THE UNIVERSITY of ADELAIDE

A 210,000-year reconstruction of subtropical climates from Fern Gully Lagoon, North Stradbroke Island (Minjerribah), Australia

Christopher Wilde Kemp

Discipline of Geography, Environment and Population
University of Adelaide
A thesis submitted for the degree of Doctor of Philosophy

October 2020

Table of Contents

Abstract

Climates during past interglacials may be an analogue for future climate change. Robust reconstructions of past interglacial climates are important for providing these analogues, as well as for better understanding ecosystem responses that are likely to accompany an increase in global temperatures. Records of interglacial climates are similarly required to understand the influence of long-term Australian climates on biota, including past extinction events, as well as long-term (~200 thousand year; kyr) patterns in Australian climate drivers. However, records of Australian palaeoclimates beyond the Last Glacial Maximum (~20 ± 2 thousand years ago; ka) are rare, limiting detailed analysis of long-term climate patterns and associated responses.

This thesis presents a review of Australian climate records beyond the last glacial stage and a new late-Quaternary multi-proxy climate record from Fern Gully Lagoon, North Stradbroke Island (Minjerribah), through the following components:

- A review and synthesis of hydroclimate data from 40 Australian marine isotope stage 3 (MIS 3; 57 – 29 ka) records, allowing a continental record of moisture availability to be created, and moisture availability during peak Australian megafauna extinction to be identified (Chapter 2).
- A chronology for a new wetland sediment record from subtropical Fern Gully Lagoon, using radiocarbon (^{14}C) and optically stimulated luminescence age determination as well as estimated hiatus locations as priors for Bayesian age-depth modelling (Chapter 3).
- Scanning micro-X-ray fluorescence geochemical analysis of Fern Gully Lagoon sediments, enabling a record of inorganic dust flux to be created and regional moisture availability for subtropical eastern Australia to be inferred for the past ~210 kyr (Chapter 3).
- Pollen, stable carbon isotope and lipid biomarker records as indicators of wetland vegetation assemblages during recent interglacial complexes and the Holocene, allowing reconstruction of relative moisture availability, changes in fire frequency and approximate mean annual air temperatures (Chapters 4 and 5).

Relatively high average Australian moisture availability for mid-MIS 3 indicates that continental climate change is unlikely to be a major driver of Australian megafauna extinction. As such, human impact rather than climate change is more likely to have driven peak megafauna loss at ~45 ka.

Fern Gully Lagoon records of aeolian flux, indicative of wind deflation, provide a record from which regional moisture availability can be inferred. Regional (pollen and charcoal) and local (stable carbon isotope and lipid biomarker) climate records were then used to refine the overall multi-proxy record, as well as determine changes in regional temperatures, fire regimes and local wetland evaporation. Along with findings related to vegetation succession and climate proxy recovery methods, the multi-proxy record indicated relatively similar moisture availability at Fern Gully Lagoon during MIS 7a–c and early MIS 5, but notably drier climates during the Holocene.

The Fern Gully Lagoon palaeoclimate record supports an interpretation of drier Holocene climates in subtropical Australia compared to recent interglacials, with increasing El Niño – Southern Oscillation variability a possible cause. As such, this study indicates that records of Australian climates during recent interglacials provide invaluable analogues of possible future climates not available during the Holocene.

Originality Statement

I certify that this work contains no material which has been accepted for the award of any other degree or diploma in my name, in any university or other tertiary institution and, to the best of my knowledge and belief, contains no material previously published or written by another person, except where due reference has been made in the text. In addition, I certify that no part of this work will, in the future, be used in a submission in my name, for any other degree or diploma in any university or other tertiary institution without the prior approval of the University of Adelaide and where applicable, any partner institution responsible for the joint-award of this degree.

I acknowledge that copyright of published works contained within this thesis resides with the copyright holder(s) of those works.

I also give permission for the digital version of my thesis to be made available on the web, via the University's digital research repository, the Library Search and also through web search engines.

Signed:

Date: 19-10-2020

Acknowledgements

This project was supported by Australian Research Council Discovery Project DP150103875 awarded to John Tibby; Patrick Moss; Melanie Leng; Jeremy Shakun and Nigel Spooner and Future Fellowship Project FT130100195, awarded to Lee Arnold. Radiocarbon dating and μXRF studies were achieved with the support of AINSE grant ALNGRA16003, and I thank ANSTO for allowing me to spend time at the radiocarbon and μXRF laboratories at Lucas Heights. OSL and sediment radioactivity determinations were supported by the Prescott Environmental Luminescence Laboratory at the University of Adelaide. I would also like to thank the University of Adelaide for three and a half years of financial support through a Faculty of Arts Divisional Scholarship.

I acknowledge Minjerribah (North Stradbroke Island; NSI) and the surrounding waters as Quandamooka Country and thank the Quandamooka Yoolooburrabee Aboriginal Corporation for permission to undertake this work.

I would like to thank Cameron Schulz, Harald Hofmann, Jon Marshall and Glenn McGregor for their enormous assistance with the NSI project. Many thanks also go to the co-authors of peer-reviewed publications completed as part of this work; your comments and feedback have been invaluable in helping me develop my scientific writing. Finally, I would like to thank Haidee Cadd, Peter Kershaw and Patrick Moss for help with pollen and spore identification, Tony Hall, Mark Rollog and Richard Lewis for lab assistance, and Sarah Gray and David Kemp for additional proof-reading.

My sincerest thanks go to my primary supervisor John Tibby, whose support in understanding contemporary climate dynamics, palaeoclimate reconstruction and academic writing over the past four years has been invaluable. I would also like to thank my co-supervisors Lee Arnold and Cameron Barr for their support and encouragement, as well as for their approachability and enthusiastic contributions to our discussions.

Finally, I would like to thank the Tuesday night crew, my friends, and family, for their support throughout my studies and their continuing interest in my work.

Relevant Publications and Presentations

The following publications and presentations have arisen over the course of writing this thesis:

Publications:

Kemp, C.W., Tibby, J., Arnold, L.J., Barr, C., 2019. "Australian hydroclimate during Marine Isotope Stage 3: A synthesis and review". *Quaternary Science Reviews* 204, 94-104. https://doi.org/10.1016/j.quascirev.2018.11.016

Kemp, C.W., Tibby, J., Arnold, L.J., Barr, C., Gadd, P.S., Marshall, J.C., McGregor, G.B., Jacobsen, G.E., 2020. "Climates of the last three interglacials in subtropical eastern Australia inferred from wetland sediment geochemistry". *Palaeogeography, Palaeoclimatology, Palaeoecology* 538. https://doi.org/10.1016/j.palaeo.2019.109463

Presentations:

12.2018 "A new >200,000 year Australian climate record from Fern Gully Lagoon, sub-tropical eastern Australia" (Kemp, C.W., Tibby, J., Arnold, L.J., Barr, C., Gadd, P.S., Marshall, J.C. and McGregor, G.B.) Australasian Quaternary Association (AQUA) conference (Canberra, Australia) Short talk.

12.2018 "Problems with normalising scanning micro-XRF data for palaeoclimate use" (Kemp, C.W., Tibby, J., Arnold, L.J., Barr, C. and Gadd, P.S.) Australasian Quaternary Association (AQUA) conference (Canberra, Australia) Poster.

11.2017 "A new ~230,000 year Australian record: Fern Gully Wetland, North Stradbroke Island" (Kemp, C.W., Tibby, J., Barr, C. and Arnold, L.J.) Geological Society of Australia Earth Sciences Student Symposium South Australia (GESSS-SA) conference (Adelaide, Australia) Short talk.

11.2017 "Precipitation in Australia during MIS3: an analysis of published palaeoclimate datasets" (Kemp, C.W., Tibby, J., Barr, C. and Arnold, L.J.) Geological Society of Australia Earth Sciences Student Symposium South Australia (GESSS-SA) conference (Adelaide, Australia) Poster.

12.2016 "A new > 100,000 year Australian palaeoclimate record: Fern Gully Lagoon" (Kemp, C.W., Tibby, J., Arnold, L.J., Barr, C., Gadd, P.S., Jacobsen, G. and Heijnis, H.) Australasian Quaternary Association (AQUA) conference (Auckland, New Zealand) Short talk.

12.2016 "Precipitation in Australia during MIS3: An analysis of published palaeoclimate datasets" (Kemp, C.W., Tibby, J., Barr, C. and Arnold, L.J.) Australasian Quaternary Association (AQUA) conference (Auckland, New Zealand) Poster.

List of Figures

List of Tables

List of Equations

Nomenclature

^{14}C: Unstable isotope of carbon used in radiocarbon dating.

BP: Before present (1950 AD).

Cal.: Calibrated using a radiocarbon calibration curve.

D-O: Dansgaard–Oeschger event; one of 25 climate events recorded during the last glacial.

D_e: Environmental dose; the total radiation dose received by a quartz grain between deposition and sampling (luminescence dating).

EAC: East Australian current; an ocean current that brings tropical warm water south from the West Pacific Warm Pool (WPWP) along the eastern Australian coastline.

ENSO: El Niño-Southern Oscillation; a major driver of global climate change.

GDGT: Glycerol dialkyl glycerol tetraether; a biochemical temperature proxy used to reconstruct mean annual air temperatures based on the distribution of cyclopentane moieties and extra methyl groups.

HS: Heinrich Stadial; an event where a large number of icebergs separate from the Northern Hemisphere ice sheets and drift into the North Atlantic, with possible impacts on thermohaline circulation and global climates.

IDW: Inverse distance weighting; an interpolation method used to construct a 'surface' from a point field in geographic information systems.

ITCZ: Inter-tropical convergence zone; the area where Hadley cells meet. Ideally, but not usually, the equator.

Kyr: Thousand years (kilo-years).

Ka: Thousand years ago (kilo-annum).

LGM: Last Glacial Maximum; the peak of the most recent glacial period (MIS 2) at ~20 ± 2 ka.

MIS: Marine Isotope Stage; cool and warm periods of Earth's climate history, as derived from the oxygen isotope composition of foraminifera in marine sediment cores.

NSI: North Stradbroke Island; a large sand island on the central eastern coast of Australia.

OSL: Optically stimulated luminescence; an age determination method utilising the measured energy of trapped electrons in the material's crystal matrix (quartz or feldspar) released via laser and measured environmental dose rate to estimate the likely burial period for a mineral grain.

SST: Sea surface temperature.

SWW: Southern westerly winds; a zonally symmetric atmospheric circulation pattern and major driver of regional climate change around 30 – 60°S.

TL: Thermo-luminescence; an age determination method similar to OSL but using heating to stimulate mineral luminescence.

WPWP: West Pacific warm pool; a collective term for a section of south-east Asian and Pacific tropical ocean with a mean annual SST >28°C.

$\delta^{13}C$: Carbon isotope ratio; measure of the ^{13}C:^{12}C ratio in a sample compared to a standard ratio (Vienna Pee Dee Belemnite; VPDB) reported in parts per thousand (per mille, ‰).

$\delta^{15}N$: Nitrogen isotope ratio; measure of the ^{15}N:^{14}N ratio in a sample compared to a standard ratio (atmospheric nitrogen) reported in parts per thousand (per mille, ‰).

$\delta^{18}O$: Oxygen isotope ratio; measure of the ^{18}O:^{16}O ratio in a sample compared to a standard ratio (Vienna Standard Mean Ocean Water; VSMOW) reported in parts per thousand (per mille, ‰).

µXRF: micro-X-ray flourescence; a method for determining the relative abundance of a limited set of elements within a sediment or clastic sample.

Chapter 1 – Introduction and thesis aims

1.1 Introduction

This thesis presents a new, discontinuous ~210 kyr climate record from Fern Gully Lagoon, a freshwater palustrine wetland on North Stradbroke Island, subtropical eastern Australia, and a review and synthesis of Australian climates during Marine Isotope Stage 3 (MIS 3; 57 – 29 ka). The ~210 kyr climate record, covering the MIS 7a–c and MIS 5 interglacial complexes as well as the Holocene, was established using multiple climate proxies for moisture availability including inorganic sediment flux, pollen relative abundances, stable carbon isotope ratios and lipid biomarkers. Interpretation of this new climate record was focussed on comparison of interglacials – recent warm periods in Earth's climate history – with the Holocene.

The work was undertaken with the goal of producing the first reconstruction of interglacial climates from the Australian subtropics and determining the relative influence of major Australian climate drivers during recent interglacials and the Holocene. This then facilitated the identification and exploration of differences between Holocene and recent interglacial subtropical climates.

1.2 Research context

Records of past climate change play a role in the prediction of future climate at local and regional scales (e.g. monsoonal rainfall patterns (Mohtadi et al., 2016), drought cycles (Allen et al., 2011)), and are used in the fine-tuning of global climate models (Stute et al., 2001; Cronin, 2009; Otto-Bliesner et al., 2017), contributing to understanding what changes are likely to accompany increasing global temperatures (Turney and Jones, 2010; Harrison and Bartlein, 2012).

Interglacial-glacial cycles in Earth's climate have been observed in benthic foraminifera records beginning at approximately 2.6 Ma, with low amplitude ~40 kyr cycles moving to stronger ~100 kyr cycles between ~1.2 – 0.6 Ma (Fig. 1.1; Lisiecki and Raymo, 2005; Berger et

al., 2015). Analysis of recent interglacial climates can be used to inform predictions of future climate change (e.g. equilibrium sea level rise (Dutton et al., 2015), or changes in major climate drivers (Harrison and Bartlein, 2012)) due to warmer mean global temperatures than current Holocene climates (Berger et al., 2015; Yin and Berger, 2015). However, orbital parameters during recent interglacials (for which the greatest number of palaeoclimate records are available) are not directly comparable to those during the Holocene, making identifying relative changes in climate complex (Yin and Berger, 2015). In addition, interglacial climate modelling combining relative changes in insolation with ice-core records of atmospheric CO_2 and CH_4 concentrations indicate that pre-industrial Holocene climates differ from those during recent interglacials (Claussen et al., 2005; Yin and Berger, 2015). Current modelling of interglacial climates is also complicated in some cases by an overestimation of subtropical precipitation and vegetation cover (Goosse et al., 2010; Yin and Berger, 2015). As such, robust subtropical interglacial palaeoclimate reconstructions are required to help bridge the gap between modelling of past climates and predictions of future climate change, as well as understand long-term changes in global climate (Turney and Jones, 2010).

Subtropical palaeoenvironmental records play an important role in the study of global climates, as the subtropics act as a link between major high and low latitude climate drivers (e.g. the Southern Westerly Winds (SWW) and the Australian summer monsoon; Chiang, 2012). Subtropical climates are affected by changes in the South Pacific Convergence Zone (SPCZ) and Hadley Cell migration (Chiang et al., 2014; Atwood et al., 2020), thus allowing past changes in major tropical climate drivers to be inferred from subtropical palaeoclimate records. For example, changes in El-Niño Southern Oscillation (ENSO) variability have been studied in depth in subtropical records (e.g. Barron et al., 2003; Barr et al., 2019). Coastal subtropical climate records can also be influenced by ocean current heat transfer between the warm tropics and cooler high latitudes, such as via the East Australian Current (EAC; Bostock et al., 2006), allowing changes in heat transfer to be tracked in some cases.

Australian continental palaeoclimate records are limited both spatially and temporally (Petherick et al., 2013; Reeves et al., 2013b). The most common form of climate records – those based on sedimentary archives – require locations with sufficient water for regular sedimentation and preservation of sequences to occur (Lowe and Walker, 2014). Australian sedimentary

climate records are therefore sparse in the arid interior where there is limited rainfall, but are more common along the south-eastern, eastern and north-eastern margins of the continent (Reeves et al., 2013a). As such, determining Australian palaeoclimates can be challenging and must sometimes rely on approximations based on distant records, such as those from Antarctica (e.g. Johnson et al., 2016). Many Australian records detailing climates prior to ~50 ka (the approximate current limit of radiocarbon dating) are also limited by chronological uncertainty, complicating study of interglacial periods (e.g. Colhoun et al., 1999; Longmore and Heijnis, 1999; Harle et al., 2002). In addition, the majority of Australian climate records do not extend beyond the Last Glacial Maximum (LGM) at ~20 ± 2 thousand years ago (ka) (Petherick et al., 2013; Reeves et al., 2013a).

There are approximately 20 published Australian climate records detailing climates during Marine Isotope Stage 5e (MIS 5e; ~124 – 119 ka), the peak of the previous interglacial complex, but records for MIS 7a–c (~220 – 200 ka) are more limited. These include those from Lynch's Crater (Kershaw et al., 2007a), and nearby ODP 820 (Moss and Kershaw, 2007) in the wet tropics of north-eastern Australia; Lake Eyre (Cohen et al., 2015; Fu et al., 2017), Lake Woods (Bowler et al., 1998) and arid-land streams (Nanson et al., 2008) in central Australia; the Naracoorte Caves (Ayliffe et al., 1998) and Lake Wangoom (Harle et al., 2002) in the south-east; Caledonia Fen (Kershaw et al., 2010) in the Australian highlands, and Lake Selina (Colhoun et al., 1999) in Tasmania. As yet, there are no published records of Australian subtropical climates beyond mid-MIS 5.

Studies of long-term Australian hydroclimates (e.g. Edney et al., 1990; Bowler et al., 2001; Kershaw et al., 2003; Fu et al., 2017) have concluded that much of the continent became progressively drier over the past ~250 kyr. Current hypotheses infer that greater ENSO variability and reduced WPWP influence on Australian summer monsoon activity during the Holocene, compared to recent interglacials, likely led to relatively dry climates (Moss and Kershaw, 2007; Nanson et al., 2008). However, gradual interglacial drying (with a drier MIS 5 than MIS 7a–c) is generally only inferred for central and south-eastern Australia (Ayliffe et al., 1998; Nanson et al., 2008; Fu et al., 2017), regions dominated by the Australian summer monsoon and the SWW. Records of interglacial climates in eastern Australia, dominated by the Australian summer monsoon and ENSO activity, instead indicate similar conditions during MIS

7a–c and MIS 5 (e.g. Kershaw et al., 2007a; Kershaw et al., 2007b). A new record of Australian subtropical interglacial climates is required to address possible sources of long-term Australian drying by providing additional records of ENSO variability and possible EAC activity separate from notable Australian summer monsoon or SWW influence.

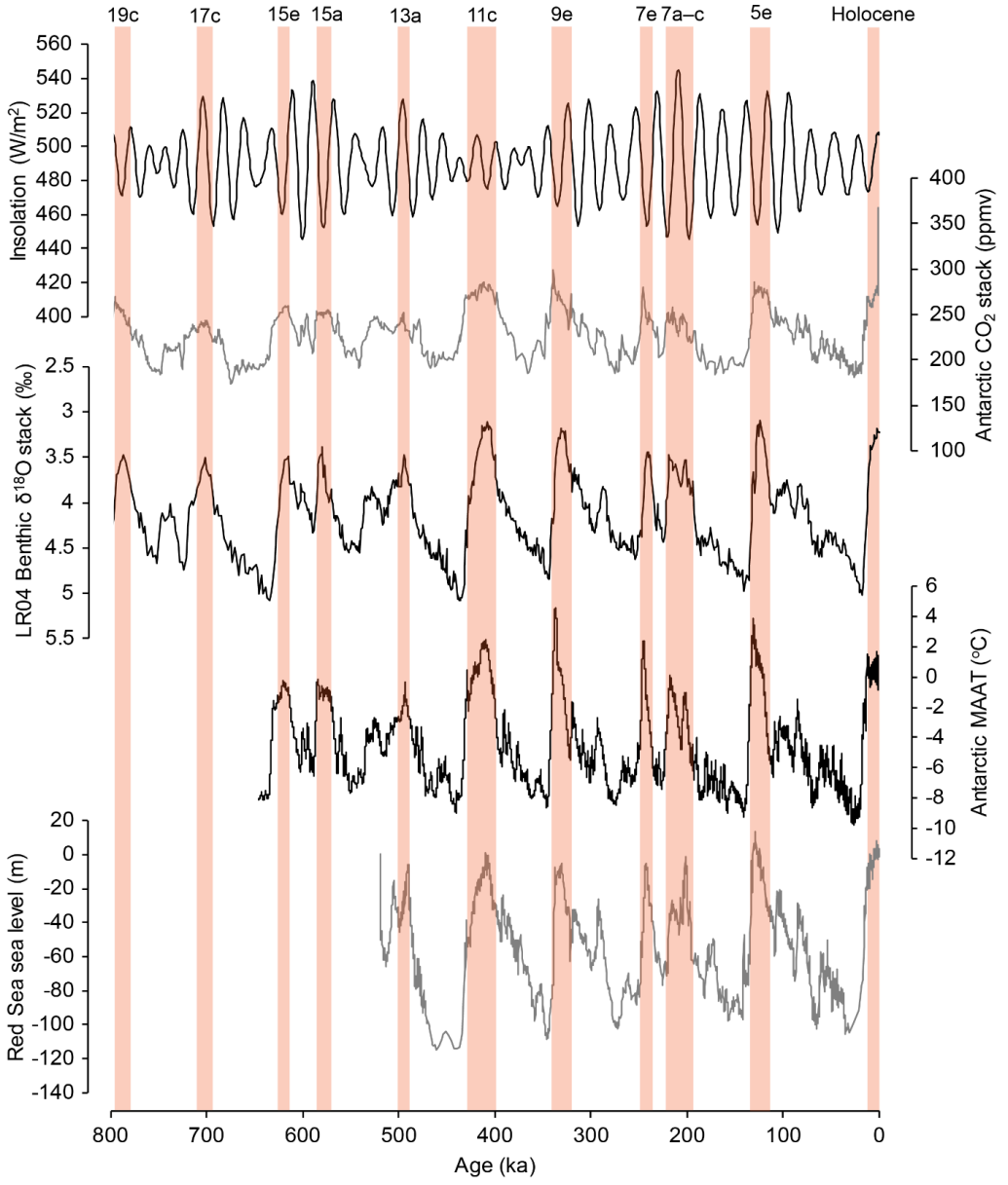

Figure 1.1: A summary of key palaeoclimate records for the past 800,000 years, with interglacials highlighted in red. Records included are December insolation at 30°S (Berger and Loutre, 1991); an Antarctic CO_2 stack (Bereiter et al., 2014); the LR04 benthic $\delta^{18}O$ stack (Lisiecki and Raymo, 2005); Antarctic mean annual air temperature reconstruction (MAAT) stack (Parrenin et al., 2013) and Global sea level (Red Sea; m compared to present; Grant et al., 2012). The interglacial numbering scheme follows Railsback et al. (2015).

In addition to the complexities involved in determining the nature of climate drivers during interglacials, understanding changes in Australian climates during MIS 3 is difficult due to limited hydroclimate records (Reeves et al., 2013a). The possible causes of Australian megafauna extinction during MIS 3, as well as the relationship between climate and the timing of human occupation have been a hotbed for scientific debate for over a century (e.g. Bird et al., 2013; Allen and O'Connell, 2014; Hamm et al., 2016). Studies have attempted to determine the exact sequence of events; whether megafauna extinction was driven by human impact in Australia (e.g. Saltré et al., 2016; van der Kaars et al., 2017), or whether a change in climate was a major factor (e.g. an increase in aridity after Cohen et al. (2015)) or some combination of the two (e.g. Bird et al., 2013). While approximately 40 Australian climate records cover part of MIS 3, no major continental synthesis of this data as has been achieved beyond ~35 ka (e.g. Petherick et al., 2013; Reeves et al., 2013a), and most studies of Australian megafauna extinction are limited to climate records of single regions (e.g. van der Kaars et al., 2017). The absence of climate syntheses, in combination with the small number of studies relative to the area of the continent, means that it has not yet been possible to provide adequate continental climate context to the extinction debate.

The development of a new >200 kyr Australian subtropical climate record would help address current spatial and temporal gaps in understanding Australian hydroclimates during MIS 3 and allow further discussion of Holocene climates relative to those of recent interglacials. Due to the large range of available analytical tools, a sedimentary source is ideally required to provide a robust multi-proxy climate record. Wetland sediment palaeoclimate records, including lakes, bogs, mires and marshes, have been instrumental in understanding climate on a global scale, including inter-hemispherical teleconnections (e.g. Turney et al., 2004; Muller et al., 2008) and large-scale drivers of Australian climates such as ENSO (e.g. Turney et al., 2004; Donders et al., 2007; Barr et al., 2019) and Southern Westerly Winds (e.g. Colhoun et al., 1999; Kirsten et al., 2018).

A new synthesis of continental MIS 3 Australian moisture availability records, and the development of a new record of Australian subtropical interglacial climates, as detailed in this thesis, provides a climate context for current scientific debates. The new synthesis of Australian MIS 3 hydroclimate addresses the lack of spatial climate context for the megafauna debate by

creating a framework where MIS 3 climates can be estimated for much of the continent. Reconstruction and validation of the first multi-proxy record of Australian subtropical climates during recent interglacials covers both spatial and temporal gaps in Australian climate history. This new subtropical wetland record allows further investigation of Australian Holocene climates as compared to recent interglacials, and identification and discussion of long-term climate drivers for Australian subtropical hydroclimates.

1.3 Methods for recording past climates

Palaeoclimate change can be inferred from variation in the properties of wetland sediments and preserved climate proxies (Table 1.1; Cronin, 2009). Multiple lines of palaeoclimate evidence are usually combined, allowing greater confidence in the final palaeoclimate interpretation. For example, increased inorganic flux may be due to drier conditions via reduced vegetation cover (e.g. McGowan et al., 2008), or may instead arise due to wetter climate with increased erosion and transport of sediment (e.g. Kemp and Rhodes, 2010). Similarly, increased charcoal flux may be due to greater fuel loads driven by wetter climates (e.g. Harrison and Sanchez Goñi, 2010), but could also be due to an increase in flammability during drier conditions (e.g. Bradstock, 2010). Comparison with a record of regional vegetation change would act as a secondary indicator of moisture availability in both these situations, and allow greater confidence in the final palaeoclimate interpretation (e.g. Kershaw et al., 2007a).

Table 1.1: A summary of common climate proxies examined in wetland sediments, with example references. *: Climate proxies utilized in this study.

Method/Proxy	Major application(s) and example reference(s)
Palynology*	Past vegetation assemblages (pollen), spores and other microfossils (algae, fungi etc.) as indicators of regional moisture availability, temperature and fire impact (Traverse, 1988; Kershaw et al., 2007a).
Scanning μXRF*	Records of changing inorganic element and oxide input due to changing aeolian flux, catchment erosion etc. in sediments – indicators of drying and weathering (Croudace and Rothwell, 2015; Burrows et al., 2016).

Stable isotope analysis (bulk sediment*, compound specific etc.)	Changing ratios of stable isotopes fractionated by environmental conditions directly or indirectly (e.g. vegetation type or stress, available nutrients). Common stable isotopes are oxygen ($\delta^{18}O$), carbon ($\delta^{13}C$), hydrogen ($\delta^{2}H$) and nitrogen ($\delta^{15}N$) (Leng, 2006; Diefendorf, 2010; Diefendorf et al., 2015).
Loss on ignition* (LOI)	Approximate changes in the proportion of organic and inorganic material and carbonates in sediment. Can be used to infer changes in catchment and wetland vegetation (Heiri et al., 2001).
Lipid biomarkers* (*n*-alkanes, GDGTs etc.)	Determination of the relative quantities of differing organic materials deposited in a wetland (e.g. terrestrial-aquatic ratio). Reconstruction of mean temperatures via the relative abundance of glycerol dialkyl glycerol tetraether (GDGT) branches (Ficken et al., 2000; Peterse et al., 2012).
Charcoal* (micro- and macro-charcoal)	Local and regional fire frequency, and a secondary indicator of vegetation assemblages and fuel availability (Mooney et al., 2011; Leys et al., 2017)
Diatom analysis	Diatom species identification to identify changes in past lake water including salinity, nutrient concentration and pH (Barr et al., 2014; Johnson et al., 2018).
Sedimentary flux	Determination of changes in wetland productivity and catchment erosion as indicators of moisture availability (Kokfelt et al., 2010; Newby et al., 2017)
Plant macrofossils (seeds etc.)	Characterisation of local vegetation assemblages as an indicator of climate (Birks, 2002; Cadd et al., 2018)
Chironomids (non-biting midge larva)	Palaeotemperature reconstruction using the relative abundance of taxa. Taxon identification via preserved head capsules (Velle et al., 2010; Eggermont and Heiri, 2012)
Trace elements – via XRF, ICP-MS or ICP-OS	Identification of sources of aeolian flux via geochemical signature (fingerprinting). Used to identify changes in wind patterns or identify tephra layers (Petherick et al., 2009; Peti et al., 2019)
Pigments	Biochemical markers used to infer past wetland state. Can determine the relative abundance of green algae, cyanobacteria, diatoms, chlorophyll etc. (Leavitt and Hodgson, 2002; Cadd et al., 2018)

Robust age-depth models are required to place palaeoclimate changes in a temporal context, to identify periods of interest, and for record comparison. To determine the extent of long climate records, previous research used either correlation-based approaches (e.g. $\delta^{18}O$ or

pollen stratigraphy (Lowe et al., 1996; van der Kaars and De Deckker, 2002)) or radiometric methods with large uncertainties (e.g. uranium-thorium dating of highly organic sediments (Heijnis and Van der Plicht, 1992; Longmore and Heijnis, 1999)). Developments in luminescence-based age determination has allowed sediment ages to be determined with increasing accuracy (Aitken, 1985; Aitken, 1998), facilitating greater chronological certainty (e.g. English et al., 2001; Rieser and Wüst, 2010). However, a large degree of error in determining the age of sediments is unavoidable in many longer records. For example, radiocarbon samples near the upper dating limit (Hogg et al., 2013), or optically stimulated luminescence (OSL) age determinations based on small grain sample sizes (Bronk-Ramsey, 2015) have inherently large age uncertainties. As such, determination of robust age-depth chronologies for many wetland sediment records (with a high likelihood of radiocarbon sample contamination and limited mineral content) almost always requires Bayesian modelling (Bronk-Ramsey, 2015; Blaauw et al., 2018). Recent advances in Bayesian modelling (e.g. Bronk-Ramsey, 2009; Blaauw et al., 2018) and single-grain OSL (e.g. Arnold et al., 2012; Arnold et al., 2014) allow notably more robust age-depth chronologies to be generated than were possible less than a decade ago (Blaauw et al., 2018).

1.4 Aims of the study

In recognition of the limited nature of MIS 3 climate records in Australia, the first aim of this study was originally to develop a new record of continental climate during MIS 3 (57 – 29 ka), thereby providing additional climate context for human settlement in Australia and peak loss of Australian megafauna. The second aim was to develop a new subtropical record of Australian climates during MIS 3 as well as during past interglacial complexes. To generate a new climate record, two sediment cores were extracted from Fern Gully Lagoon, a perched, oligotrophic, palustrine wetland on North Stradbroke Island (NSI), eastern subtropical Australia. To ensure a robust chronology I undertook detailed radiocarbon and OSL analysis to generate priors for Bayesian age-depth modelling. Combining multiple climate proxy records with a robust chronology allowed interglacial climates at Fern Gully Lagoon to be inferred, allowing an assessment of subtropical Australian Holocene climates relative to the previous two interglacials.

Specifically, the major aims of this study were to:

i) Construct a record of Australian continental climate change during MIS 3.
ii) Create a new, high resolution, discontinuous multi-proxy subtropical Australian climate record of at least two glacial cycles.

With the objectives of:

1. Creating a robust Bayesian age-depth model for the Fern Gully Lagoon record.
2. Extracting a coherent proxy signal for both regional and local climate change.
3. Comparing the climate record from Fern Gully Lagoon with other long records of climate change in Australia to determine the influence of differing Holocene climate drivers and, if possible, identify shared long-term climate trends.

1.5 Thesis outline

1.5.1 A shift in focus

The original focus of this thesis was to investigate climate change during the period of initial human colonisation of Australia, when much of the Australian megafauna became extinct (MIS 3). My work on the subject was to consist of a literature review, followed by the generation of a new Australian MIS 3 climate record from Fern Gully Lagoon. The new record would be compared to groups of other MIS 3 climate records in north-eastern and south-eastern Australia and add to current discussions of subtropical climates during MIS 3.

Initial radiocarbon and OSL dating indicated that MIS 3 was largely missing from the Fern Gully Lagoon sedimentary record. As it was no longer possible to develop a new subtropical climate record for MIS 3, the focus of this thesis moved to cover the second aim in greater detail. My Bayesian age-depth model placed the base of the Fern Gully Lagoon core at 209.3 ± 28.4 ka (2σ). As there are a very limited number of Australian climate records reaching beyond 150 ka, a new >200 ka subtropical climate record detailing conditions during three separate interglacial complexes (MIS 7a–c, MIS 5 and the Holocene) represented a rare opportunity to investigate long-term drivers of Australian interglacial climates, and the nature of Holocene climates compared to recent interglacials. Thankfully, the synthesised Australian MIS 3 moisture availability record remained a useful addition to the thesis, as it allowed an estimate

of regional moisture availability in the subtropics during a hiatus in the Fern Gully Lagoon record to be made.

1.5.2 Chapter 2

In this chapter I present a review of 40 published Australian MIS 3 hydroclimate records and provide a continental synthesis to examine temporal and spatial hydroclimate variability during this key period of Australia's prehistory (Fig. 1.2). There were notable differences in moisture availability between regions dominated by the Australian summer monsoon and the Southern Westerly Winds, with SWW-dominated regions remaining relatively wet compared to contemporary climates until the end of MIS 3. Australian climates during peak megafauna extinction at ~45 ± 5 ka (Roberts et al., 2001; Saltré et al., 2016) were relatively wet compared to modern climates, implying that human impact, rather than climate change, played a major role in the extinction of much of the Australian megafauna. The review of Australian MIS 3 climate records and synthesis of a continental record of moisture availability was published in *Quaternary Science Reviews* (Kemp et al., 2019). Minor modifications from this publication (included in Appendix E) have been made for clarity and consistency.

1.5.3 Chapter 3

In this chapter I present the chronology and age-depth model for Fern Gully Lagoon and a record of regional climates based on inorganic flux (Fig. 1.2). The chapter also includes a review of micro-X-ray fluorescence normalisation methods.

Bayesian modelling utilising 20 radiocarbon and 17 single-grain OSL ages as priors, combined with possible hiatus locations determined via change-point analysis, was used to generate a robust age-depth model for Fern Gully Lagoon. Modelling found basal sediments were deposited at 209.3 ± 28.4 ka (±2σ), in agreement with a reconnaissance core (Tibby et al., 2017), and that the sediments were deposited in four separate sedimentary phases, covering most of the Holocene as well as interglacial complexes MIS 7a–c and MIS 5.

As inorganic material in NSI wetland sediments is generally an indicator of regional vegetation density driven by regional hydroclimates, regional moisture availability can be inferred from inorganic flux (McGowan et al., 2008; Petherick et al., 2017). As such, a record of regional moisture availability was estimated from inorganic oxides present in Fern Gully Lagoon

sediments. Selected methods for identifying inorganics within Fern Gully Lagoon sediments included estimation of inorganic mass via loss on ignition (LOI) and micro-X-ray fluorescence to identify individual oxides.

The inorganic flux record indicated that regional climates during the MIS 5 interglacial complex were marginally drier than during MIS 7a–c, but that Holocene climates were notably drier than in MIS 5, with up to three times greater inorganic flux. The chronology and inorganic flux record, a detailed review of μXRF normalisation methods and the palaeoclimate interpretations have been published in *Palaeogeography, Palaeoclimatology, Palaeoecology*. Minor modifications from this publication (included in Appendix E) have been made for clarity and consistency.

1.5.4 Chapter 4

In Chapter 4 I present an extension to the regional climate record from Fern Gully Lagoon. Pollen and charcoal records were utilised to identify changes in regional moisture availability and identify any links between long-term vegetation density (hence inorganic flux) and fire frequency.

Pollen analysis allowed a record of vegetation assemblages to be established, and an approximate record of relative changes in regional moisture availability to be inferred, mainly via shifts in the relative abundance of rainforest taxa (after Kershaw et al. (2007a) and Moss et al. (2013)). The charcoal record allowed changes in fire frequency on NSI to be identified, as well as any changes due to dominant vegetation assemblages or human impact.

The pollen and charcoal studies indicated that Holocene climates on NSI were notably drier than climates during early MIS 5, consistent with climate records from north-eastern and south-eastern Australia (Kershaw et al., 2007a; Kershaw et al., 2010). They also identified a lack of rainforest taxa recovery during late MIS 2 and the early Holocene, possibly due to human impact on regional fire regimes after the LGM. Similar vegetation assemblages during MIS 5 and MIS 7a–c indicated that drying of subtropical Australia over the past two glacial-interglacial cycles is unlikely. The pollen and charcoal studies, along with discussion of possible drivers, were detailed in a manuscript submitted to the *Journal of Quaternary Science* in December 2019, which was resubmitted with changes after review in May 2020.

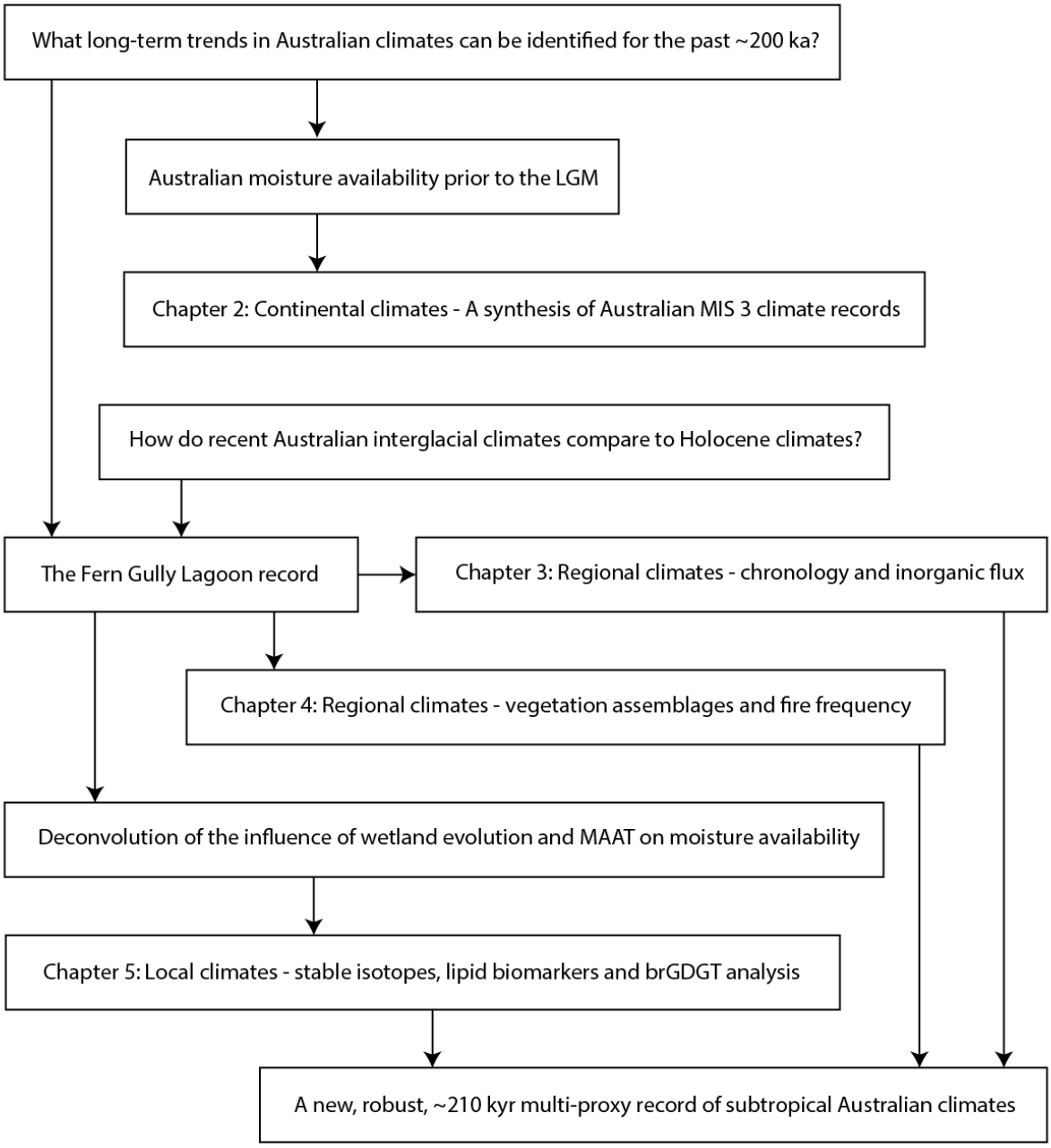

Figure 1.2: Thesis conceptual model.

1.5.5 Chapter 5

Chapter 5 details the use of bulk sediment $\delta^{13}C$ and lipid biomarkers to generate a record of local wetland conditions based on changes in wetland vegetation composition and water stress. Organic material was determined to be mostly wetland-derived by overlap with $\delta^{13}C$ and C:N values of contemporary NSI vegetation, as well as by the presence of peat indicator biomarker $C_{31}17\alpha21\beta(H)$ – homohopane in most samples.

Wetland moisture availability inferred from bulk sediment $\delta^{13}C$ and lipid biomarker records supported the climate interpretations of inorganic flux and vegetation studies: Holocene climates were relatively dry compared to recent interglacials, independent to the impact of human occupation on regional vegetation.

Glycerol dialkyl glycerol tetraether (GDGT) biomarker analysis was used to establish a palaeotemperature record for Fern Gully Lagoon, allowing comparison of interglacial mean annual temperatures. Unfortunately, GDGT calibrations used to determine interglacial temperatures at Fern Gully Lagoon were found to be unreliable, with higher temperatures inferred during glacials than during interglacials. Stable isotope and lipid biomarker analysis, as well as research detailing the local evolution of Fern Gully Lagoon and inferred local moisture availability is detailed in Chapter 5 and submission to the *Journal of Quaternary Science* is planned for July 2020.

1.5.6 Chapter 6

In Chapter 6, I summarise the key MIS 3 climate synthesis and Fern Gully Lagoon climate record findings, including how each of the objectives were addressed. Possible directions for further research are also outlined, summarising identified gaps in current knowledge and possible methods which could be used to address these gaps.

1.6 References

Aitken, M.J., 1985. "Thermoluminescence dating". Academic Press, London.

Aitken, M.J., 1998. "An introduction to optical dating: the dating of Quaternary sediments by the use of photon-stimulated luminescence". Oxford University Press, Oxford.

Allen, J., O'Connell, J.F., 2014. "Both half right: Updating the evidence for dating first human arrivals in Sahul." *Australian Archaeology* 79, 86-108.

Allen, K., Ogden, J., Buckley, B., Cook, E., Baker, P., 2011. "The potential to reconstruct broadscale climate indices associated with southeast Australian droughts from Athrotaxis species, Tasmania." *Climate Dynamics* 37, 1799-1821.

Arnold, L.J., Demuro, M., Navazo, M., Benito-Calvo, A., Pérez-González, A., 2012. "OSL dating of the Middle Palaeolithic Hotel California site, Sierra de Atapuerca, north-central Spain." *Boreas* 42, 285-305.

Arnold, L.J., Demuro, M., Parés, J.M., Arsuaga, J.L., Aranburu, A., de Castro, B., María, J., Carbonell, E., 2014. "Luminescence dating and palaeomagnetic age constraint on hominins from Sima de los Huesos, Atapuerca, Spain." *Journal of Human Evolution* 67, 85-107.

Ayliffe, L.K., Marianelli, P.C., Moriarty, K.C., Wells, R.T., McCulloch, M.T., Mortimer, G.E., Hellstrom, J.C., 1998. "500 ka precipitation record from southeastern Australia: Evidence for interglacial relative aridity." *Geology* 26, 147-150.

Barr, C., Tibby, J., Gell, P., Tyler, J., Zawadzki, A., Jacobsen, G.E., 2014. "Climate variability in south-eastern Australia over the last 1500 years inferred from the high-resolution diatom records of two crater lakes." *Quarternary Science Reviews* 95, 115-131.

Barr, C., Tibby, J., Leng, M.J., Tyler, J.J., Henderson, A.C.G., Overpeck, J.T., Simpson, G.L., Cole, J.E., Phipps, S.J., Marshall, J.C., McGregor, G.B., Hua, Q., McRobie, F.H., 2019. "Holocene El Niño–Southern Oscillation variability reflected in subtropical Australian precipitation." *Scientific Reports* 9, 1627.

Barron, J.A., Heusser, L., Herbert, T., Lyle, M., 2003. "High-resolution climatic evolution of coastal northern California during the past 16,000 years." *Paleoceanography* 18, 1-14.

Bereiter, B., Eggleston, S., Schmitt, J., Nehrbass-Ahles, C., Stocker, T.F., Fischer, H., Kipfstuhl, S., Chappellaz, J., 2014. "Revision of the EPICA Dome C CO_2 record from 800 to 600 kyr before present." *Geophysical Research Letters* 42, 542-549.

Berger, A., Crucifix, M., Hodell, D.A., Mangili, C., McManus, J.F., Otto-Bliesner, B., Pol, K., Raynaud, D., Skinner, L.C., Tzedakis, P.C., Wolff, E.W., Yin, Q.Z., Abe-Ouchi, A., Barbante, C., Brovkin, V., Cacho, I., Capron, E., Ferretti, P., Ganopolski, A., Grimalt, J.O., Hönisch, B., Kawamura, K., Landais, A., Margari, V., Martrat, B., Masson-Delmotte, V., Mokeddem, Z., Parrenin, F., Prokopenko, A.A., Rashid, H., Schulz, M.,

Riveiros, N.V., 2015. "Interglacials of the last 800,000 years." *Reviews of Geophysics* 54, 162-219.

Berger, A., Loutre, M.F., 1991. "Insolation values for the climate of the last 10 million years." *Quaternary Sciences Reviews* 10, 297-317.

Bird, M.I., Hutley, L.B., Lawes, M.J., Lloyd, J.O.N., Luly, J.G., Ridd, P.V., Roberts, R.G., Ulm, S., Wurster, C.M., 2013. "Humans, megafauna and environmental change in tropical Australia." *Journal of Quaternary Science* 28, 439-452.

Birks, H.H., 2002. "Plant macrofossils", in: Smol, J.P., Birks, H.J.B., Last, W.M., Bradley, R.S., Alverson, K. (Eds.), Tracking Environmental Change Using Lake Sediments: Terrestrial, Algal, and Siliceous Indicators. Springer Netherlands, Dordrecht, pp. 49-74.

Blaauw, M., Christen, J.A., Bennett, K.D., Reimer, P.J., 2018. "Double the dates and go for Bayes — Impacts of model choice, dating density and quality on chronologies." *Quaternary Science Reviews* 188, 58-66.

Bostock, H.C., Opdyke, B.N., Gagan, M.K., Kiss, A.E., Fifield, L.K., 2006. "Glacial/interglacial changes in the East Australian current." *Climate Dynamics* 26, 645-659.

Bowler, J.M., Duller, G.A.T., Perret, N., Prescott, J.R., Wyrwoll, K.-H., 1998. "Hydrologic changes in monsoonal climates of the last glacial cycle: stratigraphy and luminescence dating of Lake Woods, N.T. Australia." *Paleoclimates* 3, 179-207.

Bowler, J.M., Wyrwoll, K.-H., Lu, Y., 2001. "Variations of the northwest Australia summer monsoon over the last 300,000 years: The paleohydrological record of the Gregory (Mulan) Lakes system." *Quaternary International* 82-85, 63-80.

Bradstock, R.A., 2010. "A biogeographic model of fire regimes in Australia: current and future implications." *Global Ecology and Biogeography* 19, 145-158.

Bronk-Ramsey, C., 2009. "Bayesian Analysis of Radiocarbon Dates." *Radiocarbon* 51, 337-360.

Bronk-Ramsey, C., 2015. "Bayesian approaches to the building of archaeological chronologies", in: Barcelo, J.A., Bogdanovic, I. (Eds.), Mathematics and Archaeology. CRC Press, Boca Raton, pp. 272-292.

Burrows, M.A., Heijnis, H., Gadd, P., Haberle, S.G., 2016. "A new late Quaternary palaeohydrological record from the humid tropics of northeastern Australia." *Palaeogeography, Palaeoclimatology, Palaeoecology* 451, 164-182.

Cadd, H., Tibby, J., Barr, C., Tyler, J., Unger, L., Leng, M., Marshall, J., McGregor, G., Lewis, R., Arnold, L., Lewis, T., Baldock, J., 2018. "Development of a southern hemisphere subtropical wetland (Welsby Lagoon, south-east Queensland, Australia) through the last glacial cycle." *Quaternary Science Reviews* 202, 53-65.

Chiang, J.C.H., Friedman, A.R., 2012. "Extratropical cooling, interhemispheric thermal gradients, and tropical climate change." *Annual Review of Earth and Planetary Sciences* 40, 383-412.

Chiang, J.C.H., Lee, S.-Y., Putnam, A.E., Wang, X., 2014. "South Pacific Split Jet, ITCZ shifts, and atmospheric North–South linkages during abrupt climate changes of the last glacial period." *Earth and Planetary Science Letters* 406, 233-246.

Claussen, M., Brovkin, V., Calov, R., Ganopolski, A., Kubatzki, C., 2005. "Did Humankind Prevent a Holocene Glaciation?" *Climatic Change* 69, 409-417.

Cohen, T.J., Jansen, J.D., Gliganic, L.A., Larsen, J.R., Nanson, G.C., May, J.-H., Jones, B.G., Price, D.M., 2015. "Hydrological transformation coincided with megafaunal extinction in central Australia." *Geology* 43, 195-199.

Colhoun, E.A., Pola, J.S., Barton, C.E., Heijnis, H., 1999. "Late Pleistocene vegetation and climate history of Lake Selina, western Tasmania." *Quaternary International* 57–58, 5–23.

Cronin, T.M., 2009. "Paleoclimates: understanding climate change past and present". Columbia University Press, New York.

Croudace, I.W., Rothwell, R.G., 2015. "Micro-XRF Studies of Sediment Cores: Applications of a non-destructive tool for the environmental sciences". Springer, New York.

Diefendorf, A.F., 2010. "Global patterns in leaf $\delta^{13}C$ discrimination and implications for studies of past and future climate." *Proceedings of the National Academy of Sciences of the United States of America* 107, 5738-5743.

Diefendorf, A.F., Freeman, K.H., Wing, S.L., Currano, E.D., Mueller, K.E., 2015. "Paleogene plants fractionated carbon isotopes similar to modern plants." *Earth and Planetary Science Letters* 429, 33-44.

Donders, T.H., Haberle, S.G., Hope, G., Wagner, F., Visscher, H., 2007. "Pollen evidence for the transition of the eastern Australian climate system from the post-glacial to the present-day ENSO mode." *Quaternary Science Reviews* 26, 1621-1637.

Dutton, A., Carlson, A.E., Long, A.J., Milne, G.A., Clark, P.U., DeConto, R., Horton, B.P., Rahmstorf, S., Raymo, M.E., 2015. "Sea-level rise due to polar ice-sheet mass loss during past warm periods." *Science* 349, 4019.

Edney, P.A., Kershaw, A.P., De Deckker, P., 1990. "A late Pleistocene and Holocene vegetation and environmental record from Lake Wangoom, Western Plains of Victoria, Australia." *Palaeogeography, Palaeoclimatology, Palaeoecology* 80, 325-343.

Eggermont, H., Heiri, O., 2012. "The Chironomid-temperature relationship: expression in nature and paleoenvironmental implications." *Biological Reviews* 87, 430-456.

English, P., Spooner, N.A., Chappell, J., Questiaux, D.G., Hill, N.G., 2001. "Lake Lewis basin, central Australia: environmental evolution and OSL chronology." *Quaternary International* 83-85, 81-101.

Ficken, K.J., Li, B., Swain, D.L., Eglinton, G., 2000. "An *n*-alkane proxy for the sedimentary input of submerged/floating freshwater aquatic macrophytes." *Organic Geochemistry* 31, 745-749.

Fu, X., Cohen, T.J., Arnold, L.J., 2017. "Extending the record of lacustrine phases beyond the last interglacial for Lake Eyre in central Australia using luminescence dating." *Quaternary Science Reviews* 162, 88-110.

Goosse, H., Brovkin, V., Fichefet, T., Haarsma, R., Huybrechts, P., Jongma, J., Mouchet, A., Selten, F., Barriat, P.-Y., Campin, J.-M., 2010. "Description of the Earth system model of intermediate complexity LOVECLIM version 1.2." *Geoscientific Model Development* 3, 603-633.

Grant, K., Rohling, E., Bar-Matthews, M., Ayalon, A., Medina-Elizalde, M., Ramsey, C.B., Satow, C., Roberts, A., 2012. "Rapid coupling between ice volume and polar temperature over the past 150,000 years." *Nature* 491, 744-747.

Hamm, G., Mitchell, P., Arnold, L.J., Prideaux, G.J., Questiaux, D., Spooner, N.A., Levchenko, V.A., Foley, E.C., Worthy, T.H., Stephenson, B., Coulthard, V., Coulthard, C., Wilton, S., Johnston, D., 2016. "Cultural innovation and megafauna interaction in the early settlement of arid Australia." *Nature* 539, 280.

Harle, K.J., Heijnis, H., Chisari, R., Kershaw, A.P., Zoppi, U., Jacobsen, G., 2002. "A chronology for the long pollen record from Lake Wangoom, western Victoria (Australia) as derived from uranium/thorium disequilibrium dating." *Journal of Quaternary Science* 17, 707-720.

Harrison, S.P., Bartlein, P., 2012. "Records from the Past, Lessons for the Future: What the Palaeorecord Implies about Mechanisms of Global Change", in: Henderson-Sellers, A., McGuffie, K. (Eds.), The Future of the World's Climate. Elsevier Science, Oxford, pp. 403-436.

Harrison, S.P., Sanchez Goñi, M.F., 2010. "Global patterns of vegetation response to millennial-scale variability and rapid climate change during the last glacial period." *Quaternary Science Reviews* 29, 2957-2980.

Heijnis, H., Van der Plicht, J., 1992. "Uranium/thorium dating of Late Pleistocene peat deposits in NW Europe, uranium/thorium isotope systematics and open-system behaviour of peat layers." *Chemical Geology* 94, 161-171.

Heiri, O., Lotter, A., Lemcke, G., 2001. "Loss on ignition as a method for estimating organic and carbonate content in sediments: reproducibility and comparability of results." *Journal of Paleoliminology* 25, 101-110.

Hogg, A.G., Hua, Q., Blackwell, P.G., Niu, M., Buck, C.E., Heaton, T.J., Guilderson, T.P., Zimmerman, S.R.H., Palmer, J.G., Turney, C.S.M., Reimer, P.J., Reimer, R.W., 2013. "Shcal13 Southern Hemisphere calibration, 0-50,000 years cal BP." *Radiocarbon* 55, 1889-1903.

Johnson, B.E., Noble, P.J., Heyvaert, A.C., Chandra, S., Karlin, R., 2018. "Anthropogenic and climatic influences on the diatom flora within the Fallen Leaf Lake watershed, Lake Tahoe Basin, California over the last millennium." *Journal of Paleolimnology* 59, 159-173.

Johnson, C.N., Alroy, J., Beeton, N.J., Bird, M.I., Brook, B.W., Cooper, A., Gillespie, R., Herrando-Pérez, S., Jacobs, Z., Miller, G.H., Prideaux, G.J., Roberts, R.G., Rodríguez-Rey, M., Saltré, F., Turney, C.S.M., Bradshaw, C.J.A., 2016. "What caused extinction of the Pleistocene megafauna of Sahul?" *Proceedings of the Royal Society of London Series B -Biological Sciences* 283:20152399, 1-8.

Kemp, C.W., Tibby, J., Arnold, L.J., Barr, C., 2019. "Australian hydroclimate during Marine Isotope Stage 3: A synthesis and review." *Quaternary Science Reviews* 204, 94-104.

Kemp, J., Rhodes, E., 2010. "Episodic fluvial activity of inland rivers in southeastern Australia: palaeochannel systems and terraces of the Lachlan River." *Quaternary Science Reviews* 29, 732-752.

Kershaw, A.P., Bretherton, S.C., van der Kaars, S., 2007a. "A complete pollen record of the last 230 ka from Lynch's Crater, north-eastern Australia." *Palaeogeography, Palaeoclimatology, Palaeoecology* 251, 23-45.

Kershaw, A.P., McKenzie, G.M., Porch, N., Roberts, R.G., Brown, J., Heijnis, H., Orr, M.L., Jacobsen, G., Newall, P.R., 2007b. "A high-resolution record of vegetation and climate through the last glacial cycles from Caledonia Fen, southeastern highlands of Australia." *Journal of Quaternary Science* 22, 481-500.

Kershaw, P., McKenzie, G., Brown, J., Roberts, R., van der Kaars, S., 2010. "Beneath the peat: A refined pollen record from an interstadial at Caledonia Fen, highland eastern Victoria, Australia." *Terra Australis* 32, 33-48.

Kershaw, P., Moss, P., Van Der Kaars, S., 2003. "Causes and consequences of long-term climatic variability on the Australian continent." *Freshwater Biology* 48, 1274-1283.

Kirsten, K.L., Haberzettl, T., Wündsch, M., Frenzel, P., Meschner, S., Smit, A.J., Quick, L.J., Mäusbacher, R., Meadows, M.E., 2018. "A multiproxy study of the ocean-atmospheric forcing and the impact of sea-level changes on the southern Cape coast, South Africa during the Holocene." *Palaeogeography, Palaeoclimatology, Palaeoecology* 496, 282-291.

Kokfelt, U., Reuss, N., Struyf, E., Sonesson, M., Rundgren, M., Skog, G., Rosén, P., Hammarlund, D., 2010. "Wetland development, permafrost history and nutrient cycling

inferred from late Holocene peat and lake sediment records in subarctic Sweden." *Journal of Paleolimnology* 44, 327-342.

Leavitt, P.R., Hodgson, D.A., 2002. "Sedimentary pigments", in: Smol, J.P., Birks, H., Last, W.M. (Eds.), Tracking Environmental Change Using Lake Sediments: Terrestrial, Algal, and Siliceous Indicators. Kluwer Academic Publishers, Dordrecht, pp. 295-326.

Leng, M.J., 2006. "Isotopes in Palaeoenvironmental Research". Springer, Dordrecht, the Netherlands.

Leys, B.A., Commerford, J.L., McLauchlan, K.K., 2017. "Reconstructing grassland fire history using sedimentary charcoal: Considering count, size and shape." *PLOS ONE* 12, 0176445.

Lisiecki, L.E., Raymo, M.E., 2005. "A Pliocene-Pleistocene stack of 57 globally distributed benthic $\delta^{18}O$ records." *Paleoceanography* 20.

Longmore, M.E., Heijnis, H., 1999. "Aridity in Australia: Pleistocene records of palaeohydrological and palaeoecological change from the perched lake sediments of Fraser Island, Queensland, Australia." *Quaternary International* 57/58, 35–47.

Lowe, J.J., Accorsi, C.A., Bandini Mazzanti, M., Bishop, A., Van der Kaars, S., Forlani, L., Mercuri, A.M., Rivalenti, C., Torri, P., Watson, C., 1996. "Pollen stratigraphy of sediment sequences from lakes Albano and Nemi (near Rome) and from the central Adriatic, spanning the interval from oxygen isotope stage 2 to present day." *Memorie-Istitudo Italiano Di Idrobiologica* 55, 71-98.

Lowe, J.J., Walker, M.J.C., 2014. "Reconstructing quaternary environments". Routledge, New York.

McGowan, H.A., Petherick, L.M., Kamber, B.S., 2008. "Aeolian sedimentation and climate variability during the late Quaternary in southeast Queensland, Australia." *Palaeogeography, Palaeoclimatology, Palaeoecology* 265, 171-181.

Mohtadi, M., Prange, M., Steinke, S., 2016. "Palaeoclimatic insights into forcing and response of monsoon rainfall." *Nature* 533, 191-199.

Mooney, S.D., Harrison, S.P., Bartlein, P.J., Daniau, A.-L., Stevenson, J., Brownlie, K.C., Buckman, S., Cupper, M., Luly, J., Black, M., Colhoun, E., D'Costa, D., Dodson, J., Haberle, S., Hope, G.S., Kershaw, P., Kenyon, C., McKenzie, M., Williams, N., 2011. "Late Quaternary fire regimes of Australasia." *Quaternary Science Reviews* 30, 28-46.

Moss, P.T., Kershaw, A.P., 2007. "A late Quaternary marine palynological record (oxygen isotope stages 1 to 7) for the humid tropics of northeastern Australia based on ODP Site 820." *Palaeogeography, Palaeoclimatology, Palaeoecology* 251, 4-22.

Moss, P.T., Tibby, J., Petherick, L., McGowan, H., Barr, C., 2013. "Late Quaternary vegetation history of North Stradbroke Island, Queensland, eastern Australia." *Quaternary Science Reviews* 74, 257-272.

Muller, J., Kylander, M., Wüst, R.A.J., Weiss, D., Martinez-Cortizas, A., LeGrande, A.N., Jennerjahn, T., Behling, H., Anderson, W.T., Jacobson, G., 2008. "Possible evidence for wet Heinrich phases in tropical NE Australia: the Lynch's Crater deposit." *Quaternary Science Reviews* 27, 468-475.

Nanson, G.C., Price, D.M., Jones, B.G., Maroulis, J.C., Coleman, M., Bowman, H., Cohen, T.J., Pietsch, T.J., Larsen, J.R., 2008. "Alluvial evidence for major climate and flow regime changes during the middle and late Quaternary in eastern central Australia." *Geomorphology* 101, 109-129.

Newby, P.E., Killoran, P., Waldorf, M.R., Shuman, B.N., Webb, R.S., Webb, T., 2017. "14,000 Years of Sediment, Vegetation, and Water-Level Changes at the Makepeace Cedar Swamp, Southeastern Massachusetts." *Quaternary Research* 53, 352-368.

Otto-Bliesner, B., Braconnot, P., Harrison, S., P., Lunt, D., Abe-Ouchi, A., Albani, S., Bartlein, P., J, Capron, E., Carlson, A., E., Dutton, A., Fischer, H., Goelzer, H., Govin, A., Haywood, A., Joos, F., LeGrande, A., N, Lipscomb, W., H, Lohmann, G., Mahowald, N., Nehrbass-Ahles, C., Pausata, F., S R, Peterschmitt, J.-Y., Phipps, S., J, Renssen, H., Zhang, Q., 2017. "The PMIP4 contribution to CMIP6 – Part 2: Two interglacials, scientific objective and experimental design for Holocene and Last Interglacial simulations." *Geoscientific Model Development* 10, 3979-4003.

Parrenin, F., Masson-Delmotte, V., Köhler, P., Raynaud, D., Paillard, D., Schwander, J., Barbante, C., Landais, A., Wegner, A., Jouzel, J., 2013. "Antarctic Temperature Stack (ATS) from five different ice cores (EDC, Vostok, Dome Fuji, TALDICE, and EDML)", In supplement to: Parrenin, F et al. (2013): Synchronous change of atmospheric CO_2 and Antarctic temperature during the last deglacial warming. Science, 339(6123), 1060-1063, https://doi.org/10.1126/science.1226368.

Peterse, F., van der Meer, J., Schouten, S., Weijers, J.W.H., Fierer, N., Jackson, R.B., Kim, J.-H., Sinninghe Damsté, J.S., 2012. "Revised calibration of the MBT–CBT paleotemperature proxy based on branched tetraether membrane lipids in surface soils." *Geochimica et Cosmochimica Acta* 96, 215-229.

Petherick, L., Bostock, H., Cohen, T.J., Fitzsimmons, K., Tibby, J., Fletcher, M.-S., Moss, P., Reeves, J., Mooney, S., Barrows, T., Kemp, J., Jansen, J., Nanson, G., Dosseto, A., 2013. "Climatic records over the past 30 ka from temperate Australia – a synthesis from the Oz-INTIMATE workgroup." *Quaternary Science Reviews* 74, 58-77.

Petherick, L.M., McGowan, H.A., Kamber, B.S., 2009. "Reconstructing transport pathways for late Quaternary dust from eastern Australia using the composition of trace elements of long traveled dusts." *Geomorphology* 105, 67-79.

Petherick, L.M., Moss, P.T., McGowan, H.A., 2017. "An extended Last Glacial Maximum in subtropical Australia." *Quaternary International* 432, 1-12.

Peti, L., Augustinus, P.C., Gadd, P.S., Davies, S.J., 2019. "Towards characterising rhyolitic tephra layers from New Zealand with rapid, non-destructive μ-XRF core scanning." *Quaternary International* 514, 161-172.

Railsback, L.B., Gibbard, P.L., Head, M.J., Voarintsoa, N.R.G., Toucanne, S., 2015. "An optimized scheme of lettered marine isotope substages for the last 1.0 million years, and the climatostratigraphic nature of isotope stages and substages." *Quaternary Science Reviews* 111, 94-106.

Reeves, J.M., Barrows, T.T., Cohen, T.J., Kiem, A.S., Bostock, H.C., Fitzsimmons, K.E., Jansen, J.D., Kemp, J., Krause, C., Petherick, L., Phipps, S.J., Members, O.-I., 2013a. "Climate variability over the last 35,000 years recorded in marine and terrestrial archives in the Australian region: an OZ-INTIMATE compilation." *Quaternary Science Reviews* 74, 21-34.

Reeves, J.M., Bostock, H.C., Ayliffe, L.K., Barrows, T.T., De Deckker, P., Devriendt, L.S., Dunbar, G.B., Drysdale, R.N., Fitzsimmons, K.E., Gagan, M.K., 2013b. "Palaeoenvironmental change in tropical Australasia over the last 30,000 years—a synthesis by the OZ-INTIMATE group." *Quaternary Science Reviews*, 97–114.

Rieser, U., Wüst, R.A.J., 2010. "OSL chronology of Lynch's Crater, the longest terrestrial record in NE-Australia." *Quarternary Geochronology* 5, 233-236.

Roberts, R.G., Flannery, T.F., Ayliffe, L.K., Yoshida, H., Olley, J.M., Prideaux, G.J., Laslett, G.M., Baynes, A., Smith, M.A., Jones, R., 2001. "New ages for the last Australian megafauna: continent-wide extinction about 46,000 years ago." *Science* 292, 1888-1892.

Saltré, F., Rodríguez-Rey, M., Brook, B.W., Johnson, C.N., Turney, C.S.M., Alroy, J., Cooper, A., Beeton, N., Bird, M.I., Fordham, D.A., Gillespie, R., Herrando-Pérez, S., Jacobs, Z., Miller, G.H., Nogués-Bravo, D., Prideaux, G.J., Roberts, R.G., Bradshaw, C.J.A., 2016. "Climate change not to blame for late Quaternary megafauna extinctions in Australia." *Nature Communications* 7, 1-7.

Stute, M., Clement, A., Lohmann, G., 2001. "Global climate models: Past, present, and future." *Proceedings of the National Academy of Sciences* 98, 10529.

Tibby, J., Barr, C., Marshall, J.C., Mgregor, G.B., Moss, P.T., Arnold, L.J., Page, T.J., Questiaux, D., Olley, J., Kemp, J., Spooner, N., Petherick, L., Penny, D., Mooney, S., Moss, E., 2017. "Persistence of wetlands on North Stradbroke Island (south-east Queensland, Australia) during the last glacial cycle: implications for Quaternary science and biogeography." *Journal of Quaternary Science* 32, 770-781.

Traverse, A., 1988. "Paleopalynology". Unwin Hyman, Boston.

Turney, C.S.M., Jones, R.T., 2010. "Does the Agulhas Current amplify global temperatures during super-interglacials?" *Journal of Quaternary Science* 25, 839-843.

Turney, C.S.M., Kershaw, P., Clemens, S., Branch, N., Moss, P., Fifield, L.K., 2004. "Millennial and orbital variations of El Niño/Southern Oscillation and high-latitude climate in the last glacial period." *Nature* 428, 306-310.

van der Kaars, S., De Deckker, P., 2002. "A Late Quaternary pollen record from deep-sea core Fr10/95, GC17 offshore Cape Range Peninsula, northwestern Western Australia." *Review of Palaeobotany and Palynology* 120, 17-39.

van der Kaars, S., Miller, G.H., Turney, C.S.M., Cook, E.J., Nürnberg, D., Schönfeld, J., Kershaw, A.P., Lehman, S.J., 2017. "Humans rather than climate the primary cause of Pleistocene megafaunal extinction in Australia." *Nature Communications* 8, 1-7.

Velle, G., Brodersen, K.P., Birks, H., Willassen, E., 2010. "Midges as quantitative temperature indicator species: Lessons for palaeoecology." *Holocene* 20, 989-1002.

Yin, Q., Berger, A., 2015. "Interglacial analogues of the Holocene and its natural near future." *Quaternary Science Reviews* 120, 28-46.

Chapter 2 – Australian hydroclimate during Marine Isotope Stage 3: a synthesis and review

2.1 Statement of Authorship

Title of Paper	Australian hydroclimate during Marine Isotope Stage 3: a synthesis and review
Publication Status	☑ Published ☐ Accepted for Publication ☐ Submitted for Publication ☐ Unpublished and Unsubmitted work written in manuscript style
Publication Details	Kemp, C.W., Tibby, J., Arnold, L.J., Barr, C., 2019. Australian hydroclimate during Marine Isotope Stage 3: A synthesis and review. *Quaternary Science Reviews* 204, 94-104.

2.1.1 Principal Author

Name of Principal Author (Candidate)	Christopher Wilde Kemp		
Contribution to the Paper	Research, creation and testing of new synthesis methods, data acquisition and analysis, creation of the database, corresponding author and writing the manuscript.		
Overall percentage (%)	80		
Certification:	This paper reports on original research I conducted during the period of my Higher Degree by Research candidature and is not subject to any obligations or contractual agreements with a third party that would constrain its inclusion in this thesis. I am the primary author of this paper.		
Signature		Date	31-3-2020

2.1.1 Co-Author Contributions

By signing the Statement of Authorship, each author certifies that:

i. the candidate's stated contribution to the publication is accurate (as detailed above);
ii. permission is granted for the candidate in include the publication in the thesis; and
iii. the sum of all co-author contributions is equal to 100% less the candidate's stated contribution.

Name of Co-Author	John Tibby		
Contribution to the Paper	Manuscript structure, research direction, methods and discussion, as well as editing, correcting and formatting of the manuscript.		
Signature		Date	31/03/2020

Name of Co-Author	Lee Arnold		
Contribution to the Paper	Suggestions for synthesis methods as well as use of weighted averages, discussion of the score table for dating methods, editing, correcting and formatting of the manuscript.		
Signature		Date	1/4/2020

Name of Co-Author	Cameron Barr		
Contribution to the Paper	Suggestions for synthesis methods, manuscript direction and editing, correcting and formatting of the manuscript.		
Signature		Date	31/03/2020

2.2 Preamble

This chapter details Australian climate during marine isotope stage 3 (MIS 3; 57 – 29 ka), a warmer period between the MIS 4 and MIS 2 glacials. Founded on the literature review undertaken before the main focus of the project changed, this chapter was to be the stepping-off point for discussing the extinction of much of the Australian megafauna in a continental context. Due to the discovery of a sedimentary hiatus within the Fern Gully Lagoon climate which eliminated much of MIS 3, this chapter is instead used to provide continental climate context for the subtropical climate record during that period.

This chapter was published as:

Kemp, C.W., Tibby, J., Arnold, L.J., Barr, C., 2019. "Australian hydroclimate during Marine Isotope Stage 3: A synthesis and review". *Quaternary Science Reviews* 204, 94-104. https://doi.org/10.1016/j.quascirev.2018.11.016

I have re-formatted the published article as a thesis chapter, with only minor changes to the original text (see Appendix E). However, notation associated with figures, tables and equations has changed, being instead prefaced by the chapter number, e.g. Figure 1 is now Figure 2.1. The supplementary material associated with the published work is included in this thesis as Appendix A.

2.3 Abstract

Improved reconstructions of Australia's climate during Marine Isotope Stage 3 (MIS 3) are important for understanding the environmental context of widespread human settlement of the continent and the extinction of a wide range of megafauna by 45 ± 5 thousand years ago (ka). To better understand spatial and temporal climate trends during this period, we present a synthesis of hydroclimate data from 41 Australian MIS 3 records. Hydroclimate records were evaluated and weighted by a scoring system developed to evaluate dating and proxy quality and resolution before inclusion into the synthesis. Our analysis reveals that Australia experienced spatially variable climates from ~57–49 ka before becoming predominantly wet from ~49–40 ka. After ~40 ka increasingly dry climates dominated MIS 3. Records from monsoon-influenced regions indicate a rapid drying from ~48 ka to the end of MIS 3, while there was a wetter period

from ~50–40 ka in Southern Westerly Wind-influenced records. The implications of our findings are discussed in relation to other proxy records, outlining a significant relationship with regional fire history, but little correlation to atmospheric CO_2 concentration or global sea level.

2.4 Introduction

Marine Isotope Stage 3 (MIS 3: 57–29 thousand years ago (ka) (Lisiecki and Raymo, 2005)) represents an important period in Australian Quaternary history as it encompasses the widespread colonisation of the continent by humans and the extinction of an ecologically diverse range of megafauna (Bird et al., 2013; Allen and O'Connell, 2014; Hamm et al., 2016). Whether human impact, climate change or a combination of the two led to the extinction of Australian megafauna has been debated for over a century. Humans arrived on the continent by 59 ka (Clarkson et al., 2017) and widespread coastal and interior settlement appears to have taken place by 45 ka (Turney et al., 2001; Bowler et al., 2003; Hamm et al., 2016; Tobler et al., 2017).

The 50–40 ka period overlaps with broad ecological and environmental changes that have been attributed to human agency either directly, as a result of changed fire regimes, or indirectly, due to loss of megafauna and subsequent reduced grazing pressures (Rule et al., 2012; Miller et al., 2016). The peak loss of Australian megafauna species occurred at 45 ± 5 ka (Roberts et al., 2001; Cosgrove et al., 2010; Saltré et al., 2016), with evidence for human-megafauna overlap ranging from ~4 kyr (van der Kaars et al., 2017) to ~20 kyr (Clarkson et al., 2017). While many authors have argued that megafaunal extinction occurred independently of climate change (Rule et al., 2012; Saltré et al., 2016; van der Kaars et al., 2017), there is evidence to suggest that large portions of the Australian continent experienced rapid climate change at 48 ± 2 ka (Cohen et al., 2015) and, furthermore, that human activities may not have changed fire regimes beyond the limits of natural variability during MIS 3 (Mooney et al., 2011; Bird et al., 2013).

The MIS 3 climate of Australia was also influenced by extensive southern hemisphere millennial-scale temperature variability (EPICA-Members, 2006; Jouzel et al., 2007). Ocean cores from south of Australia indicate millennial-scale sea surface temperature variation of around 2ºC during late MIS 3 (De Deckker et al., 2012). A compilation study of Australasian charcoal records has attributed millennial-scale variability in biomass burning to Dansgaard–Oeschger cycles (Mooney et al., 2011), while variability in biogenic silica has been attributed to

Heinrich events (Muller et al., 2008) and variability in peat humification and charcoal to D-O cycles (Turney et al., 2004) at Lynch's Crater in north-east Australia.

Several studies have concluded that there was a gradual aridification of Australia in the second half of MIS 3, albeit with differing hypotheses as to the cause (Chen et al., 1995; Kershaw et al., 2007a; Petherick et al., 2011). Fluvial activity in central Australia strongly reflects this pattern, with a decrease in discharge and lake filling events from ~48 ka onwards (Nanson et al., 2008; Cohen et al., 2011; Cohen et al., 2015). Increased dune formation interpreted to be indicative of aridification is evident from ~35 ka in the southern half of Australia (Fitzsimmons et al., 2013). A record of continental dust deposition indicates an abrupt period of aridity, along with a change in the source of aeolian sediment at ~30 ka, suggesting a change in atmospheric circulation during the peak aridity phases (Petherick et al., 2008). As the climate dried in the lead up to the LGM, a marked change in vegetation was also noted in multiple eastern and southern Australian records (Petherick et al., 2013; Reeves et al., 2013). Elsewhere, increased fluvial activity has been reported in late MIS 3 from ~35 ka onwards in the Murray-Darling Basin, in the south east of the continent (Fig. 2.1), with 5–10 times higher discharge than today (Page et al., 1996; Kemp and Rhodes, 2010). However, instead of indicating increased rainfall, this increased flow may be due to decreased evaporation resulting in deeper winter snow pack and elevated spring runoff from alpine regions.

Large scale spatial and temporal Australian hydroclimate patterns are likely due to major changes in climate drivers affecting the Australian continent. These include the El Niño-Southern Oscillation (ENSO), the Australian monsoon, and the southern westerly winds. ENSO variability affects rainfall across much of Australia (Risbey et al., 2009; Brown et al., 2016; Freund et al., 2017), while the Australian monsoon dominates the hydroclimate in central and northern Australia (Godfred-Spenning and Reason, 2002). The position of the southern westerly winds strongly influences hydroclimate in Tasmania, southern Victoria and South Australia (Fig. 2.1; Hendon et al., 2007; De Deckker et al., 2012).

To compare MIS 3 climate with Australian megafaunal extinction history, previous studies have relied on a high-resolution Antarctic temperature record (Johnson et al., 2016), and/or palaeoclimate model experiments (Saltré et al., 2016). To better understand the climatic context of megafaunal extinctions in MIS 3 requires improved spatial and temporal

reconstructions of MIS 3 climate dynamics derived from palaeoenvironmental records. We have synthesised data from 41 Australian hydroclimate records that span MIS 3 and use a range of archives – including lake sediments, river systems, and offshore sediments – to evaluate spatial and temporal trends in hydroclimate.

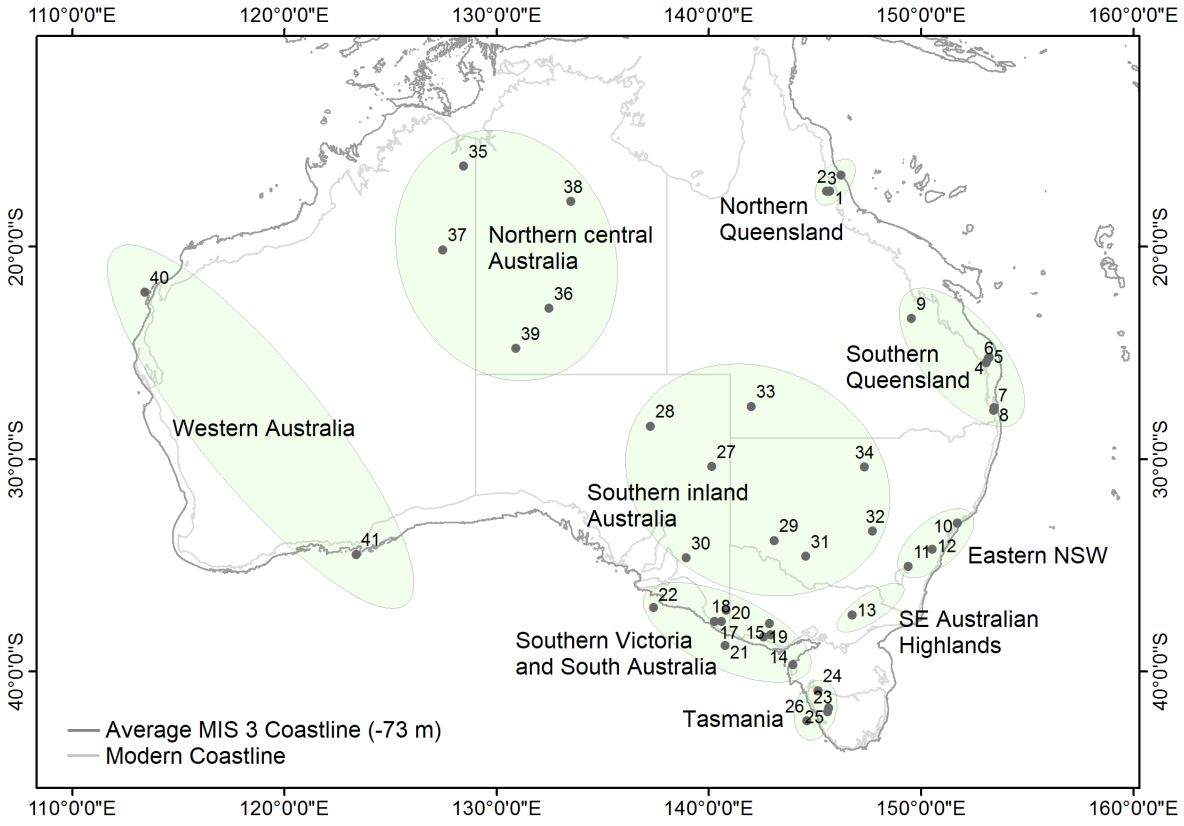

Figure 2.1: Location of study regions in Australia (green shaded areas) and the location of sites within those regions (grey dots). Average MIS 3 coastline courtesy of Phillip Arnold (pers. comm.). Numbers refer to records in Fig. 2.2.

2.5. Methods

For this MIS 3 synthesis study we have selected records from continental Australia and ocean cores within 100 km of the modern Australian coastline (to limit the influence of far-travelled pollen and dust). Forty Australian palaeoclimate MIS 3 records were located using Scopus (https://www.scopus.com/home.uri) and Web of Science, (http://www.webofknowledge.com) and separated into regions (Fig. 2.1, Supplementary Table ST1)

Radiocarbon (^{14}C) ages were re-calibrated in OxCal 4.2.4 (Bronk-Ramsey, 2009, 2016). Terrestrial records were recalibrated using SHCal13 (Hogg et al., 2013), while marine records were recalibrated using MARINE13 (Reimer et al., 2013). The re-calibrated radiocarbon ages are available in the supplementary material (Table A2). The ^{14}C ages presented in this study refer to calibrated ka before present, where present is 1950 CE. For each record, a timeline of hydroclimate as inferred in the original studies was produced (Fig. 2.2).

A rating scheme was developed to weight each study. Our scheme is conceptually similar to that developed to assess the quality of Australian Pleistocene fossil ages (Rodríguez-Rey et al., 2015), but uses a larger set of variables to assess the records. Specifically, the record quality rating scheme evaluates: (i) dating quality and resolution; (ii) proxy quality and resolution; (iii) record continuity through MIS 3; and (iv) corroborative evidence from the same region (as defined in Fig. 2.1). The overall record quality rating method is outlined in Table 2.1, with the method for assessing dating quality – a component of the quality rating – further detailed in Table 2.2. While the weighting and score assignments used in this scheme may incorporate an element of subjectivity, our approach has the advantage of being able to discriminate between high and low reliability hydroclimate records in a semi-quantitative and internally consistent manner. An example using Redhead Lagoon (Williams et al., 2006) is available in the supplementary materials.

Table 2.1: Record quality scoring system for Australian MIS 3 studies. The final score for each record is calculated as follows: dating quality (0-1) + proxy quality (0-1) + record continuity (0-0.5) + validation (0-0.5) = final score (0-3). The detailed scoring for each record is provided in the supplementary table A1.

Record quality score breakdown	**Score**
Dating quality	
1. *For the period 57 ka to 45 ka (early MIS 3)*. Scoring: 0.1 if an age estimate has been provided within this time period up to a maximum 0.2 (2 ages), 0.1 if an age has been provided for the 10 kyr period prior to the beginning of MIS 3 (acting as a maximum age constraint), and 0.1 for a spread of more than 10 kyr between the oldest and youngest ages (a measure of the temporal coverage of age control within early MIS 3).	0–0.4
2. *For the period 45 ka to 29 ka (late MIS 3).* Scoring: as above, replacing the 0.1 score awarded for a maximum constraining age with an equivalent score for a minimum constraining age during the 10 kyr period following the end of MIS 3.	0–0.4
3. Dating method (suitability of dating material and type of age control) used within the MIS 3 period. See Table 2.2. Value taken from the highest scoring dating method where more than one technique has been used.	0–0.2
Maximum subtotal:	**1**
Proxy quality	
4. Resolution of climate proxy/ies in MIS 3. Scoring: 0 = 1–5 samples; 0.1 = 6–15 samples; 0.2 = 16–30 samples, 0.3 = 31–60 samples; 0.4 = > 60 samples. The highest score is generally limited to very high-resolution proxies (e.g. micro-XRF core scans).	0–0.4
5. Number of proxies. Each additional proxy increases the score by 0.1 up to a maximum score of 0.3.	0–0.3
6. Responsiveness between proxy and hydroclimate. A fast responding proxy such as geochemical evidence of rainfall (e.g. speleothem geochemistry) or flood deposits score 0.3. Indirect or slower responding proxies such as pollen data score 0.2. Hydroclimate changes inferred from changes in charcoal score 0.1.	0–0.3
Maximum subtotal:	**1**
Record continuity	
7. Presence of a hiatus in MIS 3. A continuous record has a maximum score of 0.3. Each hiatus reduces this score by 0.1.	0–0.3
8. Hiatus above and/or below the MIS 3 record. Such occurrences introduce dating uncertainty to inferred MIS 3 ages. Each hiatus reduces the score by 0.1 from a maximum of 0.2.	0–0.2
Maximum subtotal:	**0.5**

Validation	
9. Comparable results are reported from another site in the same region (green shaded areas in Fig. 2.1) or from other proxies at the same site. Scoring: 0.1 for each additional published study from the same site detailing use of additional proxies, up to a maximum of 0.2. A score of 0.1 is assigned for each additional regional site finding discussed in relation to the new findings, up to a maximum of 0.3.	0–0.5
Maximum subtotal:	**0.5**

Table 2.2: Dating methods considered in this review and their quality scores. The latter are based on the suitability of dating material for MIS 3 records, and whether the dating technique provides a direct numerical age or age-equivalent constraint on the palaeoclimate sequence.

Dating method	Dating subtype	Type of age constraint	Sample source	Score
Radiocarbon Dating	AMS or conventional radiocarbon (^{14}C) dating	Numerical age	Bulk sediment Disseminated fine organics and/or the isolated charcoal fraction, carbonate samples. Complete or identified organics (e.g. plant macrofossils, seeds and pollen)	0.1 0.15 0.2
Luminescence Dating	Optically Stimulated Luminescence (OSL) or Thermoluminescence (TL) dating	Numerical age	Small sample size (<50 single grain equivalent dose (D_e) values or <20 multigrain aliquot D_e values per sample) Large sample size (≥50 single grain D_e values or ≥20 multigrain aliquot D_e values per sample)	0.1 0.2
Exposure dating	Cosmogenic ^{10}Be exposure dating	Numerical age	Selected boulder surface samples	0.2
Oxygen isotope stratigraphy	O^{16}/O^{18} isotope ratio of foraminifera	Relative age / age-equivalence	Shell calcite Pre-treated, etched shell calcite	0.1 0.15
Magnetics	Palaeomagnetic inclination	Relative age / age-equivalence	Bulk sediment	0.05
Uranium-Thorium	Uranium-thorium disequilibrium method	Numerical age	Bulk sediment carbonates Speleothems	0.05 0.2
Amino acid dating	Amino acid racemization	Relative age / age-equivalence	Bulk organics and egg shells	0.1

2.5.1 Hydroclimate classification scheme

There are 30 Australian records spanning MIS 3, with an additional 10 records covering only the latter parts of the period (Fig. 2.2 and Supplementary Table A1). To enable further analyses of continental hydroclimate, we have used a method similar to Harrison and Digerfeldt (1993) and Herzschuh (2006), and classified indicators of dry or wet climate into four classes before weighting by the record score, as follows:

1. We assigned hydroclimate classes to each record in 1000-year time slices. Each time slice was classed as follows; 1 = dry climate; 2 = moderately dry; 3 = moderately wet and 4 = wet climate. Dryland Australian lakes and river systems were scored on a binary scale, with 1 representing the absence of water and 4 representing the presence of water.

2. To generate an average hydroclimate record for each 1000-year time slice, the hydroclimate class for each record was first weighted by its record score. The collection of these weighted classes for each time slice was then averaged to determine the mean continental-scale hydroclimate (Equation 2.1). In this way, higher quality records have greater weight in the final synthesis.

$$water\ availiability_{time\ slice} = \frac{\sum_{record=1}^{n}(record\ score_{record} \times hydroclimate\ class_{time\ slice,record})}{\sum_{record=1}^{n} record\ score_{record}}$$

Equation 2.1: Average weighted mean equation for the moisture availability for each record at each time slice. The equation weights each record's hydroclimate class by its record score before inclusion in the synthesis.

To illustrate spatial hydroclimate variability, the classes for all records were used to create 'surface' maps of Australia at 5000-year time steps (based on the modal hydroclimate class for each record). The mapping was undertaken using the Inverse Distance Weighted (IDW) interpolation tool in ArcMap 10 (Dangermond, 2015) which was chosen because the method reduces to the overall mean value at a distance from known values (Shepard, 1968), reducing possible error due to interpolation artefacts. The IDW power was set to four, providing a drop-

off in record weighting at a short distance and reducing the influence of individual records that may record localised hydroclimate trends.

To investigate the influence of large-scale climate drivers on Australian hydroclimate, records were synthesised from two subsets of the 41-record database: records influenced by monsoonal variation (9 records) or variation in the southern westerly winds (SWW; 13 records). Defining a subset to determine MIS 3 ENSO variability was not undertaken due to a lack of unambiguously ENSO-dominated records. However, the effect of ENSO on Australia's hydroclimate during MIS 3 is detailed in the discussion. Inclusion of records in the SWW or monsoon-influenced subsets was determined by a combination of published Quaternary (e.g. monsoon records from central Australian lakes (Magee et al., 2004; Fitzsimmons et al., 2012)) and modern relationships between rainfall and remote climates drivers (Hendon et al., 2007; Fletcher and Moreno, 2011). To assess the influence of low scoring sites on the Australian average, a hydroclimate record was created using only the ten highest quality records.

Finally, to provide comparison with contemporary climate, an average climate state was derived from studies that reported the modern hydrological state. These were assigned a score between 1 and 4, as described above. Where no modern condition was described, or where landscape clearing and/or grazing has altered the study site, the record was excluded from this analysis.

2.6. Results

2.6.1 Continental trends in hydroclimate

The average weighted hydroclimate conditions of all 41 records and subsets is illustrated in Fig. 2.3. Mean continental hydroclimates were wetter than modern climates between 57–40 ka, with wettest conditions between ~49–40 ka. After ~40 ka, the climate became drier, accelerating to the end of MIS 3, reaching an average moisture availability ~30% lower than modern climate. Most sites recorded their driest conditions at the end of MIS 3 (Fig. 2.2). The ten high-quality records largely follow the Australian trend (Fig. 2.3), increasing confidence in the 41 record synthesis. The high-quality records indicate a slightly earlier commencement of drying at ~44 ka, at an increased rate compared to the continental average, indicating rapid

drying between ~41–39 ka. After ~39 ka, the high-quality records show continuing drying at a similar rate to the full Australian record until the end of MIS 3.

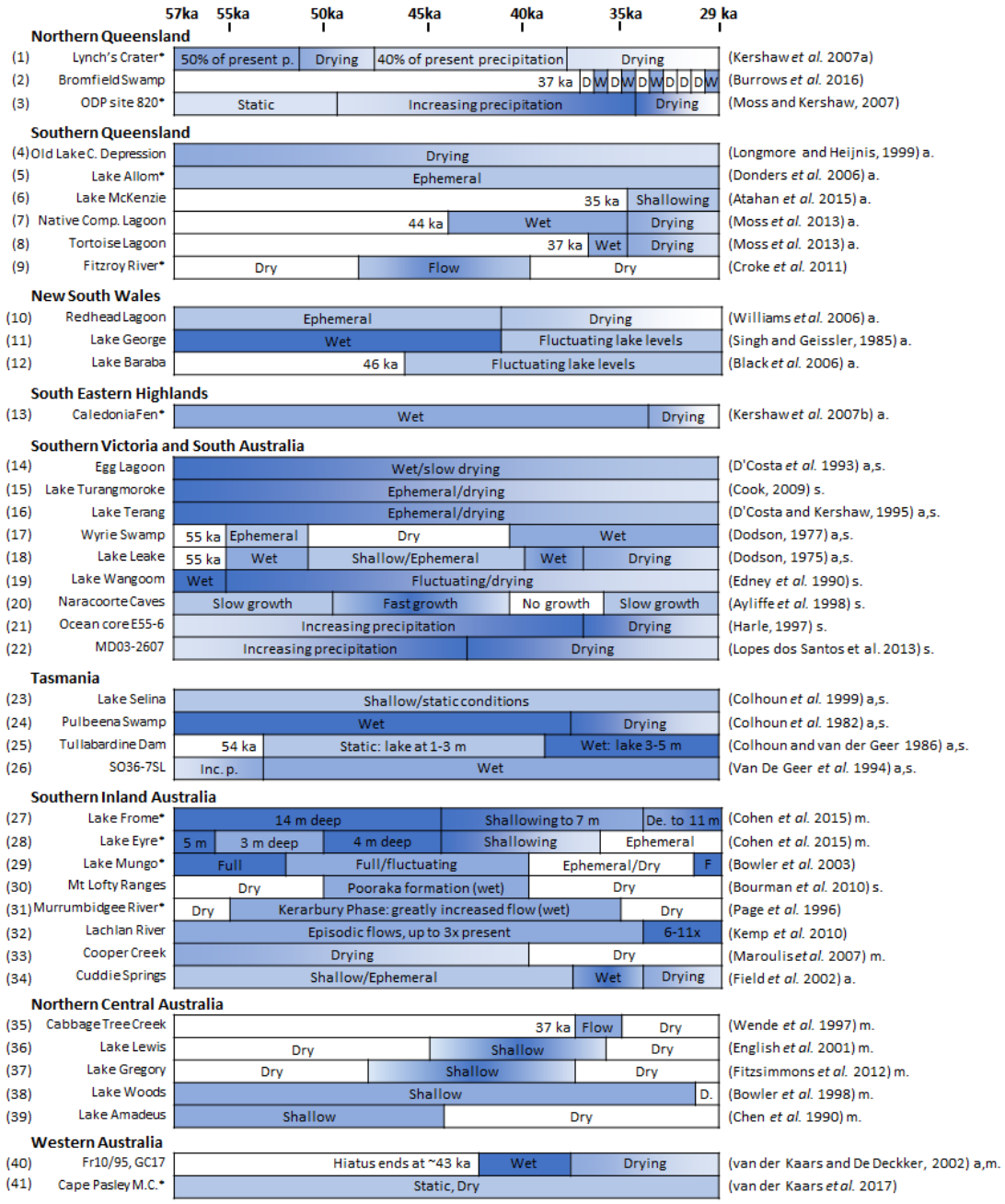

Figure 2.2: MIS 3 hydroclimate at Australian sites. Shades of blue indicate relative water availability, with darker shades representing greater water availability. Numbers refer to locations shown in Fig. 2.1. Where records are incomplete for MIS 3, the basal age is shown. Lake levels are detailed where available, in metres. Ep.: ephemeral; De.: becoming deeper; F.: full; D.: dry; W.: wet; Sh.: shallow; Dr. drying. The ten highest scoring records are marked with an asterisk. m = records included in the Australian summer monsoon-influenced subset, s = records included in the Southern Westerly Wind-influenced subset. a = records where radiocarbon ages have been recalibrated.

There are notable differences between the MIS 3 hydroclimate records in the southern westerly wind and Australian summer monsoon-influenced regions (Fig. 2.3). The SWW-influenced records are comparatively wetter than the monsoon-influenced records for all of MIS 3. Records influenced by the SWW also appear to remain wet longer, with the onset of drying in mid-MIS 3 delayed until ~39 ka. The monsoon records indicate strong hydroclimate change at ~48 ka, after which there is a gradual drying to the end of MIS 3.

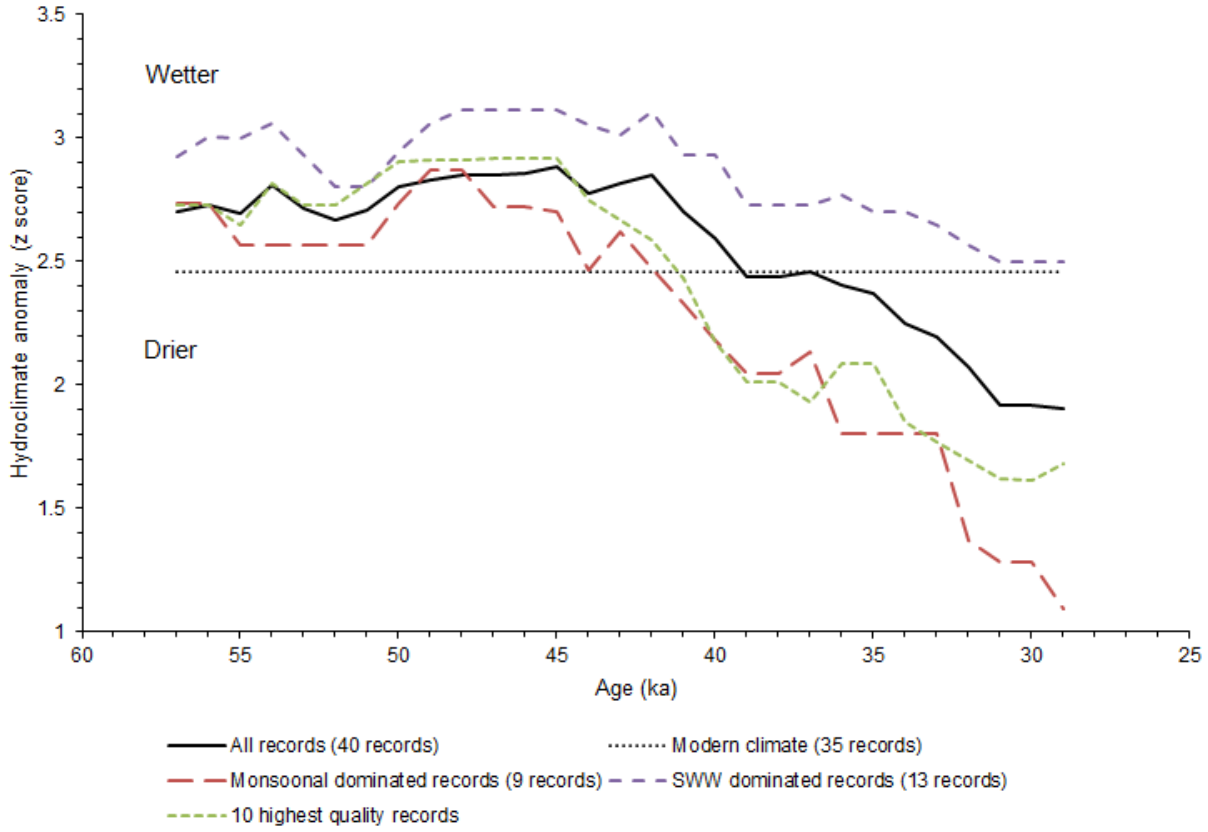

Figure 2.3: Australian MIS 3 hydroclimate anomaly at 1000-year intervals.

2.6.2 Spatial hydroclimate trends

To provide a basis for understanding the veracity of climate inferences based on spatial trends during MIS 3, the location of palaeoclimate records and quality of those records is shown in Fig. 2.4. The highest record density is in (present day) temperate south-eastern Australia, while the high scoring records are widespread – their distribution does not overlap with any single major climate driver. The distance between records in inland Australia – especially inland Western Australia – is likely to result in less accurate hydroclimate inferences for those regions.

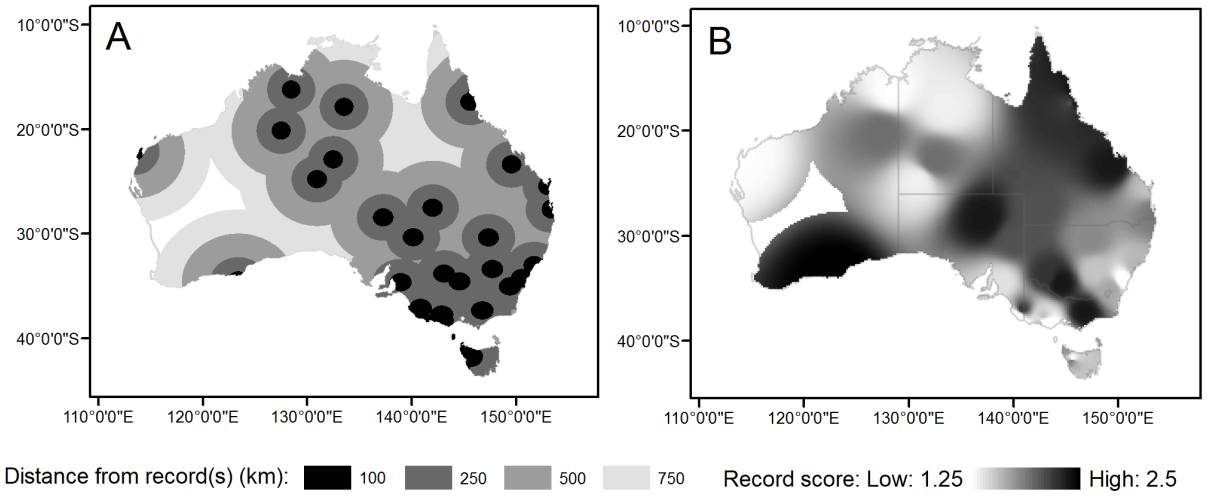

Figure 2.4: A: Record density included in this synthesis. **B:** Interpolated surface of the record quality scores, with darker shading indicating areas where greater confidence can be attributed to results.

Fig. 2.5 illustrates MIS 3 hydroclimate in six time periods. Between 57 ka and ~50 ka, central Australia was predominantly wet, though dry conditions were evident in the north-west. There were spatially variable climates in the eastern third of the continent. Between ~50–45 ka there is a trend towards a drier north-eastern Australia and generally moist climates in the southern-central and south-east parts of the continent. In the 45–40 ka period, central Australia became more arid while mildly wet conditions remained in much of the south-east of the continent. Widespread aridification of most of the continent is evident between ~40 ka and 29 ka, with peak MIS 3 aridity evident between ~35 and 29 ka. Notable exceptions to the arid late-MIS 3 climates are evident in scattered records in the south-east of the continent and Tasmania, which remained wet.

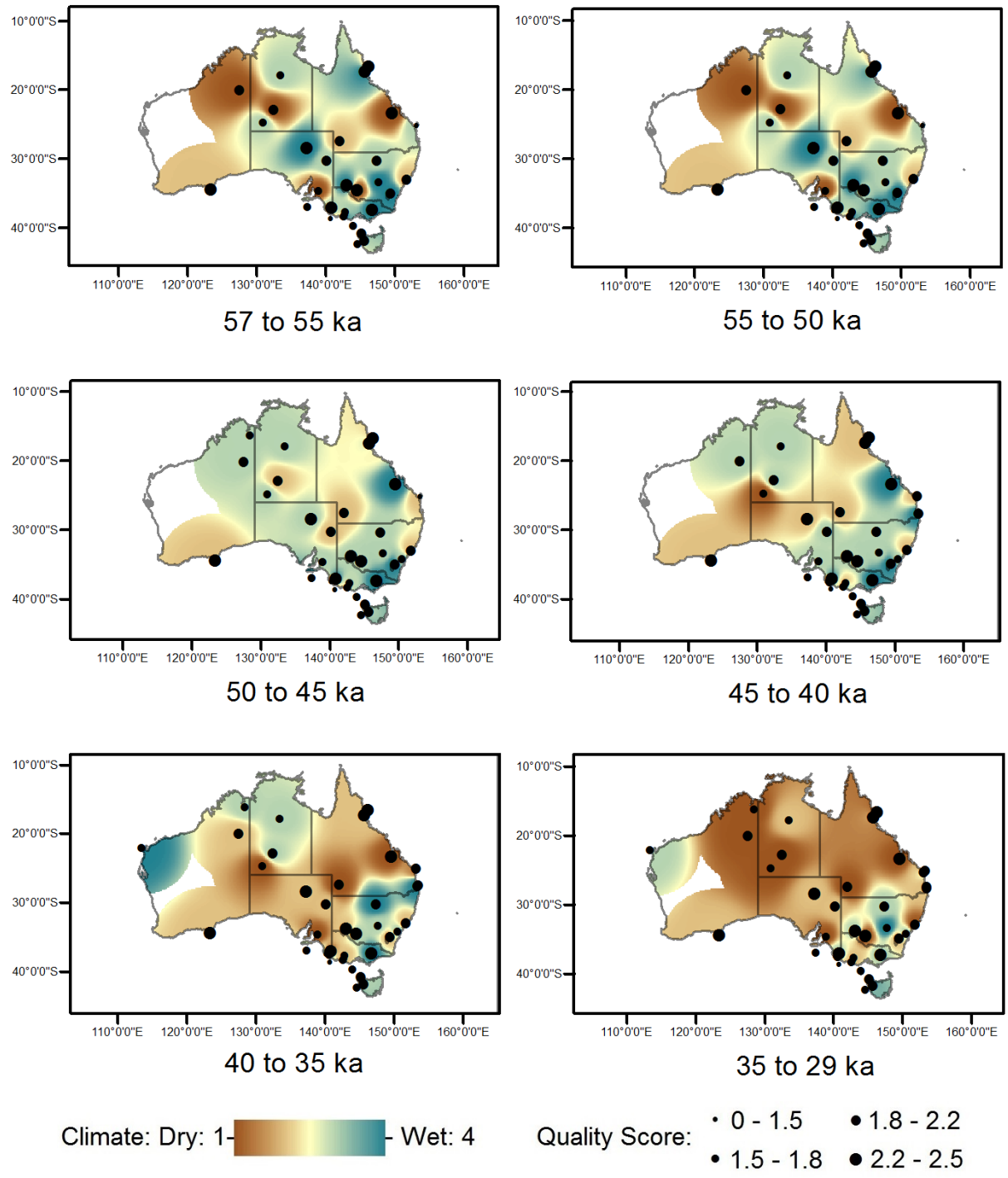

Figure 2.5: Continental-scale hydroclimate through MIS 3, showing quality score for each record. Records are only included when they have hydroclimate data pertaining to the period illustrated. The interpolated surface is limited to 750 km from the active records in each period.

2.7. Discussion

2.7.1 Temporal patterns in the Australian MIS 3 hydroclimate record

Several observations can be made about Australian climate during MIS 3 from comparison of the hydroclimate trends in Fig. 2.3. In the first half of MIS 3 the climate was wetter than present climate – as indicated by the highest-scoring records (n=10) and the continental average (n=41). After drying began at ~45 ka, the high-quality records indicate faster drying and remain drier on average to the end of MIS 3. In this context, it may be that small amounts of contamination by younger material in the lower quality records have resulted in these changes being inferred to occur later than in reality. Due to the lack of resolution in the source records, it was not possible to extract millennial scale variability with any accuracy. As such, assessment of the effect of Heinrich events or Antarctic isotope maxima, for example, was not possible.

2.7.2 Drivers of spatial and temporal hydroclimate anomalies

ENSO is a major driver of the modern hydroclimate for much of Australia, with the north-east of the continent most strongly influenced by ENSO state and variability (Risbey et al., 2009). Fossil clam shell $\delta^{18}O$ isotope records from Papua New Guinea indicate similar ENSO variability to the twentieth century at ~60 and ~40 ka (Driscoll et al., 2014), and a reduction in variability between 40–34 ka, in agreement with fossil corals from the same location (Tudhope et al., 2001). Recent ENSO modelling supports reduced ENSO variability in late MIS 3 from ~35 ka (Merkel et al., 2010), similar to previous models of ENSO 'strength' (Clement et al., 2001). The drying observed in Australian hydroclimate at ~40 ka (Fig. 2.3) may have been in part driven by the initial effect of less variable ENSO.

While clam shell $\delta^{18}O$ records indicate fewer El Niño events during MIS 3 compared to the Holocene (12 vs. 18 per century) (Driscoll et al., 2014), peat decomposition (humification) in north eastern Australia indicates a period of more frequent El Niño events centred on ~40 ka (Turney et al., 2004). The observed period of rapid drying indicated by the mean hydroclimate ~40 ka (Fig. 2.3) and multiple individual records (Fig. 2.5d–e) is likely associated with more frequent El Niño events. However, the MIS 3 hydroclimate record does not reflect a return to wetter climates associated with lower frequency of El Niño events after ~40 ka (Fig. 2.5e–f).

There is evidence that the influence of the Australian summer monsoon on continental hydroclimate may have been stronger during late MIS 3 than the present (Magee et al., 2004; Leduc et al., 2009), perhaps masking or modulating the effects of ENSO during this time (An et al., 2017).

The fluvial archives of central and northern Australia are sensitive to Australian monsoonal hydroclimate as they drain a large proportion of northern Australia (Magee et al., 2004; Fitzsimmons et al., 2012; Fitzsimmons et al., 2013). The wet climates evident in central and northern regions between ~50 and ~45 ka (Fig. 2.5c) are consistent with an intensified Australian summer monsoon during the insolation peak. Similarly, drying after ~48 ka (Fig. 2.6f) correlates with decreasing mid-latitude summer southern hemisphere insolation (Fig. 2.6a). This drying trend reflects the aridification of central Australia (Cohen et al., 2015) as well as the monsoon record inferred from Indonesian speleothems (Carolin et al., 2013). However, instead of a rapid decline in moisture availability after ~48 ka, the monsoon record indicates a more gradual, but continuous, drying of central and northern Australia.

The southern westerly winds are significantly correlated with precipitation in southern temperate Australia (Hendon et al., 2007; Fletcher and Moreno, 2011). While continental drying was occurring in late MIS 3, comparatively wetter climates persisted in records influenced by SWW variability in southern Australia and Tasmania (Fig. 2.5f). This pattern is consistent with observations during the LGM, at which time the SWW were found to either have strengthened or moved further north (Fletcher and Thomas, 2010; Kohfeld et al., 2013). Early movement or increasing SWW strength in late MIS 3 is additionally supported by dust records from North Stradbroke Island, the central tablelands of New South Wales and the southern Pacific Ocean, all of which show increased dust transport prior to the end of MIS 3 (Hesse et al., 2003; Petherick et al., 2008; Lamy et al., 2014).

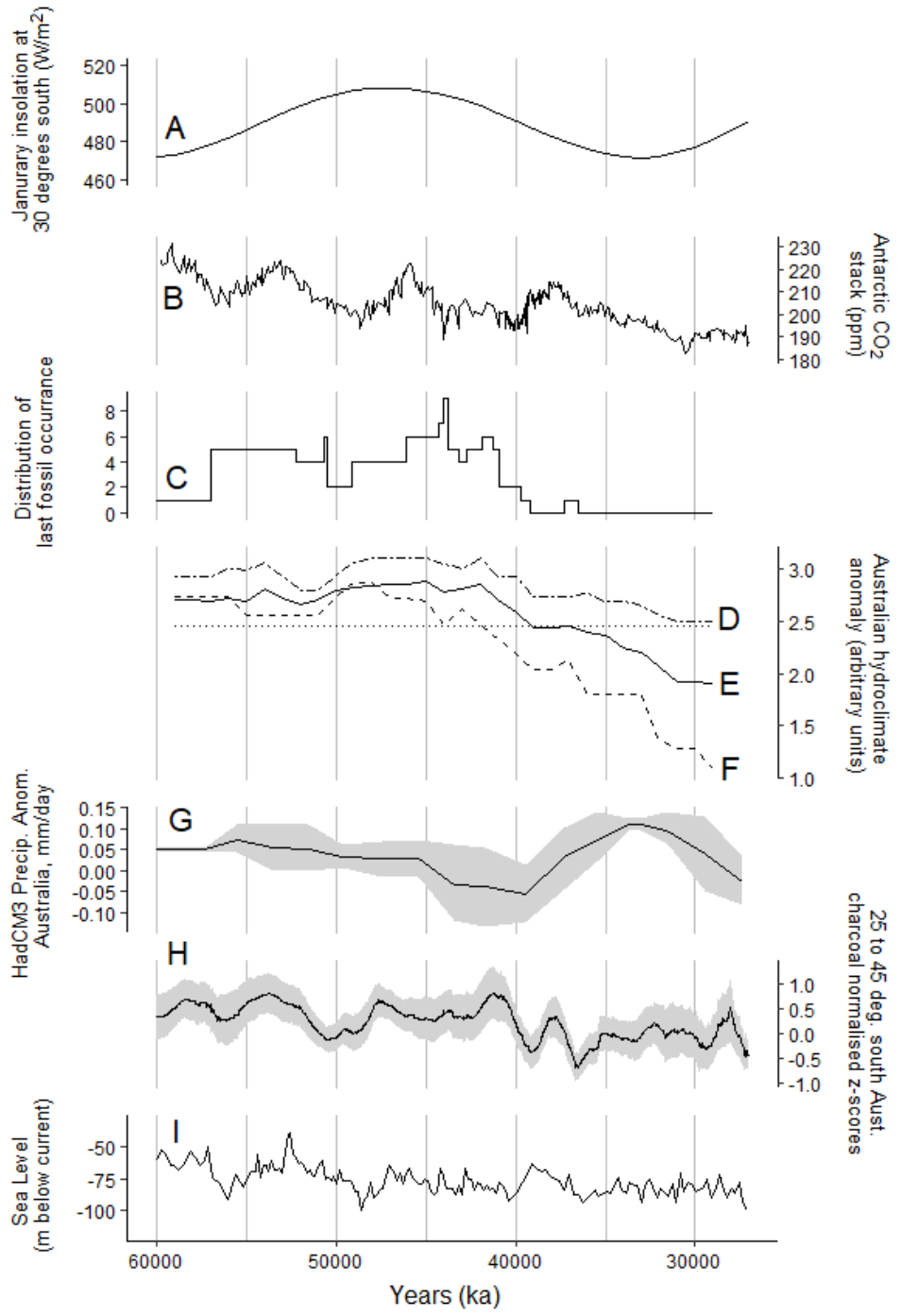

Figure 2.6: A. MIS 3 January insolation at 30°S (Berger and Loutre, 1991); **B**. Antarctic CO_2 record stack (Köhler et al., 2017); **C.** the age of last megafaunal fossil occurrences (Saltré et al., 2016); **D.** hydroclimate record for southern westerly wind influenced regions (this synthesis); **E.** Australian hydroclimate average (this synthesis); and **F.** hydroclimate record for Australian summer monsoon-influenced regions (this synthesis); **G**. HadCM3 modelled rainfall anomaly for Australia with ± 1 sigma s.d. (grey envelope) (Saltré et al., 2016); **H.** Australia and New Zealand subtropical high pressure belt (25° to 45° south) biomass burning reconstruction (Z scores of transformed charcoal influx) with ± 95% bootstrap interval (grey envelope) (Mooney et al., 2011) and, **I.** Global sea level (Grant et al., 2012).

2.7.3 The effects of changing MIS 3 climate

Human occupation of Australia, which is recorded at many sites in the the southern arid interior between ~49 and ~44 ka (Bowler et al., 2003; Allen and O'Connell, 2014; Hamm et al., 2016; Clarkson et al., 2017; Tobler et al., 2017), occurred during comparatively wetter climates (Fig. 2.5c). Bass Strait was a barrier for human migration into Tasmania until ~43 ka, when receding sea levels created a land bridge (Lambert et al., 2008). The peak loss of megafauna occurred at 45 ± 5 ka (Fig. 2.6c) (Cosgrove et al., 2010; Saltré et al., 2016), during a period where the proxy data suggest generally widespread high effective moisture (Fig. 2.6e), albeit with drying conditions in the monsoon-sensitive region (Fig. 2.6f).

Our synthesis indicates gradual continental drying from ~48 ka, which would likely have affected megafauna populations to a smaller degree than the rapid climate change indicated by the central Australian lake systems (Cohen et al., 2015). An absence of dramatic climate change corresponding to megafauna extinction has been suggested previously using modelled mean continental precipitation (Saltré et al., 2016). While our data largely support this overall conclusion, there is in fact little relationship between our mean continental hydroclimate record and modelled precipitation (Fig. 2.6e and g). The model predicts a gradually more arid MIS 3 from 57 ka, reaching its driest state at ~40 ka, before rainfall increases to a peak at ~34 ka. The model then infers a rapid decrease in rainfall until the end of MIS 3. Notably, the only major peak in rainfall in the model is ~10 kyr later than observed in our synthesis, and much closer to the end of MIS 3.

A recent charcoal compilation for Australia and New Zealand from 25° to 45° degrees south (Mooney et al., 2011) – an area containing >70% of the records in our synthesis (Fig. 2.6h) – was compared to our hydroclimate synthesis. A linear regression indicated that ~33% of the variance in the charcoal record is associated with Australian hydroclimate from records south of 25° (30 records) ($r^2 = 0.33$, $p < 0.005$). The relationship suggests that decreasing charcoal influx is associated with increasing aridity over the period, potentially reflecting reduced fuel availability in response to reduced effective moisture. A possible complication is that the charcoal record synthesis contains fewer MIS 3 records than our synthesis (all 13 of the Australian MIS 3 charcoal records are included in the synthesis) and includes records from New Zealand (Mooney et al., 2011).

Increased continentality has been argued to contribute to dry Australian glacial climates , even in near-coastal records (Dodson, 1994). This effect has been observed during MIS 4 and is argued to have had a large impact on LGM water avaliability in coastal records (e.g. Donders et al., 2006; McGowan et al., 2008; Veth et al., 2017) compared to the Holocene and MIS 5. To assess the potential influence of continentality on hydroclimates of MIS 3, we performed a regression of global sea level (Grant et al., 2012) and mean hydroclimate in the 12 records within 30 km of the coast. There was a very low r^2 of 0.05 ($p \approx 0.27$) suggesting it is unlikely that continentality during MIS 3 had a notable affect on hydroclimate.

2.7.4 Future research

The most fundamental problem in reconstructing Australian MIS 3 climate is the lack of data. While a number of published studies are available, they are restricted in two important ways: spatially, mirroring the location of wetland sediments that occur in a very small percentage of Australia's land mass; and temporally, in that there are few sedimentary records beyond 40 ka (Tibby et al., 2017). The limited number of MIS 3 studies have either low resolution (an average of approximately one sample every 1000 years, see supplementary material), and/or they have imprecise chronologies, with an average of only four constraining ages during MIS 3.

The problems of dating and proxy resolution could be partially addressed by resampling existing Australian palaeoclimate sites using improved dating methods with a focus on MIS 3. Re-analysis of older published records may also result in more detailed records due to new analytical and dating techniques. Additionally, increased focus on new sites, such as potential speleothem records in Nullarbor Plain cave systems (Lipar and Ferk, 2015; Heath et al., 2018), would help address spatial gaps (Fig. 2.4a).

Recent advances in dating of palaeoclimate archives have the potential to improve the Australian MIS 3 climate record. Refined optically stimulated luminescence (OSL) dating has significantly improved the reliability of dating beyond the radiocarbon boundary. Key recent OSL methodological improvements include the advent of single-grain techniques (e.g. Arnold et al., 2012; Arnold et al., 2014), improved statistical analyses of equivalent dose (D_e) datasets (Galbraith and Roberts, 2012), the advent of the single-aliquot regenerative protocol (Murray and Wintle, 2000) and the development of extended-range luminescence techniques (e.g. Arnold et

al., 2015; Arnold et al., 2016). Age determination has also been improved by the introduction of Bayesian age modelling (e.g. Bronk-Ramsey, 2009; Blaauw et al., 2018). Furthermore, techniques such as Monte Carlo Empirical Orthogonal Function analysis (Anchukaitis and Tierney, 2013; Tyler et al., 2015) allow the extraction of shared variance between sites while considering the age uncertainties.

Relatively new methods such as μXRF and hyperspectral core scanning allow for very high-resolution palaeoclimate inferences from sedimentary archives (e.g. Hahn et al., 2014; Sun et al., 2016). The introduction of new methods, which can determine past temperature from glycerol dialkyl glycerol tetraethers (GDGTs) (e.g. Tierney et al., 2008; Woltering et al., 2014; Atahan et al., 2015), chironomids (e.g. Larocque-Tobler et al., 2011; Eggermont and Heiri, 2012; Chang et al., 2015) and clumped isotopes (e.g. Affek et al., 2008; Zaarur et al., 2011; Saenger et al., 2012), and inferences of past precipitation from compound specific carbon or hydrogen isotopes from leaf waxes (e.g. Tierney et al., 2008; Feakins et al., 2014; Feakins et al., 2016), would greatly aid in the inference of Australia MIS 3 climate.

2.8. Conclusions

Analysis of Australian MIS 3 climate records reveals distinct hydroclimate trends. MIS 3 began relatively wet, compared to modern climates, with peak moisture availability occurring between ~49 and ~40 ka. Thereafter, continental aridity increased for the remainder of MIS 3. Southern westerly wind-influenced records indicate high moisture availability throughout MIS 3, while Australian summer monsoon-influenced records indicate a gradual drying from ~48 ka, until the end of MIS 3. Predominantly wet conditions are evident in central and northern Australia between ~50 and ~45 ka, possibly reflecting the influence of both a predominantly La Niña-like climate and a stronger Australian summer monsoon. These wet conditions may have aided migration of people across the continent. Lastly, the peak loss of megafauna at 45 ± 5 ka occurred at a time of generally high moisture availability before a transition into the comparatively dry second half of MIS 3.

2.9 References

Affek, H.P., Bar-Matthews, M., Ayalon, A., Matthews, A., Eiler, J.M., 2008. "Glacial/interglacial temperature variations in Soreq cave speleothems as recorded by 'clumped isotope' thermometry." *Geochimica et Cosmochimica Acta* 72, 5351-5360.

Allen, J., O'Connell, J.F., 2014. "Both half right: Updating the evidence for dating first human arrivals in Sahul." *Australian Archaeology* 79, 86-108.

An, S.-I., Kim, H.-J., Park, W., Schneider, B., 2017. "Impact of ENSO on East Asian winter monsoon during interglacial periods: effect of orbital forcing." *Climate Dynamics* 49, 3209-3219.

Anchukaitis, K.J., Tierney, J.E., 2013. "Identifying coherent spatiotemporal modes in time-uncertain proxy paleoclimate records." *Climate Dynamics* 41, 1291-1306.

Arnold, L.J., Demuro, M., Navazo, M., Benito-Calvo, A., Pérez-González, A., 2012. "OSL dating of the Middle Palaeolithic Hotel California site, Sierra de Atapuerca, north-central Spain." *Boreas* 42, 285-305.

Arnold, L.J., Demuro, M., Parés, J.M., Arsuaga, J.L., Aranburu, A., de Castro, B., María, J., Carbonell, E., 2014. "Luminescence dating and palaeomagnetic age constraint on hominins from Sima de los Huesos, Atapuerca, Spain." *Journal of Human Evolution* 67, 85-107.

Arnold, L.J., Demuro, M., Parés, J.M., Pérez-González, A., Arsuaga, J.L., Bermúdez de Castro, J.M., Carbonell, E., 2015. "Evaluating the suitability of extended-range luminescence dating techniques over early and Middle Pleistocene timescales: Published datasets and case studies from Atapuerca, Spain." *Quaternary International* 389, 167-190.

Arnold, L.J., Duval, M., Demuro, M., Spooner, N.A., Santonja, M., Pérez-González, A., 2016. "OSL dating of individual quartz 'supergrains' from the Ancient Middle Palaeolithic site of Cuesta de la Bajada, Spain." *Quaternary Geochronology* 36, 78-101.

Atahan, P., Heijnis, H., Dodson, J., Grice, K., Le Metayer, P., Taffs, K., Hembrow, S., Woltering, M., Zawadzki, A., 2015. "Pollen, biomarker and stable isotope evidence of late Quaternary environmental change at Lake McKenzie, southeast Queensland." *Journal of Paleoliminology* 53, 139-156.

Ayliffe, L.K., Marianelli, P.C., Moriarty, K.C., Wells, R.T., McCulloch, M.T., Mortimer, G.E., Hellstrom, J.C., 1998. "500 ka precipitation record from southeastern Australia: Evidence for interglacial relative aridity." *Geology* 26, 147-150.

Berger, A., Loutre, M.F., 1991. "Insolation values for the climate of the last 10 million years." *Quaternary Sciences Reviews* 10, 297-317.

Bird, M.I., Hutley, L.B., Lawes, M.J., Lloyd, J.O.N., Luly, J.G., Ridd, P.V., Roberts, R.G., Ulm, S., Wurster, C.M., 2013. "Humans, megafauna and environmental change in tropical Australia." *Journal of Quaternary Science* 28, 439-452.

Blaauw, M., Christen, J.A., Bennett, K.D., Reimer, P.J., 2018. "Double the dates and go for Bayes — Impacts of model choice, dating density and quality on chronologies." *Quaternary Science Reviews* 188, 58-66.

Black, M.P., Mooney, S.D., Martin, H.A., 2006. "A >43,000-year vegetation and fire history from Lake Baraba, New South Wales, Australia." *Quaternary Science Reviews* 25, 3003-3016.

Bourman, R.P., Prescott, J.R., Banerjee, D., Alley, N.F., Buckman, S., 2010. "Age and origin of alluvial sediments within and flanking the Mt Lofty Ranges, southern South Australia: A Late Quaternary archive of climate and environmental change." *Australian Journal of Earth Sciences* 57, 175-192.

Bowler, J.M., Duller, G.A.T., Perret, N., Prescott, J.R., Wyrwoll, K.-H., 1998. "Hydrologic changes in monsoonal climates of the last glacial cycle: stratigraphy and luminescence dating of Lake Woods, N.T. Australia." *Paleoclimates* 3, 179-207.

Bowler, J.M., Johnston, H., Olley, J.M., Prescott, J.R., Roberts, R.G., Shawcross, W., Spooner, N.A., 2003. "New ages for human occupation and climatic change at Lake Mungo, Australia." *Nature* 421, 837.

Bronk-Ramsey, C., 2009. "Bayesian Analysis of Radiocarbon Dates." *Radiocarbon* 51, 337-360.

Bronk-Ramsey, C., 2016. "Dealing with Outliers and Offsets in Radiocarbon Dating." *Radiocarbon* 51, 1023-1045.

Brown, J.R., Hope, P., Gergis, J., Henley, B.J., 2016. "ENSO teleconnections with Australian rainfall in coupled model simulations of the last millennium." *Climate Dynamics* 47, 79-93.

Burrows, M.A., Heijnis, H., Gadd, P., Haberle, S.G., 2016. "A new late Quaternary palaeohydrological record from the humid tropics of northeastern Australia." *Palaeogeography, Palaeoclimatology, Palaeoecology* 451, 164-182.

Carolin, S.A., Cobb, K.M., Adkins, J.F., Clark, B., Conroy, J.L., Lejau, S., Malang, J., Tuen, A.A., 2013. "Varied Response of Western Pacific Hydrology to Climate Forcings over the Last Glacial Period." *Science* 340, 1564.

Chang, J.C., Shulmeister, J., Woodward, C., 2015. "A chironomid based transfer function for reconstructing summer temperatures in southeastern Australia." *Palaeogeography, Palaeoclimatology, Palaeoecology* 423, 109-121.

Chen, X.Y., Chappell, J., Murray, A.S., 1995. "High (ground) water levels and dune development in central Australia: TL dates from gypsum and quartz dunes around Lake Lewis (Napperby), Northern Territory." *Geomorphology* 11, 311-322.

Chen, X.Y., Prescott, J.R., Hutton, J.T., 1990. "Thermoluminescence dating on gypseous dunes of Lake Amadeus, central Australia." *Australian Journal of Earth Sciences* 37, 93-102.

Chiang, J.C.H., Friedman, A.R., 2012. "Extratropical cooling, interhemispheric thermal gradients, and tropical climate change." *Annual Review of Earth and Planetary Sciences* 40, 383-412.

Clarkson, C., Jacobs, Z., Marwick, B., Fullagar, R., Wallis, L., Smith, M., Roberts, R.G., Hayes, E., Lowe, K., Carah, X., Florin, S.A., Mcneil, J., Cox, D., Arnold, L.J., Hua, Q., Huntley, J., Brand, H.E.A., Manne, T., Fairbairn, A., Shulmeister, J., Lyle, L., Salinas, M., Page, M., Connell, K., Park, G., Norman, K., Murphy, T., Pardoe, C., 2017. "Human occupation of northern Australia by 65,000 years ago." *Nature* 547, 306.

Clement, A.C., Cane, M.A., Seager, R., 2001. "An Orbitally Driven Tropical Source for Abrupt Climate Change." *Journal of Climate* 14, 2369.

Cohen, T.J., Jansen, J.D., Gliganic, L.A., Larsen, J.R., Nanson, G.C., May, J.-H., Jones, B.G., Price, D.M., 2015. "Hydrological transformation coincided with megafaunal extinction in central Australia." *Geology* 43, 195-199.

Cohen, T.J., Nanson, G.C., Jansen, J.D., Jones, B.G., Jacobs, Z., Treble, P., Price, D.M., May, J.-H., Smith, A.M., Ayliffe, L.K., Hellstrom, J.C., 2011. "Continental aridification and the vanishing of Australia's megalakes." *Geology* 39, 167-170.

Colhoun, E.A., Pola, J.S., Barton, C.E., Heijnis, H., 1999. "Late Pleistocene vegetation and climate history of Lake Selina, western Tasmania." *Quaternary International* 57–58, 5–23.

Colhoun, E.A., van de Geer, G., Mook, W.G., 1982. "Stratigraphy, pollen analysis, and palaeoclimatic interpretation of Pulbeena Swamp, northwestern Tasmania." *Quaternary Research* 18, 108-126.

Colhoun, E.A., van der Geer, G., 1986. "Holocene to middle last glaciation vegetation history at Tullabardine Dam, western Tasmania." *Proceedings of the Royal Society of London Series B, Biological Sciences* 229, 177–207.

Cook, E.J., 2009. "A record of late Quaternary environments at lunette-lakes Bolac and Turangmoroke, Western Victoria, Australia, based on pollen and a range of non-pollen palynomorphs." *Review of Palaeobotany and Palynology* 153, 185-224.

Cosgrove, R., Field, J., Garvey, J., Brenner-Coltrain, J., Goede, A., Charles, B., Wroe, S., Pike-Tay, A., Grün, R., Aubert, M., Lees, W., O'Connell, J., 2010. "Overdone overkill – the archaeological perspective on Tasmanian megafaunal extinctions." *Journal of Archaeological Science* 37, 2486–2503.

Croke, J., Jansen, J.D., Amos, K., Pietsch, T.J., 2011. "A 100 ka record of fluvial activity in the Fitzroy River Basin, tropical northeastern Australia." *Quaternary Science Reviews* 30, 1681-1695.

D'Costa, D.M., Kershaw, A.P., 1995. "A Late Pleistocene and Holocene pollen record from Lake Terang, Western Plains of Victoria, Australia." *Palaeogeography, Palaeoclimatology, Palaeoecology* 113, 57-67.

D'Costa, D.M., Grindrod, J., Ogden, R., 1993. "Preliminary environmental reconstructions from late Quaternary pollen and mollusc assemblages at Egg Lagoon, King Island, Bass Strait." *Australian Journal of Ecology* 18, 351-366.

Dangermond, J., 2015. "ArcMap". Esri, 380 New York Street, Redlands, CA 92373.

De Deckker, P., Moros, M., Perner, K., Jansen, E., 2012. "Influence of the tropics and southern westerlies on glacial interhemispheric asymmetry." *Nature Geoscience Letters* 5, 266-269.

Dodson, J.R., 1975. "Vegetation history and water fluctuations at Lake Leake, south-eastern South Australia 50,000 B.P. to 10,000 B.P." *Australian Journal of Botany* 23, 815-831.

Dodson, J.R., 1977. "Late Quaternary palaeoecology of Wyrie Swamp, southeastern South Australia." *Quaternary Research* 8, 97-114.

Dodson, J.R., 1994. "Quaternary vegetation history". Cambridge University Press, Cambridge.

Donders, T.H., Wagner, F., Visscher, H., 2006. "Late Pleistocene and Holocene subtropical vegetation dynamics recorded in perched lake deposits on Fraser Island, Queensland, Australia." *Palaeogeography, Palaeoclimatology, Palaeoecology* 241, 417-439.

Driscoll, R., Elliot, M., Russon, T., Welsh, K., Yokoyama, Y., Tudhope, A., 2014. "ENSO reconstructions over the past 60 ka using giant clams (Tridacna sp.) from Papua New Guinea." *Geophysical Research Letters* 41, 6819-6825.

Edney, P.A., Kershaw, A.P., De Deckker, P., 1990. "A late Pleistocene and Holocene vegetation and environmental record from Lake Wangoom, Western Plains of Victoria, Australia." *Palaeogeography, Palaeoclimatology, Palaeoecology* 80, 325-343.

Eggermont, H., Heiri, O., 2012. "The Chironomid-temperature relationship: expression in nature and paleoenvironmental implications." *Biological Reviews* 87, 430-456.

English, P., Spooner, N.A., Chappell, J., Questiaux, D.G., Hill, N.G., 2001. "Lake Lewis basin, central Australia: environmental evolution and OSL chronology." *Quaternary International* 83-85, 81-101.

EPICA-Members, 2006. "One-to-one coupling of glacial climate variability in Greenland and Antarctica." *Nature* 444, 195-198.

Feakins, S.J., Bentley, L.P., Salinas, N., Shenkin, A., Blonder, B., Goldsmith, G.R., Ponton, C., Arvin, L.J., Wu, M.S., Peters, T., West, A.J., Martin, R.E., Enquist, B.J., Asner, G.P., Malhi, Y., 2016. "Plant leaf wax biomarkers capture gradients in hydrogen isotopes of precipitation from the Andes and Amazon." *Geochimica et Cosmochimica Acta* 182, 155-172.

Feakins, S.J., Kirby, M.E., Cheetham, M.I., Ibarra, Y., Zimmerman, S.R.H., 2014. "Fluctuation in leaf wax D/H ratio from a southern California lake records significant variability in isotopes in precipitation during the late Holocene." *Organic Geochemistry* 66, 48-59.

Fitzsimmons, K.E., Cohen, T., Hesse, P.P., Jansen, J., Nanson, G.C., May, J.-H., Barrows, T.T., Haberlah, D., Hilgers, A., Kelly, T., Larsen, J., Lomax, J., Treble, P., 2013. "Late Quaternary palaeoenvironmental change in the Australian drylands." *Quaternary Science Reviews* 74, 78-96.

Fitzsimmons, K.E., Miller, G.H., Spooner, N.A., Magee, J.W., 2012. "Aridity in the monsoon zone as indicated by desert dune formation in the Gregory Lakes basin, northwestern Australia." *Australian Journal of Earth Sciences* 59, 469-478.

Fletcher, M.-S., Moreno, P., 2011. "Zonally symmetric changes in the strength and position of the Southern Westerlies drove atmospheric CO_2 variations over the past 14 kyr." *Geology* 39, 419-422.

Fletcher, M.-S., Thomas, I., 2010. "A quantitative Late Quaternary temperature reconstruction from western Tasmania, Australia." *Quaternary Science Reviews* 29, 2351-2361.

Freund, M., Henley, B.J., Karoly, D.J., Allen, K.J., Baker, P.J., 2017. "Multi-century cool- and warm-season rainfall reconstructions for Australia's major climatic regions." *Climate of the Past* 13, 1751-1770.

Galbraith, R.F., Roberts, R.G., 2012. "Statistical aspects of equivalent dose and error calculation and display in OSL dating: An overview and some recommendations." *Quaternary Geochronology* 11, 1-27.

Godfred-Spenning, C.R., Reason, C.J.C., 2002. "Interannual variability of lower-tropospheric moisture transport during the Australian monsoon." *International Journal of Climatology* 22, 509-532.

Grant, K., Rohling, E., Bar-Matthews, M., Ayalon, A., Medina-Elizalde, M., Ramsey, C.B., Satow, C., Roberts, A., 2012. "Rapid coupling between ice volume and polar temperature over the past 150,000 years." *Nature* 491, 744-747.

Hahn, A., Kliem, P., Oehlerich, M., Ohlendorf, C., Zolitschka, B., 2014. "Elemental composition of the Laguna Potrok Aike sediment sequence reveals paleoclimatic changes over the past 51 ka in southern Patagonia, Argentina." *Journal of Paleolimnology* 52, 349-366.

Hamm, G., Mitchell, P., Arnold, L.J., Prideaux, G.J., Questiaux, D., Spooner, N.A., Levchenko, V.A., Foley, E.C., Worthy, T.H., Stephenson, B., Coulthard, V., Coulthard, C., Wilton, S.,

Johnston, D., 2016. "Cultural innovation and megafauna interaction in the early settlement of arid Australia." *Nature* 539, 280.

Harle, K.J., 1997. "Late Quaternary vegetation and climate change in southeastern Australia: palynological evidence from marine core E55-6." *Palaeogeography, Palaeoclimatology, Palaeoecology* 131, 465–483.

Harrison, S.P., Digerfeldt, G., 1993. "European lakes as palaeohydrological and palaeoclimatic indicators." *Quaternary Science Reviews* 12, 233-248.

Heath, P., Gouthas, G., Irvine, J., Krapf, C., Dutch, R., 2018. "Microgravity surveys on the Nullarbor." *ASEG Extended Abstracts* 2018, 1-7.

Hendon, H.H., Thompson, D.W.J., Wheeler, M.C., 2007. "Australian rainfall and surface temperature variations associated with the Southern Hemisphere annular mode." *Journal of Climate* 20, 2452-2467.

Herzschuh, U., 2006. "Palaeo-moisture evolution in monsoonal Central Asia during the last 50,000 years." *Quaternary Science Reviews* 25, 163-178.

Hesse, P.P., Humphreys, G.S., Smith, B.L., Campbell, J., Peterson, E.K., 2003. "Age of loess deposits in the Central Tablelands of New South Wales." *Soil Research* 41, 1115-1131.

Hogg, A.G., Hua, Q., Blackwell, P.G., Niu, M., Buck, C.E., Heaton, T.J., Guilderson, T.P., Zimmerman, S.R.H., Palmer, J.G., Turney, C.S.M., Reimer, P.J., Reimer, R.W., 2013. "Shcal13 Southern Hemisphere calibration, 0-50,000 years cal BP." *Radiocarbon* 55, 1889-1903.

Johnson, C.N., Alroy, J., Beeton, N.J., Bird, M.I., Brook, B.W., Cooper, A., Gillespie, R., Herrando-Pérez, S., Jacobs, Z., Miller, G.H., Prideaux, G.J., Roberts, R.G., Rodríguez-Rey, M., Saltré, F., Turney, C.S.M., Bradshaw, C.J.A., 2016. "What caused extinction of the Pleistocene megafauna of Sahul?" *Proceedings of the Royal Society of London Series B -Biological Sciences* 283:20152399, 1-8.

Jouzel, J., Masson-Delmotte, V., Cattani, O., Dreyfus, G., Falourd, S., Hoffmann, G., Minster, B., Nouet, J., Barnola, J.M., Chappellaz, J., Fischer, H., Gallet, J.C., Johnsen, S., Leuenberger, M., Loulergue, L., Luethi, D., Oerter, H., Parrenin, F., Raisbeck, G., Raynaud, D., Schilt, A., Schwander, J., Selmo, E., Souchez, R., Spahni, R., Stauffer, B., Steffensen, J.P., Stenni, B., Stocker, T.F., Tison, J.L., Werner, M., Wolff, E.W., 2007. "Orbital and millennial Antarctic climate variability over the past 800,000 years." *Science* 317, 793-796.

Kemp, J., Rhodes, E., 2010. "Episodic fluvial activity of inland rivers in southeastern Australia: palaeochannel systems and terraces of the Lachlan River." *Quaternary Science Reviews* 29, 732-752.

Kershaw, A.P., Bretherton, S.C., van der Kaars, S., 2007a. "A complete pollen record of the last 230 ka from Lynch's Crater, north-eastern Australia." *Palaeogeography, Palaeoclimatology, Palaeoecology* 251, 23-45.

Kershaw, A.P., McKenzie, G.M., Porch, N., Roberts, R.G., Brown, J., Heijnis, H., Orr, M.L., Jacobsen, G., Newall, P.R., 2007b. "A high-resolution record of vegetation and climate through the last glacial cycles from Caledonia Fen, southeastern highlands of Australia." *Journal of Quaternary Science* 22, 481-500.

Kohfeld, K.E., Graham, R.M., de Boer, A.M., Sime, L.C., Wolff, E.W., Le Quéré, C., Bopp, L., 2013. "Southern Hemisphere westerly wind changes during the Last Glacial Maximum: paleo-data synthesis." *Quaternary Science Reviews* 68, 76-95.

Köhler, P., Nehrbass-Ahles, C., Schmitt, J., Stocker, T.F., Fischer, H., 2017. "Continuous record of the atmospheric greenhouse gas carbon dioxide (CO_2), raw data", In supplement to: Köhler, P et al. (2017): A 156 kyr smoothed history of the atmospheric greenhouse gases CO_2, CH_4, and N_2O and their radiative forcing. Earth System Science Data, 9(1), 363-387, https://doi.org/10.5194/essd-9-363-2017. PANGAEA.

Lambert, F., Delmonte, B., Petit, J.R., Bigler, M., Kaufmann, P.R., Hutterli, M.A., Stocker, T.F., Ruth, U., Steffensen, J.P., Maggi, V., 2008. "Dust-climate couplings over the past 800,000 years from the EPICA Dome C ice core." *Nature* 452, 616-619.

Lamy, F., Gersonde, R., Winckler, G., Esper, O., Jaeschke, A., Kuhn, G., Ullermann, J., Martinez-Garcia, A., Lambert, F., Kilian, R., 2014. "Increased dust deposition in the Pacific Southern Ocean during glacial periods." *Science* 343, 403-407.

Larocque-Tobler, I., Grosjean, M., Kamenik, C., 2011. "Calibration-in-time versus calibration-in-space (transfer function) to quantitatively infer July air temperature using biological indicators (chironomids) preserved in lake sediments." *Palaeogeography, Palaeoclimatology, Palaeoecology* 299, 281-288.

Leduc, G., Vidal, L., Tachikawa, K., Bard, E., 2009. "ITCZ rather than ENSO signature for abrupt climate changes across the tropical Pacific?" *Quaternary Research* 72, 123–131.

Lipar, M., Ferk, M., 2015. "Karst pocket valleys and their implications on Pliocene–Quaternary hydrology and climate: Examples from the Nullarbor Plain, southern Australia." *Earth-Science Reviews* 150, 1-13.

Lisiecki, L.E., Raymo, M.E., 2005. "A Pliocene-Pleistocene stack of 57 globally distributed benthic $\delta^{18}O$ records." *Paleoceanography* 20.

Longmore, M.E., Heijnis, H., 1999. "Aridity in Australia: Pleistocene records of palaeohydrological and palaeoecological change from the perched lake sediments of Fraser Island, Queensland, Australia." *Quaternary International* 57/58, 35–47.

Magee, J.W., Miller, G.H., Spooner, N.A., Questiaux, D., 2004. "Continuous 150 k.y. monsoon record from Lake Eyre, Australia; insolation-forcing implications and unexpected Holocene failure." *Geology* 32, 558-888.

Maroulis, J.C., Nanson, G.C., Price, D.M., Pietsch, T., 2007. "Aeolian–fluvial interaction and climate change: source-bordering dune development over the past ~100 ka on Cooper Creek, central Australia." *Quaternary Science Reviews* 26, 386-404.

McGowan, H.A., Petherick, L.M., Kamber, B.S., 2008. "Aeolian sedimentation and climate variability during the late Quaternary in southeast Queensland, Australia." *Palaeogeography, Palaeoclimatology, Palaeoecology* 265, 171-181.

Merkel, U., Prange, M., Schulz, M., 2010. "ENSO variability and teleconnections during glacial climates." *Quaternary Science Reviews* 29, 86-100.

Miller, G.H., Fogel, M.L., Magee, J.W., Gagan, M.K., 2016. "Disentangling the impacts of climate and human colonization on the flora and fauna of the Australian arid zone over the past 100 ka using stable isotopes in avian eggshell." *Quaternary Science Reviews* 151, 27-57.

Mooney, S.D., Harrison, S.P., Bartlein, P.J., Daniau, A.-L., Stevenson, J., Brownlie, K.C., Buckman, S., Cupper, M., Luly, J., Black, M., Colhoun, E., D'Costa, D., Dodson, J., Haberle, S., Hope, G.S., Kershaw, P., Kenyon, C., McKenzie, M., Williams, N., 2011. "Late Quaternary fire regimes of Australasia." *Quaternary Science Reviews* 30, 28-46.

Moss, P.T., Kershaw, A.P., 2007. "A late Quaternary marine palynological record (oxygen isotope stages 1 to 7) for the humid tropics of northeastern Australia based on ODP Site 820." *Palaeogeography, Palaeoclimatology, Palaeoecology* 251, 4-22.

Moss, P.T., Tibby, J., Petherick, L., McGowan, H., Barr, C., 2013. "Late Quaternary vegetation history of North Stradbroke Island, Queensland, eastern Australia." *Quaternary Science Reviews* 74, 257-272.

Muller, J., Kylander, M., Wüst, R.A.J., Weiss, D., Martinez-Cortizas, A., LeGrande, A.N., Jennerjahn, T., Behling, H., Anderson, W.T., Jacobson, G., 2008. "Possible evidence for wet Heinrich phases in tropical NE Australia: the Lynch's Crater deposit." *Quaternary Science Reviews* 27, 468-475.

Murray, A.S., Wintle, A.G., 2000. "Luminescence dating of quartz using an improved single-aliquot regenerative-dose protocol." *Radiation Measurements* 32, 57-73.

Nanson, G.C., Price, D.M., Jones, B.G., Maroulis, J.C., Coleman, M., Bowman, H., Cohen, T.J., Pietsch, T.J., Larsen, J.R., 2008. "Alluvial evidence for major climate and flow regime changes during the middle and late Quaternary in eastern central Australia." *Geomorphology* 101, 109-129.

Page, K., Nanson, G., Price, D., 1996. "Chronology of Murrumbidgee River palaeochannels on the Riverine Plain, southeastern Australia." *Journal of Quaternary Science* 11, 311-326.

Petherick, L., Bostock, H., Cohen, T.J., Fitzsimmons, K., Tibby, J., Fletcher, M.-S., Moss, P., Reeves, J., Mooney, S., Barrows, T., Kemp, J., Jansen, J., Nanson, G., Dosseto, A., 2013. "Climatic records over the past 30 ka from temperate Australia – a synthesis from the Oz-INTIMATE workgroup." *Quaternary Science Reviews* 74, 58-77.

Petherick, L., McGowan, H., Moss, P., 2008. "Climate variability during the Last Glacial Maximum in eastern Australia: evidence of two stadials?" *Journal of Quaternary Science* 23, 787-802.

Petherick, L.M., Moss, P.T., Mcgowan, H.A., 2011. "Climatic and environmental variability during the termination of the Last Glacial Stage in coastal eastern Australia: a review." *Australian Journal of Earth Sciences* 58, 563-577.

Reeves, J.M., Barrows, T.T., Cohen, T.J., Kiem, A.S., Bostock, H.C., Fitzsimmons, K.E., Jansen, J.D., Kemp, J., Krause, C., Petherick, L., Phipps, S.J., Members, O.-I., 2013. "Climate variability over the last 35,000 years recorded in marine and terrestrial archives in the Australian region: an OZ-INTIMATE compilation." *Quaternary Science Reviews* 74, 21-34.

Reimer, P.J., Bard, E., Bayliss, A., Beck, J.W., Blackwell, P.G., Bronk Ramsey, C., Buck, C.E., Cheng, H., Edwards, R.L., Friedrich, M., Grootes, P.M., Guilderson, T.P., Haflidason, H., Hajdas, I., Hatté, C., Heaton, T.J., Hoffmann, D.L., Hogg, A.G., Hughen, K.A., Kaiser, K.F., Kromer, B., Manning, S.W., Niu, M., Reimer, R.W., Richards, D.A., Scott, E.M., Southon, J.R., Staff, R.A., Turney, C.S.M., van der Plicht, J., 2013. "IntCal13 and Marine13 Radiocarbon Age Calibration Curves 0–50,000 Years cal BP." *Radiocarbon* 55, 1869-1887.

Risbey, J.S., Pook, M.J., McIntosh, P.C., Wheeler, M.C., Hendon, H.H., 2009. "On the Remote Drivers of Rainfall Variability in Australia." *Monthly Weather Review* 137, 3233-3253.

Roberts, R.G., Flannery, T.F., Ayliffe, L.K., Yoshida, H., Olley, J.M., Prideaux, G.J., Laslett, G.M., Baynes, A., Smith, M.A., Jones, R., 2001. "New ages for the last Australian megafauna: continent-wide extinction about 46,000 years ago." *Science* 292, 1888-1892.

Rodríguez-Rey, M., Herrando-Perez, S., Gillespie, R., Jacobs, Z., Saltre, F., Brook, B.W., Prideaux, G.J., Roberts, R.G., Cooper, A., Alroy, J., Miller, G.H., Bird, M.I., Johnson, C.N., Beeton, N., Turney, C.S.M., Bradshaw, C.J.A., 2015. "Criteria for assessing the quality of Middle Pleistocene to Holocene vertebrate fossil ages." *Quaternary Geochronology* 30, 69-79.

Rule, S., Brook, B.W., Haberle, S.G., Turney, C.S.M., Kershaw, A.P., Johnson, C.N., 2012. "The Aftermath of Megafaunal Extinction: Ecosystem Transformation in Pleistocene Australia." *Science* 335, 1483-1486.

Saenger, C., Affek, H.P., Felis, T., Thiagarajan, N., Lough, J.M., Holcomb, M., 2012. "Carbonate clumped isotope variability in shallow water corals: Temperature dependence and growth-related vital effects." *Geochimica et Cosmochimica Acta* 99, 224-242.

Saltré, F., Rodríguez-Rey, M., Brook, B.W., Johnson, C.N., Turney, C.S.M., Alroy, J., Cooper, A., Beeton, N., Bird, M.I., Fordham, D.A., Gillespie, R., Herrando-Pérez, S., Jacobs, Z., Miller, G.H., Nogués-Bravo, D., Prideaux, G.J., Roberts, R.G., Bradshaw, C.J.A., 2016. "Climate change not to blame for late Quaternary megafauna extinctions in Australia." *Nature Communications* 7, 1-7.

Shepard, D., 1968. "A two-dimensional interpolation function for irregularly-spaced data." *Proceedings of the 1968 ACM National Conference*, 517–524.

Singh, B.S., Geissler, E.A., 1985. "Late Cainozoic history of vegetation, fire, lake levels and climate, at Lake George, New South Wales, Australia." *Philosophical Transactions of the Royal Society of London. Series B, Biological Sciences* 311, 379-447.

Sun, Y., Liang, L., Bloemendal, J., Li, Y., Wu, F., Yao, Z., Liu, Y., 2016. "High-resolution scanning XRF investigation of Chinese loess and its implications for millennial-scale monsoon variability." *Journal of Quaternary Science* 31, 191-202.

Tibby, J., Barr, C., Marshall, J.C., Mgregor, G.B., Moss, P.T., Arnold, L.J., Page, T.J., Questiaux, D., Olley, J., Kemp, J., Spooner, N., Petherick, L., Penny, D., Mooney, S., Moss, E., 2017. "Persistence of wetlands on North Stradbroke Island (south-east Queensland, Australia) during the last glacial cycle: implications for Quaternary science and biogeography." *Journal of Quaternary Science* 32, 770-781.

Tierney, J.E., Russell, J.M., Huang, Y., Damsté, J.S.S., Hopmans, E.C., Cohen, A.S., 2008. "Northern hemisphere controls on tropical southeast African climate during the past 60,000 years." *Science* 322, 252-255.

Tobler, R., Rohrlach, A., Soubrier, J., Bover, P., Llamas, B., Tuke, J., Bean, N., Abdullah-Highfold, A., Agius, S., O'Donoghue, A., O'Loughlin, I., Sutton, P., Zilio, F., Walshe, K., Williams, A.N., Turney, C.S.M., Williams, M., Richards, S.M., Mitchell, R.J., Kowal, E., Stephen, J.R., Williams, L., Haak, W., Cooper, A., 2017. "Aboriginal mitogenomes reveal 50,000 years of regionalism in Australia." *Nature* 544, 180-184.

Tudhope, A.W., Chilcott, C.P., Mcculloch, M.T., Cook, E.R., Chappell, J., Ellam, R.M., Lea, D.W., Lough, J.M., Shimmield, G.B., 2001. "Variability in the El Niño - Southern oscillation through a glacial-interglacial cycle." *Science* 291, 1511-1517.

Turney, C.S.M., Bird, M.I., Fifield, L.K., Roberts, R.G., Smith, M., Dortch, C.E., Grün, R., Lawson, E., Ayliffe, L.K., Miller, G.H., Dortch, J., Cresswell, R.G., 2001. "Early human occupation at Devil's Lair, southwestern Australia 50,000 years ago." *Quaternary Research* 55, 3-13.

Turney, C.S.M., Kershaw, P., Clemens, S., Branch, N., Moss, P., Fifield, L.K., 2004. "Millennial and orbital variations of El Niño/Southern Oscillation and high-latitude climate in the last glacial period." *Nature* 428, 306-310.

Tyler, J.J., Mills, K., Barr, C., Sniderman, J.M.K., Gell, P.A., Karoly, D.J., 2015. "Identifying coherent patterns of environmental change between multiple, multivariate records: an

application to four 1000-year diatom records from Victoria, Australia." *Quaternary Science Reviews* 119, 94-105.

van De Geer, G., Heusser, L.E., Lynch-Stieglitz, J., Charles, C.D., 1994. "Paleoenvironments of Tasmania inferred from a 5–75 ka marine pollen record." *Palynology* 18, 33-40.

van der Kaars, S., De Deckker, P., 2002. "A Late Quaternary pollen record from deep-sea core Fr10/95, GC17 offshore Cape Range Peninsula, northwestern Western Australia." *Review of Palaeobotany and Palynology* 120, 17-39.

van der Kaars, S., Miller, G.H., Turney, C.S.M., Cook, E.J., Nürnberg, D., Schönfeld, J., Kershaw, A.P., Lehman, S.J., 2017. "Humans rather than climate the primary cause of Pleistocene megafaunal extinction in Australia." *Nature Communications* 8, 1-7.

Veth, P., Ward, I., Ditchfield, K., 2017. "Reconceptualising Last Glacial Maximum discontinuities: A case study from the maritime deserts of north-western Australia." *Journal of Anthropological Archaeology* 46, 82-91.

Wende, R., Nanson, G.C., Price, D.M., 1997. "Aeolian and fluvial evidence for late Quaternary environmental change in the east Kimberley of Western Australia." *Australian Journal of Earth Sciences* 44, 519-526.

Williams, N.J., Harle, K.J., Gale, S.J., Heijnis, H., 2006. "The vegetation history of the last glacial-interglacial cycle in eastern New South Wales, Australia." *Journal of Quaternary Science Review* 21, 735-750.

Woltering, M., Atahan, P., Grice, K., Heijnis, H., Taffs, K., Dodson, J., 2014. "Glacial and Holocene terrestrial temperature variability in subtropical east Australia: branched GDGT distributions in a sediment core from Lake McKenzie." *Quaternary Research* 82, 132–145.

Zaarur, S., Olack, G., Affek, H.P., 2011. "Paleo-environmental implication of clumped isotopes in land snail shells." *Geochimica et Cosmochimica Acta* 75, 6859-6869.

Chapter 3 – Climates of the last three interglacials in subtropical eastern Australia inferred from wetland sediment geochemistry

3.1 Statement of Authorship

Title of Paper	Climates of the last three interglacials in subtropical eastern Australia inferred from wetland sediment geochemistry
Publication Status	☑ Published ☐ Accepted for Publication ☐ Submitted for Publication ☐ Unpublished and Unsubmitted work written in manuscript style
Publication Details	Kemp, C.W., Tibby, J., Arnold, L.J., Barr, C., Gadd, P.S., Marshall, J.C., McGregor, G.B., Jacobsen, G.E., 2020. Climates of the last three interglacials in subtropical eastern Australia inferred from wetland sediment geochemistry. *Palaeogeography, Palaeoclimatology, Palaeoecology* 538.

3.1.1 Principal Author

Name of Principal Author (Candidate)	Christopher Wilde Kemp		
Contribution to the Paper	Research, testing of μXRF methods, data acquisition and analysis, creation of the XRF database, writing the manuscript and corresponding author.		
Overall percentage (%)	75		
Certification:	This paper reports on original research I conducted during the period of my Higher Degree by Research candidature and is not subject to any obligations or contractual agreements with a third party that would constrain its inclusion in this thesis. I am the primary author of this paper.		
Signature		Date	31-3-2020

3.1.2 Co-Author Contributions

By signing the Statement of Authorship, each author certifies that:

i. the candidate's stated contribution to the publication is accurate (as detailed above);
ii. permission is granted for the candidate in include the publication in the thesis; and
iii. the sum of all co-author contributions is equal to 100% less the candidate's stated contribution.

Name of Co-Author	John Tibby		
Contribution to the Paper	Manuscript structure, research direction, methods and discussion, as well as editing, correcting and formatting of the manuscript.		
Signature		Date	31/03/2020

Name of Co-Author	Lee Arnold		
Contribution to the Paper	Assistance with OSL and age-depth modelling methods and analysis, formatting of resulting figures and tables, contribution to respective sections of the manuscript, editing, correcting and formatting of the manuscript.		
Signature		Date	6/4/2020

Name of Co-Author	Cameron Barr		
Contribution to the Paper	Suggestions for synthesis methods, manuscript discussion and editing, correcting and formatting of the manuscript.		
Signature		Date	31/03/2020

Name of Co-Author	Patricia Gadd		
Contribution to the Paper	**Comments on µXRF analysis, methodology and discussion.**		
Signature		Date	6/04/20

Name of Co-Author	Jon Marshall		
Contribution to the Paper	Field work and contributions to the methods and discussion, proof reading.		
Signature		Date	06/04/2020

Name of Co-Author	Glenn McGregor		
Contribution to the Paper	Field work and contributions to the discussion, proof reading.		
Signature		Date	06/03/2020

Name of Co-Author	Geraldine Jacobsen		
Contribution to the Paper	Assistance with radiocarbon dating, analysis and discussion.		
Signature		Date	06/04/2020

3.2 Preamble

This chapter details initial work undertaken at Fern Gully Lagoon, North Stradbroke Island, presenting the first published interglacial palaeoclimate record for subtropical eastern Australia. A foundation for the next two chapters, this chapter includes considerable material on dating the record, age-depth modelling, analysis of the inorganic proportion of the wetland sediments and a discussion of other records of Australian climates during the Holocene, MIS 5 and MIS 7. Comparison of Holocene climates to those during recent interglacials is discussed in relation to Holocene climate drivers, and the long-term pattern of Australian drying observed in central and south-eastern Australia. In addition to foundational work, this chapter also reviews recent advances in scanning micro-x-ray fluorescence (μXRF) and compares the large number of normalisation methods available for μXRF data using Fern Gully Lagoon sediments.

This chapter was published as:

Kemp, C.W., Tibby, J., Arnold, L.J., Barr, C., Gadd, P.S., Marshall, J.C., McGregor, G.B., Jacobsen, G.E., 2020. "Climates of the last three interglacials in subtropical eastern Australia inferred from wetland sediment geochemistry". *Palaeogeography, Palaeoclimatology, Palaeoecology* 538. https://doi.org/10.1016/j.palaeo.2019.109463

I have re-formatted the published article as a thesis chapter, with only minor changes to the original text (see Appendix E). However, notation associated with figures, tables and equations has changed, being instead prefaced by the chapter number, e.g. Figure 1 is now Figure 3.1. The supplementary material associated with the published work is included in this thesis as Appendix B.

3.3 Abstract

Records of Australian climate during Marine Isotope Stages 5 and 7 (130–71 and 243–191 ka) are rare, preventing detailed assessments of long-term climate, drivers and ecological responses across the continent over glacial-interglacial timescales. This study presents a geochemistry-based palaeoclimate record from Fern Gully Lagoon on North Stradbroke Island (also known as Minjerribah) in subtropical eastern Australia, which records climates in MIS 7a–c, MIS 5 and much of the Holocene, in addition to MIS 4 (71–57 ka), and parts of MIS 6, MIS 3

and MIS 2 (191–130, 57–29 and 29–14 ka). Indicators of inorganic sedimentation from a 9.5 m sediment core – focussed on high-resolution estimates of sediment geochemistry supported by x-radiography, inorganic content and magnetic susceptibility – were combined with a chronology consisting of six radiocarbon (^{14}C) and thirteen single-grain optically stimulated luminescence (OSL) ages. Hiatuses occurred at ~178–153 ka, ~36–21 ka and ~7–2 ka and likely result from desiccation of the wetland and deflation. Low values of locally sourced aeolian materials indicate a wet MIS 7a–c and early MIS 6 before a relatively dry MIS 5. Inorganic flux during the Holocene was up to four times greater than during MIS 5, consistent with long-term interglacial drying observed in other regions, most notably in central Australia. This study highlights the importance of employing multiple dating approaches and calibrated geochemical proxies to derive climate reconstructions and to identify depositional complexities in organic-rich wetland records.

3.4 Introduction

Reliable reconstructions of past interglacial climates are important for providing analogues of future climate change, and allow us to better understand ecosystem responses that are likely to accompany increases in global temperature (Turney and Jones, 2010; Harrison and Bartlein, 2012). Records of interglacial climates are similarly required to understand the long-term evolution of Australian biota including past extinction events (Kershaw et al., 2003; Miller et al., 2016; van der Kaars et al., 2017). At present, the usefulness of Australian palaeoclimate records for either of these purposes is relatively limited, as most only extend to the Last Glacial Maximum (LGM) ~20 ± 2 thousand years ago (ka) (Petherick et al., 2013; Reeves et al., 2013).

Records of Australian climate during the past three interglacials are limited, but include Lynch's Crater and the nearby ODP 820 marine record (Kershaw et al., 2007a; Moss and Kershaw, 2007) in the north-east; Lake Eyre, Lake Woods and central Australian streams and lakes (Bowler et al., 1998; Nanson et al., 2008; Cohen et al., 2015; Fu et al., 2017); and the Naracoorte Caves, Lake Selina, Lake Wangoom and Caledonia Fen in the south-east (Ayliffe et al., 1998; Colhoun et al., 1999; Harle et al., 2002; Kershaw et al., 2007b). The distribution of available records is limited in geographical scope, and does not currently include equatorial or subtropical regions. Additionally, while these records infer past climate from proxies such as

pollen, charcoal and palaeoshorelines, there is not as yet an Australian interglacial record utilising μXRF geochemical analysis.

With the advent of relatively cheap, reliable, reproducable μXRF analysis, climate records derived from geochemical studies of wetland sediments have experienced a boom in the past decade (Croudace and Rothwell, 2015). Wetland geochemical records represent invaluable archives for palaeoclimatology reconstructions, providing constraints on climate change at local (e.g. Burrows et al., 2016; Eggenberger et al., 2018; Vegas-Vilarrúbia et al., 2018) and regional scales (e.g. Field et al., 2018; Pleskot et al., 2018; Profe et al., 2018), and enabling a greater understanding of internal wetland processes (e.g. Burrows et al., 2016; Kienel et al., 2017; Vegas-Vilarrúbia et al., 2018).

Here we present a multi-proxy ~210 kyr record of subtropical climatic variability from Fern Gully Lagoon focussing on past interglacials. This study is the foundation for future studies of regional climate change based on Fern Gully Lagoon sediments and assesses the validity of the site as a palaeoclimate archive. We use calibrated μXRF Itrax scanning to infer locally-derived aeolian inorganic sedimentation and assess the suitability of OSL and ^{14}C to date the complex, organic-rich sediment sequence.

3.5 Background

3.5.1 Global climate changes during recent interglacials

A recent review of global interglacial climates has demonstrated some important differences between marine isotope stage 7 (MIS 7), MIS 5 and the Holocene (Berger et al., 2015). Specifically, the MIS 7 interglacial complex was characterised by higher average global temperatures than the MIS 5 interglacial complex but had a lower temperature peak in MIS 7e than that in MIS 5e (Lisiecki and Raymo, 2005; Parrenin et al., 2013; Berger et al., 2015). The lower MIS 7e temperature is likely due to the greater difference between MIS 5e summer and winter insolation, while insolation during MIS 7e was more evenly distributed over the seasons due to lower obliquity of the Earth's orbit (Berger et al., 2015). In contrast to the warmer MIS 5e, the warmer climates of the MIS 7a–c sub-complex relative to the MIS 5a–c sub-complex are reflected in extended periods of reduced ice volume (Lisiecki and Raymo, 2005; Elderfield et al., 2012), higher sea levels (Grant et al., 2012) and higher atmospheric CO_2 concentrations (Köhler

et al., 2017). MIS 7a–c represents a rare ~20 kyr period of relatively stable, warm, mean global climate (Berger et al., 2015).

Sea surface temperature (SST) records from the West Pacific Warm Pool (WPWP) can be used to guide understanding of globally-linked, regional changes in eastern Australian climate that occurred during the previous three interglacials (Zhang et al., 2017). In particular, sea surface temperatures in the WPWP (Fig. 3.1a) can influence climate variability for the central eastern Australian coast and Tasman Sea (Martinez et al., 2002; Bostock et al., 2006; Pelejero et al., 2006). MIS 5e had the warmest WPWP SSTs of the last ~250 kyr (Tachikawa et al., 2014), but the MIS 7 interglacial complex and the Holocene were/are warmer than the MIS 5 interglacial complex by an average of ~1 – 2ºC (Lo et al., 2017).

3.5.2 Australian climates during past interglacials

The available Australian MIS 7 data permits insights into broad-scale climatic trends. During late MIS 7, Lakes Eyre and Woods in central Australia, which are predominantly fed by monsoonal rains, were full, in contrast to their present mostly dry state (Bowler et al., 1998; Fu et al., 2017). Meanwhile, wet climates and open water were present in Lynch's Crater in ENSO-dominated north-eastern Australia (Kershaw et al., 2007a; Moss and Kershaw, 2007). Similarly, the speleothem record from the Naracoorte Caves in south-eastern Australia, which primarily reflects southern westerly wind-dominated rainfall, indicates wet climates, with pronounced periods of calcitic growth between ~220 and 155 ka (Ayliffe et al., 1998). These few available records indicate that Australia was wetter during late MIS 7 than the Holocene, with a more active Australian summer monsoon in the north and stronger or more northerly southern westerly winds.

Central Australia was also wet during MIS 5 (Bowler et al., 1998; Cohen et al., 2015), though the average precipitation:evaporation ratio was lower than during late MIS 7. North-eastern Australian records indicate wet climates during MIS 5, but greater climate variability than during MIS 7 (Kershaw et al., 2007a; Moss and Kershaw, 2007). The pattern in the south-east of the continent is in general agreement with north-eastern records, with generally wet climates observed during MIS 5 (Edney et al., 1990; Ayliffe et al., 1998; Colhoun et al., 1999; Harle et al., 2002).

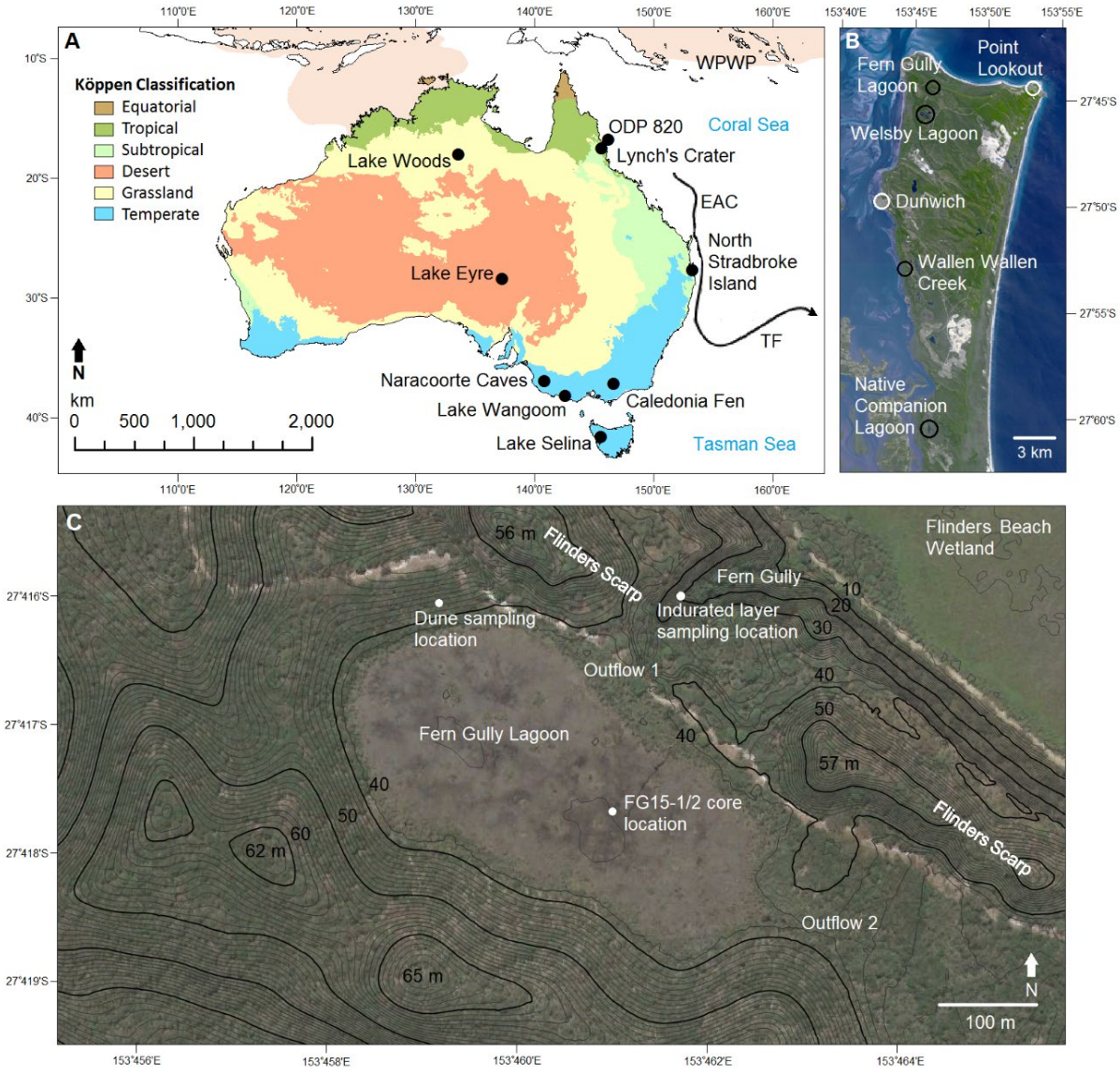

Figure 3.1: A: Modified Köppen climate zones (BOM, 2005), location of Australian interglacial climate records and the approximate current positions of the west Pacific warm pool (WPWP, mean annual SST >28˚C) boundary (pink shading; (Gagan et al., 2000)), the East Australian Current (EAC) and the Tasman Front (TF) (Bostock et al., 2006). **B:** North Stradbroke Island, with the four climate/archaeological record sites (black circles) and local towns (white circles), mentioned in the text. **C:** Fern Gully Lagoon combined topographic map and satellite image, indicating the coring location, locations of modern geochemistry samples, outflows and the height of surrounding dunes (m ASL).

Holocene hydroclimate in Australia was drier than MIS 5 and MIS 7 in most regions. Lake Eyre and Lake Frome, which were full during MIS 5, became dry and ephemeral (Cohen et al., 2015), while speleothem growth largely ceased in the Naracoorte Caves (Ayliffe et al., 1998) suggesting weakening or more southerly southern westerly winds. However, there is uncertainty about whether the Holocene was drier than MIS 5 in south-east Australia and the Wet Tropics of north-eastern Australia within each record (Edney et al., 1990; Colhoun et al., 1999; Kershaw et al., 2007a; Kershaw et al., 2007b). Uncertainty within records combined with geographical separation makes it difficult to determine climate change at a continental scale. As such, additional records from new locations are required.

3.5.3 Study site

North Stradbroke Island is a sand island located along the eastern coast of Australia (Fig. 3.1). The Island is part of the world's oldest and largest coastal dune system (Patton et al., 2019) and lies on an aeolian dust pathway from central and south-central Australia (McGowan et al., 2008; Petherick et al., 2009). The Island is a strategic location for understanding palaeoclimate, as it is situated in the subtropics (Fig. 3.1), with a contemporary climate that is strongly influenced by the El Niño – Southern Oscillation (ENSO) (Barr et al., 2019) and preserves the highest density of wetlands with sediment dating to the LGM in Australia (Tibby et al., 2017). As such, it has been the focus of several detailed palaeoenvironmental reconstructions (e.g. Moss et al., 2013; Barr et al., 2017; Petherick et al., 2017; Cadd et al., 2018), the longest of which extends to ~130 ka (Cadd et al., 2018). There is evidence for human occupation of the island from at least 21 ka at Wallen Wallen Creek (Fig. 3.1), with a Holocene increase in human occupation peaking at ~1 ka (Neal and Stock, 1986).

Fern Gully Lagoon (27.417°S, 153.460°E, 39 m ASL) is an approximately 0.8 km^2 perched, palustrine wetland (Leach, 2011) that lies within a shallow bowl of vegetated dunes at the north-western end of North Stradbroke Island. The wetland has two above-ground outflows, the largest being to the eponymous Fern Gully (Fig. 3.1c). The limited catchment area and highly permeable sandy soils mean the delivery of fluvially transported material to the wetland is limited. Single-grain OSL dating of a reconnaissance core from Fern Gully Lagoon determined a preliminary basal age of ~208.4 ± 32.5 ka (Tibby et al., 2017) at a depth of 9.25 meters.

3.6 Methods

3.6.1 Core collection and correlation

In 2015, two ~9 m-long cores were extracted from the approximate centre of Fern Gully Lagoon (27.4174°S, 153.4600°E) using a modified Bolivia corer, itself a modification of the Livingstone-square-rod piston-sampling method (Wright, 1967). The two cores were offset by one metre laterally and 50 cm vertically, in an attempt to provide a continuous sequence. Cores were extracted in black-painted PVC pipe and stored in black plastic sleeves to eliminate light contamination and ensure the sediments would be suitable for luminescence dating. The first core (FG15-1) was chosen as the master core and was sampled for single-grain OSL and ^{14}C dating. The second core (FG15-2) was used to fill gaps in the FG15-1 record and to provide additional sediment for ^{14}C and conventional wave dispersive x-ray fluorescence analyses.

Cores were aligned using CPLSlot sequence slotting software (Clark and Hounslow, 2009) using the eight elements with highest Itrax counts per second: silicon, titanium, zircon, potassium, calcium, iron and bromine. The correlation allowed the cores to be placed on a common depth scale.

Moisture and organic content were determined on 930 samples of one cubic centimetre each following Heiri et al. (2001). This record was used to target optimum OSL sample locations (i.e., locate areas with highest inorganic content, and presumably quartz content) and to calculate average water content and sediment densities for luminescence dose rate calculation (See supplementary materials).

3.6.2 Itrax µXRF, magnetic susceptibility and X-radiography

To determine changes in sediment geochemistry, Itrax second-generation micro X-ray fluorescence (µXRF; Croudace et al., 2006) scanning of both cores was undertaken at the Australian Nuclear Science and Technology Organisation. Itrax scanning utilised a molybdenum x-ray tube at 30 kV and 55 mA, with a 20 second exposure time, generating a record of elemental response (counts per second) for thirty-five elements at 2 mm intervals. An X-radiograph record using the same tube at 45 kV at 30 mA and a magnetic susceptibility record were also developed.

Micro XRF data must be normalised to mitigate the closed-sum effect (Weltje and Tjallingii, 2008; Löwemark et al., 2011). However, despite an increasing number of µXRF studies (Croudace and Rothwell, 2015), there is no standardised method for normalisation. To identify all recently published methods, we undertook a review and synthesis of µXRF in the Scopus (https://www.scopus.com/home.uri) and Web of Science (http://www.webofknowledge.com) databases. The results of this review were used to identify which normalisation methods have been utilised in recent µXRF studies, along with what (if any) validation and calibration methods were used (e.g. conventional XRF, inductively coupled plasma mass spectrometry (ICP-MS)). Further details of the database review methods and results, along with a discussion of recent µXRF methodologies are provided in the supplementary material.

The eight most common normalisation methods identified in our review were assessed to determine the best method for normalising the Fern Gully Lagoon µXRF record. These were: total counts per second normalisation (Bouchard et al., 2011; Martin et al., 2014), centred log-ratio normalisation (Weltje and Tjallingii, 2008; Weltje et al., 2015), aluminium normalisation (Brumsack, 2006; Löwemark et al., 2011), titanium normalisation (Vegas-Vilarrúbia et al., 2018), silicon normalisation, zircon normalisation, normalisation using incoherent scattering (Compton scattering) and the ratio of incoherent to coherent scattering (Rayleigh and Compton scattering) (e.g. Guyard et al., 2007; Kylander et al., 2011; Marshall et al., 2011; Berntsson et al., 2014).

The normalised µXRF data were compared to quantitative conventional XRF analyses at twenty locations from core FG15-2, following a similar method to recent studies (e.g. Hahn et al., 2014; Falster et al., 2018; Profe et al., 2018). The conventional XRF sample locations were chosen to represent the broadest range of µXRF-derived concentrations, but where there was little within-sample variability in µXRF readings. The latter consideration was important since due to the high sediment organic content, it was necessary to sample up to 1 cm of the core to ensure sufficient material for XRF. Conventional XRF analysis was undertaken at the Commonwealth Scientific and Industrial Research Organisation in Adelaide, South Australia, using lithium-borate fusion of sample material. The glass discs created from the fusion procedure

were subsequently analysed on a PANalytical Axios Advanced wavelength dispersive XRF (WD-XRF) system using an in-house silicates calibration program.

For normalisation methods without internal XRF calibration (all but centred log-ratio), µXRF counts per second were compared to absolute concentrations using simple linear regressions. The normalisation method with the highest coefficient of variation was used to identify the most suitable normalisation method for Fern Gully Lagoon sediments. For centred log-ratio we used a Matlab script after Grant et al. (2017) to produce a multivariate centred log-ratio corrected dataset. This XRF calibration was then used to calculate the approximate mass of oxides for the composite record.

The commonly utilised µXRF incoherent/coherent scattering ratio was also evaluated as a qualitative indicator of sediment organic content (e.g. Guyard et al., 2007; Jouve et al., 2013; Field et al., 2018; Woodward et al., 2018). µXRF water content corrections were also calculated after Boyle et al. (2015), as the sediments have a high water content that is likely to affect µXRF readings.

3.6.3 Identification of the aeolian component in the Fern Gully Lagoon µXRF record

McGowan et al. (2008) demonstrated that the inorganic component of wetland sediments on North Stradbroke Island (NSI) is derived from two main sources; the local silicon-rich and trace element-depleted sands, and far-travelled dust, which is more clay-rich. Petherick et al. (2009) expanded on that study, analysing source material from 149 sites in central and eastern Australia to geochemically fingerprint far-travelled dust deposited in Native Companion Lagoon (Fig. 3.1b). High quantities of scandium, gallium, thallium and nickel characterise the clay-rich, far-travelled sediment, contrasting with the Island's rare earth element-depleted silicon-rich quartz sands (McGowan et al., 2008; Petherick et al., 2009). While scandium, gallium and nickel were identified in the µXRF scan, their concentration was too low to be accurate, and they were not considered further.

Element	Material quantified by XRF	Total cts/s normalised	Centered log ratio	Raw cts/s	Al normalised	Total scatter normalised	Incoherent scatter normalised
Zircon (Zr)	pure element (ppm)	**$r^2 = 0.93$, $p < 0.05$**	**$r^2 = 0.65$, $p < 0.05$**	**$r^2 = 0.92$, $p < 0.05$**	**$r^2 = 0.83$, $p < 0.05$**	**$r^2 = 0.92$, $p < 0.05$**	**$r^2 = 0.92$, $p < 0.05$**
Titanium (Ti)	TiO_2	**$r^2 = 0.88$, $p < 0.05$**	**$r^2 = 0.66$, $p < 0.05$**	**$r^2 = 0.90$, $p < 0.05$**	**$r^2 = 0.80$, $p < 0.05$**	**$r^2 = 0.90$, $p < 0.05$**	**$r^2 = 0.89$, $p < 0.05$**
Potassium (K)	K_2O	**$r^2 = 0.83$, $p < 0.05$**	**$r^2 = 0.79$, $p < 0.05$**	**$r^2 = 0.85$, $p < 0.05$**	**$r^2 = 0.73$, $p < 0.05$**	**$r^2 = 0.85$, $p < 0.05$**	**$r^2 = 0.84$, $p < 0.05$**
Silicon (Si)	SiO_2	**$r^2 = 0.80$, $p < 0.05$**	**$r^2 = 0.57$, $p < 0.05$**	**$r^2 = 0.78$, $p < 0.05$**	**$r^2 = 0.65$, $p < 0.05$**	**$r^2 = 0.77$, $p < 0.05$**	**$r^2 = 0.76$, $p < 0.05$**
Bromine (Br)	pure element (ppm)	**$r^2 = 0.71$, $p < 0.05$**	**$r^2 = 0.84$, $p < 0.05$**	**$r^2 = 0.44$, $p < 0.05$**	**$r^2 = 0.61$, $p < 0.05$**	**$r^2 = 0.44$, $p < 0.05$**	**$r^2 = 0.42$, $p < 0.05$**
Calcium (Ca)	CaO	**$r^2 = 0.74$, $p < 0.05$**	**$r^2 = 0.78$, $p < 0.05$**	**$r^2 = 0.42$, $p < 0.05$**	**$r^2 = 0.54$, $p < 0.05$**	**$r^2 = 0.42$, $p < 0.05$**	**$r^2 = 0.43$, $p < 0.05$**
Sulfur (S)	SO_3	**$r^2 = 0.73$, $p < 0.05$**	**$r^2 = 0.70$, $p < 0.05$**	**$r^2 = 0.30$, $p < 0.05$**	**$r^2 = 0.33$, $p < 0.05$**	**$r^2 = 0.28$, $p < 0.05$**	**$r^2 = 0.26$, $p < 0.05$**
Iron (Fe)	Fe_2O_3	**$r^2 = 0.53$, $p < 0.05$**	**$r^2 = 0.55$, $p < 0.05$**	**$r^2 = 0.50$, $p < 0.05$**	**$r^2 = 0.44$, $p < 0.05$**	**$r^2 = 0.50$, $p < 0.05$**	**$r^2 = 0.49$, $p < 0.05$**
Gallium (Ga)	pure element (ppm)	$r^2 = 0.11$, $p = 0.16$	$r^2 = 0.19$, $p = 0.05$	$r^2 = 0.03$, $p = 0.48$	**$r^2 = 0.20$, $p < 0.05$**	$r^2 = 0.01$, $p = 0.69$	$r^2 = 0.01$, $p = 0.72$
Aluminum (Al)	Al_2O_3	$r^2 = 0.09$, $p = 0.19$	$r^2 = 0.09$, $p = 0.19$	**$r^2 = 0.62$, $p < 0.05$**	N/A	**$r^2 = 0.67$, $p < 0.05$**	**$r^2 = 0.69$, $p < 0.05$**
Magnesium (Mg)	MgO	$r^2 = 0.05$, $p = 0.33$	**$r^2 = 0.85$, $p < 0.05$**	$r^2 < 0.01$, $p = 0.79$	$r^2 = 0.08$, $p = 0.22$	$r^2 = 0.02$, $p = 0.60$	$r^2 = 0.02$, $p = 0.55$
Phosphorus (P)	P_2O_5	$r^2 = 0.02$, $p = 0.56$	**$r^2 = 0.46$, $p < 0.05$**	$r^2 = 0.11$, $p = 0.14$	$r^2 < 0.01$, $p = 0.76$	$r^2 = 0.12$, $p = 0.13$	$r^2 = 0.13$, $p = 0.12$

Table 3.1: Regressions of known quantities of oxides and elements via WD-XRF versus corrected µXRF data with methods ranked first in order of coefficient of determination then by number of p values < 0.05 (in bold). n = 20 for all r^2 values. Titanium, silicon and zircon normalisation had $r^2 < 0.5$, $p > 0.05$ in all cases and are not shown. cts/s: µXRF counts per second.

We derived a high-resolution record of calibrated μXRF silicon as a primary record of aeolian flux. Higher silicon input into wetlands is indicative of drier climate on NSI, which reduces protective vegetation cover (McGowan et al., 2008; Petherick et al., 2009). This effect is amplified by the sandy soils of NSI, which are generally loose and very dry due to their high permeability (Leach, 2011), which also restricts overland flow.

To identify the main directions of variation in the Fern Gully inorganic data, a principal component analysis (PCA) was performed using the vegan package (Oksanen et al., 2018) in RStudio (Team-RStudio, 2015; Ihaka and Gentleman, 2016). A subset of seven normalised elements comprising those with the highest counts per second (silicon, iron, calcium, bromine, zircon, potassium and titanium), along with LOI estimated organic content were used. A broken stick model was used to estimate the number of significant components in the μXRF record (Fig. B2) (Baczkowski, 2000). The PCA vectors were scaled by the species scores before being divided by the standard deviation of each element and multiplied by an equalising constant. In this way, element vectors were centred and standardised so that the relative variance of each element could be compared.

To characterise possible local sediment end members, samples were taken from the following locations:

- The surface of modern dunes ~30 m from the edge of Fern Gully Lagoon and ~30 m from the edge of nearby Welsby Lagoon.
- Sand three meters below the surface of dunes surrounding Fern Gully Lagoon.
- The surface of outflow one at Fern Gully Lagoon (Fig. 3.1c).
- Local rock outcrops (Point Lookout rhyolite and Dunwich sandstone).
- An indurated layer representing the B horizon of material below each of the two lagoons.

These end member samples were scanned using Itrax μXRF and placed on the PCA using the vegan predict model (Oksanen et al., 2018).

3.6.4 Dating

A preliminary age obtained from Fern Gully Lagoon exceeded the radiocarbon dating limit of ~50 ka (Tibby et al., 2017). As such, we employed two dating methods to examine different depths of the core in this study: ^{14}C dating for sediments to a depth of 288 cm, and single-grain OSL dating from 171 cm to the base of the core. Four paired OSL and ^{14}C samples were collected between 171 and 288 cm, to assess age agreement.

^{14}C dating was performed on 18 macrofossil samples, including seeds, leaf material, and bark and charcoal > 3 mm diameter. Six paired ^{14}C samples were collected from different materials to identify any offset due to material properties, including absorption of humic acids and alteration by ground water residence time (Hofmann et al., 2019). Sample preparation was undertaken at the Australian Nuclear Science and Technology Organisation, where each of the samples was dissected under a stereoscope. Any identified root fragments or other foreign objects were removed. Each sample then underwent an Acid-Base-Acid (ABA) pre-treatment to remove humic acids, following Brock et al. (2010) and were freeze-dried before graphitisation and AMS measurement. After correction for isotopic fractionation using measured $\delta^{13}C$ values, the conventional ^{14}C ages were calibrated using the Southern Hemisphere Calibration Curve (SHCal13; Hogg et al., 2013).

Single-grain OSL dating was performed on 19 quartz samples collected from core sections with the highest inorganic content. The sediment samples were extracted under filtered and subdued red LED lighting, where ~12 g of bulk sediment (dry weight) was retained from the exposed core face and margins for beta and gamma dose rate determination and beta dose rate water correction (after oven drying at 100ºC). Additional bulk sediment was collected from the overlying and underlying 10 cm depth of each OSL sample position for gamma dose rate determination and gamma dose rate water content correction. Single-grain equivalent dose (D_e) measurements and environmental dose rate assessments were made using the experimental procedures described by Demuro et al. (2013; 2015). Further details of the OSL methodologies employed in this study, including SAR suitability assessments (dose recoveries) and quality assurance criteria, are included in the supplementary materials.

The age-depth model for Fern Gully Lagoon was constructed from the ^{14}C and OSL likelihoods using a Bayesian Poisson process depositional model in OxCal v4.2.4 (P_Sequence model: Bronk-Ramsey (2009); Bronk-Ramsey and Lee (2013)), which allows for randomly variable deposition rates through the age-depth profile. The P_Sequence k_0 base rigidity parameter, which controls the ability of the model to respond to variations in the prior and likelihood data, was set to a single event per 1 cm of sedimentation but was allowed to vary between 0.01 to 100 events per centimetre to accommodate any major fluctuations in deposition rate. This additional flexibility is at the expense of precision in the final age model and results in a liberal estimate of uncertainties inherent in the data.

As part of the assessment of modelling priors, we used a common method for identifying change in linear records: pruned exact linear time (PELT) multi-changepoint analysis (Killick and Eckley, 2014). PELT was performed on the sediment inorganic content record and the μXRF Si, Ti, K and Zr data to identify any statistically significant changes in deposition mode, including potential sedimentation hiatuses (see supplementary material for further details and results). These independently assigned changepoint locations were used to identify separate depositional units in the OxCal modelling framework (Fig. 3.3, B2), each of which was represented by a separate P_Sequence with delineating start and end boundaries, nested within a master Sequence according to stratigraphic priors. Posterior dated events were automatically calculated at 1 cm intervals throughout the sequence. Further details of the Bayesian age-depth modelling method are included in the supplementary materials.

3.7 Results

3.7.1 Core correlation

Sequence slotting revealed that the top of the two cores were vertically offset by ~97 cm, rather than the 50 cm planned (Fig. 3.2). The unplanned offset meant that a total of 15 cm of sediment located at the end of several core drives was not recovered, with the largest contiguous gap being 4 cm. These lost sections did not coincide with the boundaries defined using change-point analysis.

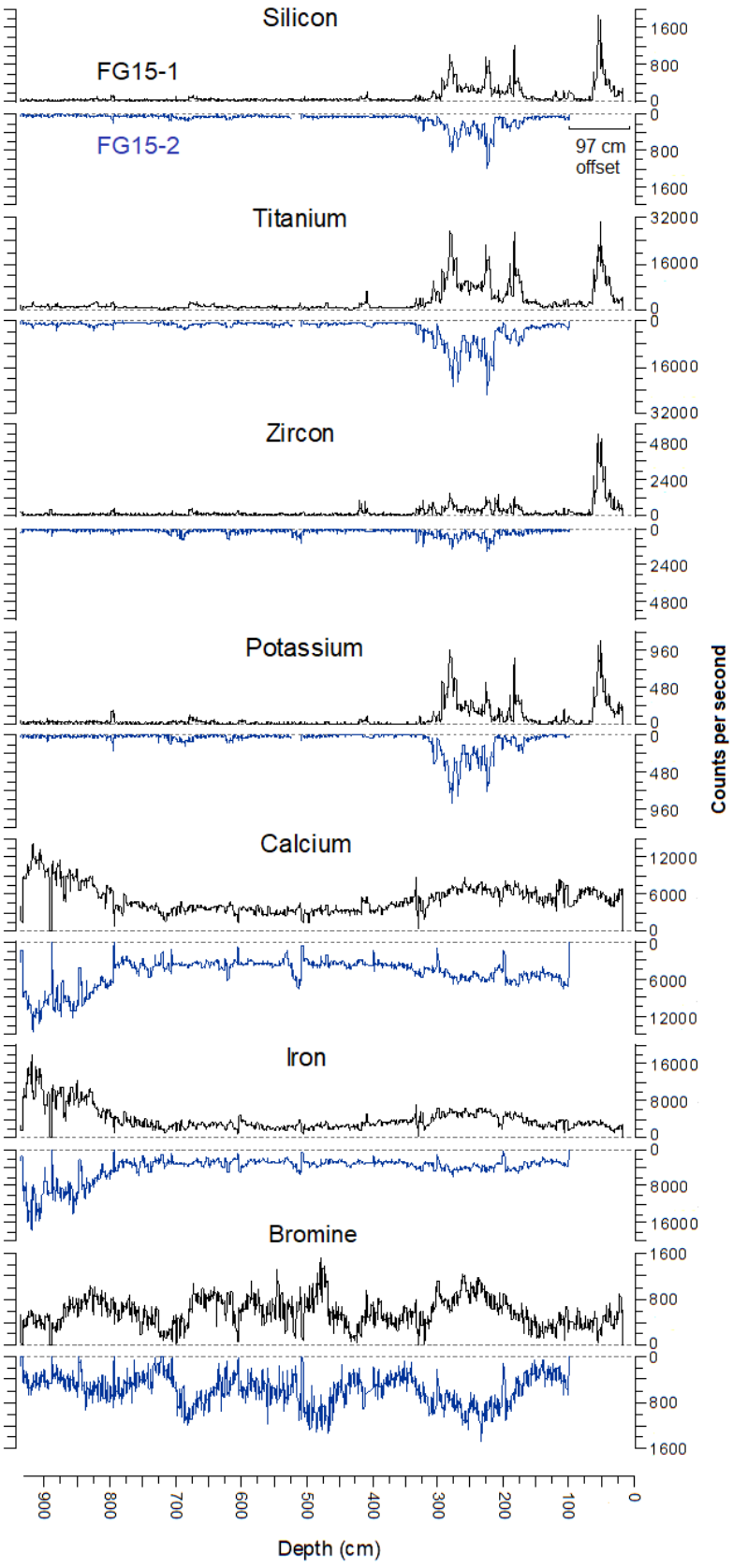

Figure 3.2: Relative position of FG15-2 (blue line, reversed vertical axis) to FG15-1 (black line) using the seven elements exhibiting the highest counts per second.

3.7.2 µXRF normalisation and calibration

Eight of the twelve elements from the µXRF Fern Gully Lagoon sequence had significant correlations (at $p < 0.05$) with the WD-XRF samples when normalised by total counts per second, with the four best correlated elements returning a coefficient of determination of $r^2 > 0.8$, $p < 0.05$ (Table 3.1, Fig. B1). Normalisation via titanium, silicon or zircon was largely unsuccessful ($r^2 < 0.5$). Of the remaining 21 recorded elements not included in WD-XRF regressions, 14 could not be considered representative of elemental concentration either due to low mean counts per second (Striberger et al., 2010; van der Bilt et al., 2015) or having >5% of data with zero values (Sáez et al., 2009).

A lack of correlation between the incoherent/coherent scattering ratio and measured water content ($r^2 = 0.05$, $p < 0.05$, $n = 804$) indicated that it was not possible to correct the µXRF record for water content (see Boyle et al., 2015). However, calibration of the µXRF record by conventional XRF accounts for any offset due to water content. Inorganic content estimated by the incoherent/coherent scattering ratio, as used in many recent studies (e.g. Guyard et al., 2007; Jouve et al., 2013; Burrows et al., 2016; Mackenzie et al., 2017), had a very weak relationship ($r^2 = 0.09$, $p < 0.05$) to inorganic content estimated by LOI, possibly due to the very high organic content of the core sequence.

3.7.3 Fern Gully Lagoon sediment composition

Fern Gully Lagoon sediments are black, finely grained and highly organic, with some macrofossils such as roots and wood fragments. They have an average of only ~8% inorganic material by dry mass (Fig. 3.3). Water content is also high, at 36–93% of wet sample weight. Sediment density and water content remained relatively constant down core with no overall monotonic trend (Fig. 3.3), demonstrating that there is little compaction of the sediments with increasing overburden pressure.

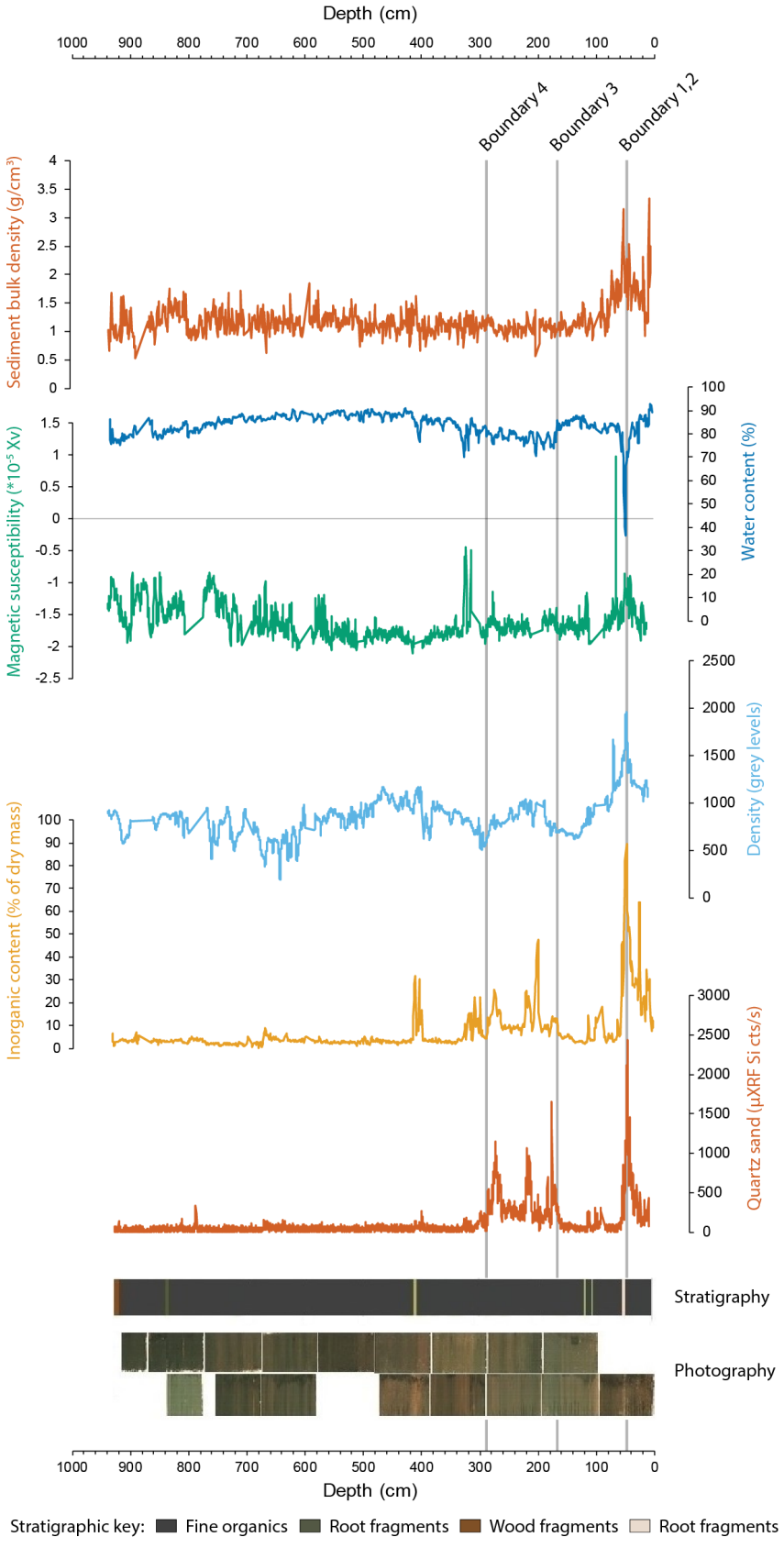

Figure 3.3: Fern Gully Lagoon sediment stratigraphy, visible wavelength photography (brightened to show colour variation), sediment bulk density, water content, magnetic susceptibility, X-radiograph derived relative density, inorganic content and µXRF derived SiO_2 content. The four depositional boundaries used in the age model were derived from silicon µXRF counts per second (cts, section 3.6.4 and supplementary material)

Both inorganic content and μXRF-derived silicon content exhibit several peaks and a plateau of ~10% inorganic content from ~170–270 cm (Fig. 3.2). Lower zircon levels in this part of the record likely indicate smaller average grain size (Cuven et al., 2010). There was a strong correlation ($r^2 = 0.70$, $p < 0.05$) between the LOI inorganic content and μXRF-derived silicon, indicating quartz sand is the major inorganic component of the sediment. While the magnetic susceptibility and X-radiograph records indicate variability in the lower part of the record, aligning with photographed banding (Fig. 3.3), the inorganic content and the μXRF silicon records indicate very little change, with largely consistent low quantities of inorganic material present.

3.7.4 ^{14}C dating

The AMS ^{14}C ages have a large degree of scatter (Table 3.2, Fig. 3.4). In general, the ^{14}C ages obtained from identifiable terrestrial macrofossils (gum nuts, seeds, leaves and bark fragments) are stratigraphically consistent over the uppermost 2 m of the core (n = 7) (Table 3.2). Three samples collected from below one metre yield very young outliers: sample RC-3 from 115 cm has a modern ^{14}C age, and samples RC-7 and RC-14 from 159 cm and 215 cm, respectively, produced ages of <2 cal. ka. These three samples were originally identified as reed stalk segments but were subsequently inferred to be root fragments. This re-interpretation was based on roots being identified during further sampling in the same core sections. Additional evidence for localised root penetration is apparent from some of the single-grain OSL D_e distributions (section 3.7.5). Encouragingly, there is a broad agreement between the paired radiocarbon ages obtained at the same depths using terrestrial seeds and terrestrial leaf fragments (Table 3.2). However, there is an age offset of ~6 kyr for the replicate bark and reed stalk samples collected from a depth of 79 cm. This offset could again be attributed to misidentification of root material at this depth.

Table 3.2: AMS Radiocarbon ages.

Sample ID	Lab ID (ANSTO)	Sample Type	Depth (cm)	$\delta^{13}C$ (‰)	pMC (%)	Conventional ^{14}C Age (^{14}C yr BP)	Calibrated ^{14}C 95.4% probability range (cal. yr BP)
Fern Gully Core 1 (FG15-1)							
FG15 RC-1	OZU189	Terrestrial gum nut	34.5–35.5	-26.0 ± 0.2	87.83 ± 0.31	1,040 ± 30	803 –960
FG15 RC-2	OZU190	Terrestrial leaf fragment	34.5–35.5	-26.2 ± 0.1	90.62 ± 0.28	790 ± 30	655–730
FG15 RC-11	OZU792	Terrestrial bark fragment	78.5–79.5	-24.6 ± 0.1	24.52 ± 0.13	11,290 ± 40	13036–13211
FG15 RC-12*	OZU793	Reed stalk segment	78.5–79.5	-24.9 [a]	46.07 ± 0.18	6,225 ± 35	6952–7238
FG15 RC-3*	OZU191	Reed stalk segment	114.5–115.5	-25.7 ± 0.1	128.18 ± 0.61	Modern	Modern
FG15 RC-4	OZU192	Terrestrial seed	134.5–135.5	-24.1 ± 0.1	15.46 ± 0.11	15,000 ± 60	17966–18366
FG15 RC-5	OZU193	Terrestrial leaf fragment	134.5–135.5	-22.6 ± 0.1	16.49 ± 0.11	14,480 ± 60	17392–17849
FG15 RC-13	OZU794	Terrestrial bark fragment	158.5–159.5	-25.0 ± 0.2	13.16 ± 0.10	16,290 ± 60	19422–19870
FG15 RC-14*	OZU795	Reed stalk segment	158.5–159.5	-25.0 [b]	78.69 ± 0.27	1,925 ± 30	1736–1896
FG15 RC-6*	OZU194	Charcoal	174.5–175.5	-28.5 ± 0.1	2.94 ± 0.04	28,330 ± 120	31637–32682
FG15 RC-7*	OZU195	Reed stalk segment	214.5–215.5	-22.1 ± 0.3	97.97 ± 0.55	165 ± 50	Modern–281
FG15 RC-8*	OZU196	Charcoal	224.5–225.5	-26.7 ± 0.1	0.70 ± 0.03	39,880 ± 330	42916–44192
FG15 RC-15**	OZU796	Terrestrial bark fragment	227.5–228.5	-24.6 ± 0.1	0.71 ± 0.07	39,730 ± 810	42343–44960
FG15 RC-16*	OZU797	Charcoal	227.5–228.5	-26.5 ± 0.3	0.35 ± 0.06	45,400 ± 1,500	46377– [c]
FG15 RC-9*	OZU197	Charcoal	234.5–235.5	-27.2 ± 0.1	0.25 ± 0.02	48,200 ± 750	46815–49875
FG15 RC-10*	OZU198	Reed stalk segment	274.5–275.5	-23.4 [a]	2.27 ± 0.07	30,420 ± 240	33945–34803
FG15 RC-17*	OZU798	Charcoal	287.5–288.5	-26.4 ± 0.1	0.41 ± 0.04	44,110 ± 850	45785–49430
FG15 RC-18*	OZU799	Reed stalk segment	287.5–288.5	-26.3 [a]	0.96 ± 0.04	37,300 ± 360	41178–42297

* denotes an age excluded from the age-depth model due to material type, while ** denotes an age eliminated from the final Bayesian model as it was identified as a major statistical outlier during initial modelling and prevented successful convergence. [a] $\delta^{13}C$ values without associated uncertainty due to a limited number of determinations. [b] $\delta^{13}C$ is assumed - measured value was not available. [c] Maximum value beyond calibration range. ^{14}C ages have been calibrated using the SHCal13 curve (Hogg et al. 2013) in OxCal v4.2.4. The calibrated age range shown is the 95.4% probability range (combining two or more potential calibration ranges, where they exist). All $\delta^{13}C$ values relate solely to the graphite derived from the fraction that was used for the radiocarbon measurement and have been derived using EA-IRMS, and are reported relative to the Pee Dee Belemnite reference standard. Uncalibrated ^{14}C ages have been corrected for isotopic fractionation using their measured $\delta^{13}C$ values and are quoted with their 1σ errors.

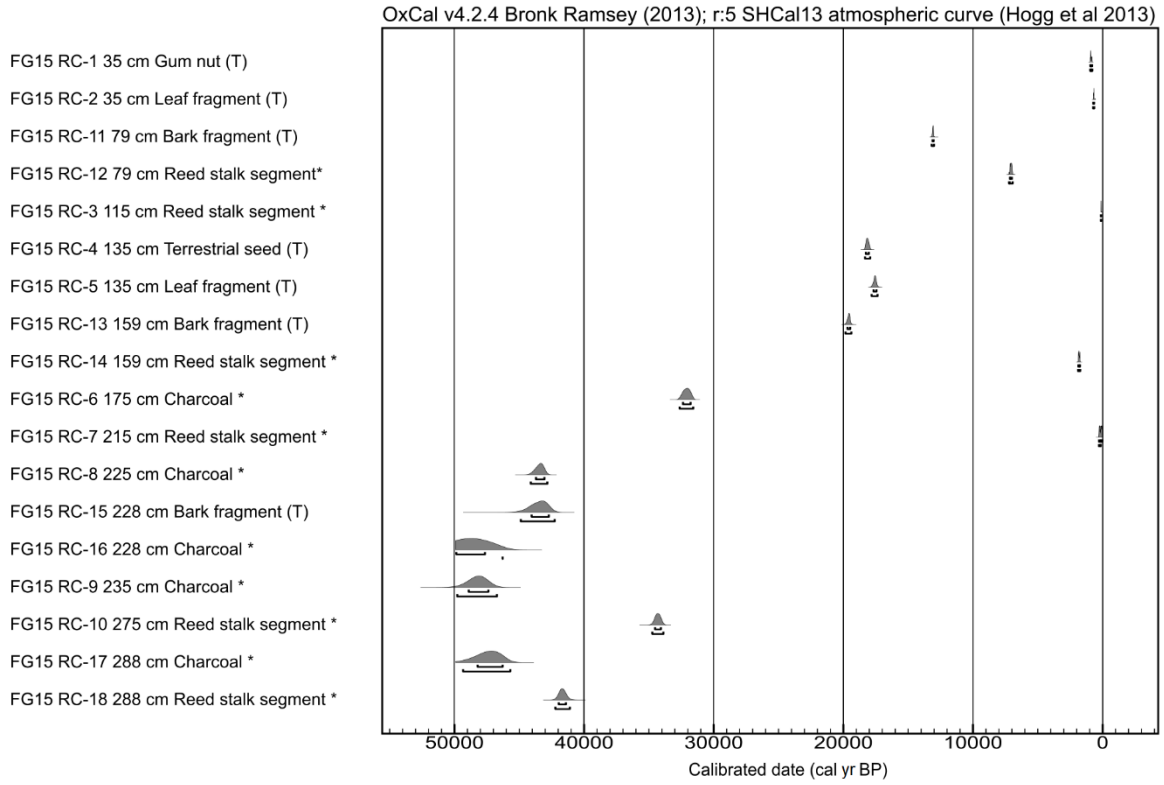

Figure 3.4: Calibrated radiocarbon age probability distributions with calibrated 68.2% and 95.4% age ranges. * denotes an age excluded from the age-depth model due to material type. (T): a confirmed terrestrial source.

Five ^{14}C samples consisted of single >3 mm charcoal fragments. ^{14}C dating of charcoal can underestimate sample age in organic-rich wetlands unless prepared using a specific method to remove humic acid contamination (Nilsson et al., 2001; Turetsky et al., 2004; Brock et al., 2011). Contamination is a particular issue in old samples where small concentrations of humic acid can produce large underestimations (e.g. 1% modern carbon contamination can cause a 15 kyr underestimation in a 50 ka sample) (Brock et al., 2011). As the charcoal samples from Fern Gully Lagoon were prepared using ABA, the resultant ages may have been inadvertently affected by humic acid contamination (Brock et al., 2010). Indeed, there is some evidence to suggest this might be the case for the three charcoal samples collected from depths of 228, 235 and 288 cm, which have statistically indistinguishable 2σ calibrated age ranges (Fig. 3.4, Table 3.2).

3.7.5 OSL dating

The single-grain OSL dating results are summarised in Table 3.3, with representative single-grain D_e distributions shown as radial plots in Figure 3.5. The OSL samples from Fern Gully Lagoon exhibit a broad range of D_e distribution characteristics, indicative of spatially and temporally variable bleaching and mixing conditions at the site (e.g. Arnold et al., 2007; Arnold et al., 2008; Arnold and Roberts, 2009; Arnold et al., 2012). Full discussions of the single-grain D_e distributions and statistical age models used to derive representative burial dose estimates for each sample are provided in the supplementary materials.

The final OSL ages exhibit good stratigraphic consistency for thirteen of the nineteen samples (Table 3.3). The remaining six samples (FG15 OSL-1, -8, -8-2, -9, -10 and -16) yield very young, outlying and inverted ages of between 6.69 ± 2.0 ka to 21.2 ± 2.6 ka for the lowermost 7 m of the core sequence. These outlying ages in the lowermost 7 m of the core are in keeping with the complex D_e distribution characteristics observed for the six samples, which are characterised by very high overdispersion values (53–119%) and multiple discrete dose components (Fig. B7). These multimodal D_e datasets are interpreted as reflecting the presence of locally intruded young grain populations. These populations could potentially be the result of sporadic lake desiccation and the formation of deep surface cracks (a process that is visible today in analogous peat-rich wetlands on NSI) or downward grain transportation via root penetration into older sediments, as has been found previously (e.g. Bateman et al., 2007; Brill et al., 2012). These interpretations are consistent with the presence of modern or near-modern organic remains at depths >1 m in the ^{14}C study (section 3.7.4).

Assuming that the multiple discrete dose components of FG15 OSL-1, -8, -8 2, -9, -10 and -16 can be explained by localised post-depositional mixing, it follows that the bulk (sample-average) dose rate of these six samples may not be entirely representative of that experienced by either dose component during burial. Owing to the impracticalities of retrospectively deriving a component-specific dose rate for the multiple identified components, these samples are not considered suitable for dating. The ages shown for these samples in Table 3.3 are included for indicative purposes only and have not been included as likelihood estimates in the Bayesian age model.

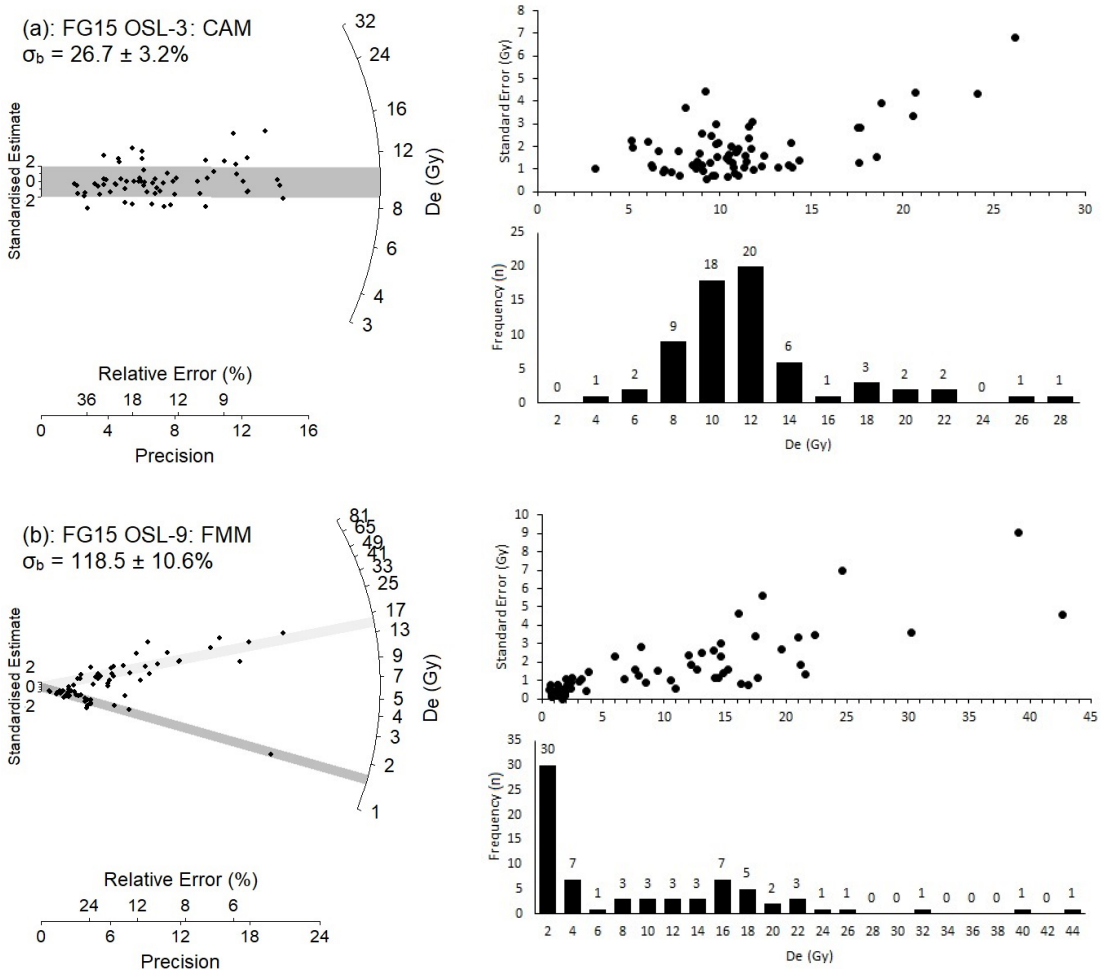

Figure 3.5: Example single-grain D_e distributions shown as radial plots and frequency histograms with ranked plots of D_e versus standard error. **(a)** Samples FG15 OSL-3 (813–832 cm depth), which was considered suitable for dating using the central age model (CAM). The grey bar on the radial plot is centred on the CAM D_e value used to derive the final burial dose of this sample; **(b)** Sample FG15 OSL-9 (326–335 cm depth), which was not considered suitable for dating because it contains multiple discrete dose populations, as identified by the finite mixture model (FMM). The two dose components identified by the FMM are shown by the light and dark grey bands in the radial plot. Individual D_e estimates are presented with their 1σ error ranges, which are derived from a random uncertainty term arising from photon counting statistics for each OSL measurement, an empirically determined instrument reproducibility uncertainty of 2.5% (following the approach outlined in Jacobs et al. (2006)) and a dose-response curve fitting uncertainty determined using 1000 iterations of the Monte Carlo method implemented in Analyst (Duller, 2015).

Table 3.3: Dose rate data, equivalent doses (D_e), overdispersion values, and OSL ages for lacustrine samples from Fern Gully Lagoon, NSI. The final OSL age of each sample has been calculated by dividing the D_e value by the total dose rate.

Sample	Depth (cm)	Water Content (% dry weight) [a]	Environmental dose rate (Gy/kyr) [b,c,d,e,f]					Equivalent dose (D_e) data			D_e (Gy) [f]	Final age (ka) [f,j]
(core)			Beta dose rate	Gamma dose rate	Internal dose rate	Cosmic dose rate	Total dose rate	No. of grains [h]	Overdispersion (σ_b) (%) [i]	Age Model [g]		
FG15 OSL-18 (1)	171–180	320/404/507	0.03±0.005	0.03±0.0007	0.02±0.007	0.03±0.003	0.11±0.01	102	50.3±4.2	MAM-3	3.60±0.8	33.2±8.0
FG15 OSL-17 (1)	181–190	342/361/497	0.03±0.005	0.03±0.0009	0.02±0.007	0.03±0.003	0.12±0.01	52	50.9±5.8	CAM	9.08±0.7	77.7±9.2
FG15 OSL-16 2 (2)	204–213	386/344/484	0.01±0.003	0.02±0.0006	0.02±0.007	0.03±0.003	0.09±0.01	117	39.5±2.9	MAM-3	14.3±0.6	128±15.3
FG15 OSL-16 (1) [k]	204–213	386/344/484	0.03±0.006	0.027±0.001	0.02±0.007	0.03±0.003	0.11±0.01	50	92.2±10.7	MAM-3	1.48±0.1	13.3±2.0
FG15 OSL-15 (1)	214–223	336/363/477	0.03±0.005	0.03±0.0009	0.02±0.007	0.03±0.003	0.12±0.01	96	41.3±3.6	CAM	11.4±0.5	95.5±9.73
FG15 OSL-14 (1)	235–244	408/378/468	0.02±0.003	0.03±0.0007	0.02±0.007	0.03±0.003	0.09±0.009	33	34.5±5.4	CAM	12.7±0.9	135±16.3
FG15 OSL-13 (1)	263–272	406/399/460	0.02±0.004	0.04±0.008	0.02±0.007	0.03±0.003	0.1±0.01	37	34.0±5.0	CAM	14.7±0.9	132±20.3
FG15 OSL-12 (1)	273–282	362/402/456	0.04±0.007	0.03±0.003	0.02±0.007	0.03±0.003	0.1±0.01	131	34.4±2.5	CAM	16.4±0.5	137±15.4
FG15 OSL-11 (1)	283–292	446/426/456	0.02±0.003	0.02±0.01	0.02±0.007	0.03±0.003	0.09±0.02	82	28.9±2.8	CAM	14.8±0.5	171±33.4
FG15 OSL-10 2 (2)	306–315	545/433/457	0.004±0.001	0.007±0.0003	0.02±0.007	0.03±0.003	0.06±0.008	63	33.2±3.7	CAM	13.8±0.6	179±22.4
FG15 OSL-10 (1) [k]	306–315	545/433/457	0.01±0.003	0.01±0.0005	0.02±0.007	0.03±0.003	0.08±0.009	86	53.3±6.1	MAM-3	1.65±0.1	21.2±2.6
FG15 OSL-9 (1) [k]	326–335	380/450/455	0.01±0.002	0.02±0.003	0.02±0.007	0.03±0.003	0.08±0.009	82	118.5±10.6	MAM-4	1.59±0.1	20.0±2.8
FG15 OSL-8 (1) [k]	405–414	572/673/477	0.009±0.002	0.02±0.0005	0.02±0.007	0.03±0.003	0.08±0.008	80	76.9±8.4	MAM-4	1.40±0.1	19.9±2.7
FG15 OSL-8 2 (2) [k]	405–414	572/673/477	0.02±0.004	0.02±0.0005	0.02±0.007	0.03±0.003	0.08±0.009	51	94.8±10.5	MAM-4	1.48±0.1	17.5±2.3
FG15 OSL-5 (1)	655–674	629/666/578	0.005±0.001	0.003±0.0002	0.02±0.007	0.02±0.002	0.05±0.008	37	39.2±5.7	CAM	12.6±0.7	248±40.6
FG15 OSL-4 (2)	777–801	438/477/577	0.007±0.001	0.007±0.0003	0.02±0.007	0.02±0.002	0.06±0.008	85	32.5±3.0	CAM	11.6±0.5	206±29.4
FG15 OSL-3 (1)	813–832	443/439/572	0.004±0.001	0.008±0.002	0.02±0.007	0.02±0.002	0.05±0.008	66	26.7±3.2	CAM	10.8±0.4	201±30.4
FG15 OSL-2 (1)	833–857	397/434/567	0.008±0.001	0.007±0.0005	0.02±0.007	0.02±0.002	0.06±0.008	50	52.4±5.8	MAM-4	10.4±0.6	180±26.4
FG15 OSL-1 (2) [k]	893–926	343/394/561	0.009±0.001	0.006±0.0005	0.02±0.007	0.02±0.002	0.06±0.008	63	88.8±12.8	MAM-3	0.38±0.1	6.69±2.0

[a] Long-term water contents used for beta / gamma / cosmic-ray dose rate attenuation, expressed as % of dry mass of mineral fraction, with an assigned relative uncertainty of ±10%. The final beta dose rates have been adjusted for moisture attenuation using the average water content from the midpoint of each OSL sample depth. The final gamma dose rates have been adjusted using the water content determined separately for the gamma dose rate bulk sediment samples, which were collected for each OSL sample depth, as well as for the overlying and underlying 10 cm depth. The final cosmic-ray dose rates have been adjusted using the average water content measured from the contiguous 1 cm^3 bulk sediment samples collected throughout the overlying core sequence.

[b] Beta, gamma and internal dose rates have been calculated on dried and powdered sediment samples using ICP-MS and ICP-OES. The beta dose rates have been calculated on bulk sediment samples collected from each OSL sample depth. The gamma dose rates have been determined separately on bulk sediment samples collected for each OSL sample depth, as well as for the overlying and underlying 10 cm depth of each OSL sample position, following De Deckker et al. (2019).

[c] Radionuclide concentrations have been converted to alpha, beta and gamma dose rates using the published conversion factors of Guérin et al. (2011) and allowing for beta-dose attenuation (Mejdahl, 1979; Brennan, 2003) and long-term water content correction (Aitken, 1985).
[d] An internal dose rate of 0.02 ± 0.007 Gy/kyr has been included in the final dose rate calculations of all samples, based on ICP-MS U and Th measurements made on etched quartz grains from associated aeolian deposits at Welsby Lagoon (Lewis et al., in prep) and an alpha efficiency factor (*a* value) of 0.04 ± 0.01 (Rees-Jones, 1995; Rees-Jones and Tite, 1997).
[e] Cosmic-ray dose rates were calculated after Prescott and Hutton (1994), and assigned a relative uncertainty of ±10%.
[f] Mean ± total uncertainty (68% confidence interval), calculated as the quadratic sum of the random and systematic uncertainties.
[g] SG OSL = single-grain optically stimulated luminescence; MAM-3 = three-parameter minimum age model (Arnold et al., 2009), MAM-4 = four-parameter minimum age model (Arnold et al., 2009); CAM = Central age model (Galbraith et al., 1999). MAM-3 and MAM-4 D_e estimates were calculated after adding, in quadrature, a relative error of 25% to each individual D_e measurement error to approximate the underlying dose overdispersion observed in an 'ideal' (well-bleached and unmixed) sedimentary sample from this core (FG15 OSL-3), which is consistent with global overdispersion datasets (Arnold and Roberts, 2009).
[h] Number of D_e measurements that passed the SAR quality assurance criteria and were used for D_e determination.
[i] The relative spread in the D_e dataset beyond that associated with the measurement uncertainties for individual D_e values, calculated using the CAM.
[j] Total uncertainty includes a systematic component of ±2% associated with laboratory beta-source calibration.
[k] Samples excluded from the Bayesian model as they contain multiple discrete dose populations when fitted with the FMM (see section 3.7.5 for details).

3.7.6 Bayesian age-depth model

Thirteen single-grain OSL ages and eighteen ^{14}C ages were included in the Bayesian age modelling procedure, separated by three depositional boundaries. A preliminary version of the model tested using these 31 likelihood estimates failed to converge owing to the identification of major statistical outliers. We excluded all potentially inaccurate charcoal and misidentified reed stalk ages from the second model (see Table 3.2). The youngest charcoal ^{14}C sample (FG15 RC-6) had an age that was consistent with the OSL sample collected at 175 cm depth (FG15 OSL-18) (see Section 3.7.4), suggesting that it may not be affected by humic acid contamination. However, for the sake of consistency, it was excluded from further consideration. These quality control measures resulted in only seven of the original eighteen ^{14}C likelihood estimates being included in the second Bayesian age model. A preliminary version of this model failed to converge owing to the identification of a major statistical outlier (sample FG15 RC-15). It was therefore, necessary to eliminate this ^{14}C likelihood estimate in the final Bayesian model.

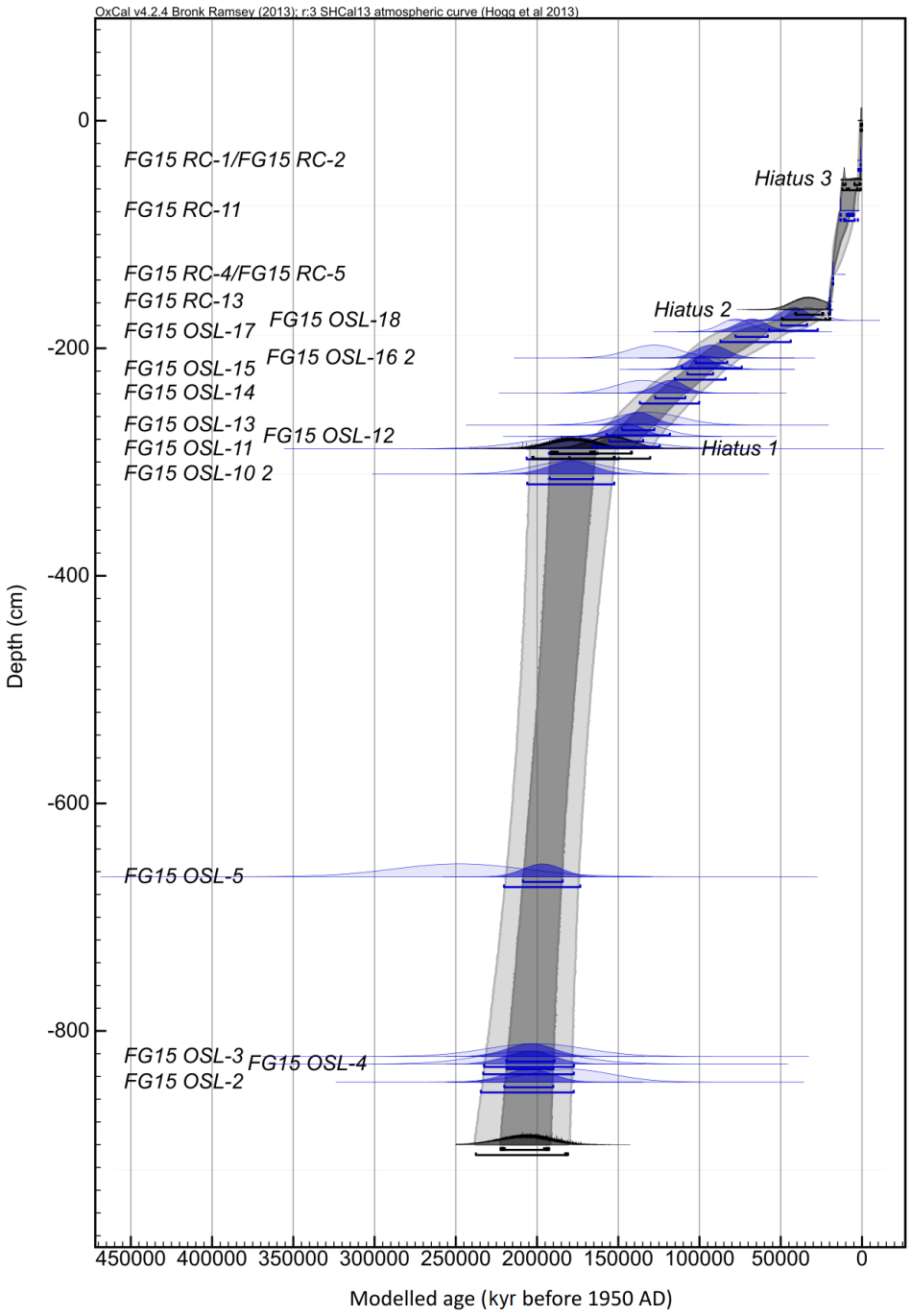

Figure 3.6: Bayesian age/depth model for the Fern Gully Lagoon sequence obtained using a non-continuous deposition scenario. The prior age distributions for the dating samples (likelihoods) are shown in light blue. The modelled posterior distributions for the dating samples and unit boundaries are shown in dark blue and grey, respectively. Likelihood and posterior ages are shown on a calendar year timescale and expressed in years before 1950 AD. The 68.2% and 95.4% ranges of the posterior probabilities are indicated by the light and dark shading.

The Bayesian model for Fern Gully Lagoon has A_{model} and $A_{overall}$ values of 62.3% and 64.6% respectively, marginally exceeding the minimum acceptance threshold of 60% and thus indicating a valid model (Bronk-Ramsey, 2009). The modelling results are summarised in Table B4 and illustrated in Fig. 3.6. The final model indicates a basal age of 209.3 ± 28.4 ka (±2σ) at 900 cm, in agreement with the previously measured basal age of 208.4 ± 32.5 ka on an adjacent preliminary core (Ad13069; Tibby et al., 2017). The model reveals four distinct sedimentation phases separated by hiatuses: a late MIS 7 to early MIS 6 phase (209.3 ± 28.4 ka to 177.5 ± 25.4 ka, 930 – 288 cm), a late MIS 6 to late MIS 3 phase (155.2 ± 24.9 to 34.7 ± 14.5, 288 – 166 cm), a mid-MIS 2 to mid-Holocene phase (20.9 ± 1.4 ka to 6.5 ± 5.6 ka, 166 – 52 cm) and a late Holocene phase (1.7 ± 1.0 ka to 0.45 ± 0.4 ka, 52 – 0 cm) (±2σ, Table B4, Fig. 3.6). The average sedimentation rates of these four phases are (from bottom to top) 0.20 m/kyr, 0.01 m/kyr, 0.08 m/kyr and 0.31 m/kyr.

3.7.7 Identifying aeolian and autochthonous wetland sediment

Broken stick analysis revealed two significant principal components in the μXRF data (Fig. B2), which combined reflect greater than 97% of the variance in the data. Co-varying silicon, titanium, potassium and zircon defined much of PC1. PC1 is very similar to the local aeolian signature identified by McGowan et al. (2008), and we therefore associate PC1 with local aeolian dust input. PC2 was defined by iron and calcium and is likely associated with a secondary aeolian source or internal wetland processes (Fig. 3.7). Unfortunately, the position of iron and calcium compounds within the sediment may have been altered post-sedimentation, such as by changing redox, rendering the identification of a source material difficult. Inorganic MIS 5 and Holocene sediments from Fern Gully Lagoon are most similar to contemporary local dune surface and subsurface samples, while the closest source material to MIS 7 inorganics is Dunwich sandstone, which contains notable quantities of iron and calcium.

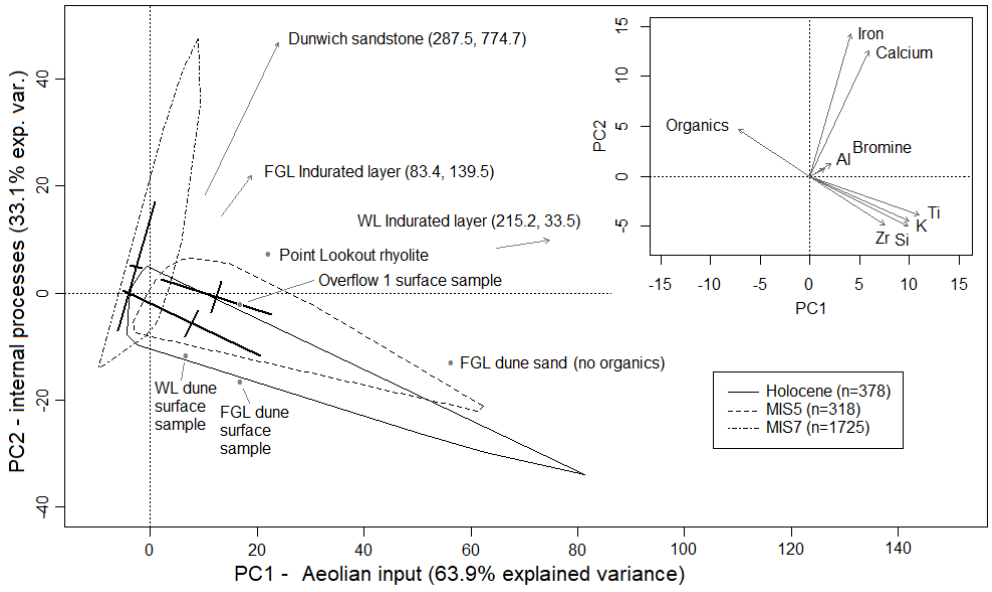

Figure 3.7: PCA biplot of µXRF elements and organic content from Fern Gully Lagoon. Crosses indicate the distribution mean and one standard deviation of the two principal axes of each distribution, while the outer polygon indicates the extent of the samples. Local inorganic source materials are indicated by grey points and grey arrows where these points lie outside the plot. Al: aluminium; Ti: titanium; K: potassium; Si: silicon; Zr: zirconium.

3.7.8 Inorganic sedimentation at Fern Gully Lagoon

The influx of aeolian inorganics was highly variable over the past 210 ka (Fig. 3.8). Aeolian inorganic input during MIS 7a–c and early MIS 6 (209.3 ± 28.4 ka to 177.5 ± 25.4 ka) was low while other inorganic sedimentation (represented by calcium and iron dominated inputs) gradually declined. The earliest phase had a high rate of total sedimentation, but no notable inorganic peaks. During the late MIS 6 to late MIS 3 phase (155.2 ± 24.9 to 34.7 ± 14.5 ka), there were aeolian inorganic peaks at ~144 ± 10 ka (LOI, magnetic susceptibility, PC1), ~100 ± 8 ka (LOI, PC1) and ~52 ± 11 ka (PC1). During the mid-MIS 2 to mid-Holocene phase (20.9 ±0.8 to 6.5 ± 2.8 ka), there were some small inorganic peaks from ~14–11 ka. Aeolian inorganic sedimentation peaks during the late Holocene, with ~95% inorganic sediments recorded at ~1.6 ± 0.5 ka (magnetic susceptibility, LOI, PC1). While wetland desiccation and cracking during dry periods, indicated by OSL D_e distributions, may have displaced quartz sand grains from their original position in the sediment, it is unlikely that this had more than a minor influence on the aeolian inorganic record, as most sediment would have remained intact.

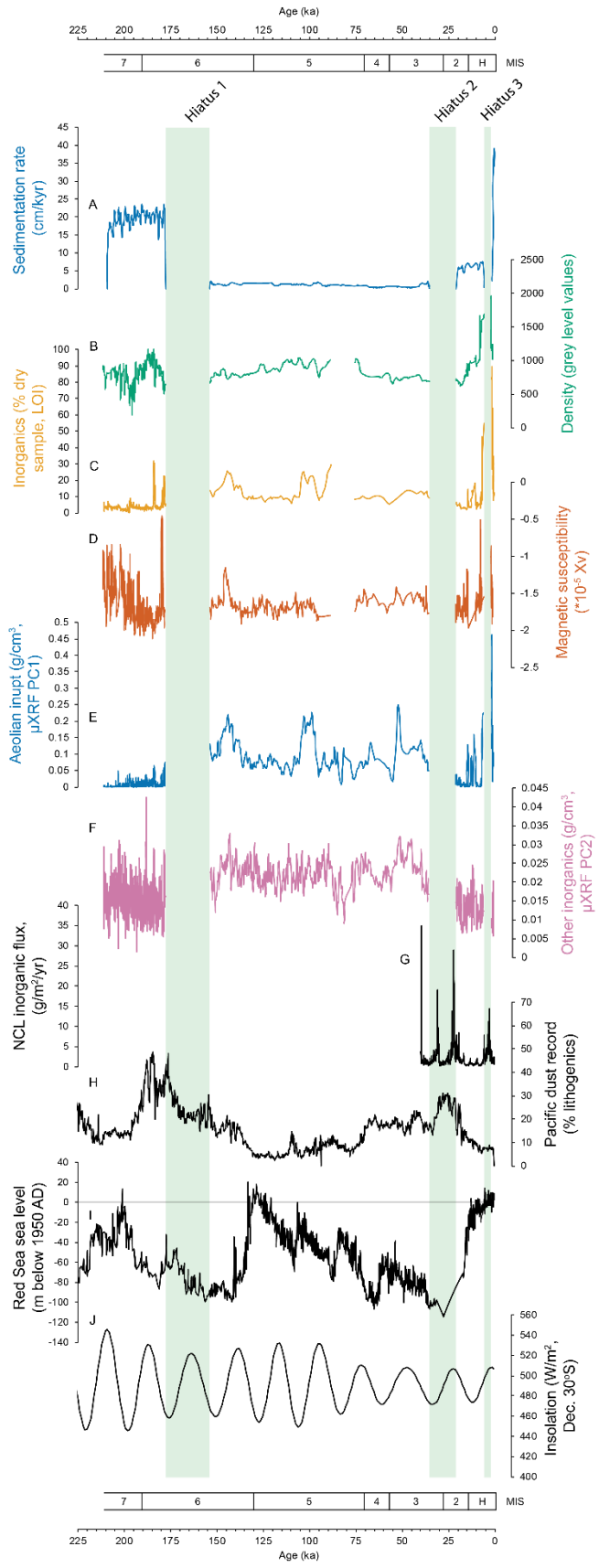

Figure 3.8: A: Sedimentation rate (3 cm moving average), **B:** sediment density (X-radiograph), **C:** inorganic content, **D:** magnetic susceptibility, **E:** calibrated µXRF aeolian input (silicon, potassium, zircon and titanium, PC1) and **F:** other calibrated µXRF inorganic sedimentation (calcium and iron, PC2). Records for comparison are **G:** Native Companion Lagoon (NCL) (Petherick et al., 2009), **H:** an Australian dust record from the South Pacific (Lamy et al., 2014), **I:** a global sea level record from the Red Sea (Grant et al., 2012) and **J:** December mean insolation for 30 degrees south (Berger and Loutre, 1991).

3.8 Discussion

3.8.1 µXRF sediment analysis of highly organic wetlands

The most commonly used µXRF normalisation method (Table B5) – normalisation by total counts per second – was the most suitable for calibrating inorganic elements in the highly organic Fern Gully Lagoon sediments. However, raw counts per second had comparable or better performance than most normalisation methods, indicating that raw data may be used in some circumstances (Table 3.1). The best performing method for correcting µXRF data appeared to depend on the element(s) under consideration. For example, centred log-ratio correction resulted in the best correlation to WD-XRF particularly for magnesium, bromine and calcium ($r^2 = 0.85$, $r^2 = 0.84$ and $r^2 = 0.78$ respectively, where $p < 0.05$, $n = 20$ for all values), while multiple normalisation methods for aluminium had similarly good r^2 values (0.62 – 0.69, Table 3.1). For µXRF analysis of highly organic sediments, the optimal method may be to determine the most suitable normalisation method for each element before calibration, rather than using a single normalisation method. If testing of multiple normalisation methods is not possible, centred log-ratio normalisation will produce the best results in the majority of cases, as it has been mathematically proven to counter the closed sum and other distorting effects inherent in µXRF data (Weltje and Tjallingii, 2008; Croudace and Rothwell, 2015).

Several recent palaeoclimate reconstructions from wetland sediments have relied on µXRF derived iron (e.g. Rees et al., 2015; Burrows et al., 2016; Stephens et al., 2018) or magnesium (Foerster et al., 2018) records to infer, for example, waterlogged soils, redox conditions and detrital input. However, our analysis indicates that these elements may not be accurately characterised by µXRF in highly organic sediment. Bromine was used as an indicator of organic content in the Paddy's Lake record (north-western Tasmania), supported by the incoherent to coherent ratio (inc/coh) (Beck et al., 2017). However, while inc/coh and bromine correlate, neither correlated well with organic content in our study ($r^2 < 0.003$, $p = 0.132$, $n = 804$ and $r^2 = 0.05$, $p < 0.05$, $n = 804$ respectively). Indeed, the use of inc/coh requires additional stages of calibration to accurately indicate organic content (Woodward and Gadd, 2019). While some recent studies have validated the use of the µXRF inc/coh for estimating organic content (e.g. Field et al., 2018; Woodward et al., 2018), a number have not (e.g. Rees et al., 2015; Turner et al., 2015; Burrows et al., 2016; Pleskot et al., 2018). Standardising normalisation and

calibration of μXRF records as a minimum requirement for μXRF derived climate studies would improve record precision and reduce uncertainty in future work.

3.8.2 Dating wetland sediments

Reliable dating of Australian palaeoclimate sequences that span multiple past interglacial periods has proved difficult, although luminescence dating offers a potentially useful means of filling chronological gaps across a range of palaeoenvironmental contexts (Fu et al., 2017; Roberts et al., 2018; De Deckker et al., 2019). This study highlights the complexities that can be encountered when using single-grain OSL and ^{14}C dating in organic-rich peaty wetlands. By employing both techniques, it has been possible to better diagnose complications related to material selection (e.g., root fragments and charcoal), post-depositional mixing, and heterogeneous bleaching of sand grains. While a relatively high proportion of the original dating samples were unsuitable for inclusion in the final age model (i.e. 67% of the eighteen ^{14}C samples and 32% of the nineteen OSL samples), our results highlight the general suitability of ^{14}C and OSL dating in this depositional context when targeting optimal sampling materials, laboratory protocols and scales of analysis. Careful consideration of dating quality control has proved critical for deriving a meaningful age-depth model at Fern Gully Lagoon. There is good scope for using systematic single-grain OSL dating studies to refine the chronology of other Australian interglacial records.

3.8.3 Fern Gully Lagoon sediment hiatuses

Age-depth modelling indicates that there were three hiatuses in sedimentation at ~177 to 155 ka, ~34.7 to 20.9 ka and 6.5 to 1.7 ka. Palaeoclimate reconstructions from nearby wetland sites on North Stradbroke and Fraser Islands have revealed sedimentary hiatuses during dry periods such as the LGM (Donders et al., 2006; Woltering et al., 2014). Unfortunately, there are no nearby records of sufficient age and resolution to allow comparison of pre-MIS 5 hiatuses at FGL. The timing of two hiatuses in the Fern Gully Lagoon record during mid-MIS 6 and late MIS 3 to mid-MIS 2 are consistent with drier climates observed in a number of Australian records, both in north-east (Kershaw et al., 2007a; Moss and Kershaw, 2007) and central Australia (Fu et al., 2017). The start of the mid-MIS 3 sedimentary hiatus in Fern Gully Lagoon aligns with the commencement of widespread drying of Australia (Chapter 2; Kemp et al., 2019), and occurs at the same time as drying in nearby Welsby Lagoon (Cadd et al., 2018). The mid-

Holocene hiatus at Fern Gully Lagoon has no equivalent from Welsby Lagoon (Cadd et al., 2018), although Fern Gully Lagoon may be more hydrologically sensitive due to its smaller catchment. Lower rainfall was noted at Swallow Lagoon after ~3 ka (Barr et al., 2019), while mid-Holocene hiatuses or drier phases were recorded at Hidden Lake and Lake Allom on nearby Fraser Island (Longmore, 1997; Donders et al., 2006).

The absence of a recorded hiatus at nearby Welsby Lagoon during the late Holocene after ~3 ka may possibly be due to a fire which burned Fern Gully Lagoon but not Welsby Lagoon. Loss of wetland peat due to fire may exceed 50 cm in a single event (in which a peatland may burn for more than a month) – high peat density and peat moisture content lower than 16% contribute to the loss of greatest material (Ballhorn et al., 2009; Davies et al., 2013; Lukenbach et al., 2015). However, an initial study of sedimentary charcoal did not indicate higher levels during this period (Chapter 4), and there is no notable change in the calcium record (Fig. 3.2) which could indicate mineralisation within the sediment as the result of a major peat fire (Smith et al., 2001). Therefore, it is more likely that Fern Gully Lagoon is more hydrologically sensitive than Welsby Lagoon, and drying led to a late-Holocene hiatus, rather than loss of peat due to a major fire event.

3.8.4 Palaeoclimate interpretation and comparison with other records

We interpret increased aeolian inorganic sedimentation in Fern Gully Lagoon as indicative of dry climates, as reduced vegetation cover increases local wind erosion (McGowan et al., 2008). While changes in wind strength could also be a major source of changing inorganic flux, records of terrestrial dust grain size from the Tasman Sea indicate that regional wind strength was secondary to continental drying in explaining regional aeolian inorganic transport (Hesse and McTainsh, 2003). Increased biomass burning on NSI is a possible additional driver for increased inorganic sedimentation. However, macrocharcoal and the proportion of sediment inorganic matter are uncorrelated at Fern Gully Lagoon ($r^2 = 0.04$, $p > 0.05$, $n = 632$ (Chapter 4; Kemp et al., submitted)), a situation similar to nearby Welsby Lagoon (Barr et al., 2017). Hence, it appears that increased biomass burning did not play a large role in increasing wind erosion on NSI. Sea-level transgression does not appear to drive inorganic flux to Fern Gully Lagoon as the major marine transgressions during late MIS 6 and after the LGM do not coincide with increased inorganic flux (Fig. 3.8). However, the lack of inorganic sediment immediately after the LGM

may also be due to a change in the dominant regional wind direction which deposited sands offshore as postulated by Walker et al. (2018).

We compared our results to the ~33 kyr inorganic flux record from Native Companion Lagoon (NCL; Fig 3.8g; McGowan et al., 2008; Petherick et al., 2008) and the ~37 kyr record from Tortoise Lagoon (Petherick et al., 2017). The NCL record indicates that a dry phase occurred during the LGM as well as an increase in inorganic sedimentation at ~3 ka (McGowan et al., 2008). While Tortoise Lagoon records a similar LGM peak, there is no increase late-Holocene inorganic sedimentation (Petherick et al., 2017). The LGM inorganic peak was not recorded at Fern Gully Lagoon due to a hiatus, but the hiatus itself indicates that Fern Gully Lagoon was similarly dry.

The Fern Gully Lagoon sequence recorded low aeolian sedimentation with low PC1 scores and the lowest inorganic content (~3%), during MIS 7a–c, indicating that it was likely the wettest interglacial of the past three in subtropical eastern Australia. This finding is similar to the record of moisture availability from central Australia, where recorded lake levels reached their highest for the past ~250 ka (Fu et al., 2017); Lynch's Crater in north-east Australia, where wet climates with open water present were found (Kershaw et al., 2007b), and at Naracoorte caves in south-east Australia, where pronounced periods of calcitic growth occurred (Ayliffe et al., 1998). In comparison, there was greater aeolian input during MIS 5e, indicating a drier local climate than in MIS 7a–c (Fig. 8; MIS 5e average ~0.24 kg/m^2/kyr vs average ~0.14 kg/m^2/kyr inorganics). The record also contains a notable MIS 5 dry period at 100 ± 15.6 ka. A similar comparatively drier mid-MIS 5b–d from ~110–90 ka has been observed in other regions, most notably in tropical north-east Australia (Kershaw et al., 2007a). Conversely, central Australian lakes Eyre and Woods maintained shallow to deep-water conditions during MIS 5 (Bowler et al., 1998; Fu et al., 2017) while calcite growth occurred after ~105 ka (Ayliffe et al., 1998).

During the Holocene, inorganic aeolian deposition at Fern Gully Lagoon averaged ~0.96 kg/m^2/kyr, four times greater than during MIS 5e and almost seven times MIS 7a–c levels. Greater inorganic flux, in combination with high PC1 scores, suggests the Holocene is the driest interglacial of the last three for subtropical eastern Australia. A drier Holocene relative to MIS 7a–c and MIS 5e is observed in several other Australian records, either via increased dry forest and herbaceous vegetation (albeit influenced by human impact; Harle et al., 2002; Moss and

Kershaw, 2007) or lower flows and lake filling (Maroulis et al., 2007; Nanson et al., 2008; Fu et al., 2017). Holocene drying has been attributed to increasing El Niño frequency compared to past interglacials (Moss and Kershaw, 2007), or to the extended period of high sea levels during the Holocene limiting WPWP influence on monsoonal precipitation and the warm East Australian Current (Nanson et al., 2008). Holocene inorganic sedimentation at Fern Gully Lagoon may also be influenced by human-induced biomass burning. There is a long record of human activity on the island (Neal and Stock, 1986) which may have also contributed to mobilisation of dune sands. However, the paucity of dated archaeology close to Fern Gully Lagoon currently precludes an assessment of human influence on the Fern Gully record.

The pattern of increasingly dry interglacials observed at Fern Gully Lagoon since MIS 7 is consistent with the few other Australian records covering this period, most notably in central Australia (Bowler et al., 2001; Cohen et al., 2015; Fu et al., 2017), but also in the north (Bowler et al., 1998) and south-east (Edney et al., 1990) of the continent. However, records from eastern Australia – tropical Lynch's Crater (Kershaw et al., 2007a) and alpine, temperate, Caledonia Fen (Kershaw et al., 2007b) – indicate similar climates during the Holocene and MIS 5e. Similar climates between the north-eastern Lynch's Crater and Fern Gully Lagoon may be explained by the behaviour of the East Australian Current (EAC). The southerly reach and hence strength of the EAC can be derived from the position of the Tasman Front (TF; Fig. 3.1), which can in turn tracked by changes in SST derived from the relative abundance of benthic and planktonic foraminifera in ocean sediments (Kawagata, 2001). SST records indicate similar temperatures for MIS 5e and the Holocene (at ~23°C for NGC100 and NGC99; Kawagata, 2001) as a result of similar TF position and hence EAC strength. A more southerly penetration of relatively warm EAC waters during interglacials likely drove higher rainfall in subtropical and temperate eastern Australia independently of major continental climate drivers such as ENSO. Similar to the influence of the Agulhas Current on regional rainfall in south-eastern Africa (Jury et al., 1993; Nkwinkwa Njouodo et al., 2018), the major driver of increased water availability in subtropical and temperate eastern Australia with a stronger EAC was likely the influence of warmer waters on regional convective rainfall.

3.9 Conclusions

Analysis of a new discontinuous sedimentary record from Fern Gully Lagoon using ^{14}C dating, single-grain OSL dating and μXRF core scanning has enabled the reconstruction of a regional palaeoclimate sequence spanning the last three interglacial complexes. An evaluation of μXRF normalisation methods indicated that normalisation by total counts per second was the most effective method for Fern Gully Lagoon sediments.

The silicon-rich elemental signature of increased aeolian input to Fern Gully Lagoon, associated with drier climates, was characterised by PC1, which also reflected variation in potassium, titanium and zircon. The record indicates a relatively wet MIS 7a–c and early MIS 6 phase, a relatively drier MIS 5 interglacial complex, MIS 4 and MIS 3, and a wetter late MIS 2 which transitioned into a drier Holocene. There is general agreement between the Fern Gully Lagoon record and central Australian lake records fed by the Australasian summer monsoon and records from the north- and south-east of the continent. Differences between ENSO driven north-eastern Australian records, and Fern Gully Lagoon may be due to the influence of the East Australian Current.

The increasingly dry interglacials observed from Fern Gully Lagoon may be due to more frequent El Niño events. Understanding how ENSO changes during interglacials is important in predicting future moisture availability due to climate change, as well as ecosystem response to increasing global temperatures. However, due to limited climate records, further study is required. The Fern Gully Lagoon climate record may assist in answering some of these questions as it represents a new record of ENSO activity at interglacial time scales as well as adding to the list of palaeoclimate records used to validate and tune new climate models.

It is difficult to determine a detailed record of hydrological change without considering changing vegetation types and biomass burning records. Ongoing analysis of multiple climate proxies such as pollen, charcoal and stable isotopes from Fern Gully Lagoon will likely result in a greater understanding of past interglacial climates and their drivers.

3.10 References

Aitken, M.J., 1985. "Thermoluminescence dating". Academic Press, London.

Arnold, L.J., Bailey, R.M., Tucker, G.E., 2007. "Statistical treatment of fluvial dose distributions from southern Colorado arroyo deposits." *Quaternary Geochronology* 2, 162-167.

Arnold, L.J., Demuro, M., Navazo, M., Benito-Calvo, A., Pérez-González, A., 2012. "OSL dating of the Middle Palaeolithic Hotel California site, Sierra de Atapuerca, north-central Spain." *Boreas* 42, 285-305.

Arnold, L.J., Roberts, R.G., 2009. "Stochastic modelling of multi-grain equivalent dose (D_e) distributions: Implications for OSL dating of sediment mixtures." *Quaternary Geochronology* 4, 204-230.

Arnold, L.J., Roberts, R.G., Galbraith, R.F., DeLong, S.B., 2009. "A revised burial dose estimation procedure for optical dating of young and modern-age sediments." *Quaternary Geochronology* 4, 306-325.

Arnold, L.J., Roberts, R.G., MacPhee, R.D.E., Willerslev, E., Tikhonov, A.N., Brock, F., 2008. "Optical dating of perennially frozen deposits associated with preserved ancient plant and animal DNA in north-central Siberia." *Quaternary Geochronology* 3, 114-136.

Ayliffe, L.K., Marianelli, P.C., Moriarty, K.C., Wells, R.T., McCulloch, M.T., Mortimer, G.E., Hellstrom, J.C., 1998. "500 ka precipitation record from southeastern Australia: Evidence for interglacial relative aridity." *Geology* 26, 147-150.

Baczkowski, A.J., 2000. "The broken-stick model for species abundances: An initial investigation." *Internal Report STAT 00/10, University of Leeds, UK*, 2-25.

Ballhorn, U., Siegert, F., Mason, M., Limin, S., 2009. "Derivation of burn scar depths and estimation of carbon emissions with LIDAR in Indonesian peatlands." *Proceedings of the National Academy of Sciences* 106, 21213.

Barr, C., Tibby, J., Leng, M.J., Tyler, J.J., Henderson, A.C.G., Overpeck, J.T., Simpson, G.L., Cole, J.E., Phipps, S.J., Marshall, J.C., McGregor, G.B., Hua, Q., McRobie, F.H., 2019. "Holocene El Niño–Southern Oscillation variability reflected in subtropical Australian precipitation." *Scientific Reports* 9, 1627.

Barr, C., Tibby, J., Moss, P.T., Halverson, G.P., Marshall, J.C., McGregor, G.B., Stirling, E., 2017. "A 25,000-year record of environmental change from Welsby Lagoon, North Stradbroke Island, in the Australian subtropics." *Quaternary International* 449, 106-118.

Bateman, M.D., Boulter, C.H., Carr, A.S., Frederick, C.D., Peter, D., Wilder, M., 2007. "Preserving the palaeoenvironmental record in Drylands: Bioturbation and its significance for luminescence-derived chronologies." *Sedimentary Geology* 195, 5-19.

Beck, K.K., Fletcher, M.-S., Gadd, P.S., Heijnis, H., Jacobsen, G.E., 2017. "An early onset of ENSO influence in the extra-tropics of the southwest Pacific inferred from a 14, 600 year high resolution multi-proxy record from Paddy's Lake, northwest Tasmania." *Quaternary Science Reviews* 157, 164-175.

Berger, A., Crucifix, M., Hodell, D.A., Mangili, C., McManus, J.F., Otto-Bliesner, B., Pol, K., Raynaud, D., Skinner, L.C., Tzedakis, P.C., Wolff, E.W., Yin, Q.Z., Abe-Ouchi, A., Barbante, C., Brovkin, V., Cacho, I., Capron, E., Ferretti, P., Ganopolski, A., Grimalt, J.O., Hönisch, B., Kawamura, K., Landais, A., Margari, V., Martrat, B., Masson-Delmotte, V., Mokeddem, Z., Parrenin, F., Prokopenko, A.A., Rashid, H., Schulz, M., Riveiros, N.V., 2015. "Interglacials of the last 800,000 years." *Reviews of Geophysics* 54, 162-219.

Berger, A., Loutre, M.F., 1991. "Insolation values for the climate of the last 10 million years." *Quaternary Sciences Reviews* 10, 297-317.

Berntsson, A., Rosqvist, G.C., Velle, G., 2014. "Late-Holocene temperature and precipitation changes in Vindelfjällen, mid-western Swedish Lapland, inferred from chironomid and geochemical data." *Holocene* 24, 78-92.

Bostock, H.C., Opdyke, B.N., Gagan, M.K., Kiss, A.E., Fifield, L.K., 2006. "Glacial/interglacial changes in the East Australian current." *Climate Dynamics* 26, 645-659.

Bouchard, F., Francus, P., Pienitz, R., Laurion, I., 2011. "Sedimentology and geochemistry of thermokarst ponds in discontinuous permafrost, subarctic Quebec, Canada." *Journal of Geophysical Research: Biogeosciences* 116.

Bowler, J.M., Duller, G.A.T., Perret, N., Prescott, J.R., Wyrwoll, K.-H., 1998. "Hydrologic changes in monsoonal climates of the last glacial cycle: stratigraphy and luminescence dating of Lake Woods, N.T. Australia." *Paleoclimates* 3, 179-207.

Bowler, J.M., Wyrwoll, K.-H., Lu, Y., 2001. "Variations of the northwest Australia summer monsoon over the last 300,000 years: The paleohydrological record of the Gregory (Mulan) Lakes system." *Quaternary International* 82-85, 63-80.

Boyle, J.F., Chiverrell, R.C., Schillereff, D., 2015. "Approaches to Water Content Correction and Calibration for μXRF Core Scanning: Comparing X-ray Scattering with Simple Regression of Elemental Concentrations", in: Croudace, I.W., Rothwell, R.G. (Eds.), Micro-XRF Studies of Sediment Cores, Developments in Paleoenvironmental Research. Springer Science and Business Media, Dordrecht.

Brennan, B.J., 2003. "Beta doses to spherical grains." *Radiation Measurements* 37, 299-303.

Brill, D., Klasen, N., Jankaew, K., Brückner, H., Kelletat, D., Scheffers, A., Scheffers, S., 2012. "Local inundation distances and regional tsunami recurrence in the Indian Ocean inferred from luminescence dating of sandy deposits in Thailand." *Natural Hazards and Earth System Sciences* 12, 2177-2192.

Brock, F., Higham, T., Ditchfield, P., Ramsey, C.B., 2010. "Current Pretreatment Methods for AMS Radiocarbon Dating at the Oxford Radiocarbon Accelerator Unit (ORAU)." *Radiocarbon* 52, 103-112.

Brock, F., Lee, S., Housley, R.A., Ramsey, B., 2011. "Variation in the radiocarbon age of different fractions of peat: A case study from Ahrenshöft, northern Germany." *Quarternary Geochronology* 6, 550–555.

Bronk-Ramsey, C., 2009. "Bayesian Analysis of Radiocarbon Dates." *Radiocarbon* 51, 337-360.

Bronk-Ramsey, C., Lee, S., 2013. "Recent and Planned Developments of the Program OxCal." *Radiocarbon* 55, 720-730.

Brumsack, H.-J., 2006. "The trace metal content of recent organic carbon-rich sediments: Implications for Cretaceous black shale formation." *Palaeogeography, Palaeoclimatology, Palaeoecology* 232, 344-361.

Burrows, M.A., Heijnis, H., Gadd, P., Haberle, S.G., 2016. "A new late Quaternary palaeohydrological record from the humid tropics of northeastern Australia." *Palaeogeography, Palaeoclimatology, Palaeoecology* 451, 164-182.

Cadd, H., Tibby, J., Barr, C., Tyler, J., Unger, L., Leng, M., Marshall, J., McGregor, G., Lewis, R., Arnold, L., Lewis, T., Baldock, J., 2018. "Development of a southern hemisphere subtropical wetland (Welsby Lagoon, south-east Queensland, Australia) through the last glacial cycle." *Quaternary Science Reviews* 202, 53-65.

Clark, M., Hounslow, M., 2009. "CPLSlot Version 2.4b", Monash University, Victoria, Australia.

Cohen, T.J., Jansen, J.D., Gliganic, L.A., Larsen, J.R., Nanson, G.C., May, J.-H., Jones, B.G., Price, D.M., 2015. "Hydrological transformation coincided with megafaunal extinction in central Australia." *Geology* 43, 195-199.

Colhoun, E.A., Pola, J.S., Barton, C.E., Heijnis, H., 1999. "Late Pleistocene vegetation and climate history of Lake Selina, western Tasmania." *Quaternary International* 57–58, 5–23.

Croudace, I.W., Rindby, A., Rothwell, R.G., 2006. "ITRAX: description and evaluation of a new multi-function X-ray core scanner." *Geological Society, London, Special Publications* 267, 51.

Croudace, I.W., Rothwell, R.G., 2015. "Micro-XRF Studies of Sediment Cores: Applications of a non-destructive tool for the environmental sciences". Springer, New York.

Cuven, S., Francus, P., Lamoureux, S., 2010. "Estimation of grain-size variability with micro X-ray fluorescence in laminated lacustrine sediments, cape bounty, Canadian High Arctic." *Journal of Paleoliminology* 44, 803–817.

Davies, G.M., Gray, A., Rein, G., Legg, C.J., 2013. "Peat consumption and carbon loss due to smouldering wildfire in a temperate peatland." *Forest Ecology and Management* 308, 169-177.

De Deckker, P., Arnold, L.J., van der Kaars, S., Bayon, G., Stuut, J.-B.W., Perner, K., Lopes dos Santos, R., Uemura, R., Demuro, M., 2019. "Marine Isotope Stage 4 in Australasia: A full glacial culminating 65,000 years ago – Global connections and implications for human dispersal." *Quaternary Science Reviews* 204, 187-207.

Demuro, M., Arnold, L.J., Froese, D.G., Roberts, R.G., 2013. "OSL dating of loess deposits bracketing Sheep Creek tephra beds, northwest Canada: Dim and problematic single-grain OSL characteristics and their effect on multi-grain age estimates." *Quaternary Geochronology* 15, 67-87.

Demuro, M., Arnold, L.J., Parés, J.M., Sala, R., 2015. "Extended-range luminescence chronologies suggest potentially complex bone accumulation histories at the Early-to-Middle Pleistocene palaeontological site of Huéscar-1 (Guadix-Baza basin, Spain)." *Quaternary International* 389, 191-212.

Donders, T.H., Wagner, F., Visscher, H., 2006. "Late Pleistocene and Holocene subtropical vegetation dynamics recorded in perched lake deposits on Fraser Island, Queensland, Australia." *Palaeogeography, Palaeoclimatology, Palaeoecology* 241, 417-439.

Edney, P.A., Kershaw, A.P., De Deckker, P., 1990. "A late Pleistocene and Holocene vegetation and environmental record from Lake Wangoom, Western Plains of Victoria, Australia." *Palaeogeography, Palaeoclimatology, Palaeoecology* 80, 325-343.

Eggenberger, S., Gobet, E., Leeuwen, J., Schwörer, C., Knaap, W., Dobben, H., Vogel, H., Tinner, W., Rambeau, C., 2018. "Millennial multi-proxy reconstruction of oasis dynamics in Jordan, by the Dead Sea." *The Journal of Quaternary Plant Ecology, Palaeoclimate and Ancient Agriculture - Official Organ of the International Work Group for Palaeoethnobotany* 27, 649-664.

Elderfield, H., Ferretti, P., Greaves, M., Crowhurst, S., McCave, I.N., Hodell, D., Piotrowski, A.M., 2012. "Evolution of Ocean Temperature and Ice Volume Through the Mid-Pleistocene Climate Transition." *Science* 337, 704-709.

Falster, G., Tyler, J., Grant, K., Tibby, J., Turney, C., Löhr, S., Jacobsen, G., Kershaw, A.P., 2018. "Millennial-scale variability in south-east Australian hydroclimate between 30,000 and 10,000 years ago." *Quaternary Science Reviews* 192, 106-122.

Field, E., Tyler, J., Gadd, P.S., Moss, P., McGowan, H., Marx, S., 2018. "Coherent patterns of environmental change at multiple organic spring sites in northwest Australia: Evidence of Indonesian-Australian summer monsoon variability over the last 14,500 years." *Quaternary Science Reviews* 196, 193-216.

Foerster, V., Deocampo, D.M., Asrat, A., Gunter, C., Junginger, A., Kramer, K.H., Stroncik, N.A., Trauth, M.H., 2018. "Towards an understanding of climate proxy formation in the

Chew Bahir basin, southern Ethiopian Rift." *Palaeogeography, Palaeoclimatology, Palaeoecology* 501, 111.

Fu, X., Cohen, T.J., Arnold, L.J., 2017. "Extending the record of lacustrine phases beyond the last interglacial for Lake Eyre in central Australia using luminescence dating." *Quaternary Science Reviews* 162, 88-110.

Galbraith, R.F., Roberts, R.G., Laslett, G.M., Yoshida, H., Olley, J.M., 1999. "Optical dating of single and multiple grains of quartz from Jinmium Rock Shelter, northern Australia: Part 1, experimental design and statistical models." *Archaeometry* 41, 339-364.

Grant, K., Rohling, E., Bar-Matthews, M., Ayalon, A., Medina-Elizalde, M., Ramsey, C.B., Satow, C., Roberts, A., 2012. "Rapid coupling between ice volume and polar temperature over the past 150,000 years." *Nature* 491, 744-747.

Grant, K.M., Rohling, E.J., Westerhold, T., Zabel, M., Heslop, D., Konijnendijk, T., Lourens, L., 2017. "A 3 million year index for North African humidity/aridity and the implication of potential pan-African Humid periods." *Quaternary Science Reviews* 171, 100-118.

Guérin, G., Mercier, N., Adamiec, G., 2011. "Dose-rate conversion factors: update." *Ancient TL* 29, 5-8.

Guyard, H., Chapron, E., St-Onge, G., Anselmetti, F.S., Arnaud, F., Magand, O., Francus, P., Mélières, M.-A., 2007. "High-altitude varve records of abrupt environmental changes and mining activity over the last 4000 years in the Western French Alps (Lake Bramant, Grandes Rousses Massif)." *Quaternary Science Reviews* 26, 2644-2660.

Hahn, A., Kliem, P., Oehlerich, M., Ohlendorf, C., Zolitschka, B., 2014. "Elemental composition of the Laguna Potrok Aike sediment sequence reveals paleoclimatic changes over the past 51 ka in southern Patagonia, Argentina." *Journal of Paleolimnology* 52, 349-366.

Harle, K.J., Heijnis, H., Chisari, R., Kershaw, A.P., Zoppi, U., Jacobsen, G., 2002. "A chronology for the long pollen record from Lake Wangoom, western Victoria (Australia) as derived from uranium/thorium disequilibrium dating." *Journal of Quaternary Science* 17, 707-720.

Harrison, S.P., Bartlein, P., 2012. "Records from the Past, Lessons for the Future: What the Palaeorecord Implies about Mechanisms of Global Change", in: Henderson-Sellers, A., McGuffie, K. (Eds.), The Future of the World's Climate. Elsevier Science, Oxford, pp. 403-436.

Heiri, O., Lotter, A., Lemcke, G., 2001. "Loss on ignition as a method for estimating organic and carbonate content in sediments: reproducibility and comparability of results." *Journal of Paleoliminology* 25, 101-110.

Hesse, P.P., McTainsh, G.H., 2003. "Australian dust deposits: modern processes and the Quaternary record." *Quaternary Science Reviews* 22, 2007-2035.

Hofmann, H., Newborn, D., Cartwright, I., Cendón, D.I., Raiber, M., 2019. "Groundwater mean residence time of a sub-tropical barrier sand island." *Hydrology and Earth System Science Discussions*, 1-32.

Hogg, A.G., Hua, Q., Blackwell, P.G., Niu, M., Buck, C.E., Heaton, T.J., Guilderson, T.P., Zimmerman, S.R.H., Palmer, J.G., Turney, C.S.M., Reimer, P.J., Reimer, R.W., 2013. "Shcal13 Southern Hemisphere calibration, 0-50,000 years cal BP." *Radiocarbon* 55, 1889-1903.

Ihaka, R., Gentleman, R., 2016. "R statistical computing program", 3.3.1 ed. The R foundation for Statistical Computing.

Jouve, G., Francus, P., Lamoureux, S., Provencher-Nolet, L., Hahn, A., Haberzettl, T., Fortin, D., Nuttin, L., 2013. "Microsedimentological characterization using image analysis and μ-XRF as indicators of sedimentary processes and climate changes during Lateglacial at Laguna Potrok Aike, Santa Cruz, Argentina." *Quaternary Science Reviews* 71, 191-204.

Jury, M.R., Valentine, H.R., Lutjeharms, J.R., 1993. "Influence of the Agulhas Current on summer rainfall along the southeast coast of South Africa." *Journal of Applied Meteorology* 32, 1282-1287.

Kawagata, S., 2001. "Tasman Front shifts and associated paleoceanographic changes during the last 250,000 years: foraminiferal evidence from the Lord Howe Rise." *Marine Micropaleontology* 41, 167-191.

Kemp, C.W., Tibby, J., Arnold, L.J., Barr, C., 2019. "Australian hydroclimate during Marine Isotope Stage 3: A synthesis and review." *Quaternary Science Reviews* 204, 94-104.

Kemp, C.W., Tibby, J., Arnold, L.J., Barr, C., submitted. "Subtropical climate, fire and vegetation dynamics on North Stradbroke Island (eastern Australia) during the last three interglacials." *Journal of Quaternary Science*.

Kershaw, A.P., Bretherton, S.C., van der Kaars, S., 2007a. "A complete pollen record of the last 230 ka from Lynch's Crater, north-eastern Australia." *Palaeogeography, Palaeoclimatology, Palaeoecology* 251, 23-45.

Kershaw, A.P., McKenzie, G.M., Porch, N., Roberts, R.G., Brown, J., Heijnis, H., Orr, M.L., Jacobsen, G., Newall, P.R., 2007b. "A high-resolution record of vegetation and climate through the last glacial cycles from Caledonia Fen, southeastern highlands of Australia." *Journal of Quaternary Science* 22, 481-500.

Kershaw, P., Moss, P., Van Der Kaars, S., 2003. "Causes and consequences of long-term climatic variability on the Australian continent." *Freshwater Biology* 48, 1274-1283.

Kienel, U., Kirillin, G., Brademann, B., Plessen, B., Lampe, R., Brauer, A., 2017. "Effects of spring warming and mixing duration on diatom deposition in deep Tiefer See, NE Germany." *Journal of Paleolimnology* 57, 37-49.

Killick, R., Eckley, I.A., 2014. "Changepoint: An R Package for Changepoint Analysis." *Journal of Statistical Software* 1.

Köhler, P., Nehrbass-Ahles, C., Schmitt, J., Stocker, T.F., Fischer, H., 2017. "Continuous record of the atmospheric greenhouse gas carbon dioxide (CO_2), raw data", In supplement to: Köhler, P et al. (2017): A 156 kyr smoothed history of the atmospheric greenhouse gases CO_2, CH_4, and N_2O and their radiative forcing. Earth System Science Data, 9(1), 363-387, https://doi.org/10.5194/essd-9-363-2017. PANGAEA.

Kylander, M.E., Ampe, L., Wohlfarth, B., Veres, D., 2011. "High-resolution X-ray fluorescence core scanning analysis of Les Echets (France) sedimentary sequence: new insights from chemical proxies." *Journal of Quaternary Science* 26, 109-117.

Lamy, F., Gersonde, R., Winckler, G., Esper, O., Jaeschke, A., Kuhn, G., Ullermann, J., Martinez-Garcia, A., Lambert, F., Kilian, R., 2014. "Increased dust deposition in the Pacific Southern Ocean during glacial periods." *Science* 343, 403-407.

Leach, L.M., 2011. "Hydrology and physical setting of North Stradbroke Island." *Proceedings of the Royal Society of Queensland* 117, 21-46.

Lisiecki, L.E., Raymo, M.E., 2005. "A Pliocene-Pleistocene stack of 57 globally distributed benthic $\delta^{18}O$ records." *Paleoceanography* 20.

Lo, L., Chang, S.-P., Wei, K.-Y., Lee, S.-Y., Ou, T.-H., Chen, Y.-C., Chuang, C.-K., Mii, H.-S., Burr, G.S., Chen, M.-T., Tung, Y.-H., Tsai, M.-C., Hodell, D.A., Shen, C.-C., 2017. "Nonlinear climatic sensitivity to greenhouse gases over past 4 glacial/interglacial cycles." *Scientific reports* 7, 4626.

Longmore, M.E., 1997. "The mid-Holocene "Dry" Anomaly on the Mid-Eastern Coast of Australia: Calibration of Palaeowater Depth as a Surrogate for Effective Precipitation using Sedimentary Loss on Ignition in the Perched Lake Sediments of Fraser island, Queensland." *Palaeoclimates* 4.

Löwemark, L., Chen, H.F., Yang, T.N., Kylander, M., Yu, E.F., Hsu, Y.W., Lee, T.Q., Song, S.R., Jarvis, S., 2011. "Normalizing XRF-scanner data: a cautionary note on the interpretation of high-resolution records from organic-rich lakes." *Journal of Asian Earth Sciences* 40, 1250–1256.

Lukenbach, M.C., Hokanson, K.J., Moore, P.A., Devito, K.J., Kettridge, N., Thompson, D.K., Wotton, B.M., Petrone, R.M., Waddington, J.M., 2015. "Hydrological controls on deep burning in a northern forested peatland." *Hydrological Processes* 29, 4114-4124.

Mackenzie, L., Heijnis, H., Gadd, P., Moss, P., Shulmeister, J., 2017. "Geochemical investigation of the South Wellesley Island wetlands: Insight into wetland development during the Holocene in tropical northern Australia." *The Holocene* 27, 566-578.

Maroulis, J.C., Nanson, G.C., Price, D.M., Pietsch, T., 2007. "Aeolian–fluvial interaction and climate change: source-bordering dune development over the past ~100 ka on Cooper Creek, central Australia." *Quaternary Science Reviews* 26, 386-404.

Marshall, M.H., Lamb, H.F., Huws, D., Davies, S.J., Bates, R., Bloemendal, J., Boyle, J., Leng, M.J., Umer, M., Bryant, C., 2011. "Late Pleistocene and Holocene drought events at Lake Tana, the source of the Blue Nile." *Global and Planetary Change* 78, 147-161.

Martin, L., Mooney, S., Goff, J., 2014. "Coastal wetlands reveal a non-synchronous island response to sea-level change and a palaeostorm record from 5.5 kyr to present." *The Holocene* 24, 569-580.

Martinez, J.I., De Deckker, P., Barrows, T.T., 2002. "Palaeoceanography of the western Pacific warm pool during the last glacial maximum: long-term climatic monitoring of the maritime continent.", in: Kershaw, P., Bruno, D., Tapper, N., Penny, D., Brown, J. (Eds.), Bridging Wallace's Line: The environmental and cultural history and dynamics of the SE-Asian-Australian Region. Advanced Geoecology, Reiskirchen, Germany, pp. 147-172.

McGowan, H.A., Petherick, L.M., Kamber, B.S., 2008. "Aeolian sedimentation and climate variability during the late Quaternary in southeast Queensland, Australia." *Palaeogeography, Palaeoclimatology, Palaeoecology* 265, 171-181.

Mejdahl, V., 1979. "Thermoluminescence Dating: Beta-Dose Attenuation in Quartz Grains." *Archaeometry* 21, 61-72.

Miller, G.H., Fogel, M.L., Magee, J.W., Gagan, M.K., 2016. "Disentangling the impacts of climate and human colonization on the flora and fauna of the Australian arid zone over the past 100 ka using stable isotopes in avian eggshell." *Quaternary Science Reviews* 151, 27-57.

Moss, P.T., Kershaw, A.P., 2007. "A late Quaternary marine palynological record (oxygen isotope stages 1 to 7) for the humid tropics of northeastern Australia based on ODP Site 820." *Palaeogeography, Palaeoclimatology, Palaeoecology* 251, 4-22.

Moss, P.T., Tibby, J., Petherick, L., McGowan, H., Barr, C., 2013. "Late Quaternary vegetation history of North Stradbroke Island, Queensland, eastern Australia." *Quaternary Science Reviews* 74, 257-272.

Nanson, G.C., Price, D.M., Jones, B.G., Maroulis, J.C., Coleman, M., Bowman, H., Cohen, T.J., Pietsch, T.J., Larsen, J.R., 2008. "Alluvial evidence for major climate and flow regime changes during the middle and late Quaternary in eastern central Australia." *Geomorphology* 101, 109-129.

Neal, R., Stock, E., 1986. "Pleistocene occupation in the south-east Queensland coastal region." *Nature* 323, 618-621.

Nilsson, M., Klarqvist, M., Bohlin, E., Possnert, G., 2001. "Variation in ^{14}C age of macrofossils and different fractions of minute peat samples dated by AMS." *The Holocene* 11, 579–586.

Nkwinkwa Njouodo, A.S., Koseki, S., Keenlyside, N., Rouault, M., 2018. "Atmospheric signature of the Agulhas Current." *Geophysical Research Letters* 45, 5185-5193.

Oksanen, J., Blanchet, F.G., Friendly, M., Kindt, R., Legendre, P., McGlinn, D., Minchin, P.R., R. B. O'Hara, Simpson, G.L., Solymos, P., Stevens, M.H.H., Szoecs, E., Wagner, H., 2018. "Community Ecology Package", 2.5-2 ed, pp. Ordination methods, diversity analysis and other functions for community and vegetation ecologists.

Parrenin, F., Masson-Delmotte, V., Köhler, P., Raynaud, D., Paillard, D., Schwander, J., Barbante, C., Landais, A., Wegner, A., Jouzel, J., 2013. "Antarctic Temperature Stack (ATS) from five different ice cores (EDC, Vostok, Dome Fuji, TALDICE, and EDML)", In supplement to: Parrenin, F et al. (2013): Synchronous change of atmospheric CO_2 and Antarctic temperature during the last deglacial warming. Science, 339(6123), 1060-1063, https://doi.org/10.1126/science.1226368.

Patton, N.R., Ellerton, D., Shulmeister, J., 2019. "High resolution remapping of the coastal dune fields of south east Queensland, Australia: a morphometric approach." *Journal of Maps* 15, 578-589.

Pelejero, C., Calvo, E., Barrows, T.T., Logan, G.A., De Deckker, P., 2006. "South Tasman Sea alkenone palaeothermometry over the last four glacial/interglacial cycles." *Marine Geology* 230, 73-86.

Petherick, L., Bostock, H., Cohen, T.J., Fitzsimmons, K., Tibby, J., Fletcher, M.-S., Moss, P., Reeves, J., Mooney, S., Barrows, T., Kemp, J., Jansen, J., Nanson, G., Dosseto, A., 2013. "Climatic records over the past 30 ka from temperate Australia – a synthesis from the Oz-INTIMATE workgroup." *Quaternary Science Reviews* 74, 58-77.

Petherick, L., McGowan, H., Moss, P., 2008. "Climate variability during the Last Glacial Maximum in eastern Australia: evidence of two stadials?" *Journal of Quaternary Science* 23, 787-802.

Petherick, L.M., McGowan, H.A., Kamber, B.S., 2009. "Reconstructing transport pathways for late Quaternary dust from eastern Australia using the composition of trace elements of long traveled dusts." *Geomorphology* 105, 67-79.

Petherick, L.M., Moss, P.T., McGowan, H.A., 2017. "An extended Last Glacial Maximum in subtropical Australia." *Quaternary International* 432, 1-12.

Pleskot, K., Tjallingii, R., Makohonienko, M., Nowaczyk, N., Szczuciński, W., 2018. "Holocene paleohydrological reconstruction of Lake Strzeszyńskie (western Poland) and its implications for the central European climatic transition zone." *Journal of Paleolimnology* 59, 443-459.

Prescott, J.R., Hutton, J.T., 1994. "Cosmic ray contributions to dose rates for luminescence and ESR dating: Large depths and long-term time variations." *Radiation Measurements* 23, 497-500.

Profe, J., Neumann, L., Novothny, Á., Barta, G., Rolf, C., Frechen, M., Ohlendorf, C., Zolitschka, B., 2018. "Paleoenvironmental conditions and sedimentation dynamics in Central Europe inferred from geochemical data of the loess-paleosol sequence at Süttő (Hungary)." *Quaternary Science Reviews* 196, 21-37.

Rees-Jones, J., 1995. "Optical dating of young sediments using fine-grain quartz." *Ancient TL* 13, 914.

Rees-Jones, J., Tite, M.S., 1997. "Optical dating results for British archaeological sediments." *Archaeometry* 36, 177-187.

Rees, A.B.H., Cwynar, L.C., Fletcher, M.-S., 2015. "Southern Westerly Winds submit to the ENSO regime: A multiproxy paleohydrology record from Lake Dobson, Tasmania." *Quaternary Science Reviews* 126, 254-263.

Reeves, J.M., Barrows, T.T., Cohen, T.J., Kiem, A.S., Bostock, H.C., Fitzsimmons, K.E., Jansen, J.D., Kemp, J., Krause, C., Petherick, L., Phipps, S.J., Members, O.-I., 2013. "Climate variability over the last 35,000 years recorded in marine and terrestrial archives in the Australian region: an OZ-INTIMATE compilation." *Quaternary Science Reviews* 74, 21-34.

Roberts, H.M., Bryant, C.L., Huws, D.G., Lamb, H.F., 2018. "Generating long chronologies for lacustrine sediments using luminescence dating: a 250,000 year record from Lake Tana, Ethiopia." *Quaternary Science Reviews* 202, 66-77.

Sáez, A., Valero-Garcés, B.L., Giralt, S., Moreno, A., Bao, R., Pueyo, J.J., Hernández, A., Casas, D., 2009. "Glacial to Holocene climate changes in the SE Pacific. The Raraku Lake sedimentary record (Easter Island, 27°S)." *Quaternary Science Reviews* 28, 2743-2759.

Smith, S.M., Newman, S., Garrett, P.B., Leeds, J.A., 2001. "Differential Effects of Surface and Peat Fire on Soil Constituents in a Degraded Wetland of the Northern Florida Everglades." *Journal of Environmental Quality* 30, 1998-2005.

Stephens, T., Augustinus, P., Rip, B., Gadd, P., Zawadski, A., 2018. "Managing land-use effects on Northland dune lakes: lessons from the past." *New Zealand Journal of Marine and Freshwater Research*, 1-21.

Striberger, J., Björck, S., Ingólfsson, Ó., Kjær, K.H., Snowball, I.A.N., Uvo, C.B., 2010. "Climate variability and glacial processes in eastern Iceland during the past 700 years based on varved lake sediments." *Boreas* 40, 28-45.

Tachikawa, K., Timmermann, A., Vidal, L., Sonzogni, C., Timm, O.E., 2014. "CO_2 radiative forcing and Intertropical Convergence Zone influences on western Pacific warm pool climate over the past 400 ka." *Quaternary Science Reviews* 86, 24-34.

Team-RStudio, 2015. "RStudio: Integrated Development for R.". RStudio, Inc, Boston, MA.

Tibby, J., Barr, C., Marshall, J.C., Mgregor, G.B., Moss, P.T., Arnold, L.J., Page, T.J., Questiaux, D., Olley, J., Kemp, J., Spooner, N., Petherick, L., Penny, D., Mooney, S., Moss, E., 2017. "Persistence of wetlands on North Stradbroke Island (south-east Queensland, Australia) during the last glacial cycle: implications for Quaternary science and biogeography." *Journal of Quaternary Science* 32, 770-781.

Turetsky, M.R., Manning, S.W., Wieder, R.K., 2004. "Dating recent peat deposits." *Wetlands* 24, 324-356.

Turner, J.N., Holmes, N., Davis, S.R., Leng, M.J., Langdon, C., Scaife, R.G., 2015. "A multiproxy (micro-XRF, pollen, chironomid and stable isotope) lake sediment record for the Lateglacial to Holocene transition from Thomastown Bog, Ireland." *Journal of Quaternary Science* 30, 514-528.

Turney, C.S.M., Jones, R.T., 2010. "Does the Agulhas Current amplify global temperatures during super-interglacials?" *Journal of Quaternary Science* 25, 839-843.

van der Bilt, W.G.M., Bakke, J., Vasskog, K., D'Andrea, W.J., Bradley, R.S., Ólafsdóttir, S., 2015. "Reconstruction of glacier variability from lake sediments reveals dynamic Holocene climate in Svalbard." *Quaternary Science Reviews* 126, 201-218.

van der Kaars, S., Miller, G.H., Turney, C.S.M., Cook, E.J., Nürnberg, D., Schönfeld, J., Kershaw, A.P., Lehman, S.J., 2017. "Humans rather than climate the primary cause of Pleistocene megafaunal extinction in Australia." *Nature Communications* 8, 1-7.

Vegas-Vilarrúbia, T., Corella, J.P., Pérez-Zanón, N., Buchaca, T., Trapote, M.C., López, P., Sigró, J., Rull, V., 2018. "Historical shifts in oxygenation regime as recorded in the laminated sediments of lake Montcortès (Central Pyrenees) support hypoxia as a continental-scale phenomenon." *Science of The Total Environment* 612, 1577-1592.

Walker, J., Lees, B., Olley, J., Thompson, C., 2018. "Dating the Cooloola coastal dunes of South-Eastern Queensland, Australia." *Marine Geology* 398, 73-85.

Weltje, G.J., Bloemsma, M.R., Tjallingii, R., Heslop, D., Röhl, U., Croudace, I.W., 2015. "Prediction of Geochemical Composition from XRF Core Scanner Data: A New Multivariate Approach Including Automatic Selection of Calibration Samples and Quantification of Uncertainties", in: Croudace, I.W., Rothwell, R.G. (Eds.), Micro-XRF Studies of Sediment Cores: Applications of a non-destructive tool for the environmental sciences. Springer Netherlands, Dordrecht, pp. 507-534.

Weltje, G.J., Tjallingii, R., 2008. "Calibration of XRF core scanners for quantitative geochemical logging of sediment cores: Theory and application." *Earth and Planetary Science Letters* 274, 423-438.

Woltering, M., Atahan, P., Grice, K., Heijnis, H., Taffs, K., Dodson, J., 2014. "Glacial and Holocene terrestrial temperature variability in subtropical east Australia: branched GDGT

distributions in a sediment core from Lake McKenzie." *Quaternary Research* 82, 132–145.

Woodward, C.A., Gadd, P.S., 2019. "The potential power and pitfalls of using the X-ray fluorescence molybdenum incoherent: Coherent scattering ratio as a proxy for sediment organic content." *Quaternary International* 514, 30-43.

Woodward, C.A., Slee, A., Gadd, P., Zawadzki, A., Hamze, H., Parmar, A., Zahra, D., 2018. "The role of earthquakes and climate in the formation of diamictic sediments in a New Zealand mountain lake." *Quaternary International* 470, 130-147.

Wright, H.E.J., 1967. "A square-rod piston sampler for lake sediments." *The Journal of Sedimentary Petrology* 37, 975–976.

Zhang, S., Li, T., Chang, F., Yu, Z., Xiong, Z., Wang, H., 2017. "Correspondence between the ENSO-like state and glacial-interglacial condition during the past 360 kyr." *Chinese Journal of Oceanology and Limnology* 35, 1018-1031.

Chapter 4 – Climate, fire, and vegetation history from subtropical North Stradbroke Island (Minjerribah), eastern Australia, during the last three interglacials

4.1 Statement of Authorship

Title of Paper	Climate, fire, and vegetation history from subtropical North Stradbroke Island (Minjerribah), eastern Australia, during the last three interglacials
Publication Status	☐ Published ☐ Accepted for Publication ☑ Submitted for Publication ☐ Unpublished and Unsubmitted w ork w ritten in manuscript style
Publication Details	Kemp, C.W., Tibby, J., Arnold, L.J., Barr, C., in prep. Climate, fire, and vegetation history from subtropical North Stradbroke Island Minjerribah), eastern Australia, during the last three interglacials. Journal of Quaternary Science.

4.1.1 Principal Author

Name of Principal Author (Candidate)	Christopher Wilde Kemp		
Contribution to the Paper	Research, sampling and material preparation, imaging and analysis, maintaining a pollen identification database, writing the manuscript and corresponding author.		
Overall percentage (%)	90		
Certification:	This paper reports on original research I conducted during the period of my Higher Degree by Research candidature and is not subject to any obligations or contractual agreements with a third party that would constrain its inclusion in this thesis. I am the primary author of this paper.		
Signature		Date	31-3-2020

4.1.2 Co-Author Contributions

By signing the Statement of Authorship, each author certifies that:

i. the candidate's stated contribution to the publication is accurate (as detailed above);
ii. permission is granted for the candidate in include the publication in the thesis; and
iii. the sum of all co-author contributions is equal to 100% less the candidate's stated contribution.

Name of Co-Author	John Tibby		
Contribution to the Paper	Suggestions for and assistance editing the manuscript structure, research direction, assistance with the methods and discussion, as well as editing, correcting and formatting of the manuscript.		
Signature		Date	31/03/2020

Name of Co-Author	Cameron Barr		
Contribution to the Paper	Assistance with palaeoclimate interpretation, help with analysis methods and discussion of findings as well as editing, correcting and formatting of the manuscript.		
Signature		Date	31/03/2020

Name of Co-Author	Lee Arnold		
Contribution to the Paper	Help with discussion of hiatuses in the age/depth model as well as editing, correcting and formatting of the manuscript.		
Signature		Date	1/4/2020

4.2 Preamble

The inorganic record of regional climates presented in Chapter 3 relies on the assumption that vegetation density on North Stradbroke Island was driven by changes in moisture availability. Pollen and charcoal studies were undertaken to infer vegetation assemblages and fire frequency during past interglacial complexes as well as to address other possible drivers of vegetation density (e.g. fire frequency, vegetation shift from closed to open woodland, temperature etc.), and to assess findings of a comparatively dry Holocene. Chapter 4 details the methods used, construction and interpretation of these records and includes discussion of regional climate drivers based on record comparison with other Australian recent interglacial climate records.

This chapter was submitted to the *Journal of Quaternary Science* in December 2019 as:

Kemp, C.W., Tibby, J., Arnold, L.J., Barr, C. (in prep) "Climate, fire, and vegetation history from subtropical North Stradbroke Island (Minjerribah), eastern Australia during the last three interglacials".

The manuscript was resubmitted with changes after peer review in May, and again in October 2020.

I have re-formatted the resubmitted article as a thesis chapter with only minor changes to the original text. However, notation associated with figures, tables and equations has changed, being instead prefaced by the chapter number, e.g. Figure 1 is now Figure 4.1. The supplementary material associated with the submitted work is included in this thesis as Appendix C.

4.3 Abstract

Records of Australian palaeoclimate beyond the last glacial cycle are rare, limiting detailed analysis of long-term climate trends and associated ecosystem responses. This study analyses a discontinuous pollen and charcoal record from Fern Gully Lagoon, North Stradbroke Island (Minjerribah), subtropical Queensland, Australia, which covers much of the last ~210 thousand years. Climate variation is inferred from changes in vegetation, while analysis of micro- and macro-charcoal is used to infer fire activity. Vegetation assemblages consist of ~40%

rainforest taxa during marine isotope stage (MIS) 7a–c and early MIS 5. These are inferred to result from high rainfall in the Australian subtropics, which was also evident in north-east and central Australia. Three periods of increased fire activity at ~198, 188, and 182 ka were associated with a temporary reduction in rainforest taxa, and corresponding transient increase in sclerophyll taxa. The relative abundance of rainforest taxa on North Stradbroke Island declined to ~5% of the terrestrial sum in late MIS 2 and never recovered. Human impact after 21 ka likely supressed rainforest recovery to some extent. However, increased abundance of Poaceae and reduced representation of aquatic taxa indicates that the Holocene was the driest interglacial of the past ~210 kyr.

4.4 Introduction

Understanding both short- and long-term impacts of human-induced climate change requires both short duration records, such as from ecological monitoring, and long-term records of past environmental change as derived from palaeoenvironmental reconstructions (Fischer et al., 2018; Hoffman et al., 2017). Palaeoenvironmental inferences ideally need to draw from multiple, comparable periods of sea levels, atmospheric CO_2 concentrations and global temperatures to separate global or continental-scale climate change from regional or local climate drivers (Harrison and Bartlein, 2012). Global mean climates during several of the past interglacial complexes were comparable to Holocene climates, with the most recent being early marine isotope stage 5 (MIS 5e) and MIS 7a–c (Berger et al., 2015).

Relatively few Australian records cover or extend beyond the previous interglacial complex (MIS 5; 130–71 ka). The majority of records that span the earlier interglacial (MIS 7a–c; 215–191 ka) to the present indicate that there has been a gradual drying of Australia over the past 230 kyr (e.g. Fu et al., 2017; Kershaw et al., 2003; Moss and Kershaw, 2007). Central Australian lake-level reconstructions provide the clearest evidence of drying, with multiple lakes and streams in both southern central (Fu et al., 2017; Nanson et al., 2008), and northern central (Bowler et al., 2001) Australia recording declining discharge and lower lake levels. Drying is also recorded in pollen records from offshore tropical north-eastern Australia (Moss and Kershaw, 2007) and speleothem growth in south-eastern Australia (Ayliffe et al., 1998).

Australian hydroclimates are influenced by a range of drivers, the most important of which, in terms of its spatial coverage, is the El Niño Southern Oscillation (ENSO; Freund et al., 2017; Risbey et al., 2009). ENSO is a major driver of rainfall variability for ~70% of the continent, with the strongest influence in northern and, particularly, north-eastern Australia (Freund et al., 2017; Lu et al., 2018). ENSO has two phases: El Niño: linked to generally drier climates in Australia, and La Niña, linked to wetter climates (Freund et al., 2017). ENSO records from the West Pacific Warm Pool (WPWP) and eastern Pacific indicate that there were either more persistent or more frequent La Niña-dominated climates during late MIS 7a–c, early MIS 6 (Pena et al., 2008) and early MIS 5 (Pena et al., 2008; Tudhope et al., 2001), likely leading to increased Australian rainfall (Kershaw et al., 2007).

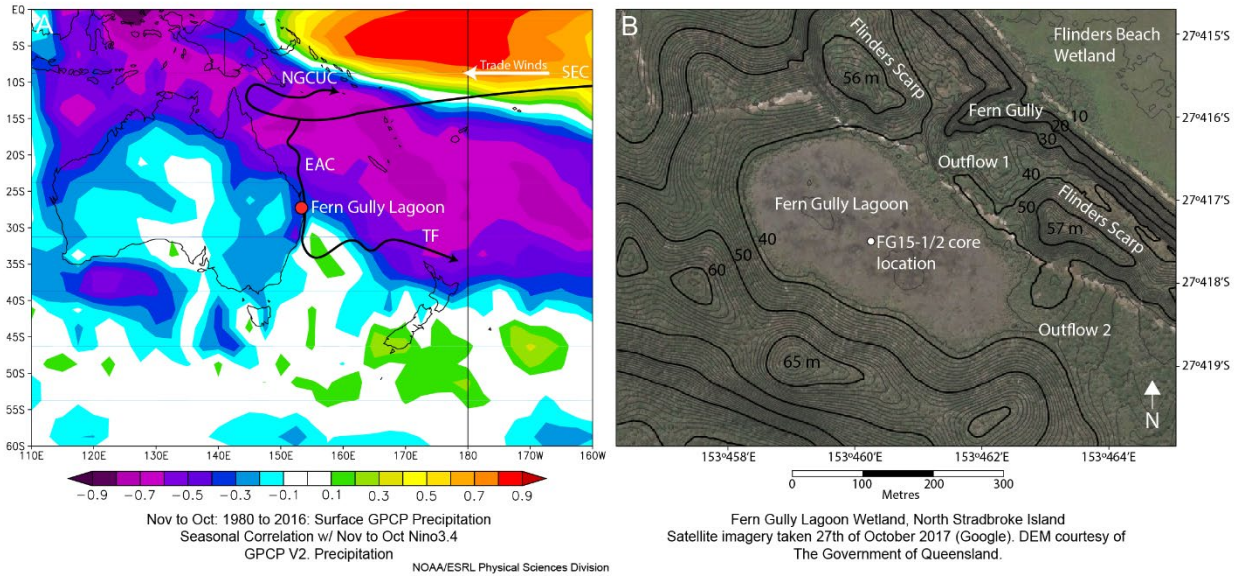

Figure 4.1: A: Mean surface Global Precipitation Climatology Project (GPCP) precipitation correlation with sea surface temperatures for the Nino 3.4 region between 1980 to 2016 (Nov–Oct: the local hydrological year), showing location of Fern Gully Lagoon, and the approximate modern routes of the East Australian Current (EAC), South Equatorial Current (SEC), Tasman Front (TF) and the New Guinea Coastal Undercurrent (NGCUC; Bostock et al. 2006), **B:** Topographic map with a satellite image of Fern Gully Lagoon, indicating the location of outflow points and the location of the core.

The Australian summer monsoon is a major source of rainfall for tropical northern and arid central Australia (Risbey et al., 2009). Above-average effective precipitation resulting from more southerly penetration of Australian summer monsoon rainfall was evident in northern and central Australia during early MIS 6, MIS 5e and MIS 5a (Bowler et al., 1998; Fu et al., 2017).

Precipitation on the north-eastern coast of Australia is strongly influenced by variability in the Southern Pacific Convergence Zone (SPCZ), which arises from low-level convergence between north-easterly trade winds and weaker westerly winds, and is in turn influenced by ENSO phases (Brown et al., 2020).

Fire is a key indicator, and consequence, of long-term climate variation in Australia (Kershaw et al., 2002). While climate exerts a direct influence on Australian fire regimes on annual timescales, this influence is modulated on longer timescales by climate-driven alterations to biomass (Mooney et al. 2011, Mariani et al., 2019). Records of microcharcoal flux have been used extensively in palaeoclimate studies, primarily as indicators of regional biomass burning (Whitlock and Larsen, 2001), with recent studies indicating that vegetation type and wind strength can also influence microcharcoal flux (e.g. Fletcher et al., 2014; Mariani et al., 2019). Human influence on regional fire regimes is also apparent in many Australian records (e.g. Kershaw et al., 2007; Fletcher et al. 2010), but is argued to have had little impact on biomass burning at a continental scale (Mooney et al. 2011).

In addition to fire, vegetation succession, due to progressive leaching of phosphorus and other nutrients from dune sequences, may be an important driver of vegetation change at glacial-interglacial time scales on sand islands such as Fraser Island and North Stradbroke Island (Longmore and Heijnis, 1999; Chen et al., 2015; Walker et al., 2018). It is argued that as dunes become phosphorus limited, vegetation progresses from mixed *Eucalyptus* and Casuarinaceae sclerophyll forests to vine forests, and low *Banksia* woodland on dunes formed before 200 ka (Chen et al., 2015).

Atmospheric CO_2 concentration may be an important driver of change vegetation at glacial-interglacial timescales, due to its direct influence on plant physiology (Prentice et al. 2017). A reduction in atmospheric CO_2 concentration results in 'drier' vegetation assemblages due to greater vegetation demand for water (Prentice et al. 2017; Dupont et al. 2019). While CO_2 concentrations were similar during early MIS 5 and the Holocene (~270 – 280 ppmv), allowing a more direct comparison of pollen-based climate inferences between these interglacials, CO_2 concentrations during MIS 7a–c and MIS 5a–c were on average ~20–30 ppmv lower (Bereiter et al. 2014).

Our study builds on a recent ~210 kyr climate record derived from sediment geochemistry at Fern Gully Lagoon (Chapter 3; Kemp et al., 2020). This study aims to:

i) Establish a record of terrestrial and wetland vegetation during past interglacial complexes and the Holocene, enabling qualitative comparison of interglacial temperatures and effective precipitation.
ii) ii) Investigate any relationship between local fire frequency and vegetation assemblages during recent interglacial complexes.

4.5 Study site

North Stradbroke Island (NSI), also known by its pre-European colonisation name Minjerribah, covers ~275.2 km^2, making NSI the world's second-largest sand island after Fraser Island. NSI and Fraser Island are part of the world's oldest and largest coastal dune system (Patton et al., 2019; Ellerton et al. 2020), which also includes the mainland Cooloola sand mass and Peregian sandhills, and Bribie and Moreton Islands (Walker et al., 2018; Patton et al., 2019). Subtropical NSI has a modern mean annual rainfall of approximately 1550 mm, a dry winter and a wet summer. The island has an average annual minimum of 15°C and maximum of 29°C (1997–2019; BOM, 2019), with ENSO as the key driver of rainfall variability at interannual timescales (Fig. 1a; Barr et al. 2019).

NSI vegetation is dominated by open *Eucalyptus* and Casuarinaceae sclerophyll forests, woodland and heath (Specht, 2011). Other vegetation types include dense low thick scrublands and dune grasses on the coastal dune sequences of the island's east coast, mangrove vegetation and saltmarsh on the sheltered western coast and an area of closed woodland in the north of the island where *Banksia* and *Callitris* are important elements (Walker et al. 1981; Specht, 2011).

Pollen records have been developed on NSI from Welsby Lagoon (~80 ka), Native Companion Lagoon (~47 ka), Blue Lake (~7.5 ka), Swallow Lagoon (~8.5 ka) and Tortoise Lagoon (~37 ka) (Petherick et al. 2008; Barr et al., 2013, Moss et al., 2013, Petherick et al. 2017; Cadd et al., 2018, Mariani et al., 2019). These records are likely to have been dominated by local vegetation, as a recent Australian study has shown that the dominant source area of pollen taxa with similar morphology to those from NSI was within a radius of ~10 km (Mariani et al., 2016).

Fern Gully Lagoon (Fig. 4.1b, 27.417°S, 153.460°E, 39 m ASL) is a ~0.8 km^2 perched, oligotrophic, palustrine wetland, situated in a shallow bowl of vegetated dunes near the north-western end of NSI (Leach, 2011). The wetland is sheltered by surrounding dunes, which reach up to ~26 m above the wetland surface. Fern Gully Lagoon has no notable overland inflow due to highly permeable surrounding sands. As such, available moisture is determined by direct rainfall. Fern Gully Lagoon has two above-ground overflow points, the most active of which drains the wetland via the eponymous Fern Gully through Flinders Scarp (Fig. 4.1b; Kemp et al. 2020).

A chronology for the Fern Gully Lagoon record has recently been established using a combination of six radiocarbon ages for the upper two metres, and 13 single-grain optically stimulated luminescence ages (Table C1, Chapter 3, Kemp et al., 2020). Age-depth modelling indicated four distinct sedimentation phases separated by hiatuses: a MIS 7a–c to early MIS 6 phase (209.3 ± 28.4 to 177.5 ± 25.4 ka), a late MIS 6 to late MIS 3 phase (155.2 ± 24.9 to 34.7 ± 14.5 ka), a mid-MIS 2 to early Holocene phase (20.9 ± 1.4 ka to 6.5 ± 5.6 ka) and a late Holocene phase (1.7 ± 1.0 ka to 0.45 ± 0.4 ka) (mean ± 2σ, Fig. C1, Table C1, Chapter 3, Kemp et al., 2020).

4.6 Methods

4.6.1 Extraction, pollen and microcharcoal

In April 2015, two nine metre cores were extracted from the approximate centre of Fern Gully Lagoon using the Bolivia modification of the Livingstone square-rod piston-corer (Myrbo and Wright, 2008). Further details are provided in Kemp et al. (2020). Pollen and microcharcoal samples of 1 cm^3 were collected every 10 cm for the top three meters of core, and every 20 cm for the remainder of the record. Sample preparation followed Faegri et al. (1989), modified to use heavy liquid instead of hydrofluoric acid to remove inorganic sediments after Field et al. (2018). A *Lycopodium* spore spike (Lund University, Batch 3862) was used to determine the absolute pollen and microcharcoal concentration, with a single tablet added to each 1 cm^3 sample during the dispersion phase.

Palynomorph counting for each of the 61 samples was limited to either 300 identified terrestrial pollen grains or two coverslips (44 x 22 mm; ~200 transects) whichever came first.

Microcharcoal particles between 10–50 µm were counted in conjunction with palynomorphs. A Zeiss Axio Scope A1 microscope, with 10x oculars and an EC Plan-NEOFLUAR 63x objective was used to identify palynomorphs and microcharcoal particles. Reference photographs of palynomorphs were taken using an Axiocam 105 colour 5-megapixel camera, using Zen Lite 2.6 software. Reference materials used for identification included the Australian National University (http://apsa.anu.edu.au/) and University of Newcastle (https://www.geo.arizona.edu/palynology/nsw/) collections. Taxa were identified to species level where possible. The term *Eucalyptus* is used in the broad sense (*sensu lato*) throughout this study. Major terrestrial habitat groups (rainforest, sclerophyll, and herb and grass taxa) are presented as relative proportions of the terrestrial pollen sum. *Melaleuca,* which grows on the surface of Fern Gully Lagoon, was classified as an aquatic taxon.

Tilia version 2.0.41 (Grimm, 2015) was used to calculate the relative abundances of taxa, both as proportion of all terrestrial grains, and as a proportion of all pollen grains in the case of aquatic taxa. Pollen zones were defined with constrained incremental sum of squares cluster analysis (CONISS; Grimm, 1987), using the terrestrial taxon subset. We applied principal component analysis to the pollen record using the vegan package for R (Oksanen et al., 2018) to determine shared variance between terrestrial taxa and identify indicator taxa, which could then be used to estimate changes in climate.

The distribution of modern taxa was used to assist in inferring climate from the Fern Gully Lagoon pollen record, after Moss and Kershaw (2000). Mean annual precipitation and mean annual air temperature envelopes were calculated using the Biodiversity and Climate Change Virtual Laboratory (http://www.bccvl.org.au/) with datasets of current taxon distributions from the Atlas of Living Australia (https://www.ala.org.au/).

4.6.2 Macrocharcoal

To derive the 930-sample macrocharcoal record, >250 µm fragments of charcoal were separated from weighed 1 cm^3 sediment samples at 1 cm increments. Following disaggregation in 5% H_2O_2 for seven days (Rhodes, 1998), washed samples were photographed on a white LED lightbox. Lightbox photos underwent image analysis using ImageJ software (v.1.8.0_66 (64-bit); Rasband, 2015), with red colour thresholding used to eliminate partially bleached non-charcoal

fragments. The area occluded by charcoal fragments was calculated after Mooney and Black (2003), calibrated to an in-picture scale. The total area of charcoal is expressed as mm^2 per dry gram of sediment (mm^2/g).

CharAnalysis was used to identify periods of increased fire activity in the macrocharcoal record, with the subset of samples for each sedimentation phase interpolated to the median age interval. The background charcoal input ($CHAR_{back}$) was determined using locally weighted scatterplot smoothing (LOWESS) and was set to 500 years. The signal to noise index (SNI) was set to determine important peaks above a threshold of three, following Kelly et al. (2011), and the fire return interval (FRI) was set with a 1000-year smoothing window. For further details of CharAnalysis see Higuera et al. (2009).

To determine whether charcoal records correlated with vegetation habitat groups (e.g. herbs and grasses; Fletcher et al., 2014; Mariani et al., 2019), or whether changes in fire frequency resulted in changes in vegetation assemblages or vice versa, macro- and micro-charcoal records were compared to the pollen record using shared sample points. Additionally, cross correlation between the pollen record and one, two, three, four and five cm leads and lags in the macrocharcoal record (~80–400 years, after Olchev et al. 2017) was used to identify any offset relationships between habitat types and fire frequency in the first sedimentation phase (~210–178 ka).

Time series analysis was performed on the macrocharcoal record between ~210 and ~178 ka (first sedimentation phase at ~80 years per sample) and between ~155 and ~35 ka (second sedimentation phase at ~1.1 kyr per sample) to identify the influence of any climate cycles on fire frequency. Monte Carlo Redfit (Schulz and Mudelsee, 2002) with a false alarm level of 99.8% (Thomson, 1990) and continuous wavelet transform analysis (Torrence and Compo, 1998) were used to identify cycle frequency and active duration.

4.7 Results

4.7.1 Pollen and Charcoal

One hundred and fifteen pollen and spore types were identified. *Pinus radiata* pollen was found on the core top and at 10 cm, indicating sedimentation above 11 cm took place following European settlement. While it was not possible to identify many grains to the genus level, it was possible to refine some inferences to family level and a few grains to the species level. For example, no Apiaceae grains were identified as belonging to *Hydrocotyle* and the Apiaceae sum is unlikely to include *Oenanthe japonica*. *Nothofagus moorei* and *Nothofagus cunninghamii* were not separated due to morphological similarities and are presented as *Nothofagus moorei/cunninghamii*. CONISS cluster analysis identified four pollen zones, with separations at 670, 288 and 165 cm (Fig. 4.2). The most pollen taxa during each sedimentation phase are listed in Table C2. Correlation statistics for relationships (including offset relationships) between macro- and micro-charcoal flux and vegetation types are listed in Table C3 and C4.

4.7.1.1 Zone FG1 – MIS 7a–c to MIS 6 transition (943 – 670 cm, ~210 – 197 ka):

Zone FG1 is dominated by Eucalyptus and Casuarinaceae. There is a gradual increase in the abundance of rainforest taxa, particularly *Araucaria* and *Agathis*, which reach around 20% of the terrestrial sum by 750 cm (~201 ka) from initial trace values, associated with a gradual decline in *Eucalyptus*. At 820 cm (~205 ka), there is a peak in the dominant aquatic taxa Cyperaceae, which gradually declines as the proportion of Restionaceae increases at the end of the zone. At the base of the core and at 880 cm (~209 and ~208 ka), there are two early peaks in fern spores, after which abundances stabilise at ~0.2% of the terrestrial sum. After two peaks at the beginning of the zone, microcharcoal abundance also declines to a low and largely constant level from 880 cm (~208 ka), while macrocharcoal peaks at 834 and 830 cm (~206 and ~205 ka).

4.7.1.2 Zone FG2 – Early MIS 6 (670 – 280 cm, ~197 – 178 ka):

Rainforest representation, driven by *Araucaria* and *Agathis*, peaks at 470 cm (~187 ka) at ~45% of the terrestrial sum, before gradually declining to the end of zone FG2. Zone FG2 contains the only major peaks of rainforest *Syzygium* and the dry-forest shrub Ericaceae at 580 and 460 cm, respectively (~192.5 and ~186.5 ka), where they account for ~12% and ~30% of the terrestrial sum. Restionaceae makes up a large part of the total pollen count, reaching ~65% of

the total sum in the early part of the zone, and peaking again at 370 cm (~182 ka), matching the timing of a Poaceae peak. There is an increase in charcoal flux from 587 cm (~192 ka), with coeval peaks at 482 cm (~188 ka).

4.7.1.3 Zone FG3 – Late MIS 6 to mid-MIS 3 (280 – 165 cm, ~155 – 35 ka):

After an initial high at ~274 cm (~142 ka), there is a gradual decline in rainforest taxa in zone FG3, but with highest values of the record for *Nothofagus moorei/cunninghamii*. The representation of sclerophyll vegetation increases gradually, driven by a ~30% increase in Casuarinaceae. Grass and herb taxa diversity is relatively high in zone FG3. The relative abundance of Poaceae increases gradually, reaching ~15% at 180 cm (~83 ka). Both micro- and macro-charcoal records have very low flux during this time.

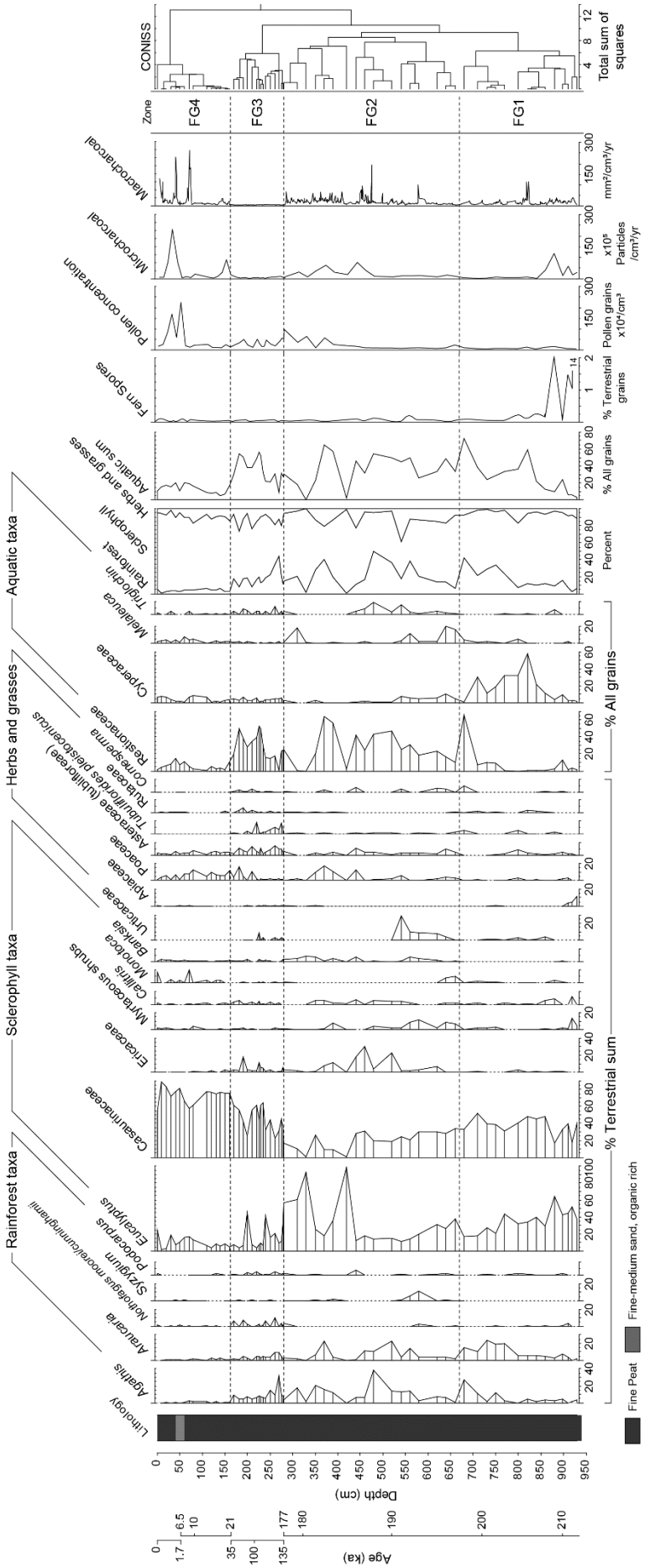

Figure 4.2: Fern Gully Lagoon lithology, pollen, spore and charcoal records.

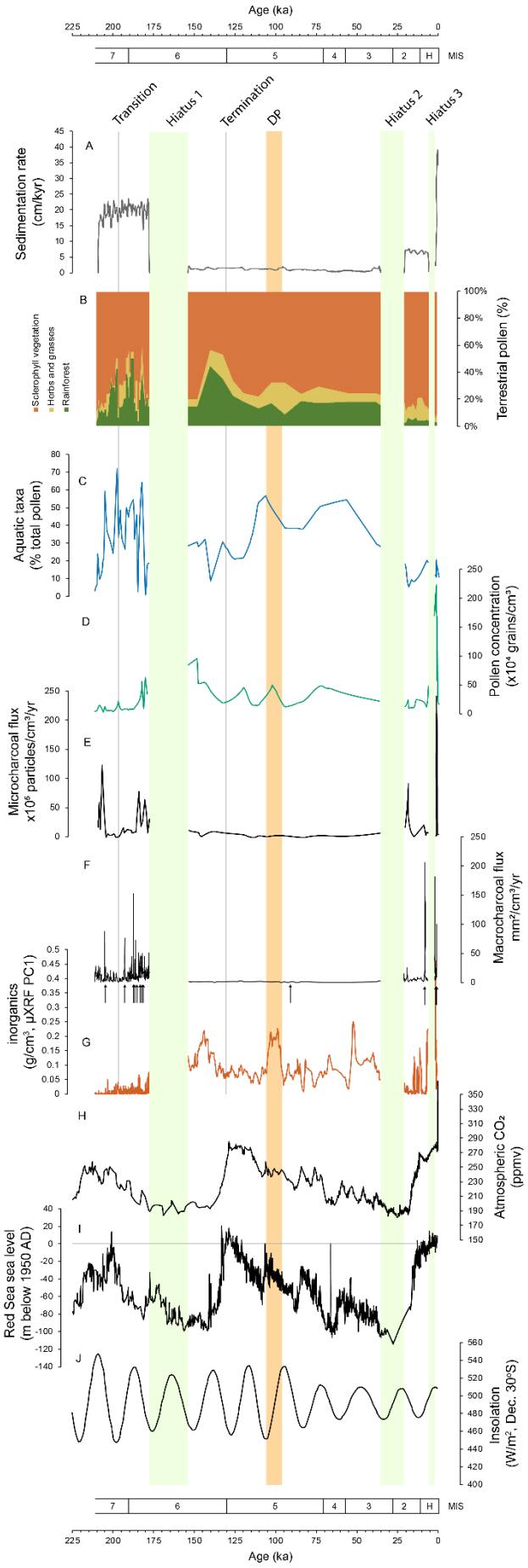

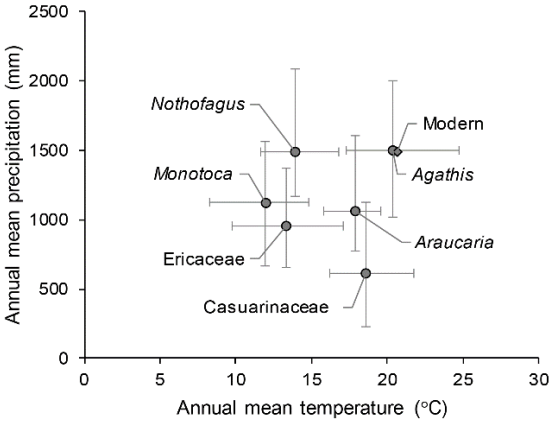

^ **Figure 4.3:** Modern mean annual precipitation and mean annual temperature distributions (10–90 percentile ranges) of selected indicator taxa (via PCA groupings, Fig. C2). *Nothofagus*: *Nothofagus moorei/cunninghamii.* Modern annual mean temperature and mean precipitation for Fern Gully Lagoon is based on the closest instrumental record to Fern Gully Lagoon: Point Lookout (1997 to 2019; BOM, 2019).

< **Figure 4.4**: Results plotted by age. **A:** Sedimentation rate as calculated from the Bayesian age-depth model. **B:** Relative abundances of terrestrial pollen. **C:** Relative abundance of aquatic taxa. **D:** Pollen concentration, in grains/cm^3. **E:** Microcharcoal flux (particles/cm^3/yr). **F:** Macrocharcoal flux (mm^2/cm^3/yr). Arrows indicate periods of increased fire activity identified by CharAnalysis. **G:** Inorganic content of Fern Gully Lagoon sediments via calibrated µXRF analysis (Chapter 3; Kemp et al., 2020). **H:** Antarctic composite CO_2 record (Bereiter et al., 2014). **I:** Global sea-level record via the Red Sea (Rohling et al., 2009). **J:** December mean insolation for 30 degrees south (Berger and Loutre, 1991). Vertical lines indicate the approximate timing of the MIS 7a–c to MIS 6 glacial transition as identified by CONISS and the approximate MIS 6 to MIS 5e glacial termination as determined by the mean age-depth model. DP.: mid-MIS 5 dry period.

4.7.1.4 Zone FG4 – late MIS 2 and the Holocene (165 – 0 cm, ~21 – 6.5, 1.7 – 0 ka):

Zone FG4 has largely constant proportions of sclerophyll, rainforest and herb taxa throughout. It has the lowest relative abundance of rainforest taxa at ~5%, and corresponding highest sclerophyll contribution at ~87%, dominated by Casuarinaceae (~65% terrestrial sum), with gradually increasing *Eucalyptus* values. Aquatic taxon abundance dips at 140 cm (~18.5 ka) before stabilising at ~20% of the total sum. There are coeval peaks in the micro- and macro-charcoal records at 150 cm (~19 ka), and at 73 cm (~7.8 ka).

4.7.2 Modern mean precipitation and temperature envelopes

The modern climate space distributions for six indicator taxa have a substantial overlap in both rainfall and temperature (Fig. 4.3). Modern precipitation climate envelopes ranged from relatively wet at ~1020–2000 mm/year for *Agathis* to relatively dry at between ~225–1125 mm/year for Casuarinaceae. Modern mean annual air temperature envelopes ranged from ~17.5–25°C for *Agathis* to ~8.5–15°C for *Monotoca*.

4.7.3 Fire frequency

CharAnalysis identified 14 periods of increased fire activity (Fig. 4.4f). Eight periods were identified during the earliest sedimentation phase (MIS 7a–c and early MIS 6; ~210–178 ka). The first period occurs during early MIS 7a–c at ~205 ka, after which burning occurs with increasing frequency through the glacial transition. Only a single period increased fire activity was identified during the second sedimentation phase, at ~95 ka, during MIS 5c. Low charcoal flux recorded during the second phase of sedimentation may, in part, result from normalisation by dry sediment mass, as there was an elevated level of inorganic sedimentation during that phase. There were five periods identified during the Holocene, with increased charcoal at ~1.5, 1.1 and 0.7 ka corresponding with three peaks of inorganic sedimentation (Fig. 4.4g).

Redfit and Wavelet analysis indicated that ~1.0 kyr biomass burning cycles were present between ~210 and ~178 ka (Fig. 4.5a). Wavelet analysis of the macrocharcoal record (Fig. 4.5b) also identified a ~5.2 kyr cycle during the first phase of sedimentation, and indicated possible fire regime change during the transition into MIS 6, with a hiatus in a ~2.5 kyr cycle. There was also a significant ~4.2 kyr biomass burning cycle during the longest sedimentation phase from late MIS 6 to late MIS 3 (~155–35 ka, Fig. C3).

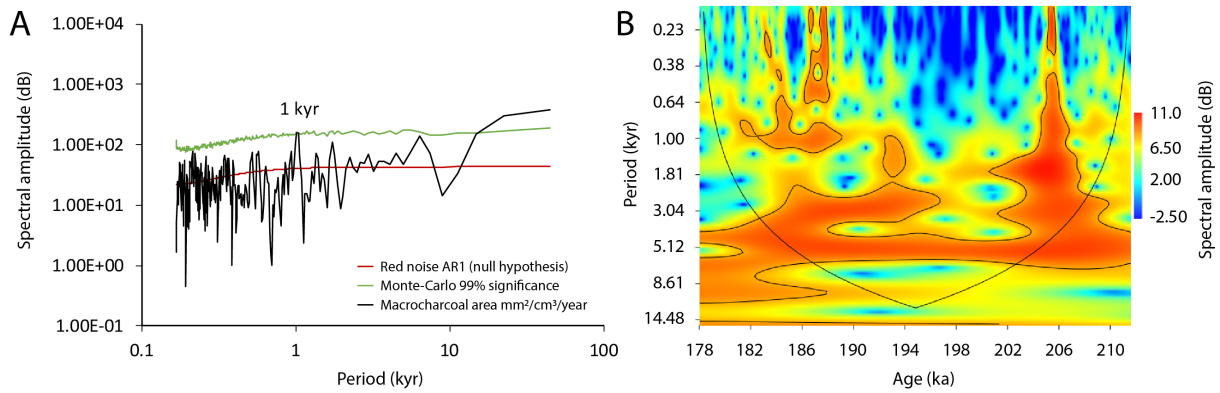

Figure 4.5: Time series analysis for ~210 to ~178 ka. **A.**: Monte-Carlo Redfit analysis of macrocharcoal area mm^2/cm^3/year; **B.**: Macrocharcoal continuous wavelet transform (black line: p = 0.05).

4.8 Discussion

4.8.1 Vegetation reconstruction

During the earliest phase of sedimentation – MIS 7a–c to MIS 6 (Zones FG1 and FG2, ~210–178 ka) – an increasing proportion of rainforest taxa and a decline in sclerophyll taxa indicates that there was a gradual transition from dry sclerophyll woodland to an *Araucaria* and Casuarinaceae-dominated assemblage (Fig. 4.2). Palustrine wetland vegetation was relatively sparse until an increase in sedges (Cyperaceae) followed by rushes (Restionaceae) from ~204 ka. During the transition into the MIS 6 glacial at ~197 ka, sedges declined, and rushes became the dominant aquatic taxon, associated with an increase in *Melaleuca*. During early MIS 6, the diversity of rainforest taxa, herbs and grasses increased.

Rainforest taxa, particularly *Agathis* and *Nothofagus moorei/cunninghamii* canopy trees, make up a notable proportion of the terrestrial sum in late MIS 6 – early MIS 5 (Zone FG3, Fig. 4.2). The predominantly sclerophyll undergrowth present in the largely Casuarinaceae and *Agathis* dominated vegetation at the start of the phase declined through MIS 5 to be replaced by a mix of herbs, grasses and rainforest taxa. At the end of MIS 5 and into MIS 4, rainforest taxa declined, leading to a more open and grassier Casuarinaceae-dominated woodland.

The largely *Agathis* and Casuarinaceae-dominated vegetation of late MIS 3 lost remaining rainforest canopy taxa during the LGM and became a true sclerophyll woodland. In

the second half of MIS 2, rainforest pollen was present only in very low quantities (Fig. 4.2) and may be indicative of an extra local source. The relative proportion of terrestrial and aquatic taxa remained broadly constant at Fern Gully Lagoon during the Holocene when compared to previous interglacials, with periodic changes in the abundance of rushes and sedges being the main feature.

4.8.2 Vegetation change due to nutrient availability

As noted earlier, gradual nutrient depletion due to leaching is argued to be an important driver of vegetation succession on sand islands (Chen et al., 2015; Walker et al., 2018). Gradual phosphorus depletion in surrounding dunes may have contributed to increasing sclerophyll vegetation at Fern Gully Lagoon, potentially complicating interpretation of changes in effective precipitation. However, no apparent increase in the relative abundance of *Banksia* on NSI, or other sclerophyll taxa associated with >200 kyr old dune sequences (Fig. 4.2), combined with the continued presence of abundant rainforest taxa until at least ~35 ka (Fig. 4.4b), indicates that vegetation succession is unlikely to be a major driver of vegetation change on NSI.

4.8.3 The impact of fire on vegetation assemblages at Fern Gully Lagoon

There is little to no linear relationship between either micro- or macrocharcoal and sclerophyll, rainforest, grass and herb, arboreal or shrub taxa habitat groups at Fern Gully Lagoon (Table C3, C4). The lack of a consistent relationship between vegetation and fire for the past ~210 kyr may indicate that vegetation-fire relationships are stronger when vegetation assemblages are dominated by sclerophyll taxa (i.e. the Holocene) or at timescales below the >1 kyr sampling interval in this study.

Several long-term (>1 kyr) relationships between periods of increased fire activity (determined by CharAnalysis) and vegetation assemblages were identified during the first phase of sedimentation (~210–178 ka), and the Holocene. Isolated periods of increased fire activity (Fig. 4.4f arrows) were generally associated with a short-term rise in herbs and grasses, as well as the gradual loss of pyrophobic rainforest taxa, with a corresponding rise in the relative abundance of pyrophytic sclerophyll taxa (Fig 4.4b,f). This pattern has been observed in other Australian vegetation records (Kershaw et al. 2007; Fletcher et al. 2014). The strongest examples in the Fern Gully Lagoon record are notable peaks in fire activity at ~198, 188, and 182 ka,

which are each associated with temporary reductions in the abundance of rainforest taxa, followed by a 1–5 ka-long recovery to ~45% of the pollen sum (Figure 4.4b,f). An increase in the number of periods of increased fire activity during early MIS 6 may be related to a change in vegetation, as there is an associated ~5% increase in the relative proportion of herbs and grasses.

4.8.4 Palaeoclimate interpretation

The basal age of the record, which has a large degree of uncertainty at 209.3 ± 28.4 ka (2σ; Chapter 3; Kemp et al., 2020), may be more tightly constrained by the presence of cool-climate taxa. The presence of cool-climate Apiaceae (Jara et al., 2015), combined with cool temperate *Nothofagus moorei/cunninghamii* (Fig. 4.2), suggests that the base of the core may have been deposited during the comparatively cooler MIS 7b (~2°C cooler than MIS 7a–c; Berger et al., 2015), or less likely, during early MIS 6.

Following these initial cool conditions, climates became wetter, and likely warmer, as indicated by increasingly abundant rainforest and aquatic taxa, and the climate space occupied by *Araucaria* and *Agathis* (Fig. 4.3). Relatively high effective precipitation at Fern Gully Lagoon during late MIS 7 (~195 ka), may have been caused by increasingly La Niña-dominated climates, as inferred from eastern Pacific SST (Pena et al., 2008). This increase in La Niña-driven precipitation during late MIS 7 coincides with stronger Australian summer monsoon influence on central Australian records as indicated by high water levels in Lake Eyre (Fig. 4.6; Fu et al., 2017).

We estimate that the MIS 7a–c to MIS 6 glacial transition at Fern Gully Lagoon was recorded at 670 cm (~197 ka), as illustrated by a marked change in taxa documented by CONISS (Fig. 4.2,4.4). This transition is defined by a switch to more sclerophyll-dominated vegetation similar to that indicated by north-eastern Australian records, albeit without extensive decline in the proportion of rainforest taxa (Fig. 4.6; Kershaw et al., 2007; Moss and Kershaw, 2007). There was also a change in millennial-scale biomass burning cycles during the transition (Fig. 4.5b). Alteration to the fire regime was likely caused by a switch to more pyrophytic vegetation and more abundant herb and grass taxa, leading to increasingly fuel-driven fire frequency as recorded elsewhere in Australia (Murphy et al. 2013).

Climates during early MIS 5 were relatively wet, as indicated by a high relative abundance of rainforest taxa, with similar inferred precipitation to that recorded during MIS 7a–c (Fig. 4.2,4.4b). However, lower CO_2 concentrations during MIS 7a–c may have increased vegetation water requirements (Prentice et al. 2017). As such, we infer that the average precipitation during MIS 7a–c was likely greater than during early MIS 5. Relatively drier conditions during MIS 5c as indicated by an increase in grass taxa and a decline in rainforest taxa when compared to either MIS 5d or MIS 5b (Fig. 4.2) likely indicates increased vegetation water stress beyond that driven by an ~20–30 ppmv drop in atmospheric CO_2 concentration. As such. there was likely a comparatively dry period during MIS 5c (DP, Fig. 4.4b), in agreement with the inorganic flux record (Fig. 4.4g, Kemp et al. 2020). Mid-MIS 5 drying was also noted at Lynch's Crater, with a reduction in rainforest taxa (Fig. 4.6; Kershaw et al., 2007).

During MIS 5, there was an elevated representation of *Nothofagus moorei/cunninghamii*, *Podocarpus*, and *Tubuliflorides pleistocenicus* (Fig. 4.2), which could indicate that warm MIS 5e may be absent from the record, and that climates were cooler than during MIS 7a–c. However, we consider this unlikely. *Nothofagus moorei/cunninghamii*, and *Tubuliflorides pleistocenicus* decline to trace values at 230 and 210 cm, likely indicating periods of warmer climates, and the probable locations of MIS 5e and MIS 5a. Given the large degree of uncertainty in the age model, it is also likely that the late MIS 6 timing of rainforest expansion at Fern Gully Lagoon is comparable to that observed in far north Queensland (Fig. 4.6; Kershaw et al., 2007; Moss and Kershaw, 2007).

Cooler regional climates for much of MIS 5 as indicated by the presence of *Nothofagus moorei/cunninghamii* and *Tubuliflorides pleistocenicus* at Fern Gully Lagoon are likely due to reduced regional sea surface temperatures, driven by lower than present average WPWP sea surface temperatures (~1–2°C cooler; Lo et al., 2017) which resulted in a cooler or less active east Australian current. *Tubuliflorides pleistocenicus* persists in the Fern Gully Lagoon record until the beginning of a hiatus at ~35 ka, indicating regional temperatures remained relatively cool until at least late MIS 3. Overlapping records from nearby Native Companion Lagoon, Welsby Lagoon and Tortoise Lagoon records indicate the continued presence of *Tubuliflorides pleistocenicus* and hence cool climates on NSI until the beginning of the Holocene (Moss et al. 2013).

Rainforest taxa *Araucaria* and *Agathis* declined to largely trace values between 35 and 21 ka, a similar decline to that observed at nearby Welsby Lagoon, Native Companion Lagoon and Tortoise Lagoon (Moss et al. 2013; Cadd et al. 2018), indicating that dry conditions during the LGM may have led to partial extinction of rainforest taxa on NSI. Rainforest abundance at Fern Gully Lagoon during the early Holocene was lower than during early MIS 5 and late MIS 7 (Fig. 4.4b,i). As such, it is possible that early Holocene climates were either notably drier than during previous interglacials, and, or that human activity on NSI (first documented at ~21 ka; Neal and Stock, 1986) had a role in limiting rainforest recovery after the LGM. Indeed, elevated late MIS 2 charcoal concentrations may indicate human influence on NSI fire frequency and hence vegetation communities (Fig. 4.4e,f).

A lower proportion of aquatic taxa compared to previous interglacials, combined with the dry climate envelope of dominant Casuarinaceae sclerophyll arboreal taxa (Fig. 4.3) and an increase in the relative proportion of Poaceae in the herb and grasses habitat group indicates that mid-Holocene climates likely remained drier than MIS 7a–c or early MIS 5 climates. The inorganic sediment flux record from Fern Gully Lagoon also indicates that mid-Holocene climates were relatively dry (Fig. 4.4g; Chapter 3; Kemp et al., 2020). Unfortunately, the chronology does not allow the timing of late Holocene climate changes to be well defined.

A drier Holocene relative to previous interglacial complexes is evident in several other Australian climate records, including in the north- and south-east with increased dry woodland and herbaceous vegetation (Harle et al., 2002; Moss and Kershaw, 2007), and reduced flows and lake filling events in central Australia (Nanson et al., 2008; Fu et al., 2017). A higher frequency of El Niño events relative to past interglacials (Moss and Kershaw, 2007), combined with the reduction of WPWP influence on Australian monsoonal precipitation (Nanson et al., 2008) have been proposed as possible causes of a relatively dry Australian Holocene. However, the exact cause of a comparatively dry Australian Holocene climates remains unresolved, and further research is required to determine the relative influence of major climate drivers during recent interglacials. Notably, increased ENSO variability and a shift to more El Niño like conditions has been inferred as a cause of drying on North Stradbroke Island from 3.2 ka BP (Barr et al. 2019).

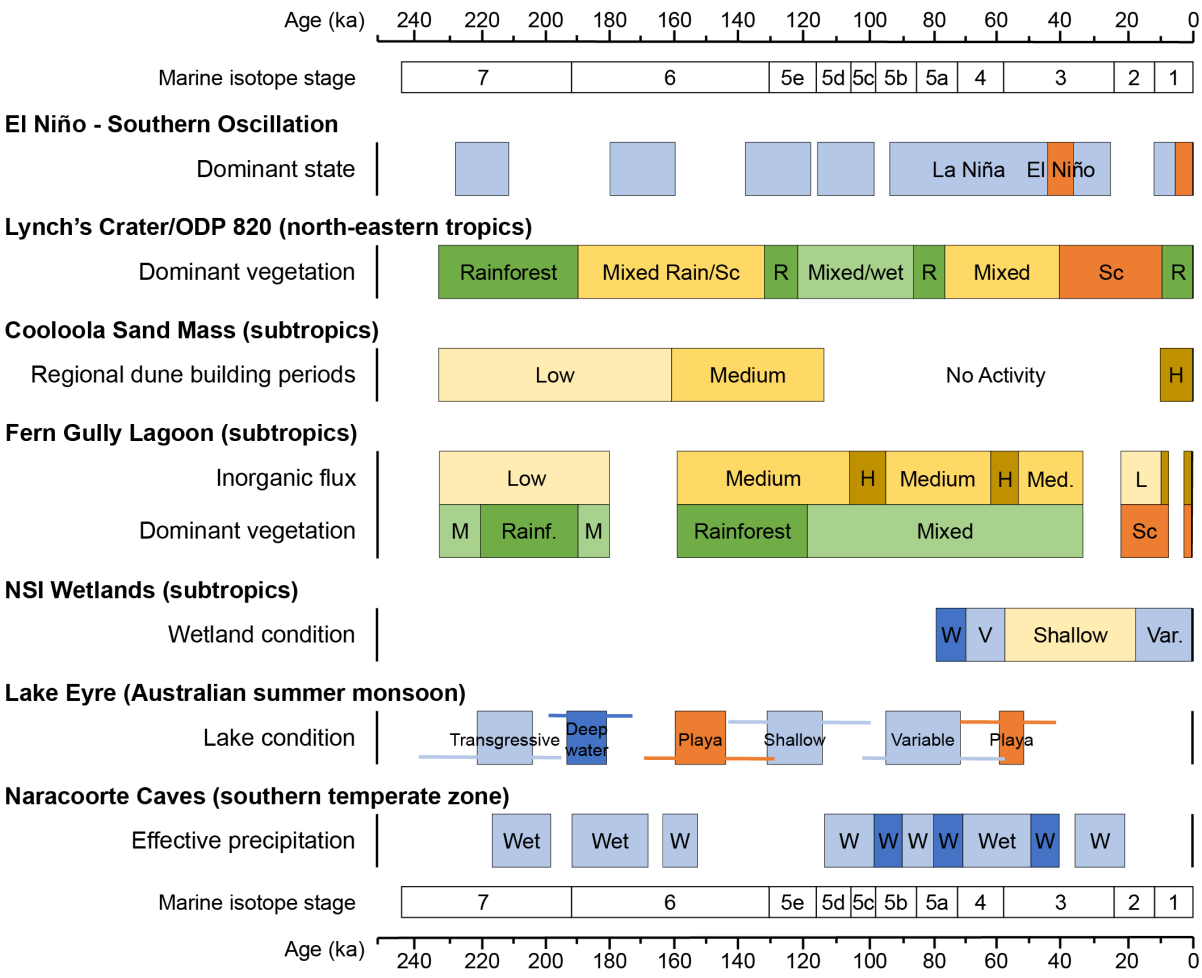

Figure 4.6: Comparison of the Fern Gully Lagoon record with a summary of palaeo-ENSO dominant state (Kukla et al., 2002; Pena et al., 2008; Driscoll et al., 2014; An et al., 2017), and records of regional climate change: Lynch's Carter/ODP 820 (Kershaw et al., 2007; Moss and Kershaw, 2007), Cooloola sand mass (Walker et al., 2018), NSI wetlands (Moss et al. 2013; Cadd et al. 2018; Lewis et al. 2020), Lake Eyre (Fu et al., 2017) and the Naracoorte caves (Ayliffe et al., 1998). H.: High, L.: Low, R.: Rainforest dominated, M.: Mixed, Sc.: Sclerophyll dominated, D.: Dry, V.: Variable and W.: Wet climates.

4.9 Conclusions

The Fern Gully Lagoon vegetation record indicates that effective precipitation during the MIS 7a–c interglacial complex was the highest of the past ~210 kyr, as evidenced by abundant rainforest taxa during a period with comparatively low atmospheric CO_2. Climates during MIS 5 are inferred to have been marginally drier and cooler than during MIS 7a–c, with woodland containing diverse rainforest and herb-grass taxa. Human impact on vegetation may have led to local extinction of several rainforest taxa after the LGM, complicating interpretation of Holocene climates. However, reduced representation of aquatic taxa, combined with the dry climate envelope of dominant sclerophyll arboreal taxa and changes in the relative proportions of herb and grass taxa indicate that the Holocene was likely notably drier than previous interglacials. This finding is in agreement with other records of interglacial climates in south-eastern and central Australia, as well as previous findings from Fern Gully Lagoon (Chapter 3; Kemp et al., 2020).

4.10 References

Ayliffe, L. K., Marianelli, P. C., Moriarty, K. C., et al. 1998. 500 ka precipitation record from southeastern Australia: Evidence for interglacial relative aridity. *Geology,* 26**,** 147-150.

Barr, C., Tibby, J., Marshall, J. C., et al. 2013. Combining monitoring, models and palaeolimnology to assess ecosystem response to environmental change at monthly to millennial timescales: the stability of Blue Lake, North Stradbroke Island, Australia. *Freshwater Biology,* 58**,** 1614–1630.

Barr, C., Tibby, J., Leng, M.J., et al. 2019. Holocene El Niño–Southern Oscillation variability reflected in subtropical Australian precipitation. *Scientific Reports* 9, 1627.

Bereiter, B., Eggleston, S., Schmitt, J., et al. 2014. Revision of the EPICA Dome C CO_2 record from 800 to 600 kyr before present. *Geophysical Research Letters,* 42**,** 542-549.

Berger, A., Crucifix, M., Hodell, D. A., et al. 2015. Interglacials of the last 800,000 years. *Reviews of Geophysics,* 54**,** 162-219.

Berger, A. & Loutre, M. F. 1991. Insolation values for the climate of the last 10 million years. *Quaternary Sciences Reviews,* 10**,** 297-317.

BOM. 2019. *Climate statistics for Australian locations: Point Lookout 1997 to 2019* [Online]. Available: http://www.bom.gov.au/climate/averages/tables/cw_040209.shtml [Accessed 5/3/2019].

Bostock, H.C., Opdyke, B.N., Gagan, M.K., et al. 2006. Glacial/interglacial changes in the East Australian current. *Climate Dynamics* 26, 645-659.

Bowler, J. M., Wyrwoll, K.-H. & Lu, Y. 2001. Variations of the northwest Australia summer monsoon over the last 300,000 years: The paleohydrological record of the Gregory (Mulan) Lakes system. *Quaternary International,* 82-85**,** 63-80.

Brown, J.R., Lengaigne, M., Lintner, B.R., et al., 2020. South Pacific Convergence Zone dynamics, variability and impacts in a changing climate. *Nature Reviews Earth & Environment*, 1-14.

Cadd, H., Tibby, J., Barr, C., et al. 2018. Development of a southern hemisphere subtropical wetland (Welsby Lagoon, south-east Queensland, Australia) through the last glacial cycle. *Quaternary Science Reviews,* 202**,** 53-65.

Chen, C. R., Hou, E. Q., Condron, L. M., et al. 2015. Soil phosphorus fractionation and nutrient dynamics along the Cooloola coastal dune chronosequence, southern Queensland, Australia. *Geoderma,* 257-258**,** 4-13.

Driscoll, R., Elliot, M., Russon, T., et al. 2014. ENSO reconstructions over the past 60 ka using giant clams (Tridacna sp.) from Papua New Guinea. *Geophysical Research Letters,* 41**,** 6819-6825.

Dupont, L.M., Caley, T., Castañeda, I.S., 2019. Effects of atmospheric CO_2 variability of the past 800 kyr on the biomes of southeast Africa. *Climate of the Past* 15, 1083-1097.

Ellerton, D., Rittenour, T., Shulmeister, J., et al. 2020. An 800 kyr record of dune emplacement in relationship to high sea level forcing, Cooloola Sand Mass, Queensland, Australia. *Geomorphology* 354, 106999.

Faegri, K., Iversen, J. & Kaland, P. E. 1989. *Textbook of Pollen Analysis*, The Blackburn Press.

Field, E., Tyler, J., Gadd, P. S., et al. 2018. Coherent patterns of environmental change at multiple organic spring sites in northwest Australia: Evidence of Indonesian-Australian summer monsoon variability over the last 14,500 years. *Quaternary Science Reviews,* 196**,** 193-216.

Fischer, H., Meissner, K. J., Mix, A. C., et al. 2018. Palaeoclimate constraints on the impact of 2°C anthropogenic warming and beyond. *Nature Geoscience,* 11**,** 474-485.

Fletcher, M.-S., Thomas, I., 2010. The origin and temporal development of an ancient cultural landscape. *Journal of Biogeography* 37, 2183-2196.

Fletcher, M.-S., Wolfe, B. B., Whitlock, C., et al. 2014. The legacy of mid-Holocene fire on a Tasmanian montane landscape. *Journal of Biogeography,* 41**,** 476-488.

Freund, M., Henley, B. J., Karoly, D. J., et al. 2017. Multi-century cool- and warm-season rainfall reconstructions for Australia's major climatic regions. *Climate of the Past,* 13**,** 1751-1770.

Fu, X., Cohen, T. J. & Arnold, L. J. 2017. Extending the record of lacustrine phases beyond the last interglacial for Lake Eyre in central Australia using luminescence dating. *Quaternary Science Reviews,* 162**,** 88-110.

Grimm, E. C. 1987. CONISS: a FORTRAN 77 program for stratigraphically constrained cluster analysis by the method of incremental sum of squares. *Computers and Geosciences,* 13.

Grimm, E. C. 2015. Tilia software. 2.0.41 ed. https://www.tiliait.com/

Harle, K. J., Heijnis, H., Chisari, R., et al. 2002. A chronology for the long pollen record from Lake Wangoom, western Victoria (Australia) as derived from uranium/thorium disequilibrium dating. *Journal of Quaternary Science,* 17**,** 707-720.

Harrison, S. P. & Bartlein, P. 2012. Records from the Past, Lessons for the Future: What the Palaeorecord Implies about Mechanisms of Global Change. *In:* Henderson-Sellers, A. & McGuffie, K. (eds.) *The Future of the World's Climate.* Elsevier Science.

Higuera, P. E., Brubaker, L. B., Anderson, P. M., et al. 2009. Vegetation mediated the impacts of postglacial climate change on fire regimes in the south-central Brooks Range, Alaska. *Ecological Monographs,* 79**,** 201-219.

Hoffman, J. S., Clark, P. U., Parnell, A. C., et al. 2017. Regional and global sea-surface temperatures during the last interglaciation. *Science,* 355**,** 276-279.

Jara, I. A., Newnham, R. M., Vandergoes, M. J., et al. 2015. Pollen–climate reconstruction from northern South Island, New Zealand (41˚S), reveals varying high- and low-latitude teleconnections over the last 16 000 years. *Journal of Quaternary Science,* 30**,** 817-829.

Kelly, R. F., Higuera, P. E., Barrett, C. M., et al. 2011. A signal-to-noise index to quantify the potential for peak detection in sediment–charcoal records. *Quaternary Research,* 75**,** 11-17.

Kemp, C. W., Tibby, J., Arnold, L. J., et al. 2020. Climates of the last three interglacials in subtropical eastern Australia inferred from wetland sediment geochemistry. *Palaeogeography, Palaeoclimatology, Palaeoecology,* 538.

Kershaw, A.P., Clark, J.S., Gill, A.M., 2002. "Flammable Australia: the Fire Regimes and Biodiversity of a Continent ", in: Bradstock, R., Williams, J., Gill, A.M. (Eds.), A history of fire in Australia. Cambridge University Press, Cambridge, pp. 3-25.

Kershaw, P., Moss, P., Van Der Kaars, S., 2003. Causes and consequences of long-term climatic variability on the Australian continent. *Freshwater Biology,* 48, 1274-1283.

Kershaw, A. P., Bretherton, S. C. & van der Kaars, S. 2007. A complete pollen record of the last 230 ka from Lynch's Crater, north-eastern Australia. *Palaeogeography, Palaeoclimatology, Palaeoecology,* 251**,** 23-45.

Kukla, G. J., Clement, A. C., Cane, M. A., et al. 2002. Last Interglacial and Early Glacial ENSO. *Quaternary Research,* 58**,** 27-31.

Leach, L.M., 2011. Hydrology and physical setting of North Stradbroke Island. *Proceedings of the Royal Society of Queensland* 117, 21-46.

Lewis, R.J., Tibby, J., Arnold, L.J., et al. 2020. Insights into subtropical Australian aridity from Welsby Lagoon, north Stradbroke Island, over the past 80,000 years. *Quaternary Science Reviews* 234, 106262.

Lo, L., Chang, S.-P., Wei, K.-Y., et al. 2017. Nonlinear climatic sensitivity to greenhouse gases over past 4 glacial/interglacial cycles. *Scientific reports,* 7**,** 4626.

Lu, Z., Liu, Z., Zhu, J., et al., 2018. A Review of Paleo El Niño-Southern Oscillation. *Atmosphere* 9.

Longmore, M. E. & Heijnis, H. 1999. Aridity in Australia: Pleistocene records of palaeohydrological and palaeoecological change from the perched lake sediments of Fraser Island, Queensland, Australia. *Quaternary International,* 57/58**,** 35–47.

Mariani, M., Connor, S. E., Theuerkauf, M., et al. 2016. Testing quantitative pollen dispersal models in animal-pollinated vegetation mosaics: An example from temperate Tasmania, Australia. *Quaternary Science Reviews,* 154**,** 214-225.

Mariani, M., Tibby, J., Barr, C., et al. 2019. Reduced rainfall drives biomass limitation of long-term fire activity in Australia's subtropical sclerophyll forests. *Journal of Biogeography,* 46**,** 1974-1987.

Mooney, S. & Black, M. 2003. A simple and fast method for calculating the area of macroscopic charcoal isolated from sediments. *Quaternary Australasia,* 21**,** 18-21.

Mooney, S. D., Harrison, S. P., Bartlein, P. J., et al. 2011. Late Quaternary fire regimes of Australasia. *Quaternary Science Reviews,* 30**,** 28-46.

Moss, P. T. & Kershaw, A. P. 2000. The last glacial cycle from the humid tropics of northeastern Australia: comparison of a terrestrial and a marine record. *Palaeogeography, Palaeoclimatology, Palaeoecology,* 155**,** 155–176.

Moss, P. T. & Kershaw, A. P. 2007. A late Quaternary marine palynological record (oxygen isotope stages 1 to 7) for the humid tropics of northeastern Australia based on ODP Site 820. *Palaeogeography, Palaeoclimatology, Palaeoecology,* 251**,** 4-22.

Moss, P. T., Tibby, J., Petherick, L., et al. 2013. Late Quaternary vegetation history of North Stradbroke Island, Queensland, eastern Australia. *Quaternary Science Reviews,* 74**,** 257-272.

Murphy, B.P., Bradstock, R.A., Boer, M.M., et al., 2013. Fire regimes of Australia: a pyrogeographic model system. *Journal of Biogeography* 40, 1048-1058.

Myrbo, A. & Wright, H. E. 2008. SOP: Livingstone-Bolivia. University of Minnesota, Limnological Research Center Core Facility.

Nanson, G. C., Price, D. M., Jones, B. G., et al. 2008. Alluvial evidence for major climate and flow regime changes during the middle and late Quaternary in eastern central Australia. *Geomorphology,* 101**,** 109-129.

Neal, R., Stock, E., 1986. Pleistocene occupation in the south-east Queensland coastal region. *Nature* 323, 618-621.

Oksanen, J., Blanchet, F. G., Friendly, M., et al. 2018. Community Ecology Package. 2.5-2 ed.

Olchev, A., Novenko, E., Popov, et al., 2017. Evidence of temperature and precipitation change over the past 100 years in a high-resolution pollen record from the boreal forest of Central European Russia. *The Holocene* 27, 740-751.

Patton, N. R., Ellerton, D. & Shulmeister, J. 2019. High resolution remapping of the coastal dune fields of south east Queensland, Australia: a morphometric approach. *Journal of Maps,* 15**,** 578-589.

Pena, L. D., Cacho, I., Ferretti, P., et al. 2008. El Niño–Southern Oscillation–like variability during glacial terminations and interlatitudinal teleconnections. *Paleoceanography,* 23**,** 1-8.

Petherick, L., McGowan, H., Moss, P., 2008. Climate variability during the last glacial maximum in eastern Australia: evidence of two stadials? *Journal of Quaternary Science,* 23, 787-802.

Petherick, L.M., Moss, P.T., McGowan, H.A., 2017. An extended last glacial maximum in subtropical Australia. *Quaternary International* 432, 1-12.

Prentice, I.C., Cleator, S.F., Huang, Y.H., et al. 2017. Reconstructing ice-age palaeoclimates: Quantifying low-CO2 effects on plants. *Global and Planetary Change* 149, 166-176.

Rhodes, A. N. 1998. A method for the preparation and quantification of microscopic charcoal from terrestrial and lacustrine sediment cores. *The Holocene,* 8**,** 113-117.

Risbey, J. S., Pook, M. J., McIntosh, P. C., et al. 2009. On the Remote Drivers of Rainfall Variability in Australia. *Monthly Weather Review,* 137**,** 3233-3253.

Rohling, E. J., Grant, K., Bolshaw, M., et al. 2009. Antarctic temperature and global sea level closely coupled over the past five glacial cycles. *Nature Geoscience,* 2**,** 500.

Schulz, M. & Mudelsee, M. 2002. REDFIT: estimating red-noise spectra directly from unevenly spaced paleoclimatic time series. *Computers & Geosciences,* 28**,** 421-426.

Specht, R. L. 2011. Plant communities of North Stradbroke Island: Development of structure and species richness. *Proceedings of the Royal Society of Queensland,* 117**,** 181-191.

Thomson, D.J., 1990. Time Series Analysis of Holocene Climate Data. *Philosophical Transactions of the Royal Society of London*. Series A, Mathematical and Physical Sciences 330, 601-616.

Torrence, C. & Compo, G. P. 1998. A practical guide to wavelet analysis. *Bulletin of the American Meteorological Society,* 79**,** 61-78.

Tudhope, A. W., Chilcott, C. P., Mcculloch, M. T., et al. 2001. Variability in the El Niño - Southern oscillation through a glacial-interglacial cycle. *Science,* 291**,** 1511-1517.

Walker, J., Thompson, C.H., Fergus, I.F., et al. 1981. Plant succession and soil development in coastal sand dunes of subtropical eastern Australia. Springer-Verlag, New York.

Walker, J., Lees, B., Olley, J., et al. 2018. Dating the Cooloola coastal dunes of South-Eastern Queensland, Australia. *Marine Geology,* 398**,** 73-85.

Whitlock, C. & Larsen, C. P. S. 2001. Charcoal as a Fire Proxy. *In:* J.P. Smol, H. J. B. B., and W. M. Last (ed.) *Tracking Environmental Change Using Lake Sediments: Volume 3 Terrestrial, Algal, and Siliceous indicators.* Dordrecht: Kluwer Academic Publishers.

Chapter 5 – Holocene and interglacial climates in subtropical eastern Australia: A case study from Fern Gully Lagoon

5.1 Statement of Authorship

Title of Paper	Holocene and interglacial climates in subtropical eastern Australia: A case study from Fern Gully Lagoon
Publication Status	☐ Published ☐ Accepted for Publication ☐ Submitted for Publication ☑ Unpublished and Unsubmitted w ork w ritten in manuscript style
Publication Details	Kemp, C.W., Naeher, S., Tibby, J., Barr, C., Arnold, L.J., Vandergoes, M.J., Stucker, V.K., Marshall, J.C., McGregor, G.B., in prep. Holocene and interglacial climates in subtropical eastern Australia: A case study from Fern Gully Lagoon.

5.1.1 Principal Author

Name of Principal Author (Candidate)	Christopher Wilde Kemp		
Contribution to the Paper	Research, stable isotope sample preparation and analysis, writing the manuscript. Palaeoclimate interpretation and discussion. Corresponding author.		
Overall percentage (%)	75		
Certification:	This paper reports on original research I conducted during the period of my Higher Degree by Research candidature and is not subject to any obligations or contractual agreements with a third party that would constrain its inclusion in this thesis. I am the primary author of this paper.		
Signature		Date	6-4-2020

5.1.2 Co-Author Contributions

By signing the Statement of Authorship, each author certifies that:

i. the candidate's stated contribution to the publication is accurate (as detailed above);
ii. permission is granted for the candidate in include the publication in the thesis; and
iii. the sum of all co-author contributions is equal to 100% less the candidate's stated contribution.

Name of Co-Author	John Tibby		
Contribution to the Paper	Suggestions for and assistance editing the manuscript structure, research direction, methods and discussion, as well as editing, correcting and formatting of the manuscript.		
Signature		Date	May 5, 2020

Name of Co-Author	Sabastian Naeher		
Contribution to the Paper	Help with stable isotope and lipid biomarker methods and analysis as well as interpretation and discussion of isotope and *n*-alkane findings. Editing, correcting, and formatting of the manuscript.		
Signature		Date	May 6, 2020

Name of Co-Author	Cameron Barr		
Contribution to the Paper	Assistance with palaeoclimate interpretation, help with discussion of basin evolution and editing, correcting, and formatting of the manuscript.		
Signature		Date	May 7, 2020

Name of Co-Author	Lee Arnold		
Contribution to the Paper	Help with discussion of possible early record timeline within the age/depth model. Editing, correcting and formatting of the manuscript.		
Signature		Date	May 7, 2020

Name of Co-Author	Valerie Stucker		
Contribution to the Paper	Assistance with biomarker laboratory methods and alkane/GDGT interpretation. Manuscript editing and figure planning.		
Signature		Date	May 12, 2020

Name of Co-Author	Marcus Vandergoes		
Contribution to the Paper	Assistance with *n*-alkane/GDGT interpretation, editing and correcting the manuscript.		
Signature		Date	May 12, 2020

Name of Co-Author	Jonathan Marshall		
Contribution to the Paper	Help with regional comparisons and discussion of emergent macrophyte growth patterns as well as editing and correcting the manuscript.		
Signature		Date	May 12, 2020

Name of Co-Author	Glenn McGregor		
Contribution to the Paper	Help with regional comparisons, editing and correcting the manuscript.		
Signature		Date	May 12, 2020

5.2 Preamble

The Fern Gully Lagoon record of regional moisture availability was inferred from inorganic flux, pollen and charcoal proxies, and relies on changes in terrestrial vegetation as an indicator of regional moisture availability. Unfortunately, there is a distinct possibility that human occupation on NSI altered post-LGM terrestrial vegetation assemblages. To address the possible misinterpretation of Holocene climates on NSI, additional climate proxy records were established based on in-wetland moisture availability proxies (stable carbon isotopes and lipid biomarkers).

A complicating factor in determining moisture availability utilising changes in vegetation on the surface of Fern Gully Lagoon was the influence of evaporation on wetland water levels. As the exposed surface area of Fern Gully Lagoon is exponentially larger with greater depth to the base of the sediment, wetland water levels would have been increasingly driven by evaporation (both directly and by exposure to wind), as much as by precipitation. In addition, mean annual air temperatures likely influenced the degree of evaporation as well as the composition of wetland vegetation assemblages. Discussion of findings, including a new moisture availability record from in-wetland climate proxies, rough estimates of Fern Gully Lagoon wind exposure over time, and discussion of reconstructed temperature records are included in Chapter 5.

This chapter is to be submitted for publication in February 2021 as:

Kemp, C.W., Naeher, S., Tibby, J., Barr, C., Arnold, L.J., Vandergoes, M.J., Stucker, V.K., Marshall, J.C., McGregor, G.B. “Holocene and interglacial climates in subtropical eastern Australia: A case study from Fern Gully Lagoon”.

I have re-formatted the manuscript as a thesis chapter, with only minor changes to the original text. However, notation associated with figures, tables and equations has changed, being instead prefaced by the chapter number, e.g. Figure 1 is now Figure 5.1. The supplementary material associated with the manuscript is included in this thesis as Appendix D.

5.3 Abstract

A drying trend has influenced climates in central and south-eastern Australia over the past ~250 kyr, but variations in subtropical Australian climates remain largely unexplored. We investigate bulk stable carbon isotopes and lipid biomarkers as indicators of changing vegetation, temperature, and moisture availability for the past ~210 kyr in sediments from Fern Gully Lagoon, a subtropical wetland. A glycerol dialkyl glycerol tetraether (GDGT) temperature reconstruction using global soil calibrations and estimated changes in wetland surface area were used to infer changes in evaporation due to wetland expansion. A change in vegetation composition inferred from increasingly negative bulk sediment $\delta^{13}C$ values and greater *n*-alkane average chain length reflects a shift in dominant vegetation community away from aquatic macrophytes and towards terrestrial vegetation. Higher terrestrial organic material contribution to wetland sediments likely indicates that Holocene climates were relatively dry when compared to previous interglacials. However, increasing wetland exposure to wind due to basin infilling may have contributed to drying during the Holocene. Inferred differences in Holocene climates between this record (using in-wetland climate proxies) and previous records of regional climates indicate the degree of human impact on terrestrial vegetation assemblages on North Stradbroke Island.

5.4 Introduction

Throughout the past 800 kyr, it has been rare for the Earth's orbital configuration to be comparable to that during the Holocene. Only two interglacials, marine isotope stage (MIS) 19 and MIS 11, had similar patterns of insolation, with comparatively low peak-to-peak amplitude (Loutre and Berger, 2000; Yin and Berger, 2015). Atmospheric composition during the Holocene also differs to that during recent interglacials - several climate models indicate that pre-industrial Holocene climates were likely driven by lower atmospheric CO_2 and CH_4 concentrations (e.g. Claussen et al., 2005; Berger and Yin, 2012; Yin and Berger, 2015). As a result, comparing climates during more recent interglacials to Holocene climates is challenging and must take into account complex interactions between multiple climate drivers (Schweger et al., 2011; Yin and Berger, 2015).

Evidence from the few available >200 kyr Australian climate records suggests that there is a pattern of increased interglacial drying in several regions, culminating in comparatively arid Holocene climates (e.g. Bowler et al., 2001; Harle et al., 2002; Kershaw et al., 2003; Lynch et al., 2007; Fu et al., 2017). Lower amplitude insolation during the Holocene than during recent interglacials (Yin and Berger, 2015) is likely at least partially responsible for the drier Holocene climates in Australia via its influence on sea surface temperatures and hence the El-Niño Southern-Oscillation (ENSO) (Kershaw et al., 2007a; Nanson et al., 2008; Fu et al., 2017). In addition, increasing ENSO variability during the Holocene when compared to recent interglacials likely contributed to Holocene drying (e.g. Kershaw et al., 2007a; Kershaw et al., 2007b; Lu et al., 2018).

Some Australian climate studies have inferred past moisture availability from sedimentation or speleothem deposition, with greater moisture availability linked to peaks in sedimentation and rapid speleothem growth (e.g. Ayliffe et al., 1998; Bowler et al., 1998; Nanson et al., 2008; Fu et al., 2017). By contrast, several studies instead inferred changes in moisture availability via changing vegetation assemblages (e.g. Colhoun et al., 1999; Harle et al., 2002; Moss and Kershaw, 2007) and, as such, may have underestimated MIS 7 moisture availability as lower atmospheric CO_2 concentrations during that interglacial may have increased vegetation moisture requirements (Prentice et al., 2017; Dupont et al., 2019). In addition, human influence on Holocene terrestrial vegetation communities via changes in fire frequency was noted in several studies as an additional source of complexity for comparative interglacial climate reconstructions (e.g. Dupont and Weinelt, 1996; Kershaw et al., 2007a; Kemp et al., submitted). Combining multiple separate palaeorecords with proxies unlikely to be influenced by human impact on terrestrial vegetation (e.g. changes in wetland vegetation) improves the accuracy of climate reconstructions and helps separate natural factors from human impact.

Climate reconstructions can be made more robust by the application of several, ideally independent climate proxies (e.g. Eggenberger et al., 2018; Fritz et al., 2018). Multi-proxy studies help to reduce confounding of climate proxies by non-climate drivers such as human influence (e.g. Dupont and Weinelt, 1996; Kershaw et al., 2007a; Johnson et al., 2018) or changes in nutrient availability (e.g. Wooller et al., 2009; Glaser et al., 2013) from climate influence on vegetation assemblages. Multi-proxy records can also help identify post-

depositional alteration of climate archives such as leaching of trace elements (e.g. Sun et al., 2016), diagenesis (e.g. Zhang et al., 2017) or dissolution of forams (e.g. Hayward et al., 2012).

Recent palaeoclimate studies have used a combination of stable isotopes and lipid biomarkers to infer past changes in moisture availability (e.g. Atahan et al., 2015; Mays et al., 2017; Sun et al., 2017). Stable carbon isotope analysis of bulk sediments, in combination with carbon to nitrogen ratios, can be used to identify organic material (OM) sources of wetland sediment, and isotope fractionation records can be combined with other climate proxies to infer changes in climate or nutrient limitation (e.g. Wooller et al., 2009; Mays et al., 2017; Cadd et al., 2018). Carbon and hydrogen isotopes can also be used to identify water stress when a narrow band of taxa or individual taxa sources can be analysed (Naafs et al., 2019). However, the use of sedimentary carbon isotopes to infer hydroclimate is limited by a wide range of potential influencing factors such as air temperature, altitude, salinity and the partial pressure of atmospheric CO_2, as well as the need to correct for atmospheric $\delta^{13}C$ (Diefendorf, 2010; Schubert and Jahren, 2012; Diefendorf and Freimuth, 2017). While bulk sediment isotope records can derive from multiple sources, lipid biomarkers and compound-specific carbon and hydrogen isotopes can provide more detailed records of changing wetland conditions (Diefendorf and Freimuth, 2017).

Lipid biomarkers provide more source-specific information than bulk organic material (OM), and a variety of parameters have been developed for reconstructing past vegetation assemblages, as well as biogeochemical, environmental and climate processes (e.g. Peters et al., 2007; Bush and McInerney, 2015; Diefendorf and Freimuth, 2017). For instance, *n*-alkane distributions are commonly used to distinguish relative contributions of algae and bacteria from those of aquatic macrophytes and terrestrial higher plants in wetland sediments, and may, therefore, reflect OM sources, vegetation composition, or climate (Ficken et al., 2000; Zhou et al., 2010; Diefendorf and Freimuth, 2017). However, inferring climate change using *n*-alkane distributions from environmental archives can be challenging due to the possible range of chain length distributions in vegetation communities (Bush and McInerney, 2013; Diefendorf and Freimuth, 2017).

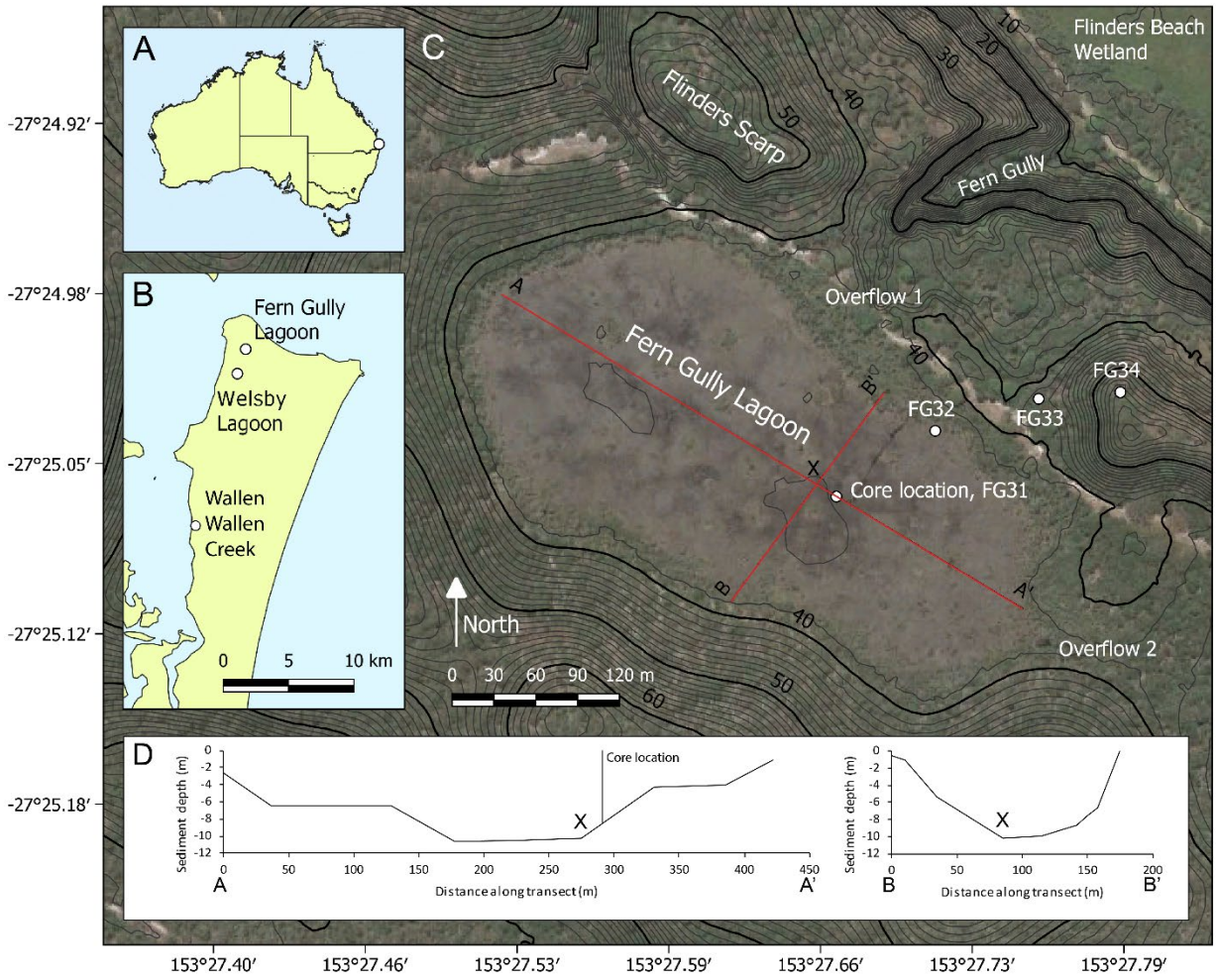

Figure 5.1: The location of North Stradbroke Island (inset **A.**). Location of Fern Gully Lagoon and Welsby Lagoon, as well as the Wallen Wallen Creek archaeological site (inset **B.**). **C:** Fern Gully Lagoon wetland sediment transects and surrounding dune topology (m above sea level). Circles FG31 – FG34 denote surface biomarker sampling locations. **D:** Transects A and B, with cross-over point X, and the location of the core.

Glycerol dialkyl glycerol tetraethers (GDGTs) are widespread in the environment and have been applied to accurately reconstruct past mean average air and water temperatures (Schouten et al., 2013; Naafs et al., 2017). The distributions of branched GDGTs in terrestrial environments are particularly promising indicators of past mean annual air temperature (MAAT) from soil and peat records, but can also be influenced by factors other than temperature such as soil pH, microbial community composition, and precipitation (Weijers et al., 2007; Weijers et al., 2011; Peterse et al., 2012; Naafs et al., 2017). The relationship with temperature was originally

formulated empirically based on the relative abundance of GDGTs via the methylation index of branched tetraethers and the cyclisation ratio of branched tetraethers, the so-called MBT–CBT proxy (Weijers et al., 2007). However, improved chromatographic separation led to the distinction of branched GDGT (brGDGT) isomers with methyl groups at C-5, which are mainly controlled by temperature, from those with methyl groups at C-6, which mainly reflect changes in soil or peat pH (De Jonge et al., 2013; De Jonge et al., 2014; Naafs et al., 2017). Global and site-specific temperature calibrations are available from the literature (e.g. Weijers et al., 2007; Peterse et al., 2012), but need to be evaluated carefully to determine which calibration is applicable and in agreement with monitoring data. GDGTs are also applied as indicators of OM source, with the branched vs isoprenoid tetraether (BIT) index commonly used to estimate relative terrestrial OM input in marine and lacustrine environments (Hopmans et al., 2004; Weijers et al., 2006).

This study is an extension and evaluation of our previous work reconstructing regional interglacial climate history at Fern Gully Lagoon (Kemp et al., 2020; Kemp et al., submitted). Since previous inferences were likely influenced by human impact on terrestrial vegetation, we utilise in-wetland climate proxies unlikely to be affected by human influence to determine water stress and characterise sources of wetland OM. In addition, this study aims to:

i) Determine a record of regional MAAT, allowing changes in temperature-driven vegetation change or evaporation to be identified.
ii) Reconstruct changes in wetland surface area, so possible evaporation, using a combination of simple basin morphology and the age-depth model.

5.5 Study site

North Stradbroke Island (NSI, also known as Minjerribah, Fig. 5.1a) is the world's second-largest sand island and is located on the subtropical central-eastern coast of Australia. NSI is part of the world's oldest and largest coastal dune system, which includes Fraser Island, the Cooloola Sand Mass, Peregian Sand Hills, and Bribie and Moreton Islands (Walker et al., 2018; Patton et al., 2019). NSI has an average annual minimum air temperature of 15°C and maximum of 29°C with a mean annual rainfall of approximately 1550 mm with a dry winter and a wetter summer (1996–2019; BOM, 2005, 2019).

NSI is host to the densest concentration of wetland records dating to the last glacial maximum (LGM) in Australia (Tibby et al., 2017), and is the focus of numerable palaeoclimate reconstructions (e.g. Moss et al., 2013; Petherick et al., 2017; Cadd et al., 2018; Barr et al., 2019; Mariani et al., 2019). Island records have allowed a greater understanding of past changes in ENSO (Barr et al., 2019) - the dominant contemporary regional climate driver (Freund et al., 2017), continental wind patterns (Petherick et al., 2009) and biomass burning (Mariani et al., 2019). The many NSI wetlands are usually waterlogged, oligotrophic and palustrine, and are dominated by rushes and sedges *Baloskion pallens* (syn. *Restio pallens*), *Baumea* spp., *Gahnia sieberiana* and *Lepironia articulata*, surrounded by open *Melaleuca quinquenervia* forest (Marshall and McGregor, 2011). Archaeological evidence of local human presence post-LGM at nearby Wallen Wallen Creek (Fig. 5.1b; Neal and Stock, 1986), combined with local extinction of arboreal rainforest taxa and changes in the local fire regime may indicate the widespread human impact on NSI vegetation assemblages during the Holocene, complicating reconstructions of moisture availability based on terrestrial pollen data (Kemp et al., submitted).

Fern Gully Lagoon (27.417°S, 153.460°E, 39 m ASL) is situated near the northern coast of NSI, above tidal wetlands and behind Flinders Scarp, a set of barrier dunes dating back to at least early MIS 5 (Patton et al., 2019). The current wetland covers approximately 0.8 km^2, lies within a shallow bowl of vegetated dunes (Leach, 2011), and is generally shallow, with an average water depth of no more than a metre. The wetland has two above-ground overflow points, the largest and most recently active being on the north-eastern side, draining into the eponymous Fern Gully, which cuts through Flinders Scarp to the tidal wetlands (Fig. 5.1c). The small catchment and highly permeable soil surrounding the perched wetland limit fluvial transport of material into the wetland, mainly restricting organic sedimentation to in situ wetland sources.

A chronology for the Fern Gully Lagoon sedimentary record was established using a combination of six radiocarbon (^{14}C) and thirteen optically stimulated luminescence (OSL) ages, along with possible hiatus priors determined using pruned exact linear time multi-changepoint analysis (Kemp et al., 2020). OxCal Bayesian age-depth modelling identified four distinct sedimentation phases separated by hiatuses: a MIS 7a–c to early MIS 6 phase (209.3 ± 28.4 to 177.5 ± 25.4 ka), a late MIS 6 to late MIS 3 phase (155.2 ± 24.9 to 34.7 ± 14.5 ka), a mid-MIS 2

to early Holocene phase (20.9 ± 1.4 ka to 6.5 ± 5.6 ka) and a late Holocene phase (1.7 ± 1.0 ka to 0.45 ± 0.4 ka) (mean ± 2σ; Kemp et al., 2020).

5.6 Methods

5.6.1 Prior research

Two overlapping nine-metre cores were extracted from the approximate geographical centre of Fern Gully Lagoon in April 2015 using a modified Livingstone-Bolivia square-rod piston-corer (Wright, 1967). Cores were aligned using CPLSlot sequence slotting software (Clark and Hounslow, 2009), allowing a joint depth record to be created. Organic and moisture content of the cores was determined according to the procedures of Heiri et al. (2001). Further details of core collection and inorganic flux records are provided in Kemp et al. (2020). A record of vegetation assemblages and fire frequency at Fern Gully Lagoon based on pollen and macro- as well as micro-charcoal analyses are to be published in Kemp et al. (submitted).

5.6.2 Bulk stable isotope analysis

Ninety bulk sediment carbon and nitrogen stable isotope samples were analysed at the University of Adelaide in South Australia using methods reported in Greer et al. (2018) and Onetto Carvallo (2018). In brief, 0.25 mg freeze-dried and powdered sediment was analysed in tin cups in a EuroVector EuroEA elemental analyser, in-line with a Nu Instruments Nu Horizon continuous flow isotope ratio mass spectrometer (EA-IRMS). The data was calibrated using in-house glycine, glutamic acid and triphenylamine standards, in turn calibrated to international standards: $\delta^{13}C$ (IAEA-C6, NBS-22, USGS 40, USGS 41 and USGS 24) and $\delta^{15}N$ (IAEA N1, N2, N3, and USGS 32, 34, 35, 40, 41). To test for sediment carbonates, a duplicate set of 20 samples were analysed after acid vapour chamber treatment in silver cups, with variation remaining within analytical error (± 0.08 ‰ for $\delta^{13}C$ and ± 0.06 ‰ for $\delta^{15}N$). To ensure reproducibility, 20 duplicate samples were also run in parallel with the analysis process, again finding values within error. Stable isotope data for bulk sediments are reported as $\delta^{13}C_{OM}$ and $\delta^{15}N_{OM}$ values in per mil relative to Vienna PeeDee Belemnite (VPDB) and atmospheric nitrogen, respectively. Carbon to nitrogen ratios (C:N) are expressed as molar ratios.

Modern average $\delta^{13}C$, total organic carbon (TOC), total nitrogen (TN) and carbon-nitrogen ratio (C:N) values for soil, terrestrial flora, emergent macrophytes and algae from NSI wetlands (Cadd et al., 2018) were used to establish possible OM sources for Fern Gully Lagoon. Nitrogen availability within Fern Gully Lagoon was calculated by assessing the degree to which nitrogen was organically bound – a lack of inorganic nitrogen (N_{in}) indicates nitrogen limitation (Talbot, 2001). Assuming a linear relationship between TOC and TN (as N is organically bound with C), the amount on inorganic nitrogen can be identified by the TN y-axis intercept when plotted against TOC (Calvert, 2004).

5.6.3 Lipid biomarkers

Thirty lipid biomarker samples from the wetland core and four samples collected from wetland surface sediments and terrestrial soils at Fern Gully Lagoon were analysed (Fig. 5.1c, FG31: wetland centre, FG32: wetland edge, FG33: 25 m from wetland edge and FG34: 50 m from the wetland edge. At the two terrestrial sites, soils were sampled in triplicate with a one-metre spacing and mixed to account for heterogeneity. Modern instrumental MAAT was calculated based on 23 years of air temperature records from Point Lookout - the closest available weather station ~7 km from Fern Gully Lagoon (1997–2019; BOM, 2019).

Lipid biomarker samples were analysed in the Organic Geochemistry Laboratory at GNS Science using the analytical procedures reported in Naeher et al. (2012; 2014) with some modifications. In brief, freeze-dried and homogenised sediment and soil (0.6–5.4 g) was extracted using dichloromethane (DCM)/ methanol (MeOH) (3:1, v:v) by ultrasonication for 20 min each time. A known mixture of 5α-cholestane, *n*-C19 alcohol and *n*-C19:0 fatty acid was added to the total lipid extract (TLE) for quantification. Elemental sulfur was removed by activated copper. After saponification of the TLE with 6% KOH in MeOH (3h, 80°C), neutrals and acid fractions were extracted with *n*-hexane, the latter fraction after addition of 6M HCl. Neutrals were divided into apolar and polar fractions via liquid chromatography over silica columns using *n*-hexane/DCM (9:1, v:v) and DCM/MeOH (1:1, v:v), respectively. Before analysis, an aliquot of the polar fraction was derivatised with BSTFA [*N,O*-bis(trimethylsilyl)trifluoroacetamide] and the FA fraction with 14% BF_3/MeOH.

The resulting fractions were analysed using gas chromatography-mass spectrometry (GC-MS) on an Agilent 7890A GC System, equipped with a SGE BPX5 capillary column (60 m × 0.25 mm inner diameter × 0.25 μm film thickness) connected to an Agilent 5975C inert MSD mass spectrometer. The temperature program of the oven was 70°C (1 min isothermal), 70–100°C at 10°C/min, 100–320°C at 4°C/min, isothermal at 320°C for 25 min. Helium was used as carrier gas with a constant flow of 1.0 mL/min. Samples were injected splitless at an inlet temperature of 280°C. The MS was operated in electron impact ionisation mode at 70 eV using a source temperature of 230°C.

GDGTs were analysed using an aliquot of the polar fraction, dissolved in *n*-hexane/isopropanol (99:1, v:v), and filtered with 0.45 μm polytetrafluoroethylene (PTFE) filters prior to analysis via high-performance liquid chromatography (HPLC). A Dionex 3000 Aunit was converted to an HPLC capable of separating the GDGTs of interest using a Grace Prevail Cyano column (150 mm x 2.1 mm; 3 μm) and new tubing and connections. A Dionex MSQ+ atmospheric chemical ionisation mass spectrometer (HPLC-APCI-MS) was used as a detector. The corona pin was set at 10 μA, cone voltage was 75 V, and the N_2 gas rate was 60 psi. The GDGTs were eluted isocratically with 100% *n*-hexane:IPA (99:1, v:v) for 5 min and then with a linear gradient to 18% *n*-hexane/isopropanol (9:1, v:v) for 40 min at 0.2 ml/min. The column was flushed for 5 minutes with 100% *n*-hexane/isopropanol (9:1, v:v) and then re-equilibrated with 100% *n*-hexane:IPA (99:1, v:v) prior to next injection. Injection volume was 25 μl of a solution of 10 mg/mL where possible and single ion monitoring of $[M+H]^+$ was used to detect GDGTs. The analytical reproducibility of GDGT analysis was within 15% based on duplicate measurements. The analytical variation in the GDGT based index values was ≤0.02.

In this study, we applied three brGDGT calibrations developed for reconstructing MAAT from soils and wetland sediments. We used the original two soil calibrations of Weijers et al. (2007) as well as the Peterse et al. (2012) soil calibration, and compared soil MAAT estimates. While lake-specific calibrations after Tierney et al. (2010) were considered, a BIT index close to 1 for all samples (Table D1), as well as abundant terrestrial biomarkers indicate that Fern Gully Lagoon is unlikely to have been a lake system at any point during the last ~210 kyr.

5.6.4 Basin shape calculations

Wetland surface area and volume are important modulators of wetland moisture responses to changes in precipitation and, or, evaporation via relative changes in direct and wind-enhanced evaporation (Anda et al., 2018; Zhai et al., 2019; Smith et al., 2020). Calculating wetland surface area also allows for identification of some vegetation changes unrelated to climate (e.g. proximity of surrounding terrestrial vegetation to the coring site during early wetland development due to small wetland size). To identify periods of rapid wetland surface area expansion at Fern Gully Lagoon, we compared changes in sedimentation rate at Fern Gully Lagoon to ideal basin models after Bennett and Buck (2016).

Sediment sounding poles were used to determine the absolute depth of highly organic peaty wetland sediments above underlying dune sequences and hence the shape of the underlying basin. Two transects were completed, totalling 19 sample locations: transect A, along the long NW to SE axis of the wetland (~422 m) and transect B, perpendicular to A across the approximate centre of the wetland from SW to NE (~175 m; Fig. 5.1c). Combined with the age-depth model (Kemp et al., 2020), and with the assumption that sediment accumulation was spatially uniform, these transects were used to reconstruct changes in wetland surface area over time.

5.7 Results

5.7.1 Stable isotopes

All stable carbon isotope samples from Fern Gully Lagoon had $\delta^{13}C_{OM}$ values consistent with those of C_3 plants or algae (-26.0 to -30.3 ‰; Fig. 5.2a; Meyers and Teranes, 2001), with most samples having C:N values close to the average values of contemporary emergent macrophyte sources as determined by Cadd et al. (2018) for NSI wetlands (~68; Fig. 5.2d). Modern plant and algae samples from nearby NSI wetlands have $\delta^{13}C$ values ranging from -23.9 to -31.6 ‰, and C:N ratios ranging from ~18 to 146, with higher than expected C:N ratios for cyanobacteria at ~47, likely due to nitrogen limitation of plants and algae in NSI wetlands (Cadd et al., 2018). Fern Gully Lagoon C:N values were higher on average than those from Welsby Lagoon sediments, with ratios ranging from ~37 to 112, with a mean of ~85 (Fig. 5.2d, Table D1).

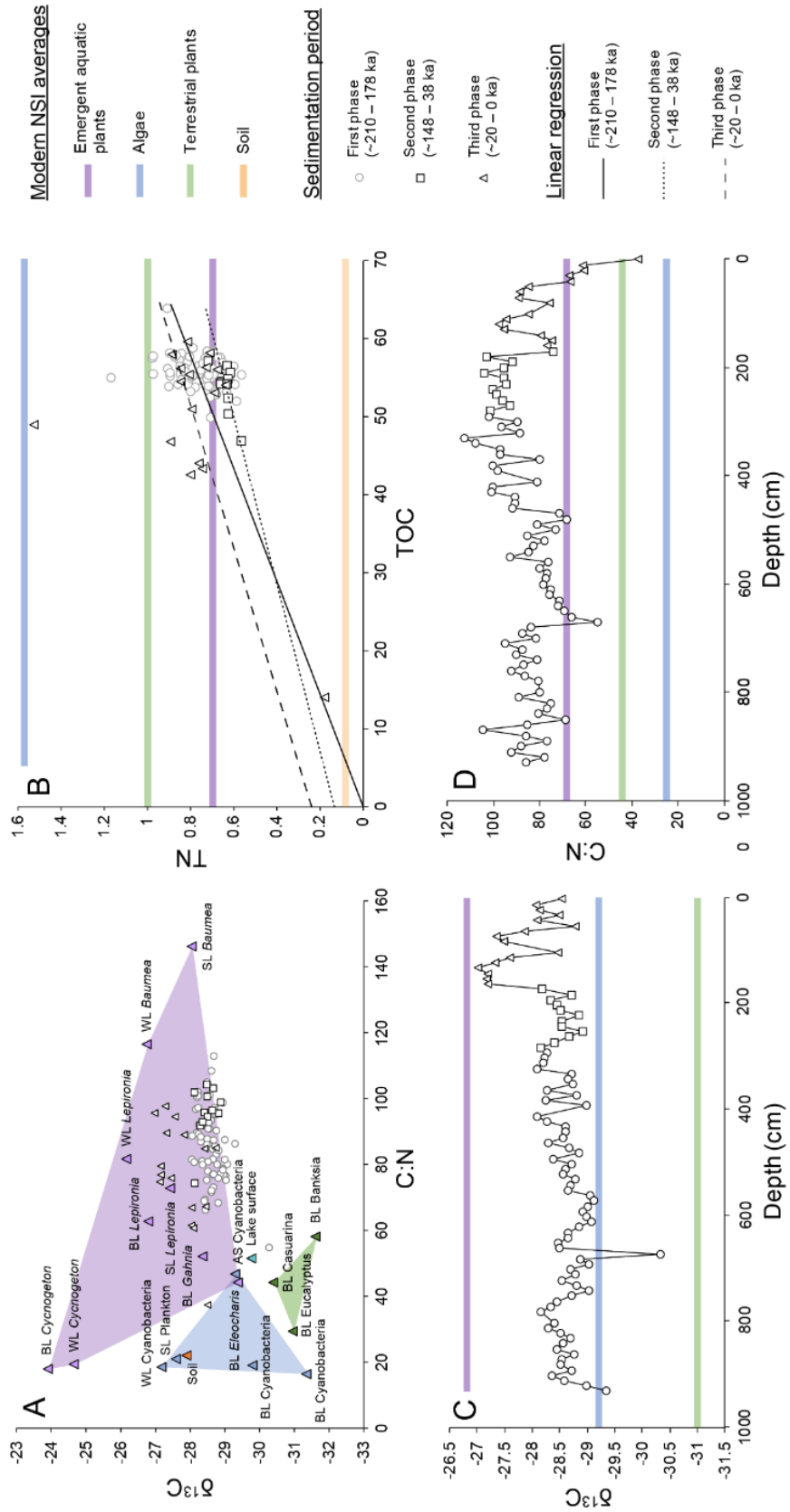

Figure 5.2: Carbon and nitrogen isotopes, with modern source samples and averages adapted from Cadd et al. (2018). **A:** $\delta^{13}C_{OM}$ vs total organic carbon-total nitrogen (C:N) ratio (Sample sources from Cadd et al. (2018): WL: Welsby Lagoon; SL: Swallow Lagoon; BL: Blue Lake and AS: Amity Swamp). **B:** Total organic carbon (TOC) vs total nitrogen (TN). Assuming a linear relationship between TOC and TN, the amount of inorganic nitrogen (N_{in}) is defined as the y-axis intercept (first phase N_{in} = ~0%, second phase N_{in} = ~0.15%, third phase ~ N_{in} = 0.25%). **C:** Sediment $\delta^{13}C$ plotted by depth. **D:** Sediment C:N plotted by depth.

The initial sedimentation phase at Fern Gully Lagoon, from 209.3 ± 28.4 ka to 177.5 ± 25.4 ka, was characterised by high TOC and C:N, and low $\delta^{13}C_{OM}$. TOC and $\delta^{13}C_{OM}$ are relatively constant during this period (55 ± 5% and 28.7 ± 1 ‰, respectively; Fig. 5.2b,c). C:N notably declines at 670 cm (~197 ka) to ~55, followed by a gradual increase to ~100 at the end of the first phase at ~177.5 ka (Fig. 5.2c). The second sedimentation phase, from 155.2 ± 24.9 to 34.7 ± 14.5 ka, is characterised by relatively constant values of C:N, TOC, $\delta^{13}C_{OM}$ and TN. The third and fourth sedimentation phases, from 20.9 ± 1.4 ka to the present, are characterised by a gradual decline in C:N, which reaches its lowest value at the end of phase four (~37, Fig. 5.2d). $\delta^{13}C_{OM}$ begins the third phase at a record high (~16.8 ‰), before gradually declining to a mean value similar to that recorded during previous phases (~28.7 ‰) at ~1.6 ka.

5.7.2 Lipid biomarkers

Lipid biomarker distributions are dominated by indicators of aquatic macrophyte and terrestrial higher plant abundances, most notably due to the dominance of mid- and long-chain *n*-alkanes (i.e., *n*-$C_{23–31}$; Fig. 5.3b), sitosterol and stigmasterol and their stanol derivatives, lupeol, lupanone and taraxerol, similar to markers indicative of shallow wetlands and terrestrial soils after Ficken et al. (2000), Ronkainen et al. (2013) and Naafs et al. (2019). However, C_{31}17α21β(H)-homohopane dominates the apolar fractions in most lipid biomarker samples (Fig. 5.3b,c), which is typical for peatlands and often attributed to the acidic depositional environment (Inglis et al., 2018). There was a rapid increase in the P_{aq} index defined by Ficken et al. (2000), which is indicative of higher contributions of submerged or floating leaf macrophytes (with values > 0.7) relative to emergent macrophytes and higher vascular plants (with values < 0.1; Ficken et al., 2000; Zhou et al., 2010; Ronkainen et al., 2013), and decline in average *n*-alkane chain length ($ACL_{C27–33}$) during the first sedimentation phase at Fern Gully Lagoon (~210–178 ka). During early MIS 5 P_{aq} values were high, and $ACL_{C27–33}$ values were low, with gradually increasing separation between the two indices (Fig. 5.4g). Holocene values were similar to those recorded during MIS 7a–c. The highest $ACL_{C27–33}$ value (30.9) occurred during the earliest part of the record, while the lowest $ACL_{C27–33}$ value (27.5) occurred during late MIS 6 to early MIS 5 (Fig. 5.4g). P_{aq} values indicate that aquatic macrophytes likely had the greatest relative OM contribution to Fern Gully Lagoon sediments for much of the past ~210 kyr.

The ACL of high molecular weight *n*-alkanes C_{27}–C_{33}, (e.g. Diefendorf and Freimuth, 2017) and relative shifts in the ratio of low to high molecular weight *n*-alkanes (Paq; Zhou et al., 2010) are generally covariant ($r^2 = 0.64$, $p < 0.05$, $n = 29$) throughout the record (Fig. 5.5b). $ACL_{C27–33}$ at Fern Gully Lagoon had a significant positive relationship with TN and the relative proportion of sclerophyll taxa ($r^2 = 0.42$ (and $r^2 = 0.42$), $p < 0.05$, $n = 30$, Fig. 5.5a,e), and negative relationships with C:N and the relative proportion of rainforest taxa ($r^2 = 0.30$ (and $r^2 = 0.36$), $p < 0.05$, $n = 30$, Fig. 5.5c,d).

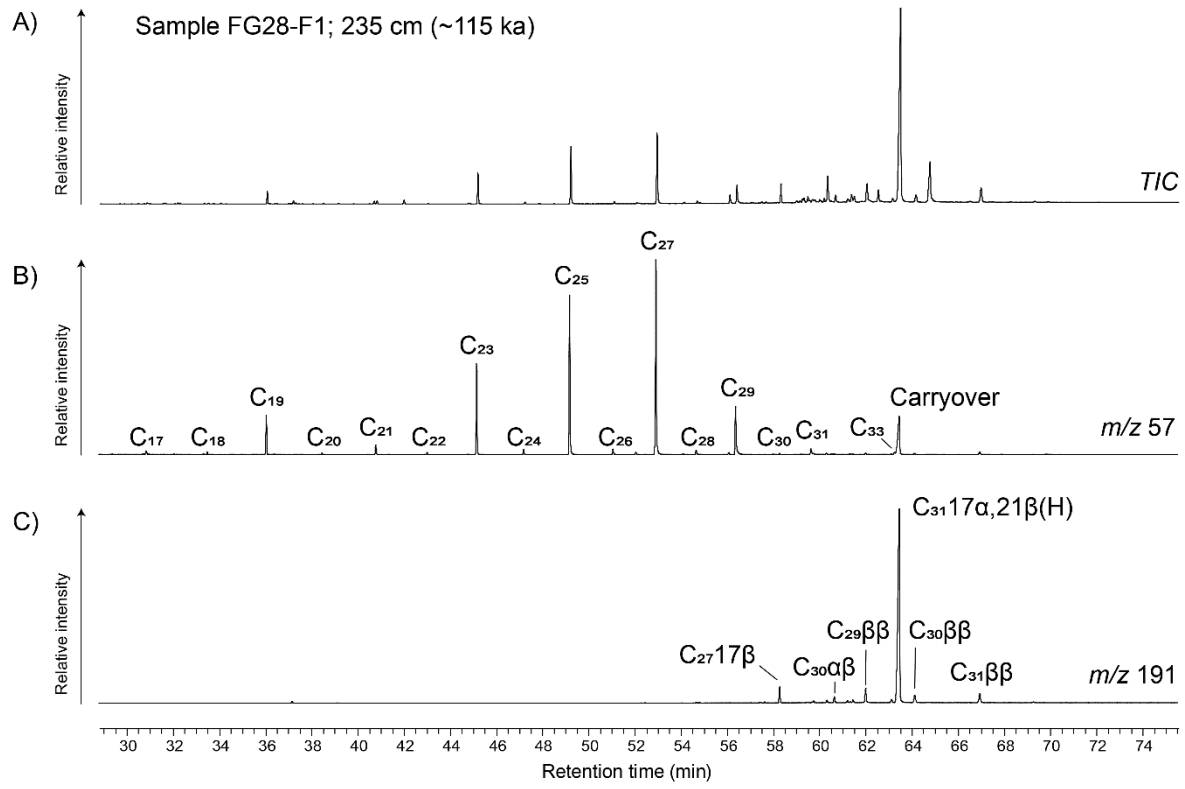

Figure 5.3: Example GC-MS chromatogram for the apolar fraction of Fern Gully Lagoon sediments. **A:** Total ion chromatogram (TIC); **B:** m/z 57, highlighting n-alkane occurrence ('Carryover' indicates the influence of $C_{31}17\alpha21\beta(H)$ - homohopane); **C:** m/z 191, highlighting hopanoid occurrence.

GDGT distributions are dominated by brGDGTs, with BIT indices close to 1, indicating the dominance of terrestrial OM in the sediments (Table D1; Weijers et al., 2006). The three selected brGDGT MAAT calibrations had substantial differences in inferred contemporary temperatures based on modern sediment and humus samples, which ranged between ~17.5 and

24.5°C. Comparison of these contemporary surface sample temperature reconstructions with mean recorded MAAT from Point Lookout (BOM, 2019) indicated that the soil calibrations of Weijers et al. (2007) are likely the best fit for Fern Gully Lagoon, with a calculated MAAT of 23.7°C compared to the instrumental 23-year average MAAT of 22.1 ± 0.2°C. However, contemporary mean annual temperatures are within root mean squared error (RSME) for both the Weijers et al. (2007) and Peterse et al. (2012) calibrations (± 4.8 and 5.0°C respectively at 1σ), indicating that both calibrations are likely suitable for Fern Gully Lagoon.

Reconstructed MAATs were above average during MIS 7a–c, before declining during the transition into MIS 6. MAAT increased during early MIS 5, albeit peaking at a value lower than during MIS 7a–c. There was a decline in MAAT mid-MIS 5, in agreement with MIS 5c MAAT inferred from plant indicator taxa (Kemp et al., submitted). Reconstructed MAAT was relatively low during the LGM, at ~1–2°C below Holocene values (Fig. 5.4g).

brGDGT derived pH values at Fern Gully Lagoon were relatively stable, ranging between ~5.4 and 6.3 over the past ~210 kyr. As such, the lipid biomarker C_{31}17α21β(H)-homohopane can be used as an indicator of wetland 'peatiness' after Inglis et al. (2018). To ensure that this relationship was not dependent on OM flux, we used a ratio of C_{31}17α21β(H)-homohopane to terrestrial OM indicators Sitosterol and Stigmasterol (Fig. D2; Ronkainen et al., 2013) to estimate changes in Fern Gully Lagoon sediment peatiness (Fig. 5.4e).

5.7.3 Wetland surface area

The two depth-sounding transects (Fig. 5.1c,d) indicated that the Fern Gully Lagoon basin is a concave bowl, reflecting with the morphology of surrounding dunes, with shallower slopes situated at ~645 and ~410 cm below the current wetland surface. The sediment is ~10.6 m deep at the centre of the basin, which has a slightly steeper north-eastern than south-western slope (Fig. 5.1c,d). An approximate reconstruction of changes in total wetland surface area (Fig. 5.6a,b) indicates relatively rapid increases in wetland size during the first phase of sedimentation (MIS 7a–c to mid-MIS 6) and during phase 4 (mid-late Holocene).

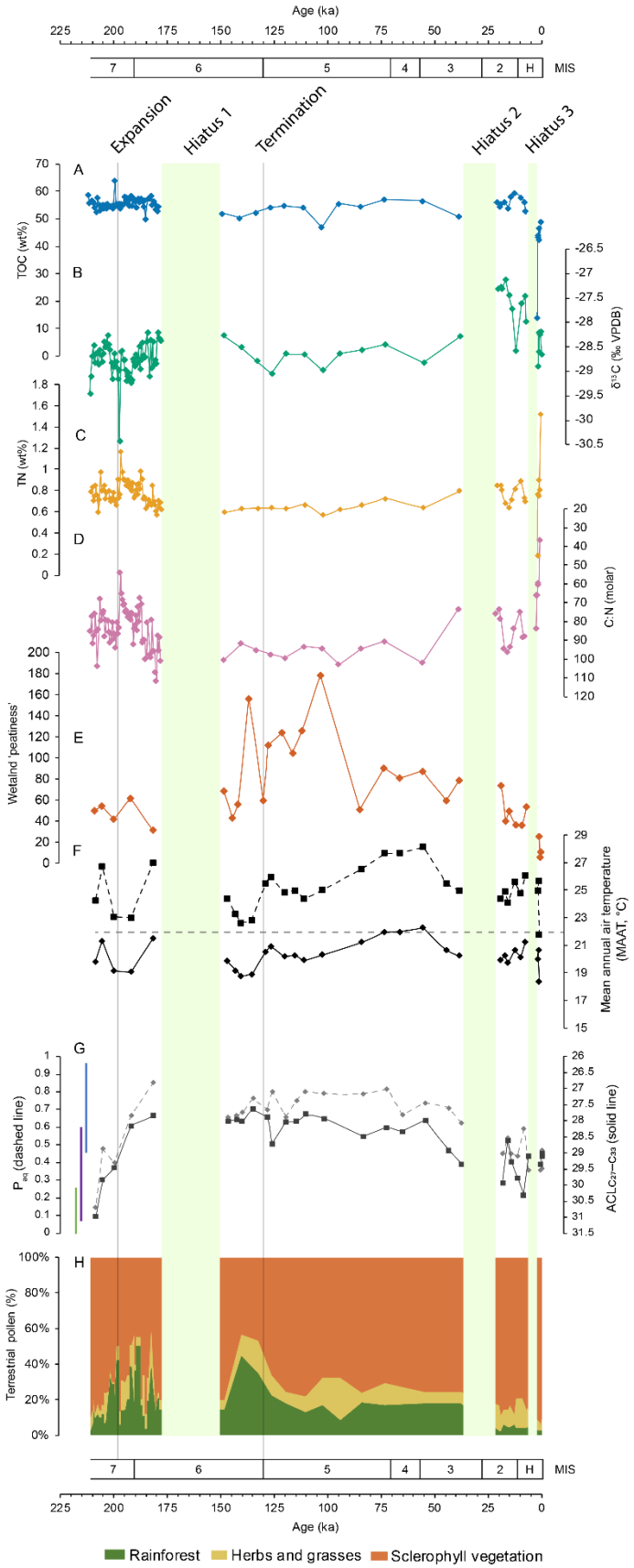

Figure 5.4: Fern Gully Lagoon organic geochemistry and summary vegetation records. **A:** Total organic carbon (TOC) %. **B:** $\delta^{13}C$. **C:** Total nitrogen (TN) %. **D:** Carbon/nitrogen molar ratio. **E:** wetland 'peatiness' indicator – the ratio of peat indicator $C_{31}17\alpha21\beta(H)$-homohopane to more terrestrial OM biomarkers Sitosterol+stanol/Stigmasterol+stanol. **F:** Mean annual air temperature (MAAT) after Weijers et al. (2007) equation 5 (dashed line) and Peterse et al. (2012) (solid line). Observed modern MAAT is shown as a horizontal grey dashed line. **G:** Average *n*-alkane chain length ($ACL_{C27–33}$, solid line) and the relative proportion of mid to long *n*-alkane chain lengths (P_{aq}, dashed line). Vertical lines on the left denote the P_{aq} ranges of (from left to right) terrestrial, emergent and aquatic taxa as described by Ficken et al. (2000). **H:** Relative proportion of rainforest, herb and grass and sclerophyllous trees and shrubs from Kemp et al. (submitted). Shaded blocks denote the three sedimentary hiatuses. Vertical lines indicate the approximate timing of wetland expansion as identified by basin mapping and the MIS 6 to MIS 5e glacial termination as identified by the OxCal Bayesian age-depth model (Kemp et al., 2020).

5.8 Discussion

5.8.1 $\delta^{13}C$ of organic material

Several factors can influence sediment $\delta^{13}C_{OM}$, including atmospheric $\delta^{13}C$ as well as atmospheric CO_2 concentration (Schubert and Jahren, 2012; Prentice et al., 2017), discrimination depending on differing dominant vegetation (Diefendorf and Freimuth, 2017), changes in MAAT, and precipitation (Bush and McInerney, 2015; Diefendorf and Freimuth, 2017). For the purposes of comparing interglacial climates using $\delta^{13}C_{OM}$, some possible influences on changing $\delta^{13}C$ can be largely eliminated: the brGDGT MAAT reconstruction indicates similar mean temperatures (±1°C, Fig. 5.4f) for MIS 7a–c, early MIS 5 and the Holocene, suggesting the influence of changing MAAT on $\delta^{13}C_{OM}$ was minor. Similarly, the strong positive relationship between $\delta^{13}C_{om}$ values and carbon isotope discrimination in plant leaves ($\Delta_{leaf,}$ after Diefendorf and Freimuth (2017); $r^2 = 0.97$, $p < 0.005$, $n = 91$; Fig. D1) indicates that changing atmospheric $\delta^{13}C$ cannot explain variations in the $\delta^{13}C_{OM}$ sedimentary record.

As there was likely very little overland flow to the wetland due to the highly permeable catchment soils, and the core as taken from the approximate centre of the wetland, introduction of OM from the surrounding catchment and overhanging vegetation is unlikely for much of the record. However, changes in the dominant wetland macrophyte taxon could influence $\delta^{13}C_{OM}$ (Diefendorf and Freimuth, 2017). Limited covariation in the relative abundance of Restionaceae pollen and $\delta^{13}C_{OM}$ ($r^2 = 0.14$, $p < 0.05$, $n = 57$), and the relative abundance of Cyperaceae pollen nd $\delta^{13}C_{OM}$ ($r^2 = 0.01$, $p = 0.55$, $n = 57$) (the two most abundant macrophyte taxa; Kemp et al., submitted), indicate that changes in dominant vegetation type are unlikely to influence $\delta^{13}C_{OM}$. By contrast, the influence of lower average atmospheric CO_2 concentrations on $\delta^{13}C_{OM}$ during MIS 7a–c (~245 ppmv; Bereiter et al., 2014) as compared to more recent interglacials (~280 ppmv) may be important, with $\delta^{13}C_{OM}$ up to 0.7‰ more negative independent of moisture availability (Schubert and Jahren, 2012).

Dry climates at Fern Gully Lagoon, which is likely to have been shallow for much of the past ~210 kyr, would have led to temporary water stress for macrophytes due to periods of wetland drying to the sediment surface, and so alteration of macrophyte $\delta^{13}C$ discrimination (Farquhar et al., 1989; Aichner et al., 2010). To restrict water loss due to drought, macrophytes

create a thickened leaf-wax layer, especially when moving from submerged to emergent conditions. Synthesis of thicker wax layers require longer n-alkane chain lengths, and hence a gradual shift to increasingly negative $\delta^{13}C_{OM}$ values for resulting bulk sediments (Aichner et al., 2010). In addition, drying of the wetland surface would have allowed terrestrial vegetation to spread, also driving resulting bulk $\delta^{13}C_{OM}$ lower. As almost all of other drivers of changing $\delta^{13}C_{OM}$ likely have only a minor influence on the record, $\delta^{13}C_{OM}$ can be used to infer the frequency of wetland drying by associated changes in macrophyte water stress and terrestrial OM contribution.

5.8.2 Carbon and nitrogen

Very low quantities of inorganic nitrogen present within Fern Gully Lagoon, as indicated by the intercept of the linear regression on the TN axis (Fig. 5.2b), suggests that almost all available nitrogen in the system at the time of sedimentation was organically bound (Talbot, 2001). Little to no inorganic nitrogen (~0 % of dry weight N_{in}) was present during the first phase of sedimentation, second phase (155.2 ± 24.9 to 34.7 ± 14.5 ka) samples indicated a N_{in} of ~0.15 %, and third to fourth phase (20.9 ± 1.4 ka to present) samples indicated a N_{in} of ~0.25 %. As such, Fern Gully Lagoon has likely been nitrogen-limited for much of the past ~210 kyr.

Nitrogen availability at nearby Welsby Lagoon was also very low throughout its history, with less than ~1 % N_{in} present for at least the past 80 kyr (Cadd et al., 2018). The Welsby Lagoon record also indicates an increase in nitrogen availability over time like that recorded at Fern Gully Lagoon. A small increase in available nitrogen in NSI wetlands at very long time scales may be linked to a possible increase in the abundance of nitrogen-fixing soil bacteria *Frankia*, as indicated by an increase in the abundance of its symbiotic partner *Casuarina* on NSI over the past ~130 kyr (see Chapter 4).

High C:N values have previously been reported for the colonial green algae *Botryococcus* (Heyng et al., 2012), and for algae dominated OM in nitrogen limited systems (e.g. Mayr et al., 2009), which can result in OM C:N values as high as 20 (Talbot and Lærdal, 2000). Abundant *Botryococcus* algae were identified in nearby Welsby Lagoon (Cadd et al., 2018), and Brown Lake (Mariani pers. com.). However, *Botryococcus* algae were not identified, neither by microscopy nor diagnostic biomarkers (i.e., lack of botryococcane), in the Fern Gully Lagoon

sediments, reducing the likelihood of possible inaccuracy in the C:N record as noted in other studies (e.g. Huang et al., 1999).

5.8.3 *n*-Alkanes and lipid biomarkers

Changes in $ACL_{C27–33}$ (Diefendorf and Freimuth, 2017; Naafs et al., 2019), and P_{aq} (Ficken et al., 2000; Nichols et al., 2006; Zhou et al., 2010), can be used to infer changes in the composition of Fern Gully Lagoon vegetation. A BIT index value close to 1 (Table D1) for all samples, the dominance of mid- and long-chain *n*-alkanes (e.g. Fig. 5.3b) and terrestrial biomarkers (Sitosterol and Stigmasterol; Ronkainen et al., 2013) indicates that Fern Gully Lagoon sediments are likely dominated by terrestrial vegetation and emergent macrophyte OM input. Due to lack of algae-derived OM (~95% of samples have a C:N greater than 70; Fig. 5.2d), we can infer that Fern Gully Lagoon has likely been shallow for much of the past ~210 kyr.

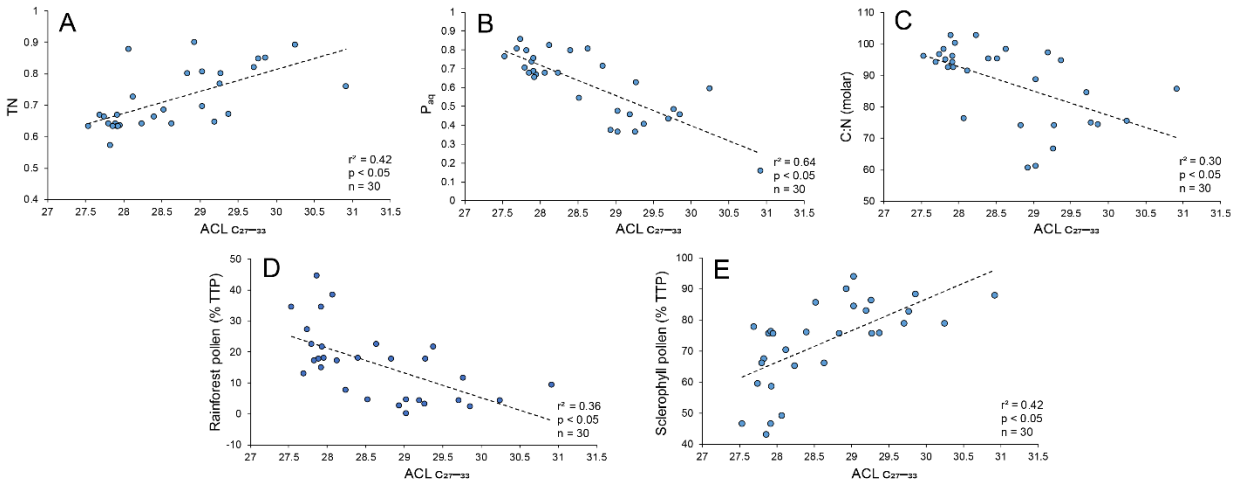

Figure 5.5: Comparison between stable isotope, alkane and pollen data from Fern Gully Lagoon and the average alkane chain length (*n*-$C_{27–33}$ ACL). Only significant correlations are shown. **A:** Total nitrogen (TN) %. **B:** Relative proportion of mid to long alkane chain length (P_{aq}, after Ficken et al. (2000)). **C:** Carbon:nitrogen (C:N) molar ratio. **D:** Rainforest taxa pollen as a percentage of total terrestrial pollen (TTP, Kemp et al., submitted). **E:** Sclerophyll taxa pollen as a percentage of TTP (Kemp et al., submitted).

The correlation between $ACL_{C27–33}$ and the relative abundance of sclerophyll taxa (and negative relationship with rainforest taxa) at Fern Gully Lagoon indicates that $ACL_{C27–33}$ values are likely linked to water stress in wetland and terrestrial vegetation ($r^2 = 0.42$ (and $r^2 = 0.36$), $p < 0.05$, $n = 30$) (Fig. 5.5d,e; Kemp et al., submitted). Similarly, the ratio of mid to long n-alkane chain lengths (P_{aq}) reflects wetland moisture availability via the relative abundance of submerged and floating macrophytes vs emergent macrophytes and terrestrial vegetation (Ficken et al., 2000; Zhou et al., 2010) and is coeval with $ACL_{C27–33}$ for much of the record. As such, P_{aq} can be used here as an approximate indicator of wetland water levels for Fern Gully Lagoon, similar to other peat hydrology studies (e.g. Zhou et al., 2005; Nichols et al., 2006; Zhou et al., 2010).

Bulk sediment *n*-alkane distributions are influenced by post-depositional in-wetland processes - preferential microbial degradation (Xie et al., 2003; Zheng et al., 2017) and peat breakdown releasing trapped hydrocarbons (Schellekens and Buurman, 2011). While preferential microbial degradation at Fern Gully Lagoon cannot be ruled out, peat degradation is unlikely as indicated by relatively high measured carbon preferential index (CPI) values for bulk sediment OM at Fern Gully Lagoon when compared to fresh material (Table D1; Schellekens and Buurman, 2011).

High levels of $C_{31}17\alpha21\beta$(H)-homohopane in most samples indicate that Fern Gully Lagoon has likely been a peat wetland for much of its history (Fig. 5.4e; after Inglis et al. (2018)). Australian *Sphagnum* peatlands are mostly found in alpine and montane regions and are not common in subtropical regions today (Whinam et al., 2003). However, changes in climate may have led to a change in the spatial distribution of *Sphagnum* peatlands. As such *Sphagnum* may have grown in NSI wetlands during glacials, altering the distribution of mid-chain length *n*-alkanes and so P_{aq} (e.g. Ortiz et al., 2010). However, no *Sphagnum* spores were identified in the pollen study (Kemp et al., submitted), indicating that *Sphagnum* was unlikely to have influenced the Fern Gully Lagoon P_{aq} record. While taraxerol has been used in the past as an indicator of mangrove abundance (e.g. Koch et al., 2003; Versteegh et al., 2004), mangrove pollen was not identified in Fern Gully Lagoon sediments (Kemp et al., submitted). Instead, taraxerol in Fern Gully Lagoon sediments likely originates from Ericaceae and peat mosses (e.g. Pancost et al., 2002; Naafs et al., 2019).

5.8.4 The influence of wetland expansion and shallowing on climate inference

Fern Gully Lagoon would have been protected from wind-driven evaporation by surrounding dunes in its early stages, and likely by trees growing around and on the wetland surface as indicated by a relatively high $ACL_{C27–33}$ and low P_{aq} in the early record (Table D1, Fig. 5.4g). As the surface area of the wetland expanded due to basin infill (Fig. 5.6), it would have received greater input from precipitation (there is little to no overland flow due to the highly permeable dunes) and been subject to greater direct evaporation. However, it also would have become more exposed to wind, and so a possible shift in the precipitation to evaporation ratio. Increasing wetland surface area and a subsequent increase wind-driven evaporation would have been modulated by the rate of wetland expansion via the apparent sedimentation rate.

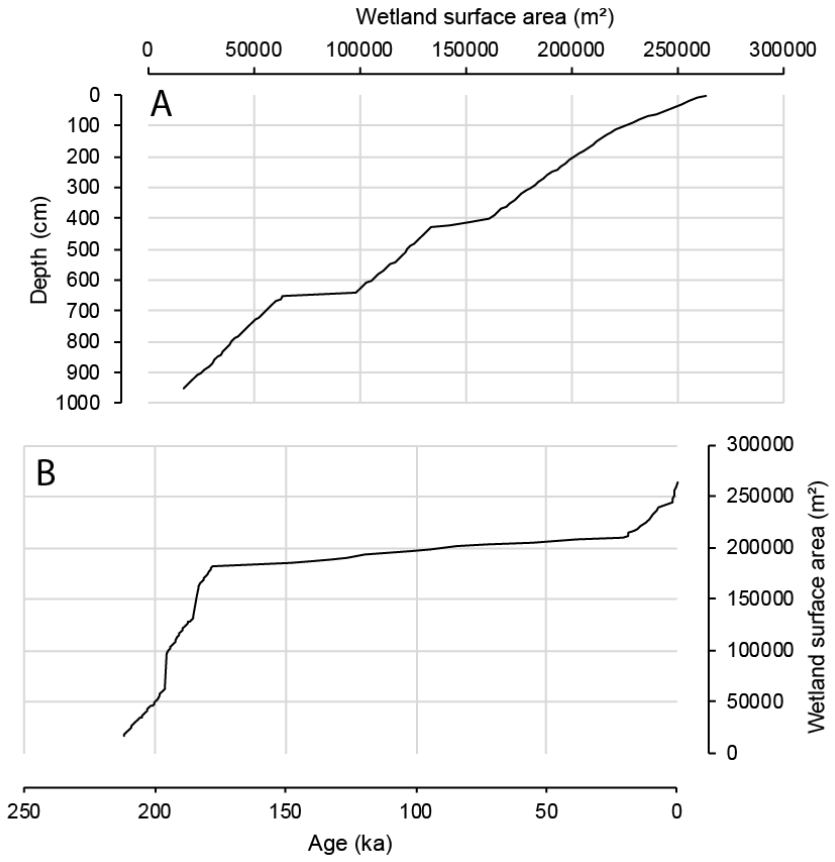

Figure 5.6: A.: Wetland surface area vs depth. **B.:** Change in the surface area of the wetland over time. The shape of a basin can alter the apparent sedimentation rate (Bennett and Buck, 2016).

Fern Gully Lagoon basin morphology is generally concave, shallow, and bowl-like (Fig. 5.1d). With a mostly constant rate of sedimentation, the sediment age-depth relationship for a bowl-shaped basin should be comparatively linear (Bennett and Buck, 2016), as observed at nearby wetlands (e.g. Petherick et al., 2009; Atahan et al., 2015). However, the strong sigmoidal shape of the age-depth profile for Fern Gully Lagoon (Kemp et al., 2020) more closely follows a sedimentation model for a bowl-shaped basin with an increasing rate of sedimentation (Bjune, 2005; Bennett and Buck, 2016).

A more rapid increase in the Fern Gully Lagoon wetland surface area during the Holocene than during MIS 5 (Fig. 5.6b) may have led to accelerated wetland shallowing due to increased wind-driven evaporation independent of changes in either precipitation or temperature. As such, greater wetland macrophyte water stress during the Holocene than during MIS 5 at Fern Gully Lagoon may be due to increased wetland evaporation rather than due to lower regional precipitation. However, the rate of Fern Gully Lagoon wetland surface area expansion during late MIS 7a–c was comparable, if not higher than that during the Holocene (Fig. 5.6b), during a period of considerably greater inferred moisture availability (Fig. 5.4h). As such, increasing wetland surface area is unlikely to have driven greater apparent wetland drying during the Holocene when compared to recent interglacials.

Basin morphology suggests that $\delta^{13}C_{OM}$ and C:N peaks of -30.3 ‰ and 55 close to the MIS 7–MIS 6 transition may result from rapid wetland expansion rather than changing climate. While only two transects constrain the basin shape, there is an apparent shallowing of basin slope present at ~650 cm (Fig. 5.1d, 5.6b; inundated somewhere between ~198 and 195 ka). Inundation of this shallow slope was associated with a relatively rapid expansion of the wetland surface area by approximately a third (~64,000 to ~98,000 m^2; Fig. 5.6b). The transition is associated with a pulse of highly terrestrial OM (Fig. 5.4b,d), and a peak in TN (Fig. 5.4c), as well as a change in dominant macrophyte taxon (Kemp et al., submitted). Similar increases in TN and $\delta^{13}C_{OM}$ were observed during the expansion of nearby Welsby Lagoon after the LGM (Barr et al., 2017).

5.8.5 brGDGTs and interglacial MAAT

The brGDGT-based paleotemperature calibration of Weijers et al. (2007) had the closest calculated modern MAAT to observed contemporary values based on two soil samples (25 and

50 m from the wetland), and two sediment samples; one from the coring location and the other from the wetland edge (Table D1), and so was selected as the most suitable of the three tested calibrations for Fern Gully Lagoon sediments. Weijers et al. (2007) calibrations have been applied successfully in peat studies (e.g. Ballantyne et al., 2010; Weijers et al., 2011; Huguet et al., 2013), and were closest to a recently developed peat-specific brGDGT calibration developed by Naafs et al. (2019). Unfortunately, 5-methyl and 6-methyl isomers in Fern Gully Lagoon samples could not be distinguished by the analytical method used for this study, which precluded the use of that calibration.

The brGDGT-based MAAT reconstruction from the Fern Gully sediments indicates that temperatures during the MIS 6 and MIS 4 glacials were similar if not warmer than during the MIS 7a–c and early MIS 5 interglacials. This result is counter to estimated glacial MAAT based on the climate envelopes of contemporary vegetation (Kemp et al., submitted), and global climate records (Lisiecki and Raymo, 2005; Elderfield et al., 2010; Tachikawa et al., 2011). Along with possible variability within considerable error margins (~5°C; Weijers et al., 2011; Peterse et al., 2012), brGDGT temperature calibrations are influenced by changes in precipitation (Weijers et al., 2007; Peterse et al., 2012) and fossil biomass (Weijers et al., 2011). As very low sedimentation rates were identified during mid-MIS 6, late MIS 5 and MIS 4 at Fern Gully Lagoon (Kemp et al., 2020), marginally increased drying of the wetland during glacials (inferred by an increase in C:N and $ACL_{C27–33}$, and decreased wetland peatiness, Fig 4d,e,g) may have resulted in altered brGDGT distributions and higher estimated MAAT than actual values. Shallowing has been previously linked to altered brGDGT distributions independent of temperature change (Tierney et al., 2010), although there related to an underestimation of MAAT. Regardless, brGDGT distributions at Fern Gully Lagoon have likely been altered unpredictably, making the current temperature reconstruction unreliable at best.

With only ±1°C of difference between reconstructed interglacial average MAAT for MIS 7a–c, early MIS 5 and the Holocene (Fig. 5.4f), it is likely that greater Holocene MAAT was not a factor in increasing evaporation or vegetation change at Fern Gully Lagoon. However, high temperatures inferred during glacials indicate a high degree of uncertainty in the temperature reconstruction, tracing the exact cause of which is unfortunately beyond the scope of this study.

5.8.6 Long-term changes in regional moisture availability

Previous studies from Fern Gully Lagoon concluded that regional climates during the Holocene were notably drier than during the previous two interglacials (Kemp et al., 2020; Kemp et al., submitted). Vegetation assemblages (taking into account lower atmospheric CO_2 concentrations) and inorganic flux records indicate MIS 7a–c may have been marginally wetter than MIS 5 (Kemp et al., 2020; Kemp et al., submitted). However, human occupation of NSI after the LGM likely led to altered vegetation assemblages and increased erosion (Kemp et al., submitted), necessitating this study of in-wetland climate proxies likely unaltered by human impact.

During early MIS 7a–c, more negative $\delta^{13}C_{OM}$ and relatively high $ACL_{C27–33}$ values indicate that Fern Gully Lagoon was at least periodically dry, with a high relative proportion of terrestrial OM and lower macrophyte input (Fig. 5.4b,g). Lower $ACL_{C27–33}$ values (likely indicative of a decrease in terrestrial water stress; Fig. 5.4g,) combined with higher $\delta^{13}C_{OM}$ values (likely indicative of a reduction in macrophyte water stress or increasing cyanobacteria input; Fig. 5.4b) during mid to late MIS 7a–c and early MIS 6 indicates increasing moisture availability. High moisture availability during late MIS 7a–c was observed in central Australia, with Lake Eyre water levels increasing during MIS 7a–c to their highest recorded levels, with wet climates continuing into early MIS 6 (Fu et al., 2017). The cause of relatively wet climates in both central Australia and the eastern subtropics during late MIS 7a–c and early MIS 6 may be due to the influence of an enhanced Australian summer monsoon combined with a more dominant La Niña ENSO phase (Pena et al., 2008; Fu et al., 2017).

P_{aq} values of between 0.6 and 0.7 indicate that a large part of the Fern Gully Lagoon basin was covered with floating or submerged macrophytes during early MIS 5 (Fig. 5.4g). Combined with peatier sediments, and lower terrestrial moisture stress during early MIS 5 than during either MIS 7a–c or the Holocene (higher $C_{31}17\alpha21\beta$(H)-homohopane proportion and lower $ACL_{C27–33}$), high P_{aq} values indicate that MIS 5e was likely the wettest interglacial in the Fern Gully Lagoon record (Fig. 5.4e,g). By contrast, shared $\delta^{13}C_{OM}$ ratios of between -28.1 and -28.9 indicate similar macrophyte water stress for MIS 7a–c and early MIS 5 (Fig. 5.4b). Due to lower atmospheric CO_2 concentrations during MIS 7a–c likely increasing vegetation water stress independent of precipitation (Prentice and Harrison, 2009; Dupont et al., 2019), the $\delta^{13}C_{OM}$

record likely underestimates MIS 7a–c moisture availability, and the wetland may have been marginally wetter during MIS 7a–c than during MIS 5. This inference is in agreement with the Fern Gully Lagoon pollen record (Kemp et al., submitted). An extended period of high moisture availability between late MIS 5 and mid-MIS 3 (Fig. 5.4b,g) may be due to more frequent La Niña phases during this period as observed in the Panama Gulf and the Bismarck Sea (Pena et al., 2008; Tachikawa et al., 2011).

Lower average $\delta^{13}C_{OM}$, higher average $ACL_{C27–33}$, and low sediment peatiness indicate that climates during the Holocene were likely drier than during previous interglacials at Fern Gully Lagoon (Fig. 5.4b,e,g). However, as $ACL_{C27–33}$ values and the relative abundance of $C_{31}17\alpha21\beta$(H)-homohopane differ only marginally between the Holocene and MIS 7a–c (Fig. 5.4e,g), it appears that estimates of very dry regional Holocene climates compared to MIS 7a–c climates (Kemp et al., 2020; Kemp et al., submitted) are not reflected in wetland conditions. As such, differences in inferred Holocene climates between this record of local wetland conditions and the regional climate records from Fern Gully Lagoon likely indicate the extent of human impact on NSI vegetation assemblages.

The influence of regional human occupation on NSI from at least ~21 ka (Neal and Stock, 1986) likely led to an increase in fire-resistant sclerophyll vegetation and increased erosion due to lower vegetation density beyond the influence of drying climates, likely altering the inorganic flux and vegetation assemblage records (Kemp et al., submitted). Compared to other records of Australian interglacial climates, the Fern Gully Lagoon wetland climate record indicates relatively mild Holocene drying when compared to southern (Ayliffe et al., 1998), or central (Bowler et al., 2001; Nanson et al., 2008; Fu et al., 2017) Australia, all of which recorded notable reductions in moisture availability during the Holocene compared to MIS 7a–c and MIS 5e climates.

A gradual decline in average $\delta^{13}C_{OM}$ values tentatively supports a hypothesis for increasingly dry interglacials in the Australian subtropics. However, a notable difference between Holocene and early MIS 5 $\delta^{13}C_{OM}$, $ACL_{C27–33}$ and wetland peatiness more supports a hypothesis for unusual subtropical Holocene climates when compared to recent interglacials. *n*-Alkane distributions and the degree of wetland peatiness similarly indicate that subtropical

Australian Holocene climates are unlikely to be the result of long-term drying, with similar inferred moisture availability for MIS 7a–c and the Holocene (Fig. 5.4g).

5.9 Conclusion

The Fern Gully Lagoon record indicates that Holocene climates in the Australian subtropics are unusual when compared to recent interglacials, likely linked to the influence of lower amplitude changes in insolation on regional climate drivers after Claussen et al. (2005) and Yin and Berger (2015), instead of the result of long-term drying as observed in central and south-eastern Australia (e.g. Ayliffe et al., 1998; Fu et al., 2017). As such, and perhaps unsurprisingly, the Fern Gully Lagoon record then indicates that drivers of subtropical climates at interglacial timescales are strongly influenced by insolation patterns, as predicted by climate modelling (e.g. Yin and Berger, 2015). More negative $\delta^{13}C_{OM,}$ higher $ACL_{C27–33}$ and less peaty wetland sediments indicate that the Holocene was likely drier than MIS 7a–c or early MIS 5 in subtropical Australia, in agreement with previous climate reconstructions (Kemp et al., 2020; Kemp et al., submitted).

Fern Gully Lagoon expanded relatively rapidly between ~198 and 195 ka, in association with the inundation of comparatively shallow basin slopes. Rapid wetland expansion had a notable impact on the carbon isotope record, which taken at face value indicated relatively dry climates but were unsupported by changes in *n*-alkane distributions or pollen-based vegetation reconstructions by Kemp et al. (submitted). Alteration of GDGT distributions independent of changes in MAAT resulted in a large degree of uncertainty in the reconstruction of interglacial temperatures, making determining whether direct evaporation may have driven increased Holocene drying and altered wetland vegetation assemblages on NSI difficult. Separation of the Fern Gully Lagoon wetland climate record from changes in wetland surface area and human influence on terrestrial vegetation assemblages illustrates the value of utilising a combination of proxies which have very different properties and provenance.

5.10 References

Aichner, B., Herzschuh, U., Wilkes, H., 2010. "Influence of aquatic macrophytes on the stable carbon isotopic signatures of sedimentary organic matter in lakes on the Tibetan Plateau." *Organic Geochemistry* 41, 706-718.

Anda, A., Simon, B., Soós, G., Menyhárt, L., da Silva, J.A.T., Kucserka, T., 2018. "Extending Class A pan evaporation for a shallow lake to simulate the impact of littoral sediment and submerged macrophytes: a case study for Keszthely Bay (Lake Balaton, Hungary)." *Agricultural and Forest Meteorology* 250-251, 277-289.

Atahan, P., Heijnis, H., Dodson, J., Grice, K., Le Metayer, P., Taffs, K., Hembrow, S., Woltering, M., Zawadzki, A., 2015. "Pollen, biomarker and stable isotope evidence of late Quaternary environmental change at Lake McKenzie, southeast Queensland." *Journal of Paleoliminology* 53, 139-156.

Ayliffe, L.K., Marianelli, P.C., Moriarty, K.C., Wells, R.T., McCulloch, M.T., Mortimer, G.E., Hellstrom, J.C., 1998. "500 ka precipitation record from southeastern Australia: Evidence for interglacial relative aridity." *Geology* 26, 147-150.

Ballantyne, A.P., Greenwood, D.R., Sinninghe Damsté, J.S., Csank, A.Z., Eberle, J.J., Rybczynski, N., 2010. "Significantly warmer Arctic surface temperatures during the Pliocene indicated by multiple independent proxies." *Geology* 38, 603-606.

Barr, C., Tibby, J., Leng, M.J., Tyler, J.J., Henderson, A.C.G., Overpeck, J.T., Simpson, G.L., Cole, J.E., Phipps, S.J., Marshall, J.C., McGregor, G.B., Hua, Q., McRobie, F.H., 2019. "Holocene El Niño–Southern Oscillation variability reflected in subtropical Australian precipitation." *Scientific Reports* 9, 1627.

Barr, C., Tibby, J., Moss, P.T., Halverson, G.P., Marshall, J.C., McGregor, G.B., Stirling, E., 2017. "A 25,000-year record of environmental change from Welsby Lagoon, North Stradbroke Island, in the Australian subtropics." *Quaternary International* 449, 106-118.

Bayon, G., De Deckker, P., Magee, J.W., Germain, Y., Bermell, S., Tachikawa, K., Norman, M.D., 2017. "Extensive wet episodes in Late Glacial Australia resulting from high-latitude forcings." *Scientific Reports* 7.

Bennett, K.D., Buck, C.E., 2016. "Interpretation of lake sediment accumulation rates." *The Holocene* 26, 1092-1102.

Bereiter, B., Eggleston, S., Schmitt, J., Nehrbass-Ahles, C., Stocker, T.F., Fischer, H., Kipfstuhl, S., Chappellaz, J., 2014. "Revision of the EPICA Dome C CO_2 record from 800 to 600 kyr before present." *Geophysical Research Letters* 42, 542-549.

Berger, A., Yin, Q., 2012. "Chapter 15 - Modelling the Past and Future Interglacials in Response to Astronomical and Greenhouse Gas Forcing", in: Henderson-Sellers, A., McGuffie, K.

(Eds.), The Future of the World's Climate (Second Edition). Elsevier, Boston, pp. 437-462.

Bjune, A.E., 2005. "Holocene vegetation history and tree-line changes on a north–south transect crossing major climate gradients in southern Norway—evidence from pollen and plant macrofossils in lake sediments." *Review of Palaeobotany and Palynology* 133, 249-275.

BOM, 2005. "Australian Köppen climate classifications based on a standard 30 year climatology (1961-1990)". Bureau of Meterology, Commonwealth of Australia.

BOM, 2019. "Climate statistics for Australian locations: Point Lookout 1997 to 2019". Bureau of Meterology, Commonwealth of Australia.

Bowler, J.M., Duller, G.A.T., Perret, N., Prescott, J.R., Wyrwoll, K.-H., 1998. "Hydrologic changes in monsoonal climates of the last glacial cycle: stratigraphy and luminescence dating of Lake Woods, N.T. Australia." *Paleoclimates* 3, 179-207.

Bowler, J.M., Wyrwoll, K.-H., Lu, Y., 2001. "Variations of the northwest Australia summer monsoon over the last 300,000 years: The paleohydrological record of the Gregory (Mulan) Lakes system." *Quaternary International* 82-85, 63-80.

Bush, R.T., McInerney, F.A., 2013. "Leaf wax n-alkane distributions in and across modern plants: Implications for paleoecology and chemotaxonomy." *Geochimica et Cosmochimica Acta* 117, 161-179.

Bush, R.T., McInerney, F.A., 2015. "Influence of temperature and C_4 abundance on n-alkane chain length distributions across the central USA." *Organic Geochemistry* 79, 65-73.

Cadd, H., Tibby, J., Barr, C., Tyler, J., Unger, L., Leng, M., Marshall, J., McGregor, G., Lewis, R., Arnold, L., Lewis, T., Baldock, J., 2018. "Development of a southern hemisphere subtropical wetland (Welsby Lagoon, south-east Queensland, Australia) through the last glacial cycle." *Quaternary Science Reviews* 202, 53-65.

Calvert, S.E., 2004. "Beware intercepts: interpreting compositional ratios in multi-component sediments and sedimentary rocks." *Organic Geochemistry* 35, 981-987.

Clark, M., Hounslow, M., 2009. "CPLSlot Version 2.4b", Monash University, Victoria, Australia.

Claussen, M., Brovkin, V., Calov, R., Ganopolski, A., Kubatzki, C., 2005. "Did Humankind Prevent a Holocene Glaciation?" *Climatic Change* 69, 409-417.

Colhoun, E.A., Pola, J.S., Barton, C.E., Heijnis, H., 1999. "Late Pleistocene vegetation and climate history of Lake Selina, western Tasmania." *Quaternary International* 57–58, 5–23.

De Jonge, C., Hopmans, E.C., Stadnitskaia, A., Rijpstra, W.I.C., Hofland, R., Tegelaar, E., Damsté, J.S.S., 2013. "Identification of novel penta-and hexamethylated branched

glycerol dialkyl glycerol tetraethers in peat using HPLC–MS2, GC–MS and GC–SMB-MS." *Organic geochemistry* 54, 78-82.

De Jonge, C., Hopmans, E.C., Zell, C.I., Kim, J.-H., Schouten, S., Damsté, J.S.S., 2014. "Occurrence and abundance of 6-methyl branched glycerol dialkyl glycerol tetraethers in soils: Implications for palaeoclimate reconstruction." *Geochimica et Cosmochimica Acta* 141, 97-112.

Diefendorf, A.F., 2010. "Global patterns in leaf $\delta^{13}C$ discrimination and implications for studies of past and future climate." *Proceedings of the National Academy of Sciences of the United States of America* 107, 5738-5743.

Diefendorf, A.F., Freimuth, E.J., 2017. "Extracting the most from terrestrial plant-derived *n*-alkyl lipids and their carbon isotopes from the sedimentary record: A review." *Organic Geochemistry* 103, 1-21.

Dupont, L., Weinelt, M., 1996. "Vegetation history of the savanna corridor between the Guinean and the Congolian rain forest during the last 150,000 years." *Vegetation History and Archaeobotany* 5, 273-292.

Dupont, L.M., Caley, T., Castañeda, I.S., 2019. "Effects of atmospheric CO_2 variability of the past 800 kyr on the biomes of southeast Africa." *Climate of the Past* 15, 1083-1097.

Eggenberger, S., Gobet, E., Leeuwen, J., Schwörer, C., Knaap, W., Dobben, H., Vogel, H., Tinner, W., Rambeau, C., 2018. "Millennial multi-proxy reconstruction of oasis dynamics in Jordan, by the Dead Sea." *The Journal of Quaternary Plant Ecology, Palaeoclimate and Ancient Agriculture - Official Organ of the International Work Group for Palaeoethnobotany* 27, 649-664.

Elderfield, H., Greaves, M., Barker, S., Hall, I.R., Tripati, A., Ferretti, P., Crowhurst, S., Booth, L., Daunt, C., 2010. "A record of bottom water temperature and seawater $\delta^{18}O$ for the Southern Ocean over the past 440 kyr based on Mg/Ca of benthic foraminiferal Uvigerina spp." *Quaternary Science Reviews* 29, 160-169.

Farquhar, G.D., Ehleringer, J.R., Hubick, K.T., 1989. "Carbon isotope discrimination and photosynthesis." *Annual review of plant biology* 40, 503-537.

Ficken, K.J., Li, B., Swain, D.L., Eglinton, G., 2000. "An *n*-alkane proxy for the sedimentary input of submerged/floating freshwater aquatic macrophytes." *Organic Geochemistry* 31, 745-749.

Freund, M., Henley, B.J., Karoly, D.J., Allen, K.J., Baker, P.J., 2017. "Multi-century cool- and warm-season rainfall reconstructions for Australia's major climatic regions." *Climate of the Past* 13, 1751-1770.

Fritz, M., Unkel, I., Lenz, J., Gajewski, K., Frenzel, P., Paquette, N., Lantuit, H., Körte, L., Wetterich, S., 2018. "Regional environmental change versus local signal preservation in

Holocene thermokarst lake sediments: A case study from Herschel Island, Yukon (Canada)." *Journal of Paleolimnology* 60, 77-96.

Fu, X., Cohen, T.J., Arnold, L.J., 2017. "Extending the record of lacustrine phases beyond the last interglacial for Lake Eyre in central Australia using luminescence dating." *Quaternary Science Reviews* 162, 88-110.

Glaser, P.H., Hansen, B.C., Donovan, J.J., Givnish, T.J., Stricker, C.A., Volin, J.C., 2013. "Holocene dynamics of the Florida Everglades with respect to climate, dustfall, and tropical storms." *Proceedings of the National Academy of Sciences* 110, 17211-17216.

Greer, J.S., McInerney, F.A., Vann, D.R., Song, X., 2018. "Evaluating methods for extraction of α-cellulose from leaves of Melaleuca quinquenervia for stable carbon and oxygen isotope analysis." *Rapid Communications in Mass Spectrometry* 32, 711-720.

Harle, K.J., Heijnis, H., Chisari, R., Kershaw, A.P., Zoppi, U., Jacobsen, G., 2002. "A chronology for the long pollen record from Lake Wangoom, western Victoria (Australia) as derived from uranium/thorium disequilibrium dating." *Journal of Quaternary Science* 17, 707-720.

Hayward, B.W., Sabaa, A.T., Kolodziej, A., Crundwell, M.P., Steph, S., Scott, G.H., Neil, H.L., Bostock, H.C., Carter, L., Grenfell, H.R., 2012. "Planktic foraminifera-based sea-surface temperature record in the Tasman Sea and history of the Subtropical Front around New Zealand, over the last one million years." *Marine Micropaleontology* 82-83, 13-27.

Heiri, O., Lotter, A., Lemcke, G., 2001. "Loss on ignition as a method for estimating organic and carbonate content in sediments: reproducibility and comparability of results." *Journal of Paleoliminology* 25, 101-110.

Heyng, A.M., Mayr, C., Lücke, A., Striewski, B., Wastegård, S., Wissel, H., 2012. "Environmental changes in northern New Zealand since the Middle Holocene inferred from stable isotope records ($\delta^{15}N$, $\delta^{13}C$) of Lake Pupuke." *Journal of paleolimnology* 48, 351-366.

Hopmans, E.C., Weijers, J.W., Schefuß, E., Herfort, L., Damsté, J.S.S., Schouten, S., 2004. "A novel proxy for terrestrial organic matter in sediments based on branched and isoprenoid tetraether lipids." *Earth and Planetary Science Letters* 224, 107-116.

Huang, Y., Street-Perrott, F.A., Perrott, R.A., Metzger, P., Eglinton, G., 1999. "Glacial–interglacial environmental changes inferred from molecular and compound-specific $\delta^{13}C$ analyses of sediments from Sacred Lake, Mt. Kenya." *Geochimica et Cosmochimica Acta* 63, 1383-1404.

Huguet, A., Fosse, C., Laggoun-Défarge, F., Delarue, F., Derenne, S., 2013. "Effects of a short-term experimental microclimate warming on the abundance and distribution of branched GDGTs in a French peatland." *Geochimica et Cosmochimica Acta* 105, 294-315.

Inglis, G.N., Naafs, B.D.A., Zheng, Y., McClymont, E.L., Evershed, R.P., Pancost, R.D., 2018. "Distributions of geohopanoids in peat: Implications for the use of hopanoid-based proxies in natural archives." *Geochimica et Cosmochimica Acta* 224, 249-261.

Johnson, B.E., Noble, P.J., Heyvaert, A.C., Chandra, S., Karlin, R., 2018. "Anthropogenic and climatic influences on the diatom flora within the Fallen Leaf Lake watershed, Lake Tahoe Basin, California over the last millennium." *Journal of Paleolimnology* 59, 159-173.

Kemp, C.W., Tibby, J., Arnold, L.J., Barr, C., submitted. "Subtropical climate, fire and vegetation dynamics on North Stradbroke Island (eastern Australia) during the last three interglacials." *Journal of Quaternary Science*.

Kemp, C.W., Tibby, J., Arnold, L.J., Barr, C., Gadd, P.S., Marshall, J.C., McGregor, G.B., Jacobsen, G.E., 2020. "Climates of the last three interglacials in subtropical eastern Australia inferred from wetland sediment geochemistry." *Palaeogeography, Palaeoclimatology, Palaeoecology* 538.

Kershaw, A.P., Bretherton, S.C., van der Kaars, S., 2007a. "A complete pollen record of the last 230 ka from Lynch's Crater, north-eastern Australia." *Palaeogeography, Palaeoclimatology, Palaeoecology* 251, 23-45.

Kershaw, A.P., McKenzie, G.M., Porch, N., Roberts, R.G., Brown, J., Heijnis, H., Orr, M.L., Jacobsen, G., Newall, P.R., 2007b. "A high-resolution record of vegetation and climate through the last glacial cycles from Caledonia Fen, southeastern highlands of Australia." *Journal of Quaternary Science* 22, 481-500.

Kershaw, P., Moss, P., Van Der Kaars, S., 2003. "Causes and consequences of long-term climatic variability on the Australian continent." *Freshwater Biology* 48, 1274-1283.

Koch, B., Rullkötter, J., Lara, R., 2003. "Evaluation of triterpenols and sterols as organic matter biomarkers in a mangrove ecosystem in northern Brazil." *Wetlands Ecology and management* 11, 257-263.

Leach, L.M., 2011. "Hydrology and physical setting of North Stradbroke Island." *Proceedings of the Royal Society of Queensland* 117, 21-46.

Lisiecki, L.E., Raymo, M.E., 2005. "A Pliocene-Pleistocene stack of 57 globally distributed benthic $\delta^{18}O$ records." *Paleoceanography* 20.

Loutre, M.F., Berger, A., 2000. "Future Climatic Changes: Are We Entering an Exceptionally Long Interglacial?" *Climatic Change* 46, 61-90.

Lu, Z., Liu, Z., Zhu, J., Cobb, K., 2018. "A Review of Paleo El Niño-Southern Oscillation." *Atmosphere* 9.

Lynch, A.H., Beringer, J., Kershaw, P., Marshall, A., Mooney, S., Tapper, N., Turney, C., Van Der Kaars, S., 2007. "Using the Paleorecord to Evaluate Climate and Fire Interactions in Australia." *Annual Review of Earth and Planetary Sciences* 35, 215-239.

Mariani, M., Tibby, J., Barr, C., Moss, P., Marshall, J.C., McGregor, G.B., 2019. "Reduced rainfall drives biomass limitation of long-term fire activity in Australia's subtropical sclerophyll forests." *Journal of Biogeography* 46, 1974-1987.

Marshall, J., McGregor, G., 2011. "The Influence of water depth on the distribution of the emergent sedge Lepironia articulata (Cyperaceae) in two dune lakes of southern Queensland Wallum wetlands." *Proceedings of the Royal of Queensland* 117, 193-199.

Mayr, C., Lücke, A., Maidana, N.I., Wille, M., Haberzettl, T., Corbella, H., Ohlendorf, C., Schäbitz, F., Fey, M., Janssen, S., 2009. "Isotopic fingerprints on lacustrine organic matter from Laguna Potrok Aike (southern Patagonia, Argentina) reflect environmental changes during the last 16,000 years." *Journal of Paleolimnology* 42, 81-102.

Mays, J.L., Brenner, M., Curtis, J.H., Curtis, K.V., Hodell, D.A., Correa-Metrio, A., Escobar, J., Dutton, A.L., Zimmerman, A.R., Guilderson, T.P., 2017. "Stable carbon isotopes ($\delta^{13}C$) of total organic carbon and long-chain n-alkanes as proxies for climate and environmental change in a sediment core from Lake Petén-Itzá, Guatemala." *Journal of Paleolimnology* 57, 307-319.

Meyers, P.A., Teranes, J.L., 2001. "Sediment organic matter", in: Last, W.M., Smol, J.P. (Eds.), Tracking Environmental Change Using Lake Sediments: physical and geochemical methods. Kluwer Academic Publishers, Dordrecht, Netherlands, pp. 239-269.

Moss, P.T., Kershaw, A.P., 2007. "A late Quaternary marine palynological record (oxygen isotope stages 1 to 7) for the humid tropics of northeastern Australia based on ODP Site 820." *Palaeogeography, Palaeoclimatology, Palaeoecology* 251, 4-22.

Moss, P.T., Tibby, J., Petherick, L., McGowan, H., Barr, C., 2013. "Late Quaternary vegetation history of North Stradbroke Island, Queensland, eastern Australia." *Quaternary Science Reviews* 74, 257-272.

Naafs, B.D.A., Inglis, G.N., Blewett, J., McClymont, E.L., Lauretano, V., Xie, S., Evershed, R.P., Pancost, R.D., 2019. "The potential of biomarker proxies to trace climate, vegetation, and biogeochemical processes in peat: A review." *Global and Planetary Change* 179, 57-79.

Naafs, B.D.A., Inglis, G.N., Zheng, Y., Amesbury, M.J., Biester, H., Bindler, R., Blewett, J., Burrows, M.A., del Castillo Torres, D., Chambers, F.M., Cohen, A.D., Evershed, R.P., Feakins, S.J., Gałka, M., Gallego-Sala, A., Gandois, L., Gray, D.M., Hatcher, P.G., Honorio Coronado, E.N., Hughes, P.D.M., Huguet, A., Könönen, M., Laggoun-Défarge, F., Lähteenoja, O., Lamentowicz, M., Marchant, R., McClymont, E., Pontevedra-Pombal, X., Ponton, C., Pourmand, A., Rizzuti, A.M., Rochefort, L., Schellekens, J., De Vleeschouwer, F., Pancost, R.D., 2017. "Introducing global peat-specific temperature and

pH calibrations based on brGDGT bacterial lipids." *Geochimica et Cosmochimica Acta* 208, 285-301.

Naeher, S., Niemann, H., Peterse, F., Smittenberg, R.H., Zigah, P.K., Schubert, C.J., 2014. "Tracing the methane cycle with lipid biomarkers in Lake Rotsee (Switzerland)." *Organic Geochemistry* 66, 174-181.

Naeher, S., Smittenberg, R.H., Gilli, A., Kirilova, E.P., Lotter, A.F., Schubert, C.J., 2012. "Impact of recent lake eutrophication on microbial community changes as revealed by high resolution lipid biomarkers in Rotsee (Switzerland)." *Organic Geochemistry* 49, 86-95.

Nanson, G.C., Price, D.M., Jones, B.G., Maroulis, J.C., Coleman, M., Bowman, H., Cohen, T.J., Pietsch, T.J., Larsen, J.R., 2008. "Alluvial evidence for major climate and flow regime changes during the middle and late Quaternary in eastern central Australia." *Geomorphology* 101, 109-129.

Neal, R., Stock, E., 1986. "Pleistocene occupation in the south-east Queensland coastal region." *Nature* 323, 618-621.

Nichols, J.E., Booth, R.K., Jackson, S.T., Pendall, E.G., Huang, Y., 2006. "Paleohydrologic reconstruction based on n-alkane distributions in ombrotrophic peat." *Organic Geochemistry* 37, 1505-1513.

Onetto Carvallo, C.A., 2018. "Identity and physiology of glycogen accumulating organisms in activated sludge", School of Agriculture, Food and Wine. University of Adelaide, Adelaide, South Australia.

Ortiz, J.E., Gallego, J.L.R., Torres, T., Díaz-Bautista, A., Sierra, C., 2010. "Palaeoenvironmental reconstruction of Northern Spain during the last 8000 cal yr BP based on the biomarker content of the Roñanzas peat bog (Asturias)." *Organic Geochemistry* 41, 454-466.

Pancost, R.D., Baas, M., van Geel, B., Damsté, J.S.S., 2002. "Biomarkers as proxies for plant inputs to peats: an example from a sub-boreal ombrotrophic bog." *Organic geochemistry* 33, 675-690.

Patton, N.R., Ellerton, D., Shulmeister, J., 2019. "High resolution remapping of the coastal dune fields of south east Queensland, Australia: a morphometric approach." *Journal of Maps* 15, 578-589.

Pena, L.D., Cacho, I., Ferretti, P., Hall, M.A., 2008. "El Niño–Southern Oscillation–like variability during glacial terminations and interlatitudinal teleconnections." *Paleoceanography* 23, 1-8.

Peters, K.E., Walters, C.C., Moldowan, J.M., 2007. "The biomarker guide: Volume 1, Biomarkers and isotopes in the environment and human history". Cambridge university press, Cambridge.

Peterse, F., van der Meer, J., Schouten, S., Weijers, J.W.H., Fierer, N., Jackson, R.B., Kim, J.-H., Sinninghe Damsté, J.S., 2012. "Revised calibration of the MBT–CBT paleotemperature proxy based on branched tetraether membrane lipids in surface soils." *Geochimica et Cosmochimica Acta* 96, 215-229.

Petherick, L.M., McGowan, H.A., Kamber, B.S., 2009. "Reconstructing transport pathways for late Quaternary dust from eastern Australia using the composition of trace elements of long traveled dusts." *Geomorphology* 105, 67-79.

Petherick, L.M., Moss, P.T., McGowan, H.A., 2017. "An extended Last Glacial Maximum in subtropical Australia." *Quaternary International* 432, 1-12.

Prentice, I.C., Cleator, S.F., Huang, Y.H., Harrison, S.P., Roulstone, I., 2017. "Reconstructing ice-age palaeoclimates: Quantifying low-CO_2 effects on plants." *Global and Planetary Change* 149, 166-176.

Prentice, I.C., Harrison, S.P., 2009. "Ecosystem effects of CO_2 concentration: evidence from past climates." *Climates of the Past* 5, 297-307.

Ronkainen, T., McClymont, E.L., Väliranta, M., Tuittila, E.-S., 2013. "The *n*-alkane and sterol composition of living fen plants as a potential tool for palaeoecological studies." *Organic Geochemistry* 59, 1-9.

Schellekens, J., Buurman, P., 2011. "*n*-Alkane distributions as palaeoclimatic proxies in ombrotrophic peat: The role of decomposition and dominant vegetation." *Geoderma* 164, 112-121.

Schouten, S., Hopmans, E.C., Damsté, J.S.S., 2013. "The organic geochemistry of glycerol dialkyl glycerol tetraether lipids: a review." *Organic geochemistry* 54, 19-61.

Schubert, B.A., Jahren, A.H., 2012. "The effect of atmospheric CO_2 concentration on carbon isotope fractionation in C_3 land plants." *Geochimica et Cosmochimica Acta* 96, 29-43.

Schweger, C., Froese, D., White, J.M., Westgate, J.A., 2011. "Pre-glacial and interglacial pollen records over the last 3 Ma from northwest Canada: Why do Holocene forests differ from those of previous interglaciations?" *Quaternary Science Reviews* 30, 2124-2133.

Smith, A., Tetzlaff, D., Gelbrecht, J., Kleine, L., Soulsby, C., 2020. "Riparian wetland rehabilitation and beaver re-colonization impacts on hydrological processes and water quality in a lowland agricultural catchment." *Science of The Total Environment* 699, 134302.

Sun, W., Zhang, E., Liu, E., Ji, M., Chen, R., Zhao, C., Shen, J., Li, Y., 2017. "Oscillations in the Indian summer monsoon during the Holocene inferred from a stable isotope record from pyrogenic carbon from Lake Chenghai, southwest China." *Journal of Asian Earth Sciences* 134, 29-36.

Sun, Y., Liang, L., Bloemendal, J., Li, Y., Wu, F., Yao, Z., Liu, Y., 2016. "High-resolution scanning XRF investigation of Chinese loess and its implications for millennial-scale monsoon variability." *Journal of Quaternary Science* 31, 191-202.

Tachikawa, K., Cartapanis, O., Vidal, L., Beaufort, L., Barlyaeva, T., Bard, E., 2011. "The precession phase of hydrological variability in the Western Pacific Warm Pool during the past 400 ka." *Quaternary Science Reviews* 30, 3716-3727.

Talbot, M.R., 2001. "Nitrogen isotopes in palaeolimnology", in: Last, W.M., Smol, J.P. (Eds.), Tracking Environmental Change Using Lake Sediments: physical and geochemical methods. Kluwer Academic Publishers, Dordrecht, Netherlands, pp. 401-439.

Talbot, M.R., Lærdal, T., 2000. "The Late Pleistocene-Holocene palaeolimnology of Lake Victoria, East Africa, based upon elemental and isotopic analyses of sedimentary organic matter." *Journal of Paleolimnology* 23, 141-164.

Tibby, J., Barr, C., Marshall, J.C., Mgregor, G.B., Moss, P.T., Arnold, L.J., Page, T.J., Questiaux, D., Olley, J., Kemp, J., Spooner, N., Petherick, L., Penny, D., Mooney, S., Moss, E., 2017. "Persistence of wetlands on North Stradbroke Island (south-east Queensland, Australia) during the last glacial cycle: implications for Quaternary science and biogeography." *Journal of Quaternary Science* 32, 770-781.

Tierney, J.E., Russell, J.M., Eggermont, H., Hopmans, E.C., Verschuren, D., Sinninghe Damsté, J.S., 2010. "Environmental controls on branched tetraether lipid distributions in tropical East African lake sediments." *Geochimica et Cosmochimica Acta* 74, 4902-4918.

Versteegh, G.J., Schefuß, E., Dupont, L., Marret, F., Damsté, J.S.S., Jansen, J.F., 2004. "Taraxerol and Rhizophora pollen as proxies for tracking past mangrove ecosystems." *Geochimica et Cosmochimica Acta* 68, 411-422.

Walker, J., Lees, B., Olley, J., Thompson, C., 2018. "Dating the Cooloola coastal dunes of South-Eastern Queensland, Australia." *Marine Geology* 398, 73-85.

Weijers, J.W., Schouten, S., Spaargaren, O.C., Damsté, J.S.S., 2006. "Occurrence and distribution of tetraether membrane lipids in soils: Implications for the use of the TEX_{86} proxy and the BIT index." *Organic Geochemistry* 37, 1680-1693.

Weijers, J.W.H., Schouten, S., van den Donker, J.C., Hopmans, E.C., Sinninghe Damsté, J.S., 2007. "Environmental controls on bacterial tetraether membrane lipid distribution in soils." *Geochimica et Cosmochimica Acta* 71, 703-713.

Weijers, J.W.H., Steinmann, P., Hopmans, E.C., Schouten, S., Sinninghe Damsté, J.S., 2011. "Bacterial tetraether membrane lipids in peat and coal: Testing the MBT–CBT temperature proxy for climate reconstruction." *Organic Geochemistry* 42, 477-486.

Whinam, J., Hope, G., Clarkson, B., Buxton, R., Alspach, P., Adam, P., 2003. "Sphagnum in peatlands of Australasia: Their distribution, utilisation and management." *Wetlands Ecology and Management* 11, 37-49.

Wooller, M.J., Behling, H., Guerrero, J.L., Jantz, N., Zweigert, M.E., 2009. "Late Holocene hydrologic and vegetation changes at Turneffe Atoll, Belize, compared with records from mainland Central America and Mexico." *Palaios* 24, 650-656.

Xie, S., Yi, Y., Huang, J., Hu, C., Cai, Y., Collins, M., Baker, A., 2003. "Lipid distribution in a subtropical southern China stalagmite as a record of soil ecosystem response to paleoclimate change." *Quaternary Research* 60, 340-347.

Yin, Q., Berger, A., 2015. "Interglacial analogues of the Holocene and its natural near future." *Quaternary Science Reviews* 120, 28-46.

Zhai, L., Wang, X., Wang, P., Miralles-Wilhelm, F., Sternberg, L.d.S.L., 2019. "Vegetation and location of water inflow affect evaporation in a subtropical wetland as indicated by the deuterium excess method." *Ecohydrology* 12, 20-82.

Zhang, Y., Zheng, M., Meyers, P.A., Huang, X., 2017. "Impact of early diagenesis on distributions of Sphagnum *n*-alkanes in peatlands of the monsoon region of China." *Organic Geochemistry* 105, 13-19.

Zheng, Y., Pancost, R.D., Liu, X., Wang, Z., Naafs, B.D.A., Xie, X., Liu, Z., Yu, X., Yang, H., 2017. "Atmospheric connections with the North Atlantic enhanced the deglacial warming in northeast China." *Geology* 45, 1031-1034.

Zhou, W., Xie, S., Meyers, P.A., Zheng, Y., 2005. "Reconstruction of late glacial and Holocene climate evolution in southern China from geolipids and pollen in the Dingnan peat sequence." *Organic Geochemistry* 36, 1272-1284.

Zhou, W., Zheng, Y., Meyers, P.A., Jull, A.J.T., Xie, S., 2010. "Postglacial climate-change record in biomarker lipid compositions of the Hani peat sequence, Northeastern China." *Earth and Planetary Science Letters* 294, 37-46.

Chapter 6 – Conclusions and suggestions for future research

6.1 Preamble

This thesis has contributed research towards a greater understanding of Australian climates during MIS 3, the nature of Australian Holocene climate drivers (relative to the previous two interglacial periods) and long-term trends in Australian climate. A review and synthesis of 40 published Australian climate records into a continental moisture availability record has provided a resource for future research on the partial extinction of Australian megafauna (Chapter 2). A ~210 kyr multi-proxy record of Australian subtropical climates covering the two most recent interglacial complexes was used to address the nature of Holocene climates in respect to gradual drying from ~200 ka as recorded in central and south eastern Australia (Chapters 3 – 5). In the following summary, outcomes of this thesis are presented in relation to the key aims and objectives of the project. Needs for further research are also outlined, summarising identified gaps in current knowledge and possible directions for future research.

6.2 Assessment of key aims

6.2.1 Construct a record of Australian continental climate change during MIS 3

Chapter 2 presented a detailed review of 40 published Australian climate records covering at least part of MIS 3. These 40 records, close to the total number of continental climate records for the period available at the time of publication (lacking only those with large degrees of age uncertainty in their chronologies) allowed synthesis of a continental mean moisture availability record. The combined moisture availability record for MIS 3 is the first such synthesis for Australia and adds greater continental climate context to the discussion of partial megafaunal extinction, where before continental climate conditions were generally approximated using distant records (e.g. Johnson et al., 2016) or climate models (Saltré et al., 2016). This research also served to define limitations in understanding Australian climates, both spatially (distance between records and geographical coverage), and chronologically (availability of long records and the generally large degree of age uncertainty beyond ~50 ka).

The MIS 3 review and synthesis indicates that:

1. Australia experienced spatially variable climates for much of MIS 3, reflecting similar variability to contemporary climates.
2. Australia was predominantly wet between ~49 and 40 ka, the period of peak loss of megafauna (Saltré et al., 2016), indicating that climate likely played a minor role, if any, in Australian megafauna extinction.
3. From ~40 ka there was a gradual reduction in Australian mean continental moisture availability.
4. Australian summer monsoon-dominated regions experienced rapid drying from ~48 ka, while southern westerly wind dominated regions were wetter from ~50 – 29 ka than during early MIS 3.
5. While a notable relationship with regional fire history was identified, there was little correlation between continental mean Australian moisture availability and atmospheric CO_2 or global sea levels.

6.2.2 Create a new, high resolution, discontinuous multi-proxy subtropical Australian climate record of at least two glacial cycles

Each of the chapters from two to five progressively refined the Fern Gully Lagoon multi-proxy records of regional and local climates, in addition to isolating the influence of biomass burning, evaporation and mean annual air temperatures on palaeoclimate proxies. Where possible, sampling locations in the core were overlapped so that all proxies were comparable during each sedimentation phase. Proxies were also sampled at high resolution where possible, with abutting samples, limiting gaps in the sedimentary record. The high number of available climate proxies made record verification by comparison between climate proxies relatively straightforward, ensuring that the Fern Gully Lagoon climate record is as robust as possible.

Multiple proxy records also allowed comparison between calibration methodologies, highlighting the limitations of each, and allowing issues to be identified and addressed where proxies indicated conflicting climate conditions. For example, a combined climate record using in-wetland climate proxies independent of human influence on terrestrial vegetation assemblages or fire frequency (used to infer climate change in Chapter 4), supported the previous findings and

indicated that Holocene wetland conditions were drier than during the previous two interglacials (Chapter 5).

Dating the Fern Gully Lagoon sedimentary sequence was not straightforward. However, utilisation of stringent testing criteria and Bayesian age-depth modelling provided the most robust age model possible under the circumstances. The Fern Gully Lagoon multi-proxy record, supported by the robust age-depth model, allowed investigation of two major climate hypothesis – that long-term Australian interglacial drying was present in the subtropics, and that differences in regional climate drivers led to drier Holocene climates compared to recent interglacials. The first hypothesis was marginally supported by regional climate trends as indicated by continental inorganic flux (Chapter 3). However, recovery of an additional information from regional vegetation reconstruction and local wetland stable carbon isotope and lipid biomarker records (Chapters 4 and 5) instead indicated that gradual drying of the Australian subtropics was unlikely, and that Holocene climates are notably different to recent interglacials, likely due to changes in regional climate drivers altered by lower amplitude Holocene insolation.

The Fern Gully Lagoon ~210 kyr climate record indicates that:

1. Holocene climates in the Australian subtropics are notably drier than climates during the previous two interglacials.
2. Climates during the MIS 7a–c and MIS 5 interglacial complexes at Fern Gully Lagoon had relatively similar moisture availability.
3. Rainforest taxa became locally extinct on NSI at around the same time as, if not before human activity peaked at nearby Wallen Wallen Creek.
4. After the LGM, human impact notably altered regional vegetation assemblages and fire regimes, leading to an initial over-estimation of Holocene drying.
5. While some monsoonal influence is possible during glacials, interglacial moisture availability at Fern Gully Lagoon has likely been dominated by ENSO activity for the past ~210 kyr.

The record from Fern Gully Lagoon supports the hypothesis of differing Holocene climates as compared to recent interglacials as proposed by Yin and Berger (2015), reflecting findings from interglacial climate models (Claussen et al., 2005; Yin and Berger, 2015) and

several interglacial climate records (e.g. Cheddadi et al., 2005; Schweger et al., 2011). While it was not possible to directly tie differing Holocene climates in subtropical Australia to differing insolation patterns (after Yin and Berger 2015), notable differences in subtropical climate drivers during the Holocene compared to MIS 7a–c and early MIS 5 climates indicate the influence of changes in ENSO variability after Kershaw et al. (2007). As such, this record supports a cautious approach when using MIS 7a–c and MIS 5 climate records to predict or interpret future changes in Holocene climates, in agreement with Yin and Berger (2015) and Schweger et al. (2011).

Relatively wetter MIS 7a–c and MIS 5 climates compared to a drier Holocene observed at Fern Gully Lagoon is most similar to the climate record from Lynch's Crater, on the tropical Atherton Tablelands ~1,400 km north of NSI (Kershaw et al., 2007) than any other record of Australian interglacial climates. However, unsurprisingly, the subtropical Fern Gully Lagoon record has a lower relative proportion of rainforest taxa present throughout, with increased average relative proportions of both sclerophyll and herb and grass taxa, reflecting lower annual mean precipitation. The similarity of these records is most likely due to a shared long-term climate driver – ENSO – but the Australian summer monsoon likely had only had a minor influence on the Fern Gully Lagoon record. Periods of increased moisture availability on NSI were coeval with increased La Niña frequency as recorded in north-eastern Australia (Moss and Kershaw, 2007) and in ocean-core records (e.g. Pena et al., 2008) and during periods of increased strength of the Australian Summer Monsoon, as recorded in central Australia (Nanson et al., 2008; Fu et al., 2017). Greater climate stability on NSI when compared to the Atherton Tablelands is likely indicative of reduced influence on climate of orbital forcing.

The Fern Gully Lagoon climate record indicated that there were notable changes in both terrestrial vegetation assemblages and fire regime after the Last Glacial Maximum (LGM) likely due to human impact. While there was continuity of sclerophyll and herb-grass vegetation assemblages on either side the LGM sedimentary hiatus, arboreal rainforest taxa became locally extinct. While local extinction may have been driven by relatively dry Holocene climates, similar stable carbon isotope ratios and *n*-alkane biomarker distributions for the Holocene and late MIS 3 (when rainforest taxa were still abundant) suggest that any reduction in mean annual precipitation is unlikely to have been sufficient to lead to almost total loss of rainforest taxa. The most likely cause of combined regional rainforest extinction and a change in fire regime is

human impact. A change in fire regime (Chapter 4), as well as coeval peaks in charcoal flux at Fern Gully Lagoon with peaks in human activity at ~21 ka and ~1 ka (Neal and Stock, 1986), and differences between local wetland and regional climate records (Chapter 5) indicates that human impact likely led to the local extinction of rainforest taxa.

6.3 Suggestions for future research

The new continental synthesis of Australian climate change during MIS 3 addressed the lack of continental climate context for Australian megafauna sites and indicated that drying was unlikely to be the major cause of peak megafauna extinction in Australia at ~45 ka (Chapter 2). The combined continental hydroclimate record provides scope for a new synthesis when combined with MIS 3 archaeological studies, with a focus on identifying changes in human occupation due to moisture availability (i.e. food and water availability). Additionally, the continental MIS 3 moisture availability record identified spatial gaps in Australian MIS 3 records and therefore areas of focus for further research. One promising location for future research are potential speleothem records in Nullarbor Plain cave systems (Lipar and Ferk, 2015; Heath et al., 2018), and new marine cores, which record regional climate (e.g. Moss and Kershaw, 2007; van der Kaars et al., 2017) could also help to fill spatial gaps. Additionally, if the search for new MIS 3 climate records is focussed on areas predicted to contain megafauna remains after Block et al. (2016) – south-eastern and south-western Australia, along with much of South Australia – new reconstructions could support palaeontological studies by providing climate context.

The Fern Gully Lagoon record of regional vegetation through time allowed moisture availability on NSI to be inferred for much of the past 210 kyr (Chapter 4). However, change associated with vegetation succession due to nutrient depletion was not observed. In addition to changes due to climate, vegetation assemblages on sand dune systems are thought to be driven by nutrient leaching and limitation over long time periods (>100 kyr), as observed on the Cooloola Sand Mass ~160 km to the north of NSI (Chen et al., 2015). While dune sequences at both locations have comparable ages and periods of deposition, changes in vegetation assemblages due to aging dunes were not observed on NSI. The lack of expected vegetation succession on NSI (Chapter 4) indicates that the theory of vegetation succession on dune systems due to nutrient depletion may be flawed, or that the Fern Gully Lagoon pollen record has a large enough catchment to smooth out succession-related vegetation trends. Investigation would be

relatively straightforward: comparing the Fern Gully Lagoon vegetation assemblage record and a new chronosequence study on NSI would support the case for either a flawed hypothesis (if differing vegetation sequences are found to those on the Cooloola Sand Mass), or the impracticality of tracking vegetation succession using pollen records.

Hiatuses in the Fern Gully Lagoon sediment record during glacials were inferred to be due to drier conditions on NSI, including the LGM hiatus, which matches the timing of hiatuses found in nearby wetland records (Chapter 3; e.g. Atahan et al., 2015; Lewis et al., 2020). As such, the Fern Gully Lagoon record supports an extended dry subtropical LGM, as proposed by Petherick et al. (2017), rather than stable LGM climates as inferred from a review of NSI climate records by Tibby et al. (2017). However, the timing of the MIS 6 glacial hiatus at Fern Gully Lagoon, even when taking into account 2-sigma error in the age-depth model, only partially overlaps the period of maximum drying during MIS 6 observed in other interglacial records (Fig. 4.6; e.g. Kershaw et al., 2007). This uncertainty in the climate record, combined with the shape of the wetland basin (Chapter 5), the lack of any sedimentary indicators of drying at hiatus locations (Chapter 2), and sediments indicative of wet climates around the hiatus points, indicate that the wetland may have suffered collapse at least once in the past ~210 kyr. Wetland collapse leading to loss of a notable volume of sediment as has been observed at contemporary sites (Loffler, 2006), and a lack of sedimentation until the wetland could again hold water would be represented in the wetland record as a sedimentary hiatus. To address possible misidentification of hiatuses at Fern Gully Lagoon as dry periods, additional work is required. Fern Gully, the main overflow below the wetland, has already been sampled for sedimentary analysis and OSL dating of the alluvial fan, but analysis has not yet taken place. Matching ages for Fern Gully alluvial sequences and Fern Gully Lagoon sedimentary hiatuses would support a hypothesis for relatively stable climates for the past ~210 kyr, in line with LGM stability observed in other NSI sites (Tibby et al., 2017).

Mapping basin morphology helped to identify changes in wetland exposure and moisture storage over time for Fern Gully Lagoon, and so identify the influence of changing evaporation on the moisture availability record (Chapter 5). However, the method used to map the basin – sounding pole transects – does not provide a very detailed record of basin shape and sounding poles do not always record the existence or absence of sand lenses. It is likely that shallower

slopes within the Fern Gully Lagoon basin led to anomalies in the stable isotope record, as a $\delta^{13}C_{OM}$ peak in the record coincides with relatively shallower basin slopes identified using sounding-poles. To investigate this anomaly, a more detailed map of basin morphology and identification of any sand lenses within the sediment using ground penetrating radar (for example) is required. Identification of the influence of basin morphology on stable isotope ratios over time would additionally add to current understanding of wetland evolution and help future studies to identify non-climate changes in stable isotope records.

Additional work on reconstructing MAAT at Fern Gully Lagoon would help to provide a high-resolution temperature reconstruction for subtropical Australia, in turn assisting in discussion of relative changes in Australian MAAT during glacials (e.g. Miller et al., 1997; Chang et al., 2015) and in the improvement of global climate models (Turney and Jones, 2010; Harrison and Bartlein, 2012). The most recent GDGT calibration for peat systems (using the degree of methylation of 5-methyl brGDGTs after Naafs et al. (2017)) was not used for this study due to difficulties distinguishing between 5-methyl and 6-methyl isomers in Fern Gully Lagoon sediments. Re-sampling of the Fern Gully Lagoon cores at a higher resolution, and analysis using the latest calibrations, including co-eluting GDGTs separated using other HPLC columns and solvent mixtures, would result in a much-improved temperature reconstruction. In addition, establishing an additional temperature proxy record (e.g. chironomids after Eggermont and Heiri (2012)) would help validate the record. Further research could also include a new GDGT calibration study focused on Australian wetland sediments and utilising a climate gradient similar to Australian chironomid calibrations after Chang et al. (2015), allowing greater accuracy for Australian temperature reconstructions.

Regional climate change

Moisture availability records from Fern Gully Lagoon indicated that changing wetland conditions for the past ~210 kyr were predominantly driven by ENSO. As such, increased sample resolution may allow extraction of a detailed ~210 kyr record of ENSO activity from Fern Gully Lagoon. A new terrestrial ENSO record would assist with ongoing debates about ENSO activity (e.g. whether there was greater ENSO activity during glacials (Koutavas and Joanides, 2012) or whether there is a consistent relationship between ENSO and orbital forcing (An et al., 2017)), as currently almost all available long records are based on marine studies (e.g.

Pena et al., 2008; Ford et al., 2015; Zhang et al., 2017) or climate modelling (Singarayer and Valdes, 2010; Brady et al., 2013). Terrestrial records of ENSO activity are important due to the discrepancy in the timing of changes in ENSO inferred from ocean records (Mariani et al., 2016; Beck et al., 2017), and some disagreement in the dominant ENSO phase between terrestrial and marine records (Emile-Geay et al., 2013). Methods for increasing the resolution and certainty of the Fern Gully Lagoon climate record beyond additional pollen sampling include $\delta^{18}O$ extracted from wetland cellulose (e.g. Wolfe et al., 2007), pigments (e.g. Cadd et al., 2018) and leaf wax $\delta^{2}H$ analysis (e.g. Goldsmith et al., 2019).

6.4 References

An, S.-I., Kim, H.-J., Park, W., Schneider, B., 2017. "Impact of ENSO on East Asian winter monsoon during interglacial periods: effect of orbital forcing." *Climate Dynamics* 49, 3209-3219.

Atahan, P., Heijnis, H., Dodson, J., Grice, K., Le Metayer, P., Taffs, K., Hembrow, S., Woltering, M., Zawadzki, A., 2015. "Pollen, biomarker and stable isotope evidence of late Quaternary environmental change at Lake McKenzie, southeast Queensland." *Journal of Paleoliminology* 53, 139-156.

Beck, K.K., Fletcher, M.-S., Gadd, P.S., Heijnis, H., Jacobsen, G.E., 2017. "An early onset of ENSO influence in the extra-tropics of the southwest Pacific inferred from a 14, 600 year high resolution multi-proxy record from Paddy's Lake, northwest Tasmania." *Quaternary Science Reviews* 157, 164-175.

Block, S., Saltré, F., Rodriguez-Rey, M., Fordham, D.A., Unkel, I., Bradshaw, C.J.A., 2016. "Where to dig for fossils: Combining climate-envelope, taphonomy and discovery models." *PLoS one* 11, 1-16.

Brady, E.C., Otto-Bliesner, B.L., Kay, J.E., Rosenbloom, N., 2013. "Sensitivity to Glacial Forcing in the CCSM4." *Journal of Climate* 26, 1901-1925.

Cadd, H., Tibby, J., Barr, C., Tyler, J., Unger, L., Leng, M., Marshall, J., McGregor, G., Lewis, R., Arnold, L., Lewis, T., Baldock, J., 2018. "Development of a southern hemisphere subtropical wetland (Welsby Lagoon, south-east Queensland, Australia) through the last glacial cycle." *Quaternary Science Reviews* 202, 53-65.

Chang, J.C., Shulmeister, J., Woodward, C., 2015. "A chironomid based transfer function for reconstructing summer temperatures in southeastern Australia." *Palaeogeography, Palaeoclimatology, Palaeoecology* 423, 109-121.

Chen, C.R., Hou, E.Q., Condron, L.M., Bacon, G., Esfandbod, M., Olley, J., Turner, B.L., 2015. "Soil phosphorus fractionation and nutrient dynamics along the Cooloola coastal dune chronosequence, southern Queensland, Australia." *Geoderma* 257-258, 4-13.

Eggermont, H., Heiri, O., 2012. "The Chironomid-temperature relationship: expression in nature and paleoenvironmental implications." *Biological Reviews* 87, 430-456.

Emile-Geay, J., Cobb, K.M., Mann, M.E., Wittenberg, A.T., 2013. "Estimating central equatorial Pacific SST variability over the past millennium. Part II: Reconstructions and implications." *Journal of Climate* 26, 2329-2352.

Ford, H.L., Ravelo, A.C., Polissar, P.J., 2015. "Reduced El Nino-Southern Oscillation during the Last Glacial Maximum." *Science* 347, 255-258.

Fu, X., Cohen, T.J., Arnold, L.J., 2017. "Extending the record of lacustrine phases beyond the last interglacial for Lake Eyre in central Australia using luminescence dating." *Quaternary Science Reviews* 162, 88-110.

Goldsmith, Y., Polissar, P.J., deMenocal, P.B., Broecker, W.S., 2019. "Leaf Wax δD and $\delta^{13}C$ in Soils Record Hydrological and Environmental Information Across a Climatic Gradient in Israel." *Journal of Geophysical Research: Biogeosciences* 124, 2898-2916.

Harrison, S.P., Bartlein, P., 2012. "Records from the Past, Lessons for the Future: What the Palaeorecord Implies about Mechanisms of Global Change", in: Henderson-Sellers, A., McGuffie, K. (Eds.), The Future of the World's Climate. Elsevier Science, Oxford, pp. 403-436.

Johnson, C.N., Alroy, J., Beeton, N.J., Bird, M.I., Brook, B.W., Cooper, A., Gillespie, R., Herrando-Pérez, S., Jacobs, Z., Miller, G.H., Prideaux, G.J., Roberts, R.G., Rodríguez-Rey, M., Saltré, F., Turney, C.S.M., Bradshaw, C.J.A., 2016. "What caused extinction of the Pleistocene megafauna of Sahul?" *Proceedings of the Royal Society of London Series B -Biological Sciences* 283:20152399, 1-8.

Kershaw, A.P., Bretherton, S.C., van der Kaars, S., 2007. "A complete pollen record of the last 230 ka from Lynch's Crater, north-eastern Australia." *Palaeogeography, Palaeoclimatology, Palaeoecology* 251, 23-45.

Koutavas, A., Joanides, S., 2012. "El Niño–Southern Oscillation extrema in the Holocene and Last Glacial Maximum." *Paleoceanography* 27.

Lewis, R.J., Tibby, J., Arnold, L.J., Barr, C., Marshall, J., McGregor, G., Gadd, P., Yokoyama, Y., 2020. "Insights into subtropical Australian aridity from Welsby Lagoon, north Stradbroke Island, over the past 80,000 years." *Quaternary Science Reviews* 234, 106262.

Loffler, T., 2006. "First Creek – Waterfall Gully November 2005 Erosion Event Site Inspection and Observations". EarthTech, Adelaide, SA.

Mariani, M., Fletcher, M.S., Holz, A., Nyman, P., 2016. "ENSO controls interannual fire activity in southeast Australia." *Geophysical Research Letters* 43, 10,891-810,900.

Miller, G.H., Magee, J.W., Jull, A.J.T., 1997. "Low-latitude glacial cooling in the Southern Hemisphere from amino-acid racemization in emu eggshells." *Nature* 385, 241-244.

Moss, P.T., Kershaw, A.P., 2007. "A late Quaternary marine palynological record (oxygen isotope stages 1 to 7) for the humid tropics of northeastern Australia based on ODP Site 820." *Palaeogeography, Palaeoclimatology, Palaeoecology* 251, 4-22.

Naafs, B.D.A., Inglis, G.N., Zheng, Y., Amesbury, M.J., Biester, H., Bindler, R., Blewett, J., Burrows, M.A., del Castillo Torres, D., Chambers, F.M., Cohen, A.D., Evershed, R.P., Feakins, S.J., Gałka, M., Gallego-Sala, A., Gandois, L., Gray, D.M., Hatcher, P.G., Honorio Coronado, E.N., Hughes, P.D.M., Huguet, A., Könönen, M., Laggoun-Défarge, F., Lähteenoja, O., Lamentowicz, M., Marchant, R., McClymont, E., Pontevedra-Pombal,

X., Ponton, C., Pourmand, A., Rizzuti, A.M., Rochefort, L., Schellekens, J., De Vleeschouwer, F., Pancost, R.D., 2017. "Introducing global peat-specific temperature and pH calibrations based on brGDGT bacterial lipids." *Geochimica et Cosmochimica Acta* 208, 285-301.

Nanson, G.C., Price, D.M., Jones, B.G., Maroulis, J.C., Coleman, M., Bowman, H., Cohen, T.J., Pietsch, T.J., Larsen, J.R., 2008. "Alluvial evidence for major climate and flow regime changes during the middle and late Quaternary in eastern central Australia." *Geomorphology* 101, 109-129.

Neal, R., Stock, E., 1986. "Pleistocene occupation in the south-east Queensland coastal region." *Nature* 323, 618-621.

Pena, L.D., Cacho, I., Ferretti, P., Hall, M.A., 2008. "El Niño–Southern Oscillation–like variability during glacial terminations and interlatitudinal teleconnections." *Paleoceanography* 23, 1-8.

Petherick, L.M., Moss, P.T., McGowan, H.A., 2017. "An extended Last Glacial Maximum in subtropical Australia." *Quaternary International* 432, 1-12.

Saltré, F., Rodríguez-Rey, M., Brook, B.W., Johnson, C.N., Turney, C.S.M., Alroy, J., Cooper, A., Beeton, N., Bird, M.I., Fordham, D.A., Gillespie, R., Herrando-Pérez, S., Jacobs, Z., Miller, G.H., Nogués-Bravo, D., Prideaux, G.J., Roberts, R.G., Bradshaw, C.J.A., 2016. "Climate change not to blame for late Quaternary megafauna extinctions in Australia." *Nature Communications* 7, 1-7.

Schweger, C., Froese, D., White, J.M., Westgate, J.A., 2011. "Pre-glacial and interglacial pollen records over the last 3 Ma from northwest Canada: Why do Holocene forests differ from those of previous interglaciations?" *Quaternary Science Reviews* 30, 2124-2133.

Singarayer, J.S., Valdes, P.J., 2010. "High-latitude climate sensitivity to ice-sheet forcing over the last 120 kyr." *Quaternary Science Reviews* 29, 43-55.

Tibby, J., Barr, C., Marshall, J.C., Mgregor, G.B., Moss, P.T., Arnold, L.J., Page, T.J., Questiaux, D., Olley, J., Kemp, J., Spooner, N., Petherick, L., Penny, D., Mooney, S., Moss, E., 2017. "Persistence of wetlands on North Stradbroke Island (south-east Queensland, Australia) during the last glacial cycle: implications for Quaternary science and biogeography." *Journal of Quaternary Science* 32, 770-781.

Turney, C.S.M., Jones, R.T., 2010. "Does the Agulhas Current amplify global temperatures during super-interglacials?" *Journal of Quaternary Science* 25, 839-843.

van der Kaars, S., Miller, G.H., Turney, C.S.M., Cook, E.J., Nürnberg, D., Schönfeld, J., Kershaw, A.P., Lehman, S.J., 2017. "Humans rather than climate the primary cause of Pleistocene megafaunal extinction in Australia." *Nature Communications* 8, 1-7.

Wolfe, B.B., Falcone, M.D., Clogg-Wright, K.P., Mongeon, C.L., Yi, Y., Brock, B.E., Amour, N.A.S., Mark, W.A., Edwards, T.W., 2007. "Progress in isotope paleohydrology using lake sediment cellulose." *Journal of Paleolimnology* 37, 221-231.

Yin, Q., Berger, A., 2015. "Interglacial analogues of the Holocene and its natural near future." *Quaternary Science Reviews* 120, 28-46.

Zhang, S., Li, T., Chang, F., Yu, Z., Xiong, Z., Wang, H., 2017. "Correspondence between the ENSO-like state and glacial-interglacial condition during the past 360 kyr." *Chinese Journal of Oceanology and Limnology* 35, 1018-1031.

Appendix A – Supplementary material for Chapter 2

A.1 Supplementary tables

Supplementary table A1 is very large and could not be included in its entirety in the printed version of the thesis. However, a copy can be downloaded from this address:

https://ars-els-cdn-com.proxy.library.adelaide.edu.au/content/image/1-s2.0-S0277379118306978-mmc1.xlsx

The caption for this table has been included below:

Table A1: Australian MIS 3 sites, scoring and metadata.

Table A2: Calibrated radiocarbon ages for Australian MIS 3 records.

Site	Sample Code	Radiocarbon age (years)	±1σ error	Calibrated age (years)	±1σ error	Curve
Lake Leake	ANU1146	35000	1500	39730	1635	SHCal13
	ANU1147	37900	1250	42175	1020	SHCal13
	ANU1279	38900	2400	43380	2260	SHCal13*
	ANU1148	34900	NR	39375		SHCal13
	ANU1149	35100	NR	39625		SHCal13
Wyrie Swamp	ANU1275	26450	650	30495	605	SHCal13
	ANU1276	29950	950	33990	990	SHCal13
	ANU1350	31100	1000	35100	1010	SHCal13
	ANU1277	35100	1400	39830	1490	SHCal13
	ANU1349	39700	2600	44050	2340	SHCal13*
	ANU1278	24100	600	28185	535	SHCal13
	ANU1351	21800	950	26185	1000	SHCal13
Pulbeena Swamp	GrN-7689	22130	180	26295	215	SHCal13
	GrN-9458	42200	800	45510	730	SHCal13
	GrN-8589	42700	900	45980	880	SHCal13
	GrN-8636	41100	800	44570	725	SHCal13
	GrN-9438	41450	700	44890	620	SHCal13
	GrN-9483	42620	200	45800	240	SHCal13
Lake George	N-1815	28400	1600	32590	1590	SHCal13
	N-1816	27100	1050	31340	1180	SHCal13
	N-1817	35700	3525	40290	3790	SHCal13*
	N-1513	12400	460	14475	685	SHCal13
	N-1514	31300	1170	35310	1260	SHCal13
	N-1818	30300	1550	34480	1810	SHCal13
	N-1819	23000	1650	27380	1750	SHCal13
	N-1515	37800	NR	42080		SHCal13
	N-1516	22500	640	26730	595	SHCal13
	N-1518	29600	2500	34110	3010	SHCal13
	N-1519	37800	NR	42080		SHCal13
Tullabardine Dam	SUA-1045	21250	270	25540	270	SHCal13
	ANU-4816	10730	660	12380	880	SHCal13
	SUA-1046	31500	900	35445	950	SHCal13
	SUA-1047	43800	NR	46880		SHCal13
Egg Lagoon	SUA-2929	39400	850	43220	680	SHCal13
Lake Selina	SUA 3040	14200	230	17230	330	SHCal13
	OZA 237U	18900	220	22720	240	SHCal13
	OZA 238U	33800	1100	38010	1340	SHCal13
Old Lake Coomboo Depression	ANU 4282	21800	1270	26090	1340	SHCal13
	ANU 4283	31700	1370	35900	1570	SHCal13
Fr10/95, GC17	Undefined1	27730	770	31810	780	MARINE13
	Undefined2	40560	1200	44140	1020	MARINE13
Lake Baraba	NZA-21524 (Wk-15818)	19411	196	23315	255	SHCal13
	Undefined3	43630	NR	46695		SHCal13
Redhead Lagoon	OZG348	19740	100	23730	150	SHCal13
	OZG788	23750	140	27785	120	SHCal13
	OZG351	33750	320	38145	445	SHCal13
	Wk-8571	34020	340	38480	410	SHCal13
	Wk-8574	32350	280	36190	315	SHCal13
	Wk-7702	35660	790	40275	830	SHCal13
	Wk-7703	39530	1320	43440	1070	SHCal13
	Wk-7704	40200	1450	43950	1220	SHCal13*
	Wk-7705	36060	830	40660	805	SHCal13
Lake Allom	R.J. Van de Graaff laboratory 13183	32500	400	36395	530	SHCal13
	R.J. Van de Graaff laboratory 13184	35900	800	40515	805	SHCal13
	R.J. Van de Graaff laboratory 13493	45200	1500	>47440		SHCal13
	R.J. Van de Graaff laboratory 13185	44600	2400	>46410		SHCal13
	R.J. Van de Graaff laboratory 13494	45900	1900	>47850		SHCal13
Caledonia Fen	OZ793	23460	260	27605	185	SHCal13
	OZ794	36540	780	41085	705	SHCal13
	OZ795	40900	1200	44390	1060	SHCal13
	OZ796	48600	3200	>45430		SHCal13
	OZ797	43100	1800	>44970		SHCal13
	OZ798	46200	2400	>47700		SHCal13
Native Companion Lagoon	NC-1-394	19311	157	23215	215	SHCal13
	NC-1-528	28684	456	32675	640	SHCal13
	NC-1-567	33187	816	37385	985	SHCal13
	NC-1-677	35757	1147	40340	1120	SHCal13
Lunette-lakes Bolac and Turangn	OZE 007	14830	100	17995	135	SHCal13
Tortoise Lagoon	Tor-D-005	18630	140	22465	150	SHCal13
	Tor-D-006	23860	180	27875	170	SHCal13
Lake McKenzie	OZO412	15100	70	18300	115	SHCal13
	OZN687	18670	100	22485	105	SHCal13
	OZN688	23270	120	27495	110	SHCal13
	OZN689	30940	190	34805	185	SHCal13
	OZN690	31870	180	35750	230	SHCal13
Cuddie Springs	Beta 81377	28770	300	32890	475	SHCal13
	Beta 81378	32900	510	37000	710	SHCal13
	Beta 81379	33660	530	37895	725	SHCal13
	Beta 81380	33300	530	37520	725	SHCal13
	Beta 81381	30990	360	34880	360	SHCal13
	Beta 81382	32580	510	36590	710	SHCal13
	Beta 81383	32420	460	36305	600	SHCal13
	Beta 81384	29170	360	33320	395	SHCal13

A.2 An example of record scoring from Redhead Lagoon

The study of Redhead Lagoon (Williams et al., 2006) was chosen to demonstrate our scoring method as it contains elements which score at either end of our scale and is also typical of a number of MIS 3 records. The record is a composite sequence developed from multiple cores which, collectively, provide a continuous record of the last ~75 ka. The age model for the composite 6 metre sequence is based on twenty ^{14}C and four OSL ages. The MIS 3 component of the record consists of approximately 2.4 m of sediment, with seven ^{14}C ages. The environmental record is based on pollen analysis, and climate changes are derived from palynology and the study of stratigraphic boundaries and layers. Within the MIS 3 section of the record, there are approximately 45 pollen samples.

Dating quality: The record has seven ^{14}C ages within the first half of MIS 3. The four OSL ages constrain the MIS 4 portion of the core, thereby providing additional maximum age constraint for the composite record. In the first dating category (57-45 ka) there are no numerical ages, hence no points have been awarded for two of the three criteria (dates within the period, age range of dates in the period). Due to the older OSL ages constraining the age/depth model for the record with the closest at ~70±7 ka, there is a <10 ky overlap with the MIS 3 period, gaining +0.1. In total, 0.1 is awarded for this category.

For the second dating quality category (the period 45–29 ka), ^{14}C ages immediately following MIS 3 help to constrain the start of the early MIS 3 part of the record (scoring +0.1). The number of numerical ages in the early MIS 3 range (45–29 ka) exceeds two (scoring +0.2) but the dating samples all fall within a period of ~4.6 ky (there is no spread of dating results spanning >10 ka; scoring +0.0). Taken together, the score for category 2 is 0.3.

The ^{14}C ages for the MIS 3 period score 0.15 as they are based on charcoal. This dating quality score would have been increased to 0.2 (the maximum possible) if OSL dating had been used to constrain the older part of the record within MIS 3 (category 3). Overall, the study scores 0.4 out of 0.8 for the number of ages obtained and dating resolution employed (categories 1 and 2), and a further 0.15 out of 0.2 for dating quality (category 3), giving a combined score of 0.55 out of a possible 1.

Proxy Quality: There are 45 pollen samples in the period between 57 and 29 ka, which provides good proxy resolution in MIS 3. This sample coverage receives a score of 0.3 out of 0.4 according to proxy quality (category 4). As only a single type of proxy data is presented, the record scores 0.1 according to category 5. Vegetation (pollen) responds on millennial or shorter timescales to climate (Kershaw et al., 2007; Muller et al., 2008; Harrison and Sanchez Goñi, 2010), and so the record scores 0.2 out of 0.3 for proxy responsiveness (category 6). The total score for proxy quality is therefore 0.6 out of a possible 1.

Continuity of the record: As the authors conclude that the record is almost continuous, covering the whole of MIS 3, the study scores 0.5 out of 0.5 for categories 7 and 8.

A.3 References

Harrison, S.P., Sanchez Goñi, M.F., 2010. "Global patterns of vegetation response to millennial-scale variability and rapid climate change during the last glacial period." *Quaternary Science Reviews* 29, 2957-2980.

Kershaw, A.P., Bretherton, S.C., van der Kaars, S., 2007. "A complete pollen record of the last 230 ka from Lynch's Crater, north-eastern Australia." *Palaeogeography, Palaeoclimatology, Palaeoecology* 251, 23-45.

Muller, J., Kylander, M., Wüst, R.A.J., Weiss, D., Martinez-Cortizas, A., LeGrande, A.N., Jennerjahn, T., Behling, H., Anderson, W.T., Jacobson, G., 2008. "Possible evidence for wet Heinrich phases in tropical NE Australia: the Lynch's Crater deposit." *Quaternary Science Reviews* 27, 468-475.

Williams, N.J., Harle, K.J., Gale, S.J., Heijnis, H., 2006. "The vegetation history of the last glacial-interglacial cycle in eastern New South Wales, Australia." *Journal of Quaternary Science Review* 21, 735-750.

Appendix B – Supplementary material for Chapter 3

B.1 µXRF Calibration plots, indicating the relationship between calibrated and normalised µXRF and WD-XRF elemental determinations

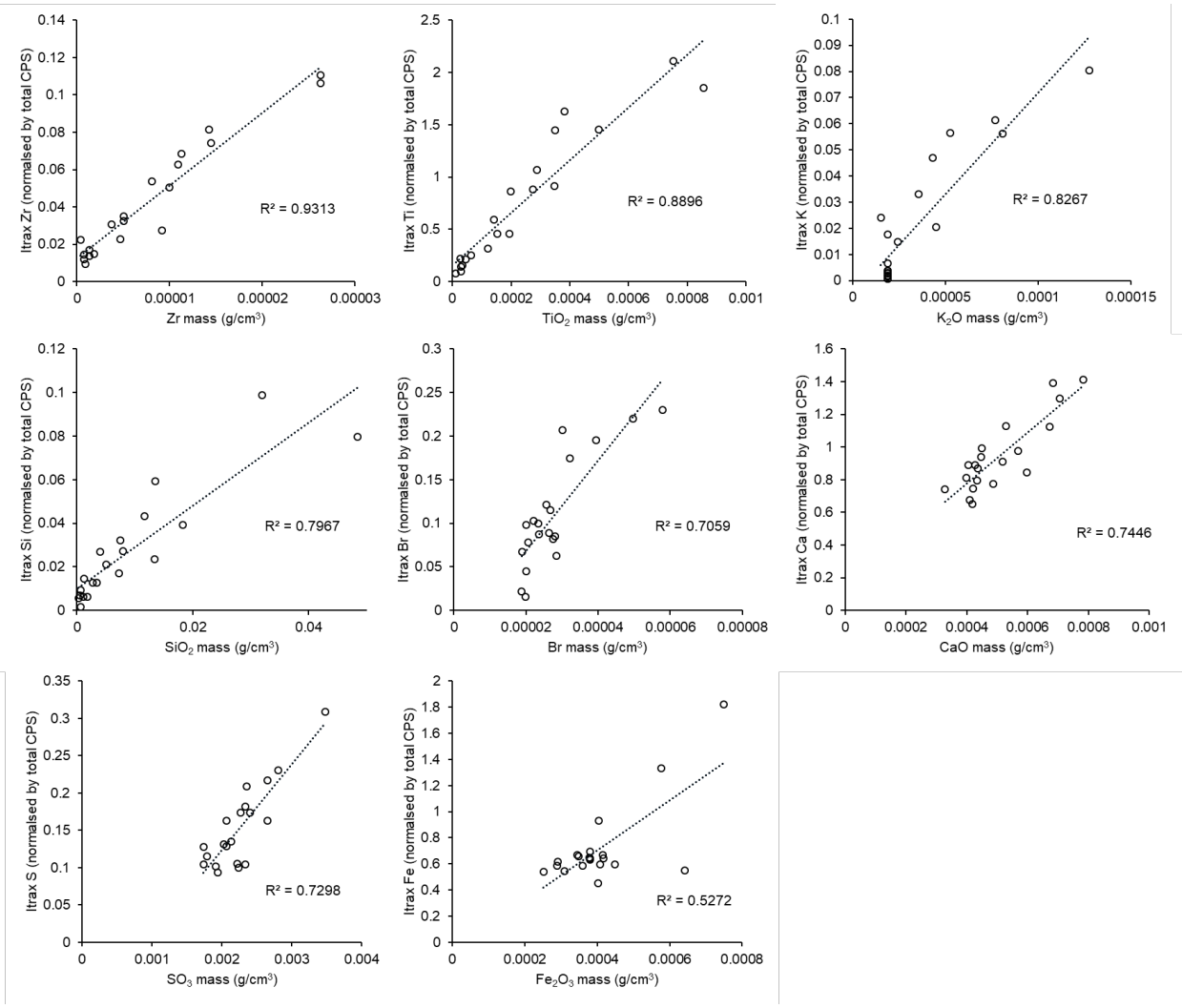

Figure B1: Regression plots, used for the determination of the mass of each inorganic oxide per wetland sediment volume from Itrax counts per second (after normalisation by total counts per second). CPS: Itrax counts per second.

B.2 Principal Components Analysis (PCA) used to determine the significant signals present within the µXRF record

The broken stick model (Fig B2), calculated using a subset of seven normalised elements comprising those with the highest counts per second (silicon, iron, calcium, bromine, zircon, potassium and titanium), and LOI derived inorganic content, indicates that axis one and two were significant (i.e. above the broken stick variance).

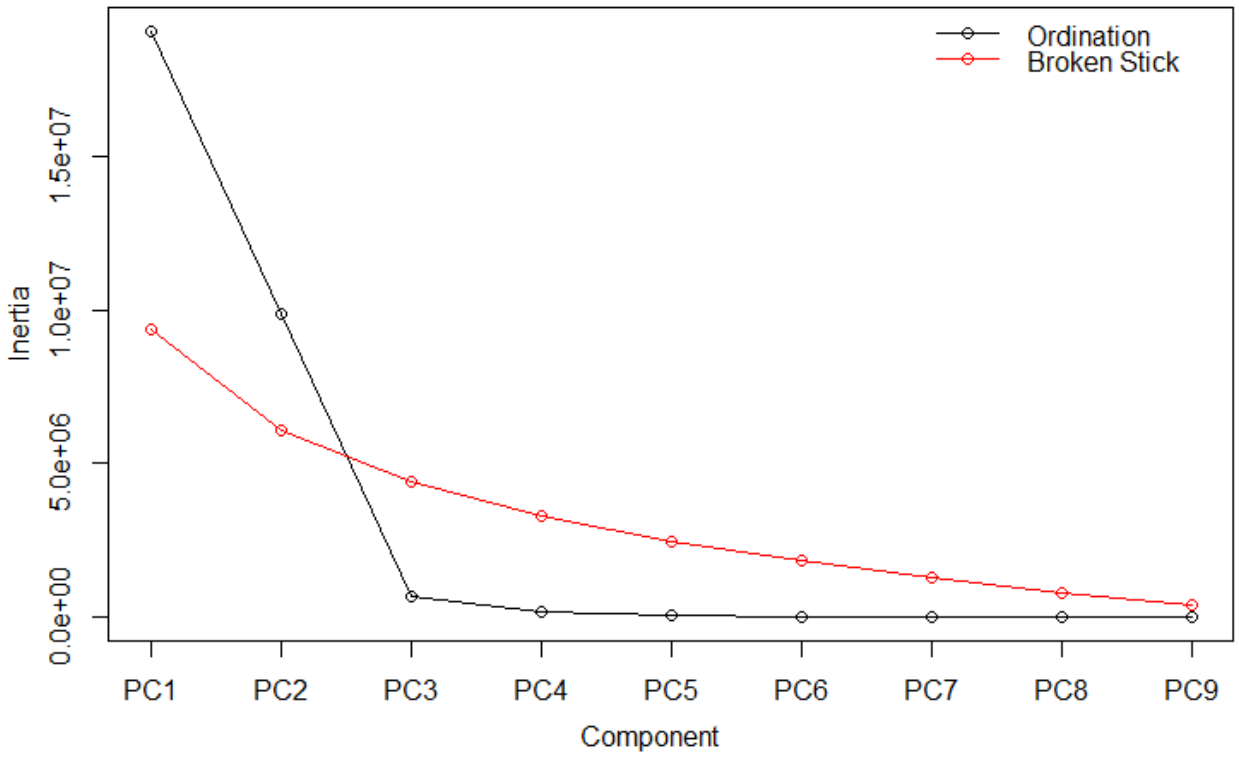

Figure B2: Broken stick model vs Fern Gully Lagoon PCA.

B.3 Changepoint Analysis used to determine the location of possible sedimentary hiatuses

Pruned exact linear time (PELT) multi-changepoint analysis (Killick and Eckley, 2014) was used to identify major changes in inorganic content through the Fern Gully core sequence, which are inferred to be associated with the location of sedimentary boundaries and potential depositional hiatuses. The results of this changepoint analysis have been used as a means of independently assigning OxCal Bayesian modelling priors on stratigraphic grounds.

The PELT multi-changepoint analysis performed on the LOI inorganic estimate log and the µXRF Si, Ti, K and Zr data identified four statistically significant stratigraphic changes or potential hiatuses in sedimentation at 42, 52, 166 and 288 cm (Fig. 3.3, B3). On the basis of these results, we have included four separate depositional units in the OxCal modelling priors with delineating *boundaries* at depths of 52, 166 and 288 cm. As there are no intervening likelihood estimates (OSL or ^{14}C dating constraints) specified between depths of 42 and 52 cm in the Fern Gully Lagoon sequence, the 42 cm changepoint was considered redundant and was not added to the model priors to avoid over-parameterization.

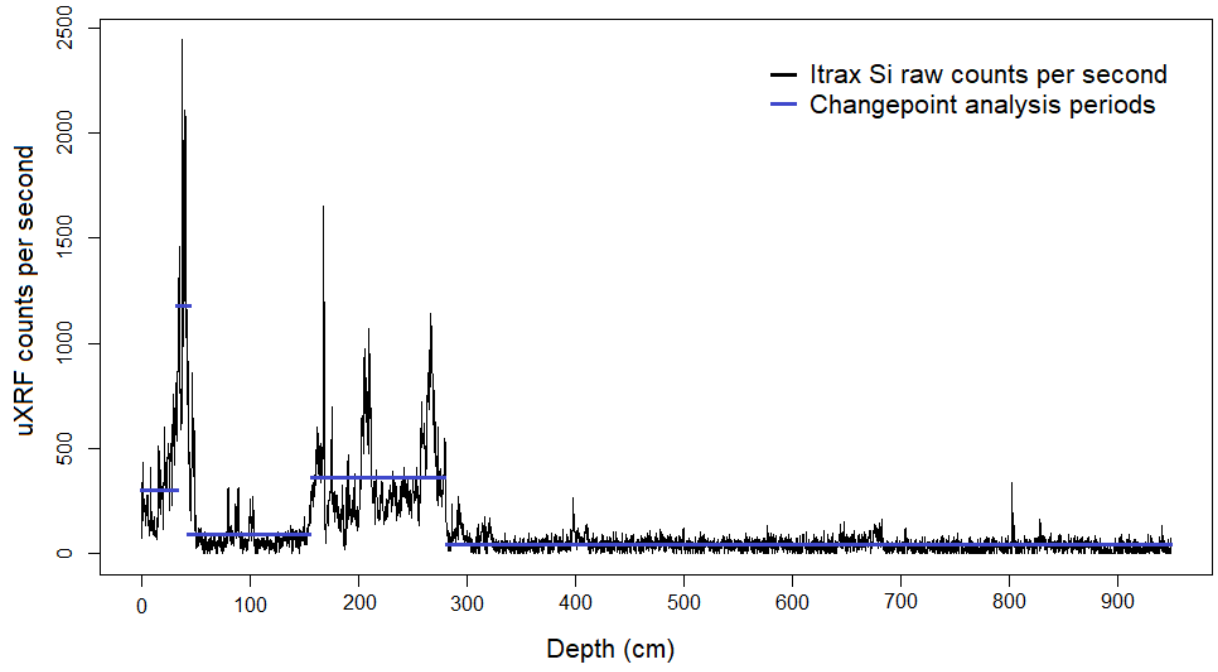

Figure B3: Changepoint analysis using µXRF silicon counts per second to identify statistically significant changes in mean inorganic sedimentation.

B.4 Optically stimulated luminescence (OSL) laboratory methods, quality control and radial plots

B.4.1 OSL methodology

Due to the low inorganic content of the core below 3 m, it was necessary to extract larger sediment samples (up to 24 cm in length instead of the standard 10 cm long sections) to ensure sufficient quartz yields for OSL dating. However, even with extended sampling, it was not possible to recover enough quartz grains for two planned OSL samples at 590 and 633 cm (FG15 OSL-6 and -7).

Purified quartz grains were extracted after Aitken (1998), including chemical disaggregation, digestion of organics, wet sieving of six grain size fractions ranging from 63 to 250 μm, with heavy liquid separation following Arnold et al. (2011). After etching with 48% hydrofluoric acid (40 minutes) to remove alpha-irradiated outer layers, individual grains from the 180–250 μm quartz fraction were mounted in aluminium discs drilled with a 10 × 10 array of chambers (300 μm wide and 300 μm deep) for single-grain OSL measurements (Arnold et al., 2012). Single-grain equivalent dose (De) measurements were made using the instrumentation and experimental procedures described by Demuro et al. (2013; 2015) and the Single-Aliquot Regenerative-dose (SAR) protocol (Murray and Wintle, 2000) shown in Table B1.

The preheating conditions used in the SAR D_e determination protocol were verified prior to use through a 20 Gy single-grain dose recovery test performed on sample FG15 OSL-5, following the approach outlined in Arnold et al. (2016). The dose-recovery test yielded a measured-to-given dose ratio of 1.01 ± 0.02 and an overdispersion value of 10 ± 2%, supporting the suitability of the chosen SAR protocol. Individual grain D_e values were only included in the final age calculation if they satisfied a series of standard quality assurance criteria (Arnold et al., 2012; Arnold et al., 2016), as summarized in Table B2.

Table B1: SAR protocol used for D_e determination with the Fern Gully OSL samples.

Step	Treatment	Signal
1	Give dose (natural or laboratory)	
2[a]	IRSL stimulation (50°C for 60 s)	
3	Preheat 1 (PH_1 = 260°C for 10 s)	
4	Single grain OSL stimulation (125°C for 2 s)	L_n or L_x
5	Test dose (10 Gy)	
6	Preheat 2 (PH_2 = 220°C for 10 s)	
7	Single grain OSL stimulation (125°C for 2 s)	T_n or T_x
8	Repeat cycle for five different sized regenerative doses, a 0-Gy dose, and a repeated regenerative dose	

L_x = regenerative-dose OSL signal response; L_n = natural dose OSL signal response; T_x = test dose OSL signal response for a laboratory dose cycle; T_n = test dose OSL signal response for the natural dose cycle.
[a] Step 2 is only included in the single-grain OSL SAR procedure when measuring the OSL IR depletion ratio (Duller, 2003) (Duller, 2004).

We considered a range of statistical age models to characterise each single-grain De distribution and derive representative burial dose estimates: the central age model (CAM), the three-parameter minimum age model (MAM-3), the four-parameter minimum age model (MAM-4) and the finite mixture model (FMM) (Galbraith and Green, 1990; Galbraith et al., 1999). The rationale behind the age model choice for each sample is provided in section 3.5 and is based on consideration of De overdispersion, the presence of discrete dose populations, and the statistical suitability of the various age model fit (maximum log-likelihood criterion after Arnold and Roberts, 2009).

Environmental dose rates were determined from the radioactive elemental concentrations of the beta and gamma dose-rate bulk sediment samples. Elemental concentrations were determined on dried and powdered sediments using a combination of (ICP-MS) and inductively coupled plasma optical emission spectrometry (ICP-OES), which were converted to beta and gamma dose rates using the conversion factors of Guérin et al. (2011). The calculated environmental dose rates were corrected for beta-dose attenuation and long-term water corrections following Mejdahl (1979), Brennan (2003), Aitken (1985) and Readhead (1987). Cosmic-ray dose rate contributions were calculated using the approach outlined by Prescott and

Hutton (1994), assuming a constant, gradual build-up of overburden and an average wetland water depth of 1 m – equivalent to observed conditions during core extraction.

To eliminate possible water content measurement error due to drying in storage, contiguous water contents were calculated immediately after opening the cores. Discrete water content assessments were subsequently made on the beta and gamma dose rate bulk sediments during the OSL sampling procedure. No substantial changes in water content were noted between these two evaluations, demonstrating the representativeness of the water content used for dose rate assessments.

The P_Sequence model was run with the general outlier function (Bronk-Ramsey, 2016), and prior outlier probabilities of 5% were equally assigned to all dating samples to identify potentially significant statistical outliers. Likelihood estimates that yielded minor posterior outlier probabilities >5% were not excluded from the final model but were proportionally down-weighted in the iterative Monte Carlo runs, thereby producing an averaged chronological model (Bronk-Ramsey, 2016).

B.4.2 OSL results

Figures B4 and B5 show representative OSL dose-response and decay curve for grains that passed the SAR quality assurance criteria and were used for dating. The samples have very low environmental dose rates (0.05 – 0.12 Gy/kyr), consistent with the organic-rich nature of the peaty sediments and their high long-term water content (Table 2.2). No moisture versus depth trend was noted, indicating that dewatering and compaction of the sediments did not occur, no compaction correction was applied to the water content estimates used for dose rate calculation.

The single grain De distributions of the Fern Gully Lagoon OSL samples are shown as radial plots in Figure 5, B6 and B7. Sample FG15 OSL-3 exhibits the lowest overdispersion (26.7 ± 3.2%) and the most homogenous De distribution of the nineteen samples (Fig. 3.5a). These De characteristics are consistent with those typically reported for ideal (well-bleached and unmixed) single-grain De datasets at 2σ (global average overdispersion = 20 ± 1% (Arnold and Roberts, 2009)). Sample FG15 OSL-3 has therefore been used to derive a site-specific baseline assessment of overdispersion expected for well-bleached and unmixed samples at Fern Gully

Lagoon. The final burial dose of this 'best-case scenario' sample has been calculated using the CAM.

Seven OSL samples (FG15 OSL-14, -13, -12, -11, -10-2, -5, -4) exhibit slightly higher De scatter and overdispersion values of 29-39% (Fig. B6). However, the overdispersion values of these samples are all consistent at 2σ with the overdispersion value of sample FG15 OSL-3, suggesting limited influences of additional extrinsic De scatter. The final burial doses of these samples have also been derived using the CAM, as their dose dispersion properties are statistically indistinguishable from FG15 OSL-3.

The remaining eleven OSL samples exhibit significant De scatter, and a more significant proportion of the measured De values do not overlap with the 2σ standardised estimates of the weighted mean burial dose (Fig. B6). These De datasets also exhibit higher overdispersion values of 39 – 119%, which are not consistent at 2σ with the overdispersion value obtained for the well-bleached and unmixed baseline sample (FG15 OSL-3). Several De datasets are characterised by largely unstructured and broadly symmetric De scatter, with a similar number of outlying De values found on both sides of the weighted mean (e.g., FG15 OSL-17). Some of the samples are significantly positively skewed (Bailey and Arnold, 2006) (Bailey and Arnold, 2006) and show clear leading-edges of low De values or elongated clusters of higher De values (e.g., FG15 OSL-18, -2). Six samples exhibit very high overdispersion values (53–119%) and contain multiple discrete dose populations when fitted with the FMM (Fig. 3.5b, B7). Collectively, these complex De distribution characteristics are consistent with those commonly reported for heterogeneously bleached single-grain OSL samples (e.g. Arnold et al., 2007; Arnold et al., 2008), samples affected by post-depositional mixing (e.g. Arnold and Roberts, 2009; Arnold et al., 2012) and samples affected by certain sources of beta dose heterogeneity (e.g. Nathan et al., 2003; Mayya et al., 2006; Arnold et al., 2014). The final De values of these eleven samples have been derived using either the CAM, MAM-3 or MAM-4 according to the maximum log-likelihood (l_{max}) criterion of Arnold et al. (2009) (i.e., using the age model that provides the most statistically suitable fit for each empirical dataset after taking into consideration model parameterisation complexity).

It is worth noting that three of the samples exhibiting multiple discrete dose components in core 1 (FG15 OSL-8, -10, -16) also have counterpart samples from equivalent depths in core 2

(samples FG15 OSL-8-2, -10-2 and -16-2, respectively). Interestingly, two of these replicate samples (FG15 OSL-10-2, -16-2) from core 2 exhibit much lower overdispersion values and are characterized by single dose components that yield stratigraphically consistent age estimates using the L_{max} age model selection criterion of Arnold et al. (2009) (Tab. 3). These results suggest that the influences of post-depositional mixing may be localised and spatially variable across Fern Gully Lagoon rather than affecting entire sediment phases or units.

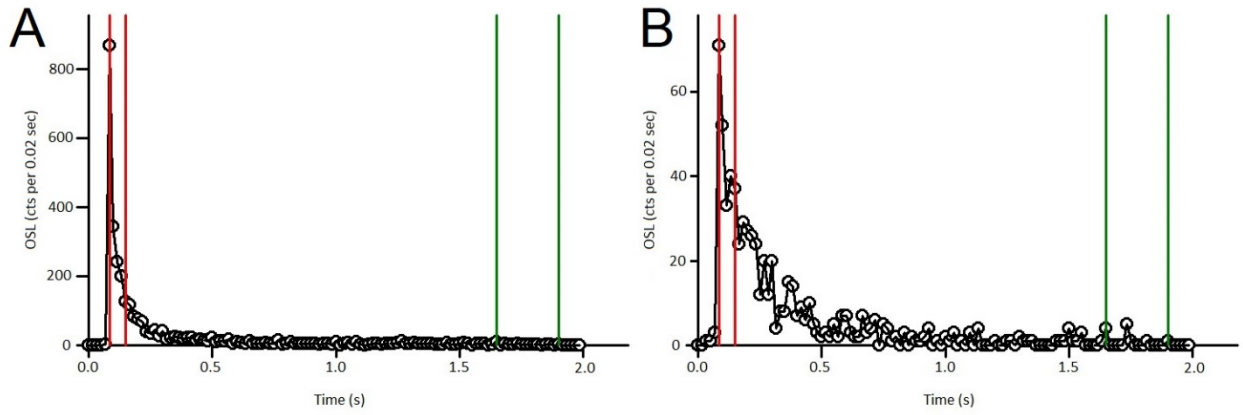

Figure B4: Representative natural test-dose (10 Gy) OSL decay curves for quartz grains that passed the SAR quality assurance criteria from sample FG15 OSL-3. (a) Example of an accepted grain that displayed a typical OSL signal brightness and relatively rapid decay within the first 0.5 s of stimulation. (b) Example of an accepted grain with a dimmer OSL signal and slightly slower decay (reaching background within 0.5-1 s of stimulation). Sensitivity-corrected dose-response curves (Fig. B5) were constructed using the first 0.08 s of each green laser stimulation (shown by the two red vertical lines) after subtracting a mean background count obtained from the last 0.25 s of the signal (shown by the two green lines).

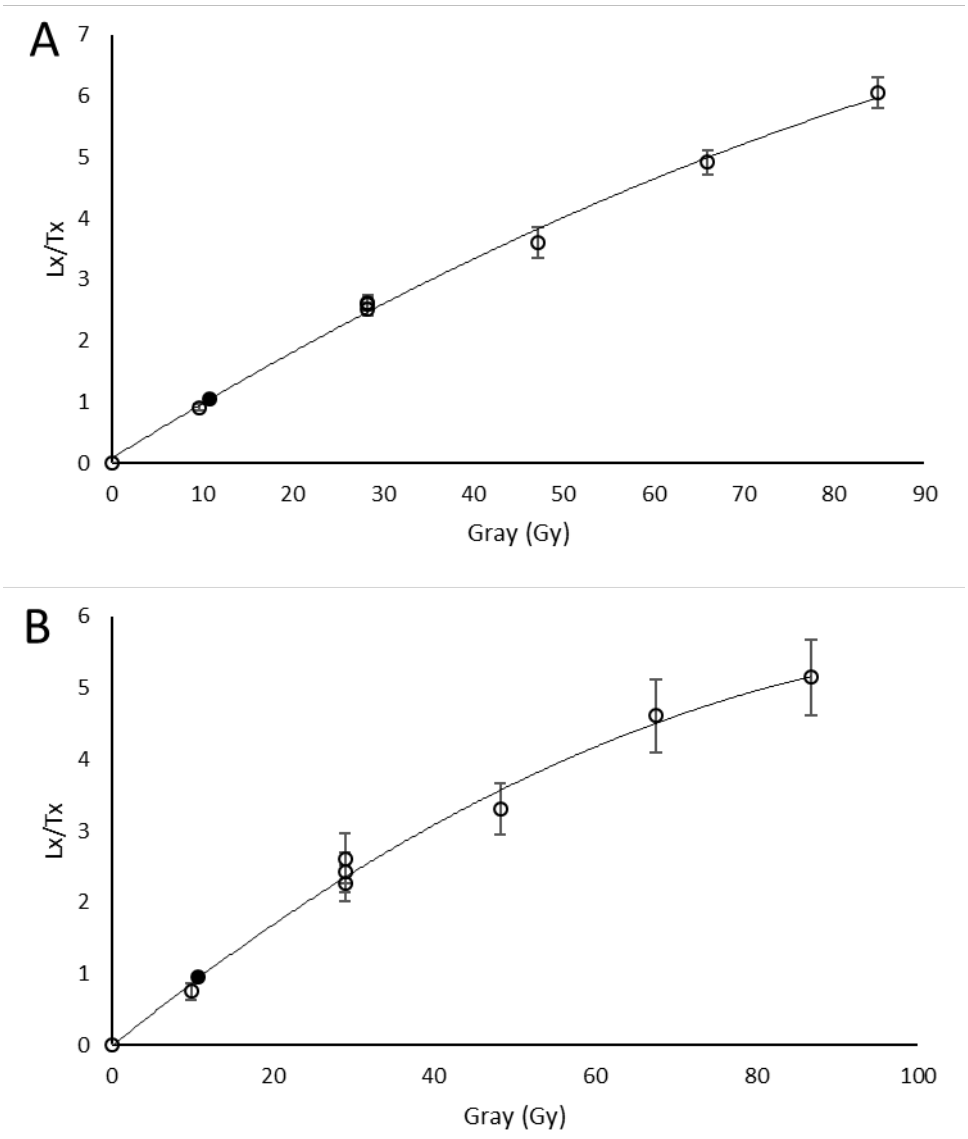

Figure B5: Example single-grain OSL dose-response curves for quartz grains from sample FG15 OSL-3. The filled circle denotes the sensitivity-corrected natural OSL signal, and open circles denote the sensitivity-corrected regenerated OSL signals.

Table B2: Single-grain quality assurance criteria and details (following Arnold et al., 2012; 2016).

Rule		Detail
1	Weak OSL signal	The net intensity of the natural test-dose signal (T_n) is less than three times the standard deviation of the late-light background signal.
2	Poor recycling ratio	The ratio of sensitivity-corrected luminescence responses (L_x/T_x) for two identical regenerative doses is not consistent with unity at 2σ.
3	High signal recuperation	The sensitivity-corrected luminescence response of the 0 Gy regenerative dose point amounts to >5% of the sensitivity-corrected natural signal response (L_n/T_n) at 2σ.
4	Feldspar contamination	The ratio of the L_x/T_x values obtained for two identical regenerative doses measured with and without prior IR stimulation (OSL IR depletion ratio; Duller, 2003) is less than unity at 2σ).
5	Signal saturation	The L_n/T_n value is equal to the I_{max} saturation limit of the dose-response curve at 2σ.
6	Non-intersecting natural signal	The L_n/T_n value is greater than the I_{max} saturation limit of the dose-response curve, and D_e interpolation is not possible.
7	Poor or anomalous dose-response	Dose-response curves display a zero or negative response with increasing dose or dose-response curves display very scattered L_x/T_x values (i.e., those that could not be successfully fitted with the Monte Carlo procedure and, hence, did not yield finite D_e values and uncertainty ranges).

Sample name	FG15 18	FG15 17	FG15 16 2	FG15 16	FG15 15	FG15 14	FG15 13	FG15 12	FG15 11	FG15 10 2	FG15 10	FG15 9	FG15 8 2	FG15 8	FG15 5	FG15 4	FG15 3	FG15 2	FG15 1
Depth (cm central)	175.5	185.5	208.5	208.5	218.5	239.5	267.5	277.5	287.5	310.5	310.5	325.5	409.5	409.5	664.5	829	822.5	845	909
Total measured grains	600	500	800	600	600	400	600	500	600	800	1100	800	800	1200	600	900	700	600	400
Rejection criteria																			
	%	%	%	%	%	%	%	%	%	%	%	%	%	%	%	%	%	%	%
1: Weak OSL signal	38	54.6	25.3	47.5	34.1	58.5	54.6	33	35.1	41.8	53.4	44.2	40.1	45.1	52.3	48.6	47.2	49.5	51.7
2: Poor recycling	3.8	1.6	3	1.1	2.3	0.5	1.5	4.2	4.5	1	2	5.7	2.5	2.8	2.5	2.6	2.4	3.8	1.2
3: High recuperation	2	1	0.7	1	1.3	0	0.5	2.2	1.3	0.5	1.9	4.3	0.6	3.9	1.8	1.2	3.1	3.3	4.5
4: Feldspar contamination	1.6	0.6	2.3	0.8	1.6	0.2	1.5	2	2.8	1.5	1.1	4	1.5	3.4	2.5	1.5	2.2	2	1.2
5: Signal saturation	0	0	0.1	0	0	0	0	0	1	0.1	0	0.3	0	0	0.3	0	0.4	0	0
6: Non-intersecting natural signal	0	0	1.3	0	0	0.5	0.1	0.4	3.1	1	0	0.6	0	0	0.1	0.4	0.5	0.6	1.5
7: Poor or anomalous dose-response	37.5	31.8	52.3	41.1	44.5	32	35.6	32.4	38.3	46.1	34.5	32.2	48.8	30.9	34.1	35.8	35.1	31.6	25.2
Sum of rejected grains (%)	82.9	89.6	85.0	91.5	83.8	91.7	93.8	74.2	86.1	92.0	92.9	91.3	93.5	86.1	93.6	90.1	90.9	90.8	85.3
Sum of accepted grains (%)	17.1	10.4	15.0	8.5	16.2	8.3	6.2	25.8	13.9	8.0	7.1	8.7	6.5	13.9	6.4	9.9	9.1	9.2	14.7

Table B3: Single-grain OSL classification statistics for the Fern Gully Lagoon sequence samples, following the quality assurance criteria of Arnold et al. (2012; 2016). The proportion of grains that were rejected from the final D_e estimation after applying the various quality assurance criteria are shown in rows 6-12.

Figure B6 (below): Radial plots showing the single-grain D_e distributions of OSL samples that were considered in the final age evaluations. The grey band on each plot is centered on the D_e value used to derive the final burial dose estimate, which has been derived using the age model indicated in the plot heading. CAM: Central Age Model; MAM3, 3-parameter Minimum Age Model; MAM4, 4-parameter Minimum Age Model; σ_b, overdispersion value.

FG15 18 – MAM3 – σ_b = 50.3 ± 4%

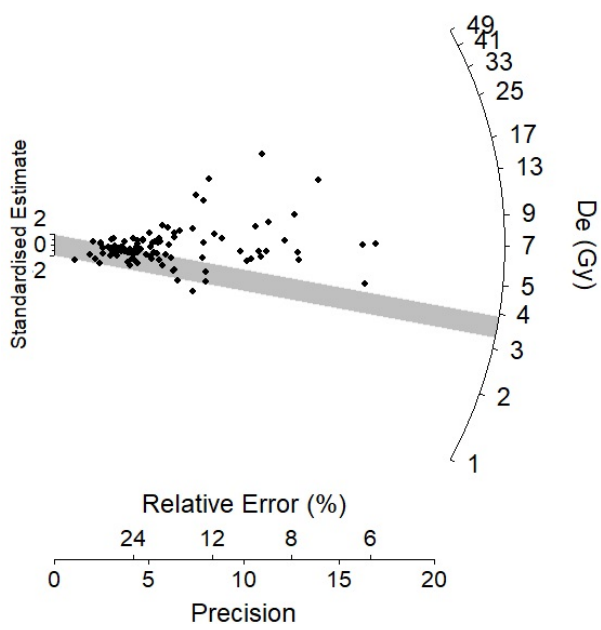

FG15 17 – CAM – σ_b = 50.9 ± 6%

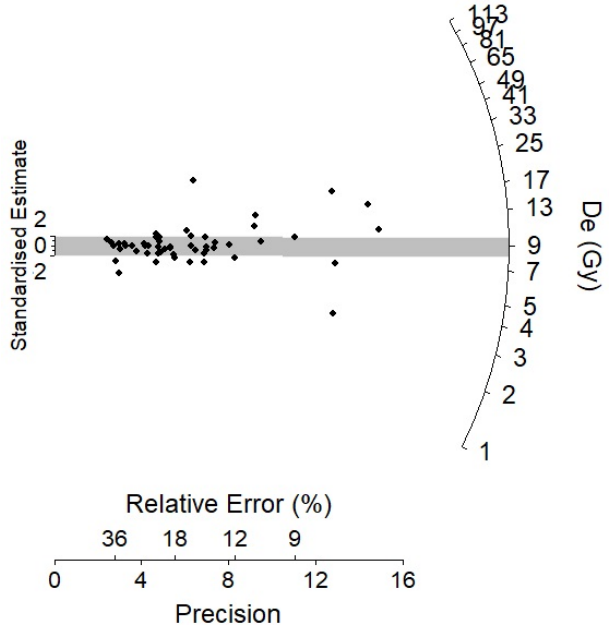

FG15 16 2 – MAM3 – σ_b = 39.5 ± 3%

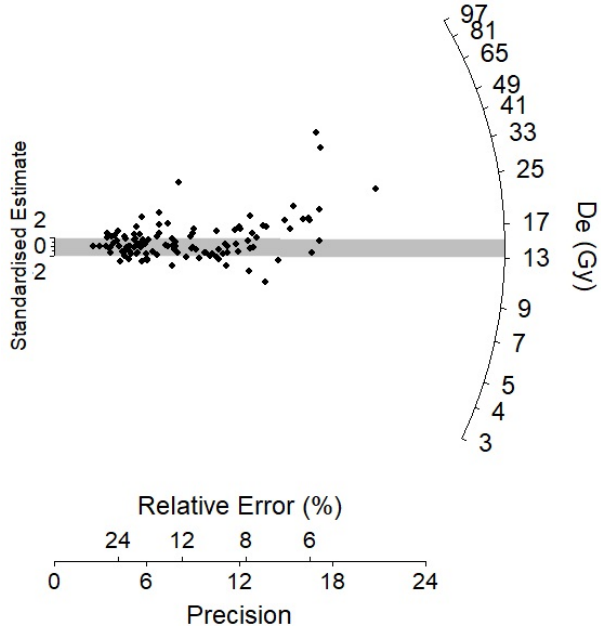

FG15 15 – CAM – σ_b = 41.3 ± 4%

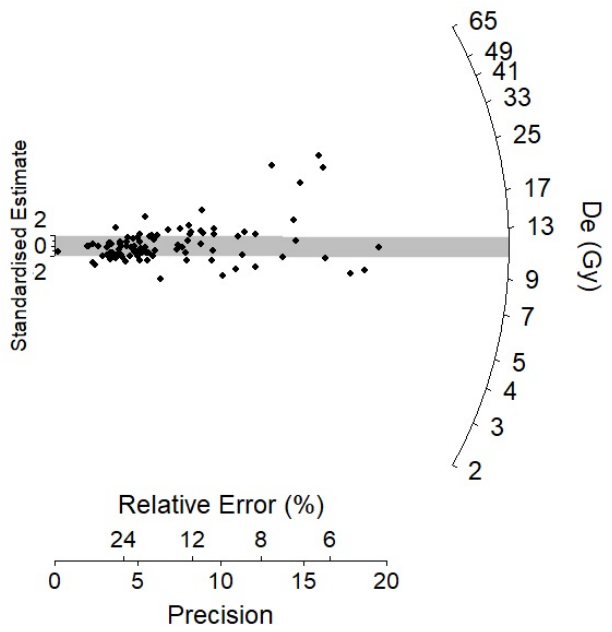

FG15 14 – CAM – σ_b = 34.5 ± 5%

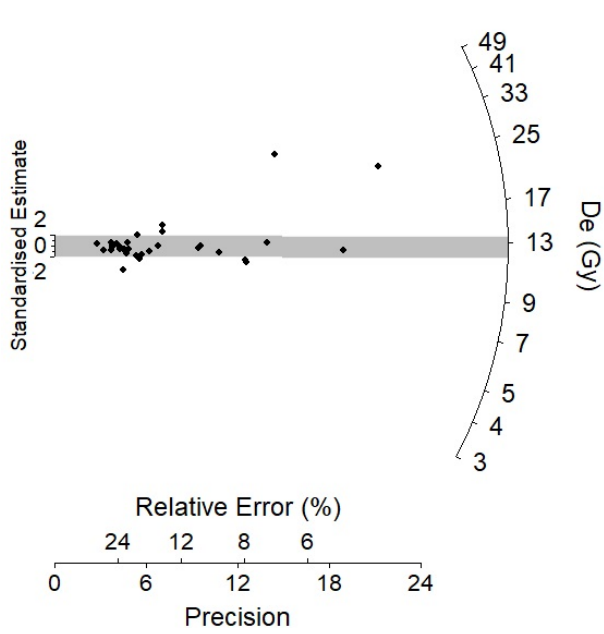

FG15 13 – CAM – σ_b = 34 ± 5%

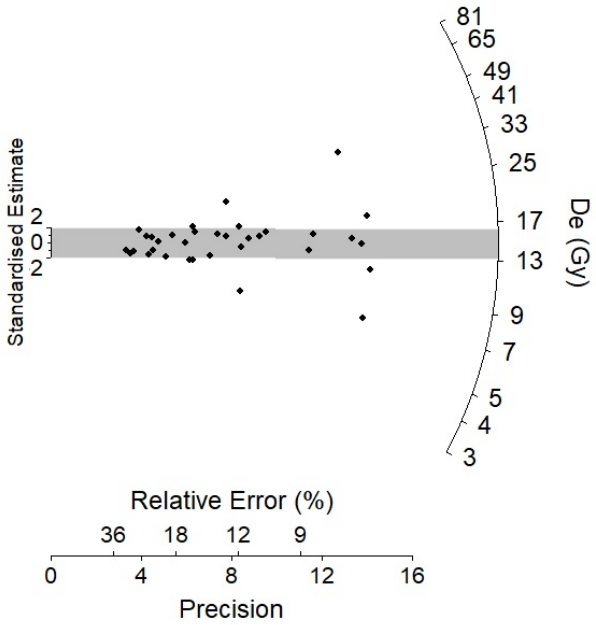

FG15 12 – CAM – σ_b = 34.4 ± 2%

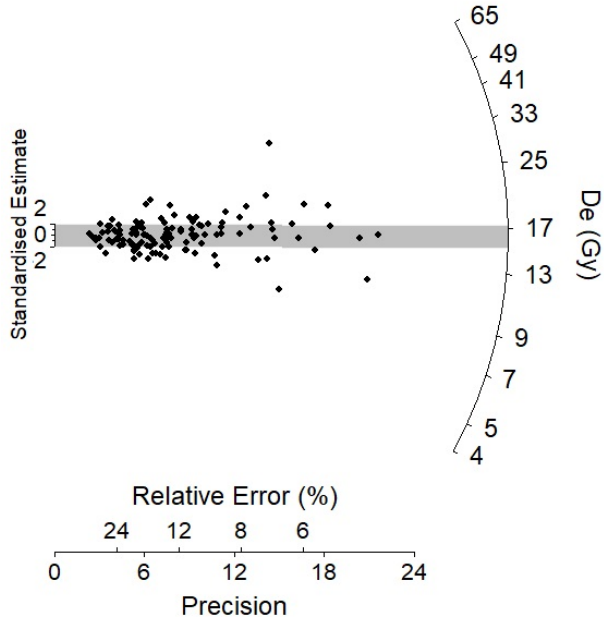

FG15 11 – CAM – σ_b = 28.9 ± 3%

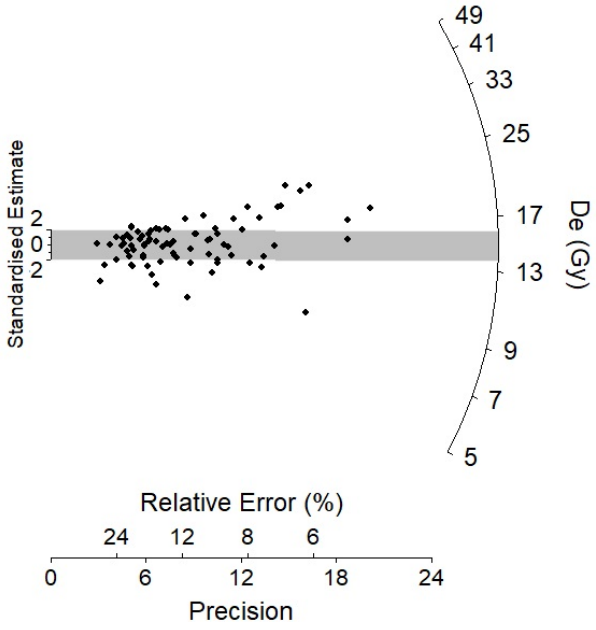

FG15 10 2 – CAM – σ_b = 33.2 ± 4%

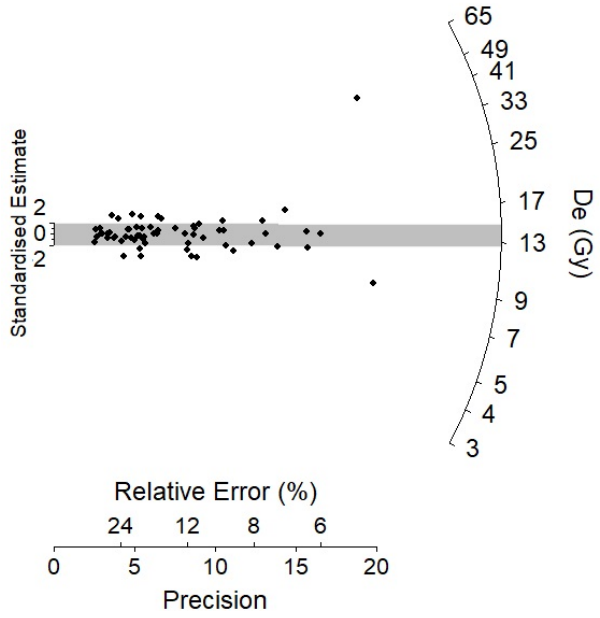

FG15 5 – CAM – σ_b = 39.2 ± 6%

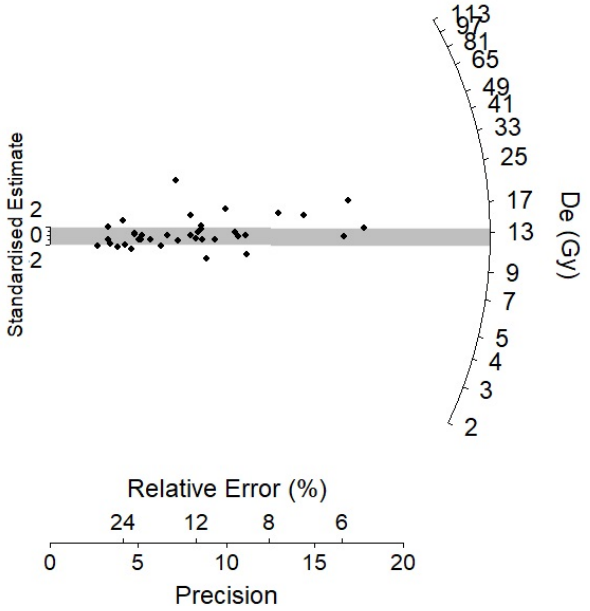

FG15 4 – CAM – σ_b = 32.5 ± 3%

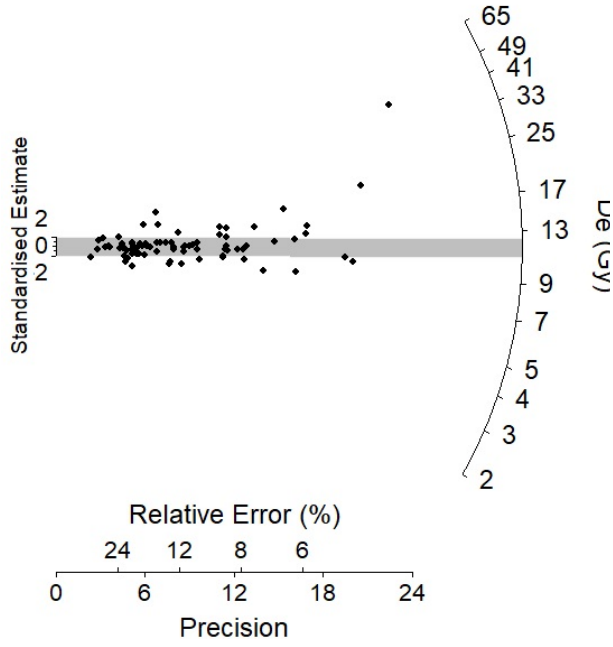

FG15 3 – CAM – σ_b = 26.7 ± 3%

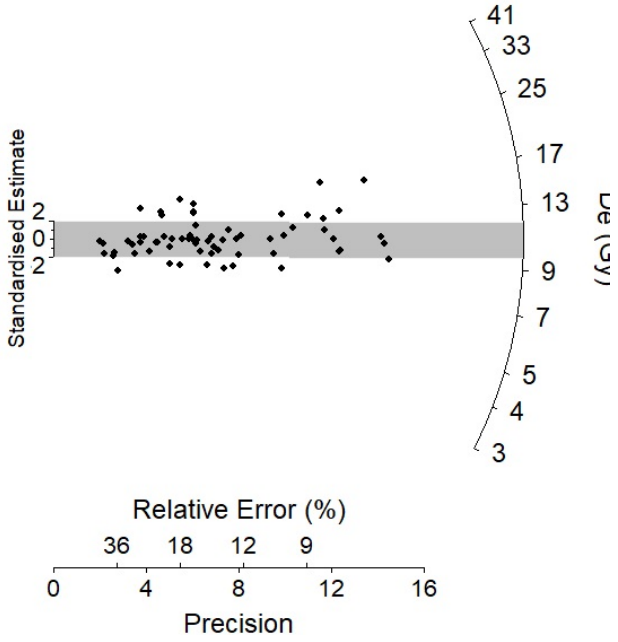

FG15 2 – MAM4 – σ_b = 52.4 ± 6%

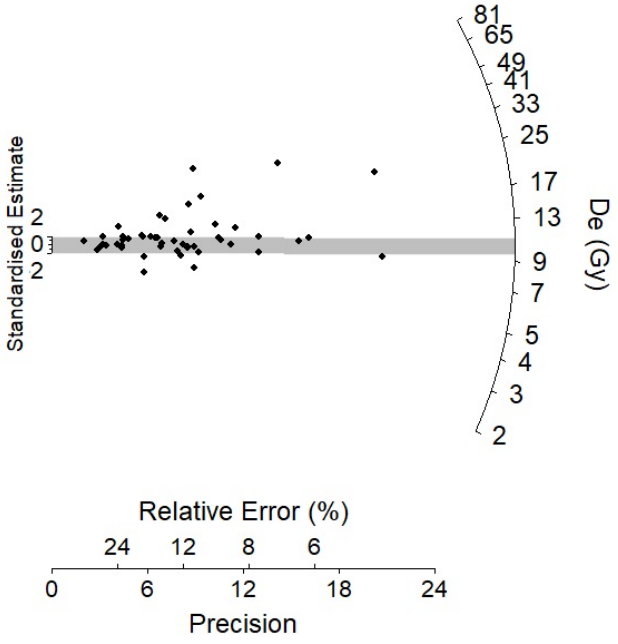

Figure B7 (below): Radial plots showing the single-grain D_e distributions of OSL samples that were not considered in the final age evaluations because of the presence of discrete multiple grain populations. The discrete dose populations identified using the finite mixture model are shown as dark grey bands (dominant dose populations), light grey bands and grey lines (minor dose populations).

FG15 16 – FMM – σ_b = 92.2 ± 10%

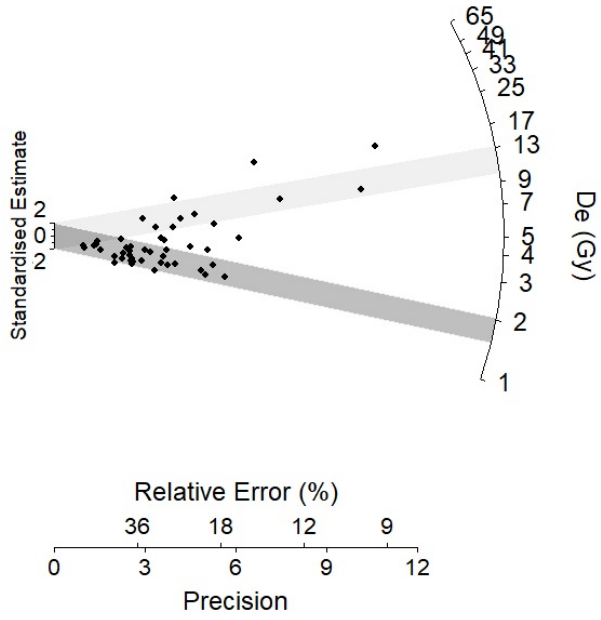

FG15 10 – FMM - σ_b = 53.3 ± 6%

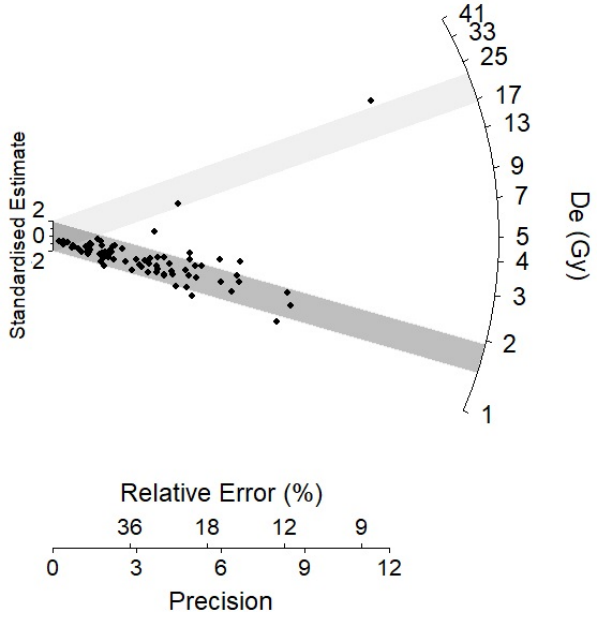

FG15 9 – FMM – σ_b = 118.5 ± 10%

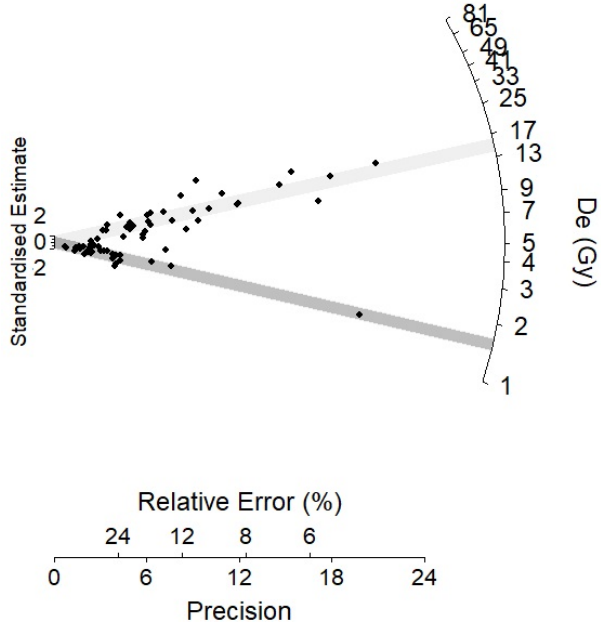

FG15 8 – FMM – σ_b = 76.9 ± 8%

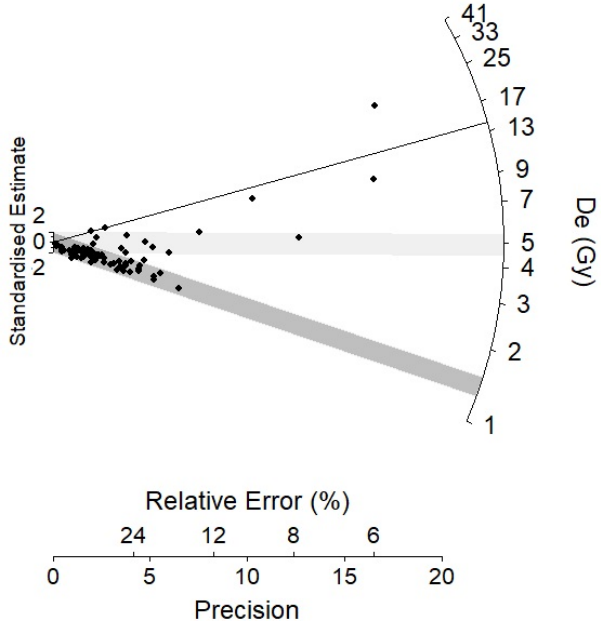

FG15 8 2 – FMM – σ_b = 94.8 ± 10%

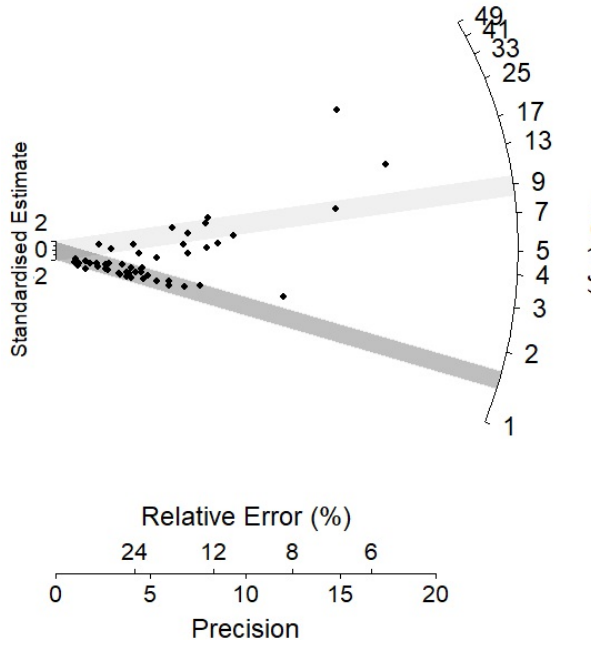

FG15 1 – FMM – σ_b = 88.8 ± 13%

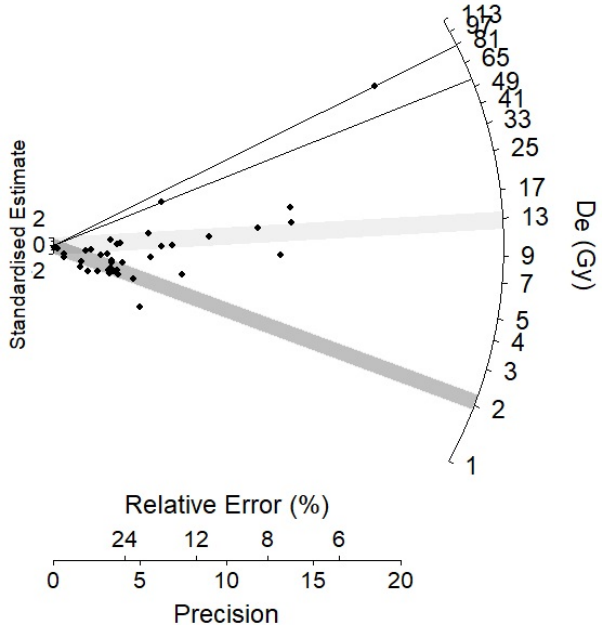

B.5 Bayesian age/depth modelling

B.5.1 Modelling method

The k_0 (base rigidity) parameter of the model was configured to respond to variations in deposition rate on the order of 1 event per cm of sedimentation and was allowed to vary over a factor of 10^{-2} to 10^{2} (i.e., 0.01 to 100 events per cm) to accommodate any major fluctuations in deposition rate supported by the data. The model adopted in this study does not presume continuous lacustrine deposition and is able to accommodate potential hiatuses and/or erosional discontinuities between different units identified on stratigraphic grounds (see details in section 2.4 and 3.6). This model structure is designed to accommodate two potential event boundaries (e.g., the end of one depositional event and the beginning of a subsequent depositional event) at the same depth in the *Sequence* framework, thereby enabling hiatus events to be more explicitly represented in the model.

B.5.2 Modelling results

The statistical validity of the modelling results was tested using the model agreement index (A_{model}), which measures the overlap between measured data and the modelled posterior distributions, and the overall agreement index ($A_{overall}$), which is a product of the individual agreement indices (A_i, Tab. 4) for each dating sample (Bronk-Ramsey, 2009). None of the three identified *boundary* hiatuses are considered statistically significant at the 95% confidence interval, as indicated by the OxCal *difference* query. The three *boundary* points are therefore only considered potential gaps in sedimentation that cannot be resolved beyond our current dating uncertainties.

Table B4: Summary of Bayesian modelling results. The likelihood (unmodelled) and posterior (modelled) age ranges are presented for each of the numerical dating samples. Posterior (modelled) age ranges are also shown for the boundaries of each stratigraphic unit. Posterior ages are presented as the 68.2% and 95.4% highest probability density ranges. The mean and 1σ uncertainty ranges of the modelled posterior distributions are shown for comparison (assuming a normally distributed probability density function). The unmodelled and modelled age estimates have been rounded to the nearest 50 years.

Boundary	Dating sample	Depth (cm)	Unmodelled age (years before 1950 CE)			Modelled age (years before 1950 CE)			Agreement index (A_i) (%)	Posterior outlier probability (%)
			68.2% range	95.4% range	Mean ± 1σ	68.2% range	95.4% range	Mean ± 1σ		
Unit 0 top		0				0–700	0–900	450 ± 200		
	FG15 RC-1,2	-35	750–800	700–850	800 ± 50	750–800	650–2100	1400 ± 350	95.2	10
Unit 0 bottom		-52				750–1150	700–2700	1700 ± 500		
Unit 1 top		-52				1350–11750	950–12100	6500 ± 2800		
	FG15 RC-11	-79	13050–13150	13050–13200	13100 ± 50	5100–13300	2500–13300	7900 ± 2700	56.5	48
	FG15 RC-4,5	-135	17800–18000	17750–18050	17900 ± 100	17800–17950	17700–18050	17900 ± 100	103.9	1
	FG15 RC-13	-159	19500–19700	19400–19850	19650 ± 100	19500–19750	19450–19900	19650 ± 100	103	0
Unit 1 bottom		-180				19650–20500	19400–22500	20950 ± 750		
Unit 2 top		-180				23950–40950	20150–49250	34700 ± 7250		
	FG15 OSL-18	-175.5	24950–41350	17100–49200	33150 ± 8050	33800–49700	27200–57100	42150 ± 7450	78.9	0
	FG15 OSL-17	-185.5	68200–87100	59100–96150	77650 ± 9250	58000–77800	43850–87100	65450 ± 10800	74.8	13
	FG15 OSL-16 2	-208.5	111950–143950	96550–159300	127950 ± 15700	82950–102250	74000–110900	92450 ± 9200	18.3	39
	FG15 OSL-15	-218.5	85500–105400	75950–114950	95450 ± 9750	91650–107450	83950–115250	99600 ± 7850	108.9	1
	FG15 OSL-14	-239.5	118600–151450	102850–167200	135050 ± 16100	108750–127250	100200–136750	118450 ± 9150	81.8	7
	FG15 OSL-13	-267.5	111400–152800	91500–172700	132100 ± 20300	127800–147700	118250–157250	137750 ± 9750	127.8	2
	FG15 OSL-12	-277.5	121150–152350	106150–167350	136750 ± 15300	134700–155500	124450–165750	145100 ± 10300	110	1
Unit 2 bottom		-280				141700–167200	130350–180100	155200 ± 12450		
Unit 3 top		-280				164250–191200	152200–202900	177550 ± 12700		
	FG15 OSL-11	-287.5	136900–205400	104000–238300	171150 ± 33550	162700–192600	149650–206350	178000 ± 14200	131	3
	FG15 OSL-10 2	-310.5	156700–202000	134900–223800	179350 ± 22200	165350–192250	152450–206000	179250 ± 13400	123.9	3
	FG15 OSL-5	-664.5	207050–288900	167750–328200	247950 ± 40100	184200–208700	173400–220300	196850 ± 11750	61.6	10
	FG15 OSL-3	-822.5	169450–231750	139550–261700	200600 ± 30550	189250–218850	177300–232600	204950 ± 13800	130.6	3
	FG15 OSL-4	-829	176000–235500	147400–264100	205750 ± 29200	189900–218800	177350–233100	205200 ± 13950	129.7	3
	FG15 OSL-2	-845	153050–206500	127350–232150	179750 ± 26200	190000–220150	177450–234550	206000 ± 14300	88.9	1
Unit 3 bottom		-900				192500–222500	180950–237650	209300 ± 14200		

B.6 Database review of µXRF studies

Our review of recent scanning µXRF studies has revealed >500 sediment records published in the past ten years. An examination of the most relevant 100 studies (as defined by Scopus and Web of Science, using the search terms 'sediment AND (micro-XRF OR (scanning XRF) OR XRF-sc OR µXRF))' was conducted to identify the most commonly utilised hardware, normalisation and validation methods (Table B5). The most common equipment used was Itrax (Cox analytical systems), accounting for ~71% of studies. Over a third of the Itrax studies (~39%) did not present any elemental ratios or use any normalisation or validation methods, instead inferring the abundance of individual elements directly from the µXRF counts per second.

Of the normalised records, the most commonly used approach was either normalisation by total counts (Bouchard et al., 2011; Martin et al., 2014) or the log ratio method (Weltje and Tjallingii, 2008; Weltje et al., 2015) (~21% of records each). The third- and fourth-most popular normalisation methods involved using ratios of selected scanned elements (e.g. Fe/Mn, Ca/Si or Rb/Sc) and a combination of incoherent and coherent scattering (incoherent + coherent or incoherent/coherent or normalisation by coherent or incoherent scatter alone) (~19% each). Normalisation by titanium, aluminum or other data (e.g. LOI) were each utilised in ~10% of studies.

Approximately 19% of studies in some way validated and/or calibrated the scanning µXRF data utilising a second method of sediment analysis, with the most common method being calibration by conventional XRF of inorganic oxides (~7% of studies). Approximately 4% of studies validated and corrected inorganic oxides by inductively coupled plasma mass spectrometry. The remaining ~3% of studies used other methods for validation, including SEM energy dispersive X-ray analysis (EDXA) (Field et al., 2018) and/or atomic absorption spectrometry (Martín-Puertas et al., 2011). Validation of the incoherent/coherent scattering ratio by LOI organic content estimation was also performed in some cases (~5%).

This review indicates that while multiple normalisation and validation methods exist, a large percentage of recent palaeoclimate records from µXRF analysis of sediments remains either unnormalised or unvalidated (>40%). From this percentage, we can infer that many of the

µXRF-based records published in the last ten years may be based on an assumed correlation of µXRF elements with absolute elementary concentrations, adding to the difficulty of reliably reconstructing past climate change.

B.7 Additional supplementary table

There is an additional supplementary table associated with chapter 3, which lists the µXRF studies used when reviewing recent published methods. It is unfortunately too large to be included in the printed version of this thesis, but can be found online at this address:

https://ars-els-cdn-com.proxy.library.adelaide.edu.au/content/image/1-s2.0-S0031018219307503-mmc2.xlsx

The caption for this table has been included below:

Table B5: A list of 100 scanning micro-XRF sediment studies used to determine common equipment, normalisation methods, elements and validation methods as well as sediment types.

B.8 References

Aitken, M.J., 1985. "Thermoluminescence dating". Academic Press, London.

Aitken, M.J., 1998. "An introduction to optical dating: the dating of Quaternary sediments by the use of photon-stimulated luminescence". Oxford University Press, Oxford.

Arnold, L.J., Bailey, R.M., Tucker, G.E., 2007. "Statistical treatment of fluvial dose distributions from southern Colorado arroyo deposits." *Quaternary Geochronology* 2, 162-167.

Arnold, L.J., Demuro, M., Navazo, M., Benito-Calvo, A., Pérez-González, A., 2012. "OSL dating of the Middle Palaeolithic Hotel California site, Sierra de Atapuerca, north-central Spain." *Boreas* 42, 285-305.

Arnold, L.J., Demuro, M., Parés, J.M., Arsuaga, J.L., Aranburu, A., de Castro, B., María, J., Carbonell, E., 2014. "Luminescence dating and palaeomagnetic age constraint on hominins from Sima de los Huesos, Atapuerca, Spain." *Journal of Human Evolution* 67, 85-107.

Arnold, L.J., Duval, M., Demuro, M., Spooner, N.A., Santonja, M., Pérez-González, A., 2016. "OSL dating of individual quartz 'supergrains' from the Ancient Middle Palaeolithic site of Cuesta de la Bajada, Spain." *Quaternary Geochronology* 36, 78-101.

Arnold, L.J., Roberts, R.G., 2009. "Stochastic modelling of multi-grain equivalent dose (D_e) distributions: Implications for OSL dating of sediment mixtures." *Quaternary Geochronology* 4, 204-230.

Arnold, L.J., Roberts, R.G., Galbraith, R.F., DeLong, S.B., 2009. "A revised burial dose estimation procedure for optical dating of young and modern-age sediments." *Quaternary Geochronology* 4, 306-325.

Arnold, L.J., Roberts, R.G., Macphee, R.D.E., Haile, J.S., Brock, F., Möller, P.E.R., Froese, D.G., Tikhonov, A.N., Chivas, A.R., Thomas, M., Gilbert, P., Willerslev, E., 2011. "Paper II – Dirt, dates and DNA: OSL and radiocarbon chronologies of perennially frozen sediments in Siberia, and their implications for sedimentary ancient DNA studies." *Boreas* 40, 417-445.

Arnold, L.J., Roberts, R.G., MacPhee, R.D.E., Willerslev, E., Tikhonov, A.N., Brock, F., 2008. "Optical dating of perennially frozen deposits associated with preserved ancient plant and animal DNA in north-central Siberia." *Quaternary Geochronology* 3, 114-136.

Bailey, R.M., Arnold, L.J., 2006. "Statistical modelling of single grain quartz D_e distributions and an assessment of procedures for estimating burial dose." *Quaternary Science Reviews* 25, 2475-2502.

Bouchard, F., Francus, P., Pienitz, R., Laurion, I., 2011. "Sedimentology and geochemistry of thermokarst ponds in discontinuous permafrost, subarctic Quebec, Canada." *Journal of Geophysical Research: Biogeosciences* 116.

Brennan, B.J., 2003. "Beta doses to spherical grains." *Radiation Measurements* 37, 299-303.

Bronk-Ramsey, C., 2009. "Bayesian Analysis of Radiocarbon Dates." *Radiocarbon* 51, 337-360.

Bronk-Ramsey, C., 2016. "Dealing with Outliers and Offsets in Radiocarbon Dating." *Radiocarbon* 51, 1023-1045.

Demuro, M., Arnold, L.J., Froese, D.G., Roberts, R.G., 2013. "OSL dating of loess deposits bracketing Sheep Creek tephra beds, northwest Canada: Dim and problematic single-grain OSL characteristics and their effect on multi-grain age estimates." *Quaternary Geochronology* 15, 67-87.

Demuro, M., Arnold, L.J., Parés, J.M., Sala, R., 2015. "Extended-range luminescence chronologies suggest potentially complex bone accumulation histories at the Early-to-Middle Pleistocene palaeontological site of Huéscar-1 (Guadix-Baza basin, Spain)." *Quaternary International* 389, 191-212.

Duller, G.A.T., 2004. "Luminescence dating of Quaternary sediments: recent advances." *Journal of Quaternary Science* 19, 183-192.

Field, E., Tyler, J., Gadd, P.S., Moss, P., McGowan, H., Marx, S., 2018. "Coherent patterns of environmental change at multiple organic spring sites in northwest Australia: Evidence of Indonesian-Australian summer monsoon variability over the last 14,500 years." *Quaternary Science Reviews* 196, 193-216.

Galbraith, R.F., Green, P.F., 1990. "Estimating the component ages in a finite mixture." *International Journal of Radiation Applications & Instrumentation. Part D, Nuclear Tracks & Radiation Measurements* 17, 197-206.

Galbraith, R.F., Roberts, R.G., Laslett, G.M., Yoshida, H., Olley, J.M., 1999. "Optical dating of single and multiple grains of quartz from Jinmium Rock Shelter, northern Australia: Part 1, experimental design and statistical models." *Archaeometry* 41, 339-364.

Guérin, G., Mercier, N., Adamiec, G., 2011. "Dose-rate conversion factors: update." *Ancient TL* 29, 5-8.

Killick, R., Eckley, I.A., 2014. "Changepoint: An R Package for Changepoint Analysis." *Journal of Statistical Software* 1.

Martín-Puertas, C., Valero-Garcés, B.L., Mata, M.P., Moreno, A., Giralt, S., Martínez-Ruiz, F., Jiménez-Espejo, F., 2011. "Geochemical processes in a Mediterranean Lake: a high-resolution study of the last 4,000 years in Zoñar Lake, southern Spain." *Journal of Paleolimnology* 46, 405-421.

Martin, L., Mooney, S., Goff, J., 2014. "Coastal wetlands reveal a non-synchronous island response to sea-level change and a palaeostorm record from 5.5 kyr to present." *The Holocene* 24, 569-580.

Mayya, Y.S., Morthekai, P., Murari, M.K., Singhvi, A.K., 2006. "Towards quantifying beta microdosimetric effects in single-grain quartz dose distribution." *Radiation Measurements* 41, 1032-1039.

Mejdahl, V., 1979. "Thermoluminescence Dating: Beta-Dose Attenuation in Quartz Grains." *Archaeometry* 21, 61-72.

Murray, A.S., Wintle, A.G., 2000. "Luminescence dating of quartz using an improved single-aliquot regenerative-dose protocol." *Radiation Measurements* 32, 57-73.

Nathan, R.P., Thomas, P.J., Jain, M., Murray, A.S., Rhodes, E.J., 2003. "Environmental dose rate heterogeneity of beta radiation and its implications for luminescence dating: Monte Carlo modelling and experimental validation." *Radiation Measurements* 37, 305-313.

Prescott, J.R., Hutton, J.T., 1994. "Cosmic ray contributions to dose rates for luminescence and ESR dating: Large depths and long-term time variations." *Radiation Measurements* 23, 497-500.

Readhead, M.L., 1987. "Thermoluminescence dose rate data and dating equations for the case of disequilibrium in the decay series." *International Journal of Radiation Applications & Instrumentation. Part D, Nuclear Tracks & Radiation Measurements* 13, 197-207.

Weltje, G.J., Bloemsma, M.R., Tjallingii, R., Heslop, D., Röhl, U., Croudace, I.W., 2015. "Prediction of Geochemical Composition from XRF Core Scanner Data: A New Multivariate Approach Including Automatic Selection of Calibration Samples and Quantification of Uncertainties", in: Croudace, I.W., Rothwell, R.G. (Eds.), Micro-XRF Studies of Sediment Cores: Applications of a non-destructive tool for the environmental sciences. Springer Netherlands, Dordrecht, pp. 507-534.

Weltje, G.J., Tjallingii, R., 2008. "Calibration of XRF core scanners for quantitative geochemical logging of sediment cores: Theory and application." *Earth and Planetary Science Letters* 274, 423-438.

Appendix C – Supplementary material for Chapter 4

C.1 Fern Gully Lagoon age-depth model

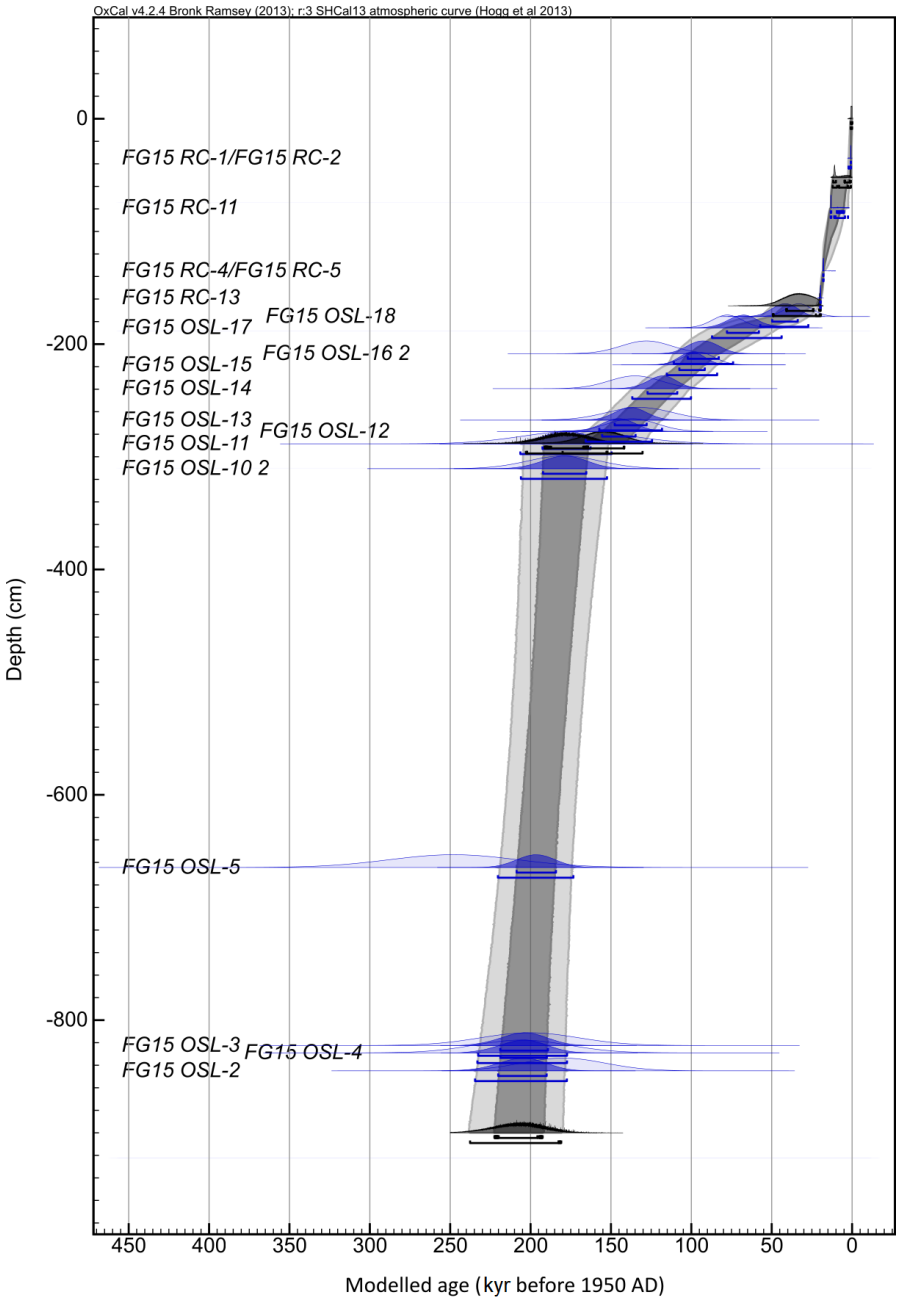

Figure C1: Age-depth model for Fern Gully Lagoon (Chapter 3; Kemp et al., 2020). This is a duplicate figure, added to preserve links in the manuscript as submitted.

C.2 Principal component analysis, indicating the relationship between major taxa

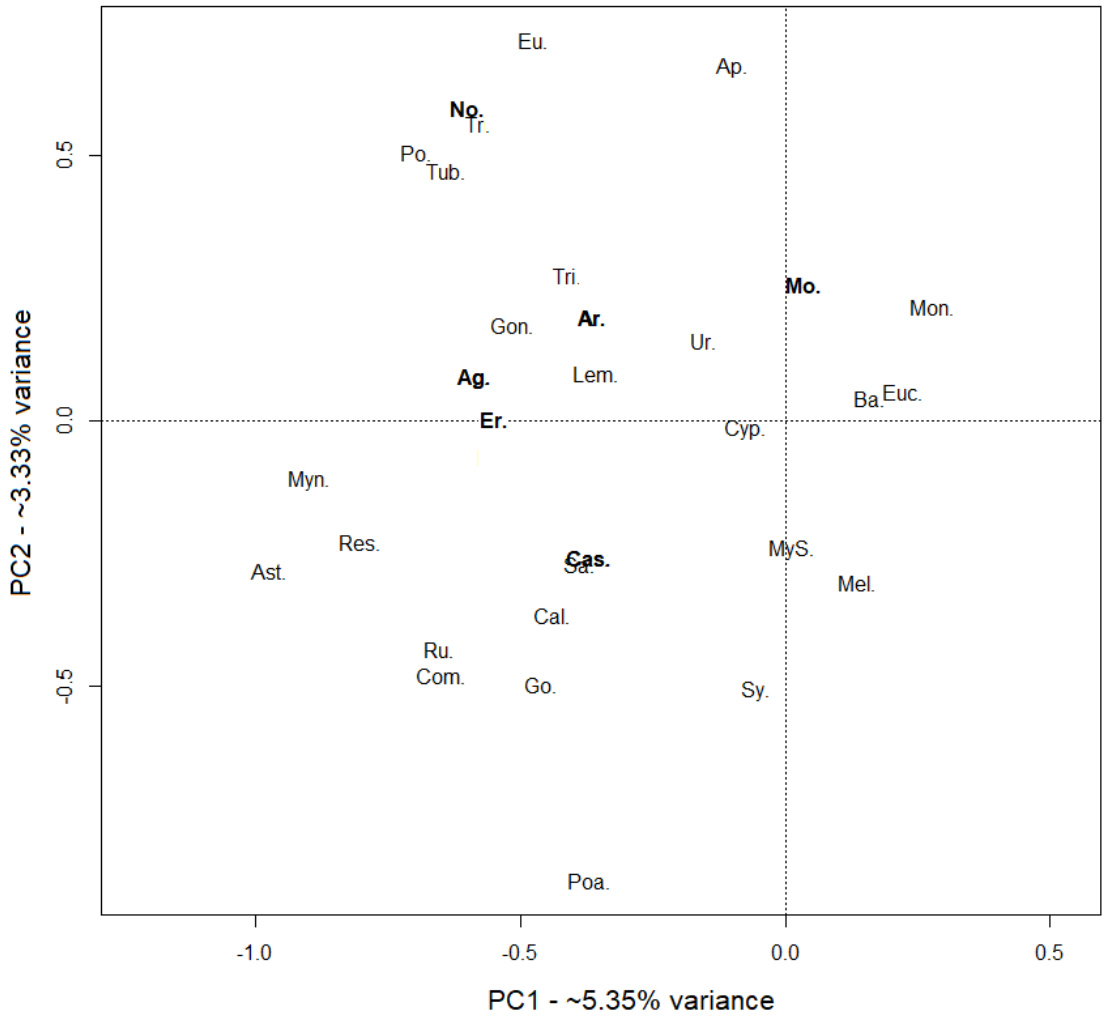

Figure C2: PCA of all major taxa (containing ~99% of all counted grains) recorded in the FGL sediments. Indicator taxa (Fig. 3) are in bold. Ar.: *Araucaria*, Ag.: *Agathis*, Po.: *Podocarpus*, Sa.: Sapotaceae, Sy.: *Syzygium*, No.: *Nothofagus*, Eu.: Euphorbiaceae, MyS.: Myrtaceous shrubs, Euc.: *Eucalyptus* spp., Cas.: Casuarinaceae, Cal.: *Callitris*, Er.: Ericaceae, Mo.: *Monotoca*, Ba.: *Banksia*, Poa.: Poaceae, Ast.: Asteraceae (tublifloreae), Tub.: *Tubuliflorides pleistocenicus*, Ur.: *Urtica*, Ru.: Rutaceae, Go.: Goodenicaeae, Ap.: Apiaceae, Com.: *Comesperma*, Cyp.: Cyperaceae, Res.: Restionaceae, Mel.: *Melaleuca*, Myn.: *Myriophyllum* sp., Gon.: *Gonocarpus* sp., Tr.: *Triglochin* sp., Lem.: *Lemna* sp., Mon.: Monolete fern spores and Tri.: Trilete fern spores.

C.3 Macrocharcoal spectral analysis

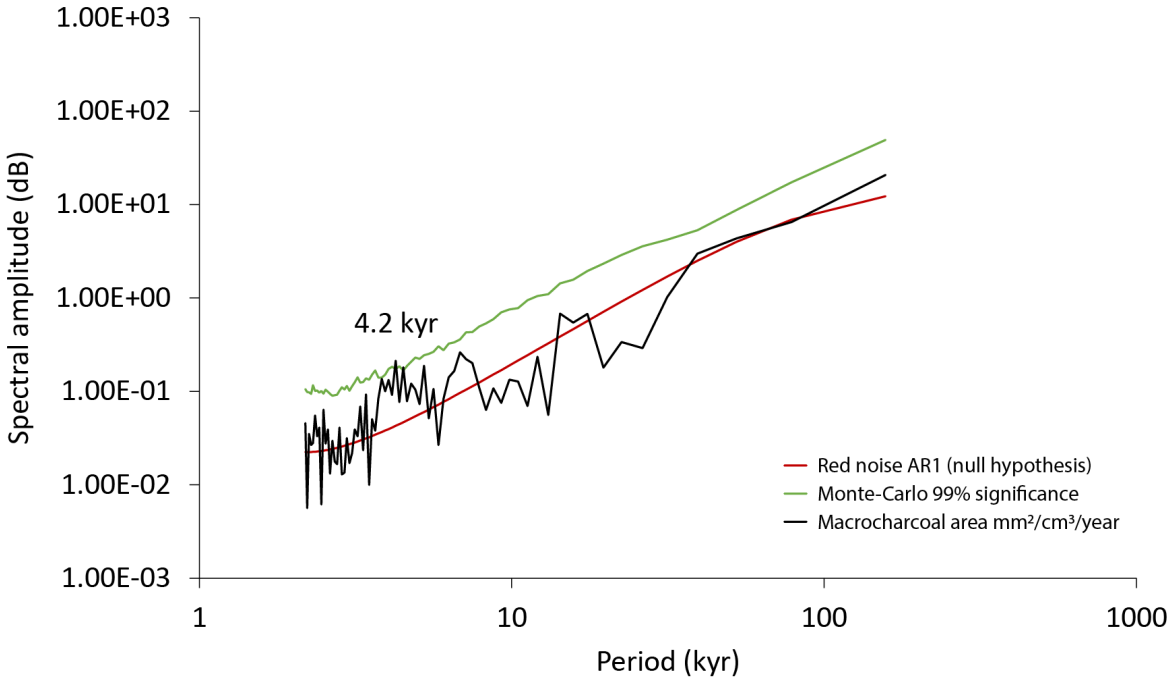

Figure C3: Redfit spectral analysis of macrocharcoal data for the late MIS 6 to late MIS 3 sedimentation phase (155–35 ka).

C.4 Bayesian priors and modelling results

Table C1: Summary of Bayesian modelling results (Chapter 3; Kemp et al., 2020). The likelihood (unmodelled) and posterior (modelled) age ranges are presented for each of the numerical dating samples. Posterior (modelled) age ranges are also shown for the boundaries of each stratigraphic unit. Posterior ages are presented as the 68.2% and 95.4% highest probability density ranges. The mean and 1σ uncertainty ranges of the modelled posterior distributions are shown for comparison (assuming a normally distributed probability density function). The unmodelled and modelled age estimates have been rounded to the nearest 50 years.

Boundary	Dating sample	Depth (cm)	Unmodelled age (years before 1950 CE)			Modelled age (years before 1950 CE)			Agreement index (A_i) (%)	Posterior outlier probability (%)
			68.2% range	95.4% range	Mean ± 1σ	68.2% range	95.4% range	Mean ± 1σ		
Unit 0 top		0				0–700	0–900	450 ± 200		
	FG15 RC-1,2	-35	750–800	700–850	800 ± 50	750–800	650–2100	1400 ± 350	95.2	10
Unit 0 bottom		-52				750–1150	700–2700	1700 ± 500		
Unit 1 top		-52				1350–11750	950–12100	6500 ± 2800		
	FG15 RC-11	-79	13050–13150	13050–13200	13100 ± 50	5100–13300	2500–13300	7900 ± 2700	56.5	48
	FG15 RC-4,5	-135	17800–18000	17750–18050	17900 ± 100	17800–17950	17700–18050	17900 ± 100	103.9	1
	FG15 RC-13	-159	19500–19700	19400–19850	19650 ± 100	19500–19750	19450–19900	19650 ± 100	103	0
Unit 1 bottom		-180				19650–20500	19400–22500	20950 ± 750		
Unit 2 top		-180				23950–40950	20150–49250	34700 ± 7250		
	FG15 OSL-18	-175.5	24950–41350	17100–49200	33150 ± 8050	33800–49700	27200–57100	42150 ± 7450	78.9	0
	FG15 OSL-17	-185.5	68200–87100	59100–96150	77650 ± 9250	58000–77800	43850–87100	65450 ± 10800	74.8	13
	FG15 OSL-162	-208.5	111950–143950	96550–159300	127950 ± 15700	82950–102250	74000–110900	92450 ± 9200	18.3	39
	FG15 OSL-15	-218.5	85500–105400	75950–114950	95450 ± 9750	91650–107450	83950–115250	99600 ± 7850	108.9	1
	FG15 OSL-14	-239.5	118600–151450	102850–167200	135050 ± 16100	108750–127250	100200–136750	118450 ± 9150	81.8	7
	FG15 OSL-13	-267.5	111400–152800	91500–172700	132100 ± 20300	127800–147700	118250–157250	137750 ± 9750	127.8	2
	FG15 OSL-12	-277.5	121150–152350	106150–167350	136750 ± 15300	134700–155500	124450–165750	145100 ± 10300	110	1
Unit 2 bottom		-280				141700–167200	130350–180100	155200 ± 12450		
Unit 3 top		-280				164250–191200	152200–202900	177550 ± 12700		
	FG15 OSL-11	-287.5	136900–205400	104000–238300	171150 ± 33550	162700–192600	149650–206350	178000 ± 14200	131	3
	FG15 OSL-102	-310.5	156700–202000	134900–223800	179350 ± 22200	165350–192250	152450–206000	179250 ± 13400	123.9	3
	FG15 OSL-5	-664.5	207050–288900	167750–328200	247950 ± 40100	184200–208700	173400–220300	196850 ± 11750	61.6	10
	FG15 OSL-3	-822.5	169450–231750	139550–261700	200600 ± 30550	189250–218850	177300–232600	204950 ± 13800	130.6	3
	FG15 OSL-4	-829	176000–235500	147400–264100	205750 ± 29200	189900–218800	177350–233100	205200 ± 13950	129.7	3
	FG15 OSL-2	-845	153050–206500	127350–232150	179750 ± 26200	190000–220150	177450–234550	206000 ± 14300	88.9	1
Unit 3 bottom		-900				192500–222500	180950–237650	209300 ± 14200		

C.5 Dominant pollen taxa by sedimentation phase

Table C2: A list of dominant pollen taxa (occurring in >15 pollen samples), taxonomic affiliation and plant habitat at Fern Gully Lagoon, with sedimentation phases in which each family has greater than background relative abundances. Taxa that make up the terrestrial pollen sum are shown in bold.

Major pollen taxon	Family	Plant habitat	210-177 ka	155-35 ka	21-0.6 ka
Rainforest taxa					
Araucaria Juss.	Araucariaceae	Emergent rainforest trees	*	*	*
Agathis Salisb.	Araucariaceae	Emergent rainforest trees	*	*	*
Podocarpus L'Hér ex Pers.	Podocarpaceae	Canopy and subcanopy rainforest trees	*	*	
Sapotaceae Juss.	Sapotaceae	Canopy and second canopy rainforest trees	*	*	*
Syzygium R.Br. ex Gaertn.	Myrtaceae	Canopy rainforest trees	*	*	
Nothofagus moorei/cunninghamii F.Muell./ (Hook.f.) Heenan & Smissen	Nothofagaceae	Canopy temperate rainforest trees		*	*
Euphorbiaceae Juss.	Euphorbiaceae	Rainforest trees, shrubs and herbs		*	*
Sclerophyll taxa					
Myrtaceous shrubs Juss.	Myrtaceae	*Leptospermum*, *Baeckea* and *Tristania* shrubs that can occur on dunes, in sclerophyll forest and heaths across NSI	*	*	*
Eucalyptus sensu lato	Myrtaceae	Dryland canopy trees	*	*	*
Casuarinaceae R.Br.	Casuarinaceae	Dryland canopy trees	*	*	*
Callitris Vent.	Cupressaceae	Dryland canopy trees	*	*	
Ericaceae Juss.	Ericaceae	Heath shrubs and herbs	*	*	*
Monotoca R.Br.	Ericaceae	Heath shrub			*
Banksia L.f.	Proteaceae	Heath and Dryland secondary trees and shrubs	*	*	*
Herb and grass taxa					
Poaceae Barnhart	Poaceae	Dryland and aquatic grasses		*	*
Asteraceae (Tubulifloreae) Bercht. & J.Presl	Asteraceae	Dryland herbs and shrubs		*	*

Tubuliflorides pleistocenicus Martin	Asteraceae	Spineless or short spined Asteraceae pollen grain, which became extinct or highly restricted during the late Pleistocene. Thought to be a dryland herb.		*	
Urtica L.	Urticaceae	Dryland herbs	*	*	
Rutaceae Juss.	Rutaceae	Dryland herbs		*	
Goodeniaceae R.Br.	Goodeniaceae	Dryland herbs		*	
Apiaceae Lindl.	Apiaceae	Dryland herbs		*	
Comesperma Labill.	Polygalaceae	Dryland herbs		*	
Aquatic taxa					
Cyperaceae Juss.	Cyperaceae	Sedge	*	*	*
Restionaceae R.Br.	Restionaceae	Rush	*	*	*
Melaleuca L. nom. cons.	Myrtaceae	Wetland canopy tree	*		*
Myriophyllum L.	Haloragaceae	Submerged		*	
Gonocarpus Thunb.	Haloragaceae	Marsh herb		*	
Triglochin L.	Juncaginaceae	Marsh herb		*	
Lemna L.	Araceae	Floating plant		*	*
Fern spores					
Pteridium Gled. ex Scop.	Dennstaedtiaceae	Ground ferns, disturbance indicator	*	*	
Aspidiaceae Herter	Aspidiaceae	Ground ferns	*		
Monolete fern spores	Various	Tree or ground ferns	*	*	*
Trilete fern spores	Various	Tree or ground ferns	*	*	

C.6 Correlation matrices for charcoal and pollen relative abundances

Table C3: Correlations between charcoal data and the relative abundances of pollen within taxon subsets (r values, n = 61 for all calculations,***: p < 0.05; **: p > 0.05 and < 0.1; *: p > 0.1).

	Micro-charcoal	Macro-charcoal
Rainforest taxa	-0.21*	-0.18*
Sclerophyll taxa	0.24**	0.23**
Herbs and grasses	-0.11*	-0.15*
Arboreal taxa	0.05*	-0.05*
Shrub taxa	-0.06*	0.09*

Table C4: Correlations between macrocharcoal data and the relative abundances of taxon subsets before and after pollen sampling points during the first phase of sedimentation (r values, p values Bonferroni adjusted for the number of comparisons (11), n = 30 for all calculations,***: p < 0.0045; **: p > 0.0045 and < 0.01; *: p > 0.01).

	Correlation to fire frequency (approx. years before)					At event	Correlation to fire frequency (approx. years after)				
	400	320	240	160	80	0	80	160	240	320	400
Rainforest taxa	-0.25**	-0.24**	-0.08*	0.04*	-0.06*	-0.09*	0.06*	0.37***	-0.14*	-0.14*	-0.04*
Sclerophyll taxa	0.26***	0.25**	0.14*	-0.12*	-0.03*	0.05*	-0.04*	-0.24**	0.12*	0.12*	0*
Herbs and grasses	-0.07*	-0.07*	-0.12*	0.14*	0.14*	0.05*	-0.03*	-0.14*	0*	0*	0.06*
Arboreal taxa	0.09*	0.12*	0.08*	0.04*	0.02*	0.11*	0.01*	0.18*	0.02*	-0.07*	-0.06*
Shrub taxa	-0.01*	-0.06*	0.01*	-0.17*	-0.03*	-0.09*	0.09*	-0.09*	0.07*	0*	-0.04*

C.7 References

Kemp, C.W., Tibby, J., Arnold, L.J., Barr, C., Gadd, P.S., Marshall, J.C., McGregor, G.B., Jacobsen, G.E., 2020. "Climates of the last three interglacials in subtropical eastern Australia inferred from wetland sediment geochemistry." *Palaeogeography, Palaeoclimatology, Palaeoecology* 538.

Appendix D – Supplementary material for Chapter 5

D.1 Data results table for stable isotopes, *n*-alkanes and brGDGTs

Depth	Sample	Age (2σ)	Stable isotopes				*n*-Alkanes			GDGTs							brGDGT based mean annual temperature (MAAT °C)				brGDGT based soil pH	
																	Weijers et al. (2007) Eq. 3	Weijers et al. (2007) Eq. 6	Peterse et al. (2012) using MBT'	Tierney et al. (2010)	Weijers et al. (2007)	Peterse et al. (2012) using MBT'
cm		ka	$\delta^{15}N$	$\delta^{13}C$	TN (%)	TOC (%)	C/N(a)	ACL (C27-C33)	P_{aq}	C31αβ-hopane ng/g TOC	BIT	CPI	MBT	MBT'	CBT							
10	FG 11	0.96 ± 0.69	-2.47	-28.07	0.81	42.6	61.4	29.0	0.5	99.6	1.00	7.81	0.73	0.73	0.92		21.8	22.4	18.3	18.2	6.3	6.1
20	FG 12	1.51 ± 0.78	-2.35	-28.13	0.9	46.8	60.6	28.9	0.4	55.1	1.00	9.36	0.82	0.82	0.97		25.7	26.0	20.7	18.7	6.2	6.0
40	FG 13	7.25 ± 0.81	-1.64	-28.08	0.77	44.0	66.7	29.3	0.4	162.9	1.00	9.13	0.85	0.84	1.2		25.0	24.6	20.0	17.5	5.6	5.5
60	FG 14	9.38 ± 5.56	-1.48	-27.87	0.7	53.0	88.7	29.0	0.4	303.6	1.00	11.28	0.84	0.85	1.03		26.1	26.2	21.3	18.7	6.1	5.9
80	FG 15	12.16 ± 4.84	-1.39	-27.49	0.89	58.0	75.7	30.2	0.6	235.20	1.00	4.91	0.85	0.85	1.24		24.7	24.3	20.1	17.5	5.5	5.5
100	FG 16	15.24 ± 4.48	-1.13	-28.46	0.82	59.6	84.6	29.7	0.4	259.9	1.00	4.79	0.84	0.84	1.11		25.6	25.5	20.6	18.0	5.8	5.7
120	FG 17	16.84 ± 2.73	-2.03	-27.32	0.65	54.0	97.4	29.2	0.5	306.3	1.00	5.23	0.83	0.83	1.21		24.1	23.7	19.7	17.5	5.6	5.5
130	FG 18	19.05 ± 1.22	-1.48	-27.01	0.69	56.0	95.3	28.5	0.5	276.3	1.00	6.22	0.82	0.83	1.09		24.9	24.9	20.2	18.2	5.9	5.7
150	FG 19	38.27 ± 0.7	-1.49	-27.16	0.85	54.5	74.5	29.8	0.5	444.4	1.00	3.91	0.83	0.83	1.18		24.4	24.1	19.9	17.8	5.6	5.6
170	FG 20	44.18 ± 15.12	-0.44	-28.17	0.8	51.0	74.1	29.3	0.6	466.1	1.00	7.6	0.84	0.84	1.15		25.0	24.8	20.2	18.2	5.7	5.6
175	FG 21	55.11 ± 17.25	-0.44	-28.17	0.8	51.0	74.1	28.8	0.7	380.3	1.00	10.93	0.84	0.84	1.09		25.5	25.5	20.6	18.6	5.9	5.8
180	FG 22	65.72 ± 21.98	0.13	-28.7	0.64	56.5	102.8	27.9	0.7	412.5	1.00	17.4	0.86	0.86	0.92		28.1	28.5	22.3	20.0	6.3	6.1
185	FG 23	73.02 ± 21.3	0.13	-28.7	0.64	56.5	102.8	28.2	0.7	376.8	1.00	14.94	0.85	0.85	0.93		27.7	28.0	22.0	19.9	6.3	6.1
190	FG 24	84.01 ± 21.9	0.63	-28.33	0.73	57.1	91.5	28.1	0.8	499.6	1.00	19.24	0.85	0.86	0.96		27.7	28.0	21.9	19.6	6.2	6.0
200	FG 25	102.2 ± 20.47	0.76	-28.44	0.67	54.5	95.5	28.4	0.8	342.3	1.00	13.97	0.84	0.84	1		26.5	26.7	21.2	19.2	6.1	5.9
220	FG 26	110.71 ± 16.39	1.01	-28.86	0.57	46.9	95.2	27.8	0.8	354.1	1.00	15.38	0.82	0.82	1.05		25.0	25.1	20.3	19.0	6	5.8
230	FG 27	114.93 ± 17.72	0.09	-28.54	0.67	54.2	94.2	27.7	0.8	462.6	1.00	11.01	0.82	0.82	1.13		24.4	24.3	19.9	17.6	5.8	5.7
235	FG 28	119.92 ± 17.7	0.09	-28.54	0.67	54.2	94.2	27.9	0.8	367.8	1.00	9.85	0.83	0.83	1.14		25.0	24.8	20.2	18.2	5.8	5.7
240	FG 29	126.24 ± 17.99	-0.33	-28.53	0.64	54.8	100.3	27.9	0.7	462.3	1.00	14.34	0.84	0.84	1.16		24.8	24.6	20.2	18.9	5.7	5.6
250	FG 9	128.52 ± 18.57	-0.07	-28.92	0.64	54.2	98.6	28.6	0.8	377.8	1.00	8.46	0.84	0.84	1.04		25.9	25.8	20.9	19.0	6.0	5.8
253.2	FG 30	135.25 ± 18.78	-0.07	-28.92	0.64	54.2	98.6	27.8	0.7	219.8	1.00	23.07	0.81	0.81	0.97		25.5	26.0	20.5	19.2	6.2	6.0
263.4	FG 8	140.29 ± 18.95	0.1	-28.68	0.64	52.4	96.2	27.5	0.8	394.2	0.99	33.54	0.77	0.77	1.03		22.8	23.1	18.9	18.6	6.0	5.9
269.8	FG 4	142.78 ± 19.29	0.1	-28.68	0.64	52.4	96.2	27.9	0.7	231.2	1.00	18.62	0.78	0.78	1.1		22.6	22.7	18.8	18.2	5.9	5.7
273.8	FG 1	146.64 ± 19.93	0.15	-28.4	0.63	50.3	92.6	27.9	0.7	212.6	1.00	25.72	0.79	0.79	1.08		23.3	23.4	19.2	18.3	5.9	5.8
277.8	FG 10	181.4 ± 20.73	0.15	-28.4	0.63	50.3	92.6	27.9	0.7	374.3	1.00	17.37	0.81	0.81	1.06		24.3	24.4	19.8	18.6	6.0	5.8
356.6	FG 7	191.77 ± 24.53	0.77	-28.74	0.66	55.2	96.9	27.7	0.9	88.8	1.00	34.51	0.87	0.87	1.12		27.0	26.8	21.5	18.8	5.8	5.7
565	FG 6	199.57 ± 21.49	0.42	-29.06	0.88	57.6	76.4	28.1	0.7	204.3	1.00	26.99	0.82	0.82	1.28		23.0	22.5	19.0	17.3	5.4	5.4
719.8	FG 5	205.04 ± 23.6	-0.81	-28.78	0.67	54.6	94.8	29.4	0.4	252.8	1.00	11.39	0.82	0.82	1.25		23.1	22.7	19.1	17.9	5.5	5.4
822.5	FG 2	208.34 ± 26.37	-0.34	-28.52	0.85	54.7	75.1	29.8	0.5	289.2	1.00	5.8	0.85	0.86	1.06		26.7	26.7	21.3	19.0	6.0	5.8
880.8	FG 3	211 ± 28.7	-0.2	-28.52	0.76	55.9	85.8	30.9	0.2	293.6	1.00	20.9	0.81	0.81	1.07		24.2	24.3	19.8	18.8	5.9	5.8
Sediment – core location	FG 31	Modern	-2.47	-28.07	0.81	42.6	61.4	27.7	0.2	6.7	1.00	6.52	0.85	0.86	1.29		24.2	23.6	20.0	17.8	5.4	5.4
Sediment – wetland edge	FG 32	Modern						27.6	0.5	10.2	1.00	10.46	0.87	0.88	1.37		24.7	23.9	20.2	17.3	5.2	5.2
Catchment soil – near to wetland	FG 33	Modern						28.6	0.1	0.0	1.00	19.44	0.97	0.98	1.73		26.4	24.4	21.4	16.8	4.2	4.5
Catchment soil – distant from wetland	FG 34	Modern						28.5	0.2	0.0		29.34	1.00		1.38					19.4		

Table D1: Results of stable isotope and lipid biomarker analysis from Fern Gully Lagoon. Alkane average chain length (ACL) after Eglinton and Hamilton (1967) and aqueous proportion (P_{aq}) after Ficken et al. (2000), MBT–CBT proxy calculated values (methylation of branched tetraethers/cyclisation of branched tetraethers (Weijers et al., 2007; Peterse et al., 2012), GDGT based mean annual air temperature (MAAT) and soil pH (Weijers et al., 2007; Tierney et al., 2010; Peterse et al., 2012) and stable isotope data

D.2 Linear regression of raw bulk sediment $\delta^{13}C$ and corrected $\delta^{13}C$ based on atmospheric CO_2 concentration

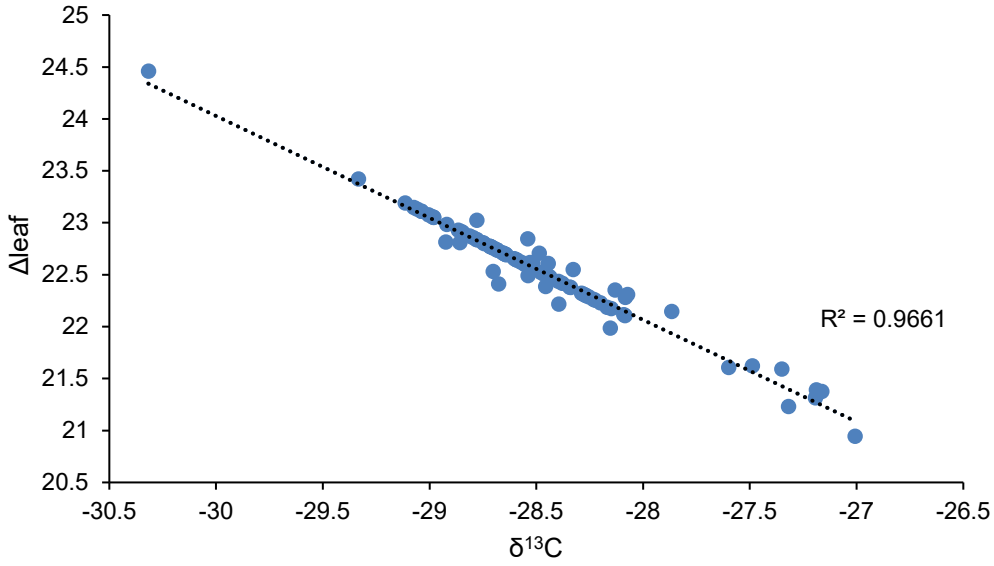

Figure D1: Linear regression of Fern Gully Lagoon raw bulk sediment $\delta^{13}C$ values and $\delta^{13}C$ corrected for changing atmospheric CO_2 concentration (Δleaf; Diefendorf and Freimuth, 2017).

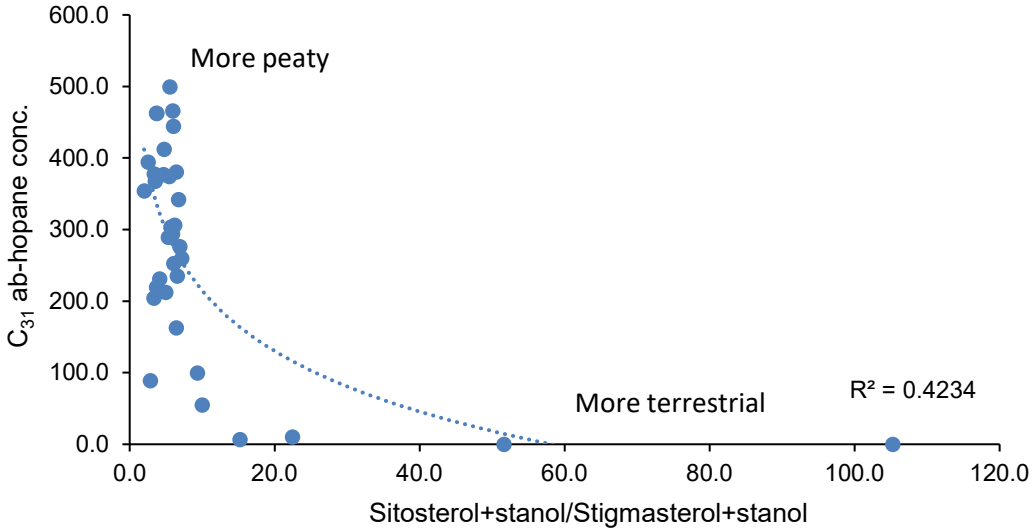

Figure D2: Relationship between $C_{31}17\alpha21\beta(H)$-homohopane and the terrestrial indicators Sitosterol and Stigmasterol, indicating more terrestrial OM with reduced wetland 'peatiness'.

D.3 References

Diefendorf, A.F., Freimuth, E.J., 2017. "Extracting the most from terrestrial plant-derived *n*-alkyl lipids and their carbon isotopes from the sedimentary record: A review." *Organic Geochemistry* 103, 1-21.

Eglinton, G., Hamilton, R.J., 1967. "Leaf Epicuticular Waxes." *Science* 156, 1322-1335.

Ficken, K.J., Li, B., Swain, D.L., Eglinton, G., 2000. "An *n*-alkane proxy for the sedimentary input of submerged/floating freshwater aquatic macrophytes." *Organic Geochemistry* 31, 745-749.

Peterse, F., van der Meer, J., Schouten, S., Weijers, J.W.H., Fierer, N., Jackson, R.B., Kim, J.-H., Sinninghe Damsté, J.S., 2012. "Revised calibration of the MBT–CBT paleotemperature proxy based on branched tetraether membrane lipids in surface soils." *Geochimica et Cosmochimica Acta* 96, 215-229.

Tierney, J.E., Russell, J.M., Eggermont, H., Hopmans, E.C., Verschuren, D., Sinninghe Damsté, J.S., 2010. "Environmental controls on branched tetraether lipid distributions in tropical East African lake sediments." *Geochimica et Cosmochimica Acta* 74, 4902-4918.

Weijers, J.W.H., Schouten, S., van den Donker, J.C., Hopmans, E.C., Sinninghe Damsté, J.S., 2007. "Environmental controls on bacterial tetraether membrane lipid distribution in soils." *Geochimica et Cosmochimica Acta* 71, 703-713.

Appendix E – Modifications to published works included in this thesis

This appendix provides a list of minor changes made to the publications included as chapters in this thesis (Chapters 2 and 3).

For both Chapters:

- Correction of the term 'south westerly winds' to the climate driver 'Southern Westerly Winds' as appropriate.
- Addition of 'summer' to 'Australian summer monsoon' where appropriate.
- Updates from 'in prep' citations to published citations where available.
- Minor changes to word choice for thesis consistency (e.g. change from 'isolated' to 'identified', and 'conditions' to 'climate' in some cases).
- Minor improvements in grammar and comma placement.
- Addition of several 'trimmed' references lost due to word count limits when submitting the manuscript.
- Modified bibliography style to match the Thesis style.
- Changes based on recommendations from Thesis reviewers, including grammar, figure consistency, and additional discussion of cool-climate taxa present on NSI during MIS 5, the organic material record and the EAC.

For Chapter 2:

- Addition of a new record (Ocean core MD03-2607) to the synthesis.

For Chapter 3:

- Addition of 'Chapter 2' alongside citations of the published paper Kemp et al. (2019).

Appendix F – Publications arising from this thesis

This appendix comprises two published journal articles arising from this thesis. These papers are identical in content to Chapters 2 and 3, aside from some minor changes for formatting and consistency, and the addition of a new record to the MIS 3 climate synthesis (Appendix E).

Quaternary Science Reviews 204 (2019) 94–104

Contents lists available at ScienceDirect

Quaternary Science Reviews

journal homepage: www.elsevier.com/locate/quascirev

Australian hydroclimate during Marine Isotope Stage 3: A synthesis and review

C.W. Kemp [a, *], J. Tibby [a], L.J. Arnold [b], C. Barr [a]

[a] Department of Geography, Environment and Population, and Sprigg Geobiology Centre, The University of Adelaide, Adelaide, Australia
[b] School of Physical Sciences, The Environment Institute, Sprigg Geobiology Centre and the Institute for Photonics and Advanced Sensing, The University of Adelaide, Adelaide, Australia

ARTICLE INFO

Article history:
Received 28 August 2018
Received in revised form
6 November 2018
Accepted 14 November 2018

Keywords:
Quaternary
Paleoclimatology
Australia
Data analysis
Australian monsoon
Water availability
South westerly winds

ABSTRACT

Improved reconstructions of Australia's climate during Marine Isotope Stage 3 (MIS 3) are important for understanding the environmental context of widespread human settlement of the continent and the extinction of a wide range of megafauna by 45 ± 5 thousand years ago (ka). To better understand spatial and temporal climate trends during this period, we present a synthesis of hydroclimate data from 40 Australian MIS 3 records. Hydroclimate records were evaluated and weighted by a scoring system developed to evaluate dating and proxy quality and resolution before inclusion into the synthesis. Our analysis reveals that Australia experienced spatially variable climates from ~57 to 49 ka before becoming predominantly wet from ~49 to 40 ka. After ~40 ka increasingly dry climates dominated MIS 3. Records from monsoon-influenced regions indicate a rapid drying from ~48 ka to the end of MIS 3, while there was a wetter period from ~50 to 40 ka in south westerly wind-influenced records. The implications of our findings are discussed in relation to other proxy records, with there being a significant relationship with regional fire history, but little correlation to atmospheric CO_2 concentration or global sea level.

1. Introduction

Marine Isotope Stage 3 (MIS 3: 57–29 thousand years ago (ka) (Lisiecki and Raymo, 2005)) represents an important period in Australian Quaternary history as it encompasses the widespread colonisation of the continent by humans and the extinction of an ecologically diverse range of megafauna (Bird et al., 2013; Allen and O'Connell, 2014; Hamm et al., 2016). Whether human impact, climate change or a combination of the two led to the extinction of Australian megafauna has been debated for over a century. Humans arrived on the continent by 59 ka (Clarkson et al., 2017) and widespread coastal and interior settlement appears to have taken place by 45 ka (Turney et al., 2001; Bowler et al., 2003; Hamm et al., 2016; Tobler et al., 2017).

The 50–40 ka period overlaps with broad ecological and environmental changes that have been attributed to human agency either directly, as a result of changed fire regimes, or indirectly, due to loss of megafauna and subsequent reduced grazing pressures (Rule et al., 2012; Miller et al., 2016). The peak loss of Australian megafauna species occurred at 45 ± 5 ka (Cosgrove et al., 2010; Saltré et al., 2016), with evidence for human-megafauna overlap ranging from ~4 ky (van der Kaars et al., 2017) to ~20 ky (Clarkson et al., 2017). While many authors have argued that megafaunal extinction occurred independently of climate change (Rule et al., 2012; Saltré et al., 2016; van der Kaars et al., 2017), there is evidence to suggest that large portions of the Australian continent experienced rapid climate change at 48 ± 2 ka (Cohen et al., 2015) and, furthermore, that human activities may not have changed fire regimes beyond the limits of natural variability during MIS 3 (Mooney et al., 2011; Bird et al., 2013).

The MIS 3 climate of Australia was also influenced by extensive southern hemisphere millennial-scale temperature variability (EPICA-Members, 2006; Jouzel et al., 2007). Ocean cores from south of Australia indicate millennial-scale sea surface temperature variation of around 2 °C during late MIS 3 (De Deckker et al., 2012). A compilation study of Australasian charcoal records has attributed millennial-scale variability in biomass burning to Dansgaard–Oeschger cycles (Mooney et al., 2011), while variability in biogenic silica and peat humification has been attributed to Heinrich events at Lynch's Crater in north-east Australia (Turney

* Corresponding author. Department of Geography, Environment and Population, The University of Adelaide, North Terrace, Adelaide, South Australia, 5005, Australia.
E-mail address: Christopher.kemp@adelaide.edu.au (C.W. Kemp).

https://doi.org/10.1016/j.quascirev.2018.11.016
0277-3791/

et al., 2004; Muller et al., 2008).

Several studies have concluded that there was a gradual aridification of Australia in the second half of MIS 3, albeit with differing hypotheses as to the cause (Chen et al., 1995; Kershaw et al., 2007a; Petherick et al., 2011). Fluvial activity in central Australia strongly reflects this pattern, with a decrease in discharge and lake filling events from ~48 ka onwards (Nanson et al., 2008; Cohen et al., 2011, 2015). Increased dune formation interpreted to be indicative of aridification is evident from ~35 ka in the southern half of Australia (Fitzsimmons et al., 2013). A record of continental dust deposition indicates an abrupt period of aridity, along with a change in the source of aeolian sediment at ~30 ka, suggesting a change in atmospheric circulation during the peak aridity phases (Petherick et al., 2008). As the climate dried in the lead up to the LGM, a marked change in vegetation was also noted in multiple eastern and southern Australian records (Petherick et al., 2013; Reeves et al., 2013). Elsewhere, increased fluvial activity has been reported in late MIS 3 from ~35 ka onwards in the Murray-Darling Basin, in the south east of the continent (Fig. 1), with 5–10 times higher discharge than today (Page et al., 1996; Kemp and Rhodes, 2010). However, instead of indicating increased rainfall, this increased flow may be due to decreased evaporation resulting in deeper winter snow pack and elevated spring runoff from alpine regions.

Large scale spatial and temporal Australian hydroclimate patterns are likely due to major changes in climate drivers affecting the Australian continent. These include the El Niño-Southern Oscillation (ENSO), the position of the Inter-Tropical Convergence Zone (ITCZ) and its effect on the Australian monsoon, and the southern westerly winds. ENSO variability affects rainfall across much of Australia (Risbey et al., 2009; Brown et al., 2016; Freund et al., 2017), while the Australian monsoon dominates the hydroclimate in central and northern Australia (Godfred-Spenning and Reason, 2002). The position of the southern westerly winds strongly influences hydroclimate in Tasmania, southern Victoria and South Australia (Fig. 1; Hendon et al., 2007; De Deckker et al., 2012).

To compare MIS 3 climate with Australian megafaunal extinction history, previous studies have relied on a high-resolution Antarctic temperature record (Johnson et al., 2016), and/or palaeoclimate model experiments (Saltré et al., 2016). To better understand the climatic context of megafaunal extinctions in MIS 3 requires improved spatial and temporal reconstructions of MIS 3 climate dynamics derived from palaeoenvironmental records. We have synthesised data from 40 Australian hydroclimate records that span MIS 3 and use a range of archives – including lake sediments, river systems, and offshore sediments – to evaluate spatial and temporal trends in hydroclimate.

2. Methods

For this MIS 3 synthesis study we have selected records from continental Australia and ocean cores within 100 km of the modern Australian coastline (to limit the influence of far-travelled pollen and dust). Forty Australian palaeoclimate MIS 3 records were located using Scopus (https://www.scopus.com/home.uri) and Web of Science (http://www.webofknowledge.com), and separated into regions (Fig. 1, Supplementary Table ST1).

Radiocarbon (^{14}C) ages were re-calibrated in OxCal 4.2.4 (Bronk Ramsey, 2009, 2016). Terrestrial records were recalibrated using SHCal13 (Hogg et al., 2013), while marine records were recalibrated using MARINE13 (Reimer et al., 2013). The re-calibrated radiocarbon ages are available in the supplementary material (Table ST2). The ^{14}C ages presented in this study refer to calibrated ka before present, where present is 1950 CE. For each record, a timeline of hydroclimate as inferred in the original studies was produced (Fig. 2).

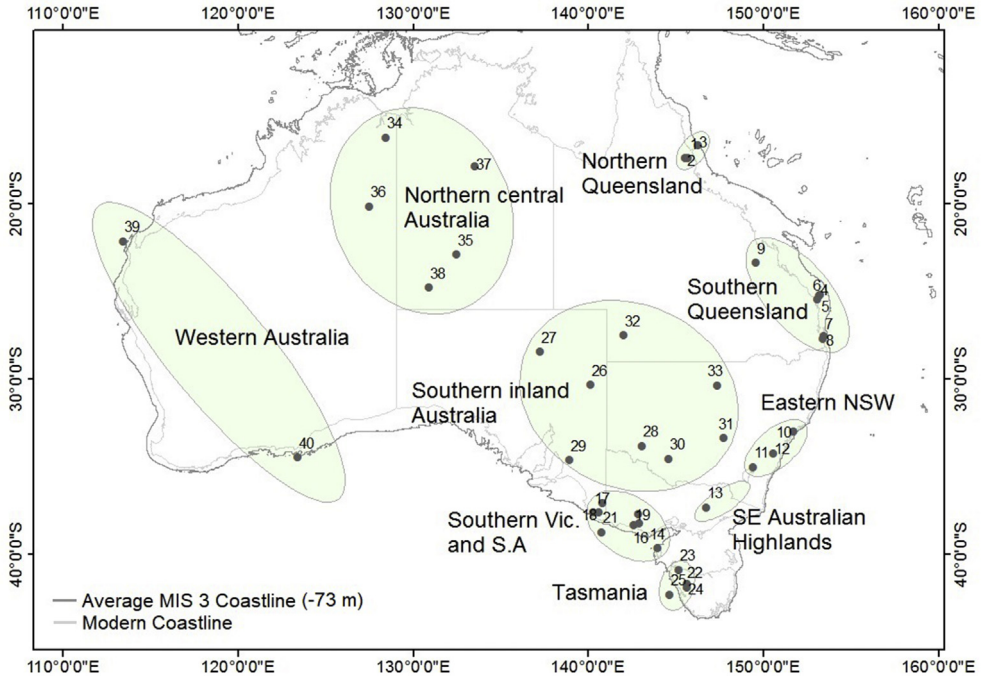

Fig. 1. Location of study regions in Australia (green shaded areas) and the location of sites within those regions (grey dots). Average MIS 3 coastline courtesy of Phillip Arnold (pers. comm.). Numbers refer to records in Fig. 2. (Ayliffe et al., 1998; Black et al., 2006; Bourman et al., 2010; Bowler et al., 1998; Burrows et al., 2016; Chen et al., 1990; Colhoun et al., 1999; Colhoun et al., 1982; Colhoun and van der Geer, 1986; Cook, 2009; Croke et al., 2011; D'Costa and Kershaw, 1995; D'Costa et al., 1993; Dodson, 1975; Dodson, 1977; Edney et al., 1990; Harle, 1997; Kershaw et al., 2007b; Longmore and Heijnis, 1999; Maroulis et al., 2007; Moss and Kershaw, 2007; Moss et al., 2013; Singh and Geissler, 1985; van De Geer et al., 1994; van der Kaars and De Deckker, 2002; Wende et al., 1997) (For interpretation of the references to colour in this figure legend, the reader is referred to the Web version of this article.)

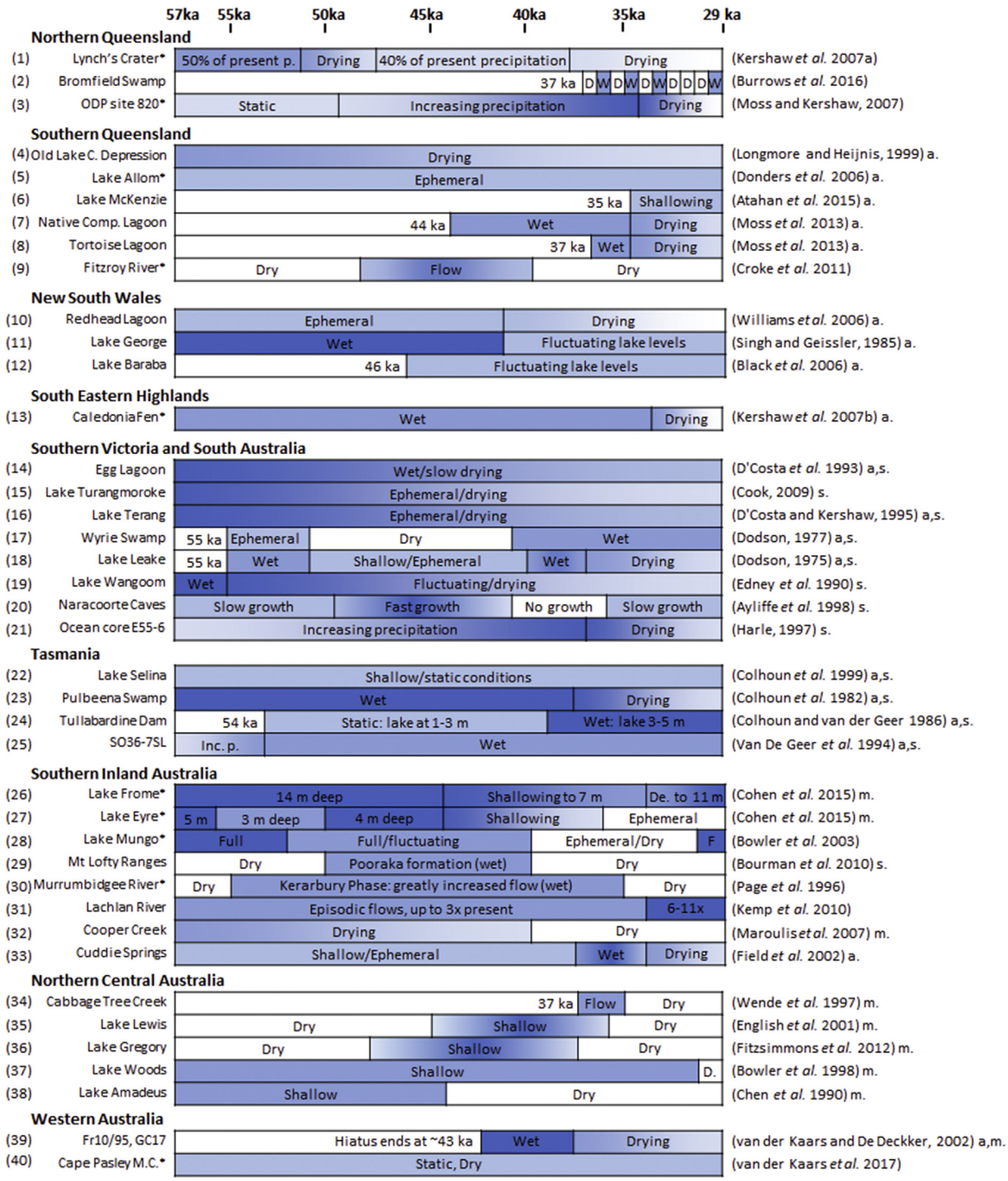

Fig. 2. MIS 3 hydroclimate at Australian sites. Numbers refer to locations shown in Fig. 1. Primary sources for each record are indicated on the right. Where records are incomplete for MIS 3, the basal age is shown. Lake levels are detailed where available, in metres. Ep.: ephemeral; De.: becoming deeper; F.: full; D.: dry; W.: wet; Sh.: shallow; Dr. drying. The ten highest scoring records are marked with an asterisk. m = records included in the monsoon-influenced subset, s = records included in the south westerly wind-influenced subset. a = records where radiocarbon ages have been recalibrated.

A rating scheme was developed to weight each study. Our scheme is conceptually similar to that developed to assess the quality of Australian Pleistocene fossil ages (Rodríguez-Rey et al., 2015), but uses a larger set of variables to assess the records. Specifically, the record quality rating scheme evaluates: (i) dating quality and resolution; (ii) proxy quality and resolution; (iii) record continuity through MIS 3; and; (iv) corroborative evidence from the same region (as defined in Fig. 1). The overall record quality rating method is outlined in Table 1, with the method for assessing dating quality – a component of the quality rating – further detailed in Table 2. While the weighting and score assignments used in this scheme may incorporate an element of subjectivity, our approach has the advantage of being able to discriminate between high and low reliability hydroclimate records in a semi-quantitative and

Table 1
Record quality scoring system for Australian MIS 3 studies. The final score for each record is calculated as follows: dating quality (0–1) + proxy quality (0–1) + record continuity (0–0.5) + validation (0–0.5) = final score (0–3). The detailed scoring for each record is provided in the supplementary table ST1.

Record quality score breakdown	Score
Dating quality	
1. *For the period 57 ka to 45 ka (early MIS 3)*. Scoring: 0.1 if an age estimate has been provided within this time period up to a maximum 0.2 (2 ages), 0.1 if an age has been provided for the 10 ky period prior to the beginning of MIS 3 (acting as a maximum age constraint), and 0.1 for a spread of more than 10 ky between the oldest and youngest ages (a measure of the temporal coverage of age control within early MIS 3).	0–0.4
2. *For the period 45 ka to 29 ka (late MIS 3)*. Scoring: as above, replacing the 0.1 score awarded for a maximum constraining age with an equivalent score for a minimum constraining age during the 10 ky period following the end of MIS 3.	0–0.4
3. Dating method (suitability of dating material and type of age control) used within the MIS 3 period. See Table 2. Value taken from the highest scoring dating method where more than one technique has been used.	0–0.2
Maximum subtotal:	**1**
Proxy quality	
4. Resolution of climate proxy/ies in MIS 3. Scoring: 0 = 1–5 samples; 0.1 = 6–15 samples; 0.2 = 16–30 samples, 0.3 = 31–60 samples; 0.4 = > 60 samples. The highest score is generally limited to very high-resolution proxies (e.g. micro-XRF core scans).	0–0.4
5. Number of proxies. Each additional proxy increases the score by 0.1 up to a maximum score of 0.3.	0–0.3
6. Responsiveness between proxy and hydroclimate. A fast responding proxy such as geochemical evidence of rainfall (e.g. speleothem geochemistry) or flood deposits score 0.3. Indirect or slower responding proxies such as pollen data score 0.2. Hydroclimate changes inferred from changes in charcoal score 0.1.	0–0.3
Maximum subtotal:	**1**
Record continuity	
7. Presence of a hiatus in MIS 3. A continuous record has a maximum score of 0.3. Each hiatus reduces this score by 0.1.	0–0.3
8. Hiatus above and/or below the MIS 3 record. Such occurrences introduce dating uncertainty to inferred MIS 3 ages. Each hiatus reduces the score by 0.1 from a maximum of 0.2.	0–0.2
Maximum subtotal:	**0.5**
Validation	
9. Comparable results are reported from another site in the same region (green shaded areas in Fig. 1) or from other proxies at the same site. Scoring: 0.1 for each additional published study from the same site detailing use of additional proxies, up to a maximum of 0.2. A score of 0.1 is assigned for each additional regional site finding discussed in relation to the new findings, up to a maximum of 0.3.	0–0.5
Maximum subtotal:	**0.5**

Table 2
Dating methods considered in this review and their quality scores. The latter are based on the suitability of dating material for MIS 3 records, and whether the dating technique provides a direct numerical age or age-equivalent constraint on the palaeoclimate sequence.

Dating method	Dating subtype	Type of age constraint	Sample source	Score
Radiocarbon Dating	AMS or conventional radiocarbon (^{14}C) dating	Numerical age	Bulk sediment	0.1
			Disseminated fine organics and/or the isolated charcoal fraction, carbonate samples.	0.15
			Complete or identified organics (e.g. plant macrofossils, seeds and pollen)	0.2
Luminescence Dating	Optically Stimulated Luminescence (OSL) or Thermoluminescence (TL) dating	Numerical age	Small sample size (<50 single grain equivalent dose (D_e) values or <20 multigrain aliquot D_e values per sample)	0.1
			Large sample size (≥50 single grain D_e values or ≥20 multigrain aliquot D_e values per sample)	0.2
Exposure dating	Cosmogenic ^{10}Be exposure dating	Numerical age	Selected boulder surface samples	0.2
Oxygen isotope stratigraphy	O^{16}/O^{18} isotope ratio of foraminifera	Relative age/age-equivalence	Shell calcite	0.1
			Pre-treated, etched shell calcite	0.15
Magnetics	Palaeomagnetic inclination	Relative age/age-equivalence	Bulk sediment	0.05
Uranium-Thorium	Uranium-thorium disequilibrium method	Numerical age	Bulk sediment carbonates	0.05
			Speleothems	0.2
Amino acid racemization	Amino acid dating	Relative age/age-equivalence	Bulk organics and egg shells	0.1

internally consistent manner. An example using Redhead Lagoon (Williams et al., 2006) is available in the supplementary materials.

2.1. Hydroclimate classification scheme

There are 30 Australian records spanning MIS 3, with an additional 10 records covering only the latter parts of the period (Fig. 2 and Supplementary Table ST1). To enable further analyses of continental hydroclimate, we have used a method similar to Harrison and Digerfeldt (1993) and Herzschuh (2006), and classified indicators of dry or wet climate into four classes before weighting by the record score, as follows:

1. We assigned hydroclimate classes to each record in 1000-year time slices. Each time slice was classed as follows; 1 = dry climate; 2 = moderately dry; 3 = moderately wet and 4 = wet climate. Dryland Australian lakes and river systems were scored on a binary scale, with 1 representing the absence of water and 4 representing the presence of water.
2. To generate an average hydroclimate record for each 1000-year time slice, the hydroclimate class for each record was first weighted by its record score. The collection of these weighted classes for each time slice was then averaged to determine the mean continental-scale hydroclimate (Equation 1). In this way, higher quality records have greater weight in the final synthesis.

Equation 1: Average weighted mean equation for the water availability for each record at each time slice. The equation weights each record's hydroclimate class by its record score before inclusion in the synthesis.

$$water\ availiability_{time\ slice} = \frac{\sum_{record=1}^{n}(record\ score_{record} \times hydroclimate\ class_{time\ slice,\ record})}{\sum_{record=1}^{n} record\ score_{record}}$$

To illustrate spatial hydroclimate variability, the classes for all records were used to create 'surface' maps of Australia at 5000-year time steps (based on the modal hydroclimate class for each record). The mapping was undertaken using the Inverse Distance Weighted (IDW) interpolation tool in ArcMap 10 (Dangermond, 2015) which was chosen because the method reduces to the overall mean value at a distance from known values (Shepard, 1968), reducing possible error due to interpolation artefacts. The IDW power was set to four, providing a drop-off in record weighting at a short distance and reducing the influence of individual records that may record localised hydroclimate trends.

To investigate the influence of large-scale climate drivers on Australian hydroclimate, records were synthesised from two subsets of the 40-record database: records influenced by monsoonal variation (9 records) or variation in the south westerly winds (SWW; 13 records). Defining a subset to determine MIS 3 ENSO variability was not undertaken due to a lack of unambiguously ENSO-dominated records. However, the effect of ENSO on Australia's hydroclimate during MIS 3 is detailed in the discussion. Inclusion of records in the SWW or monsoon-influenced subsets was determined by a combination of published Quaternary (e.g. monsoon records from central Australian lakes (Magee et al., 2004; Fitzsimmons et al., 2012)) and modern relationships between rainfall and remote climates drivers (Hendon et al., 2007; Fletcher and Moreno, 2011). To assess the influence of low scoring sites on the Australian average, a hydroclimate record was created using only the ten highest quality records.

Finally, to provide comparison with contemporary climate, an average climate state was derived from studies that reported the modern hydrological state. These were assigned a score between 1 and 4, as described above. Where no modern condition was described, or where landscape clearing and/or grazing has altered the study site, the record was excluded from this analysis.

3. Results

3.1. Continental trends in hydroclimate

The average weighted hydroclimate conditions of all 40 records and subsets is illustrated in Fig. 3. Mean continental hydroclimates were wetter than modern climates between 57 and 40 ka, with wettest conditions between ~49 and 40 ka. After ~40 ka, the climate became drier, accelerating to the end of MIS 3, reaching an average water availability ~30% lower than modern climate. Most sites recorded their driest conditions at the end of MIS 3 (Fig. 2). The ten high-quality records largely follow the Australian trend (Fig. 3), increasing confidence in the 40 record synthesis. The high-quality records indicate a slightly earlier commencement of drying at ~44 ka, at an increased rate compared to the continental average, indicating rapid drying between ~41 and 39 ka. After ~39 ka, the high-quality records show continuing drying at a similar rate to the full Australian record until the end of MIS 3.

There are notable differences between the MIS3 hydroclimate records in the south westerly wind and Australian monsoon-influenced regions (Fig. 3). The SWW-influenced records are comparatively wetter than the monsoon-influenced records for all of MIS 3. Records influenced by the SWW also appear to remain wet longer, with the onset of drying in mid-MIS 3 delayed until ~39 ka. The monsoon records indicate strong hydroclimate change at ~48 ka, after which there is a gradual drying to the end of MIS 3.

3.2. Spatial hydroclimate trends

To provide a basis for understanding the veracity of climate inferences based on spatial trends during MIS 3, the location of palaeoclimate records and quality of those records is shown in Fig. 4. The highest record density is in (present day) temperate south-eastern Australia, while the high scoring records are widespread – their distribution does not overlap with any single major climate driver. The distance between records in inland Australia – especially inland Western Australia – is likely to result in less accurate hydroclimate inferences for those regions.

Fig. 5 illustrates MIS 3 hydroclimate in six time periods. Between 57 ka and ~50 ka, central Australia was predominantly wet, though dry conditions were evident in the north-west. There were spatially variable climates in the eastern third of the continent. Between ~50 and 45 ka there is a trend towards a drier north-eastern Australia and generally moist climates in the southern-central and south-east parts of the continent. In the 45–40 ka period, central Australia became more arid while mildly wet conditions remained in much of the southeast of the continent. Widespread aridification of most of the continent is evident between ~40 ka and 29 ka, with peak MIS 3 aridity evident between ~35 and 29 ka. Notable exceptions to the arid late-MIS 3 climates are evident in scattered records in the south-east of the continent and Tasmania, which remained wet.

4. Discussion

4.1. Temporal patterns in the Australian MIS 3 hydroclimate record

Several observations can be made about Australian climate during MIS 3 from comparison of the hydroclimate trends in Fig. 3. In the first half of MIS 3 the climate was wetter than present climate

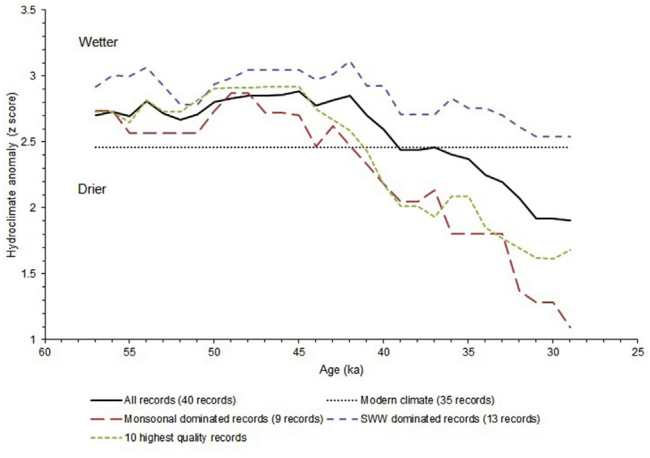

Fig. 3. Australian MIS 3 hydroclimate anomaly at 1000-year intervals.

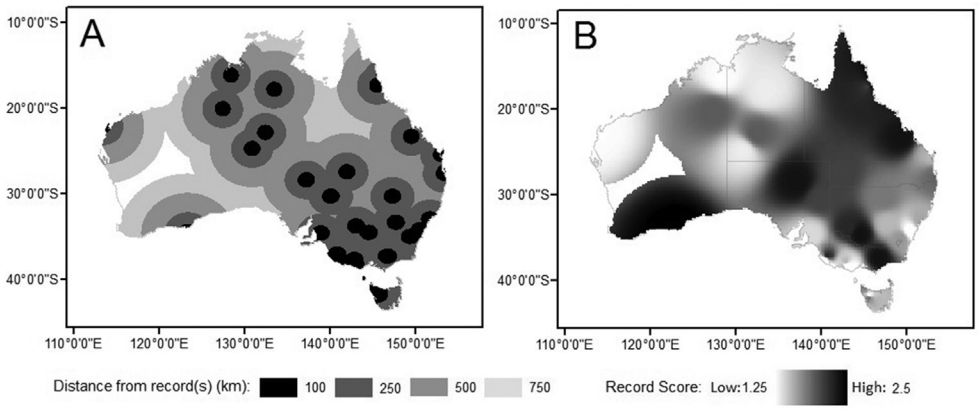

Fig. 4. A: Record density during MIS 3. B: Interpolated surface of the record quality scores, with darker shading indicating areas where greater confidence can be attributed to results.

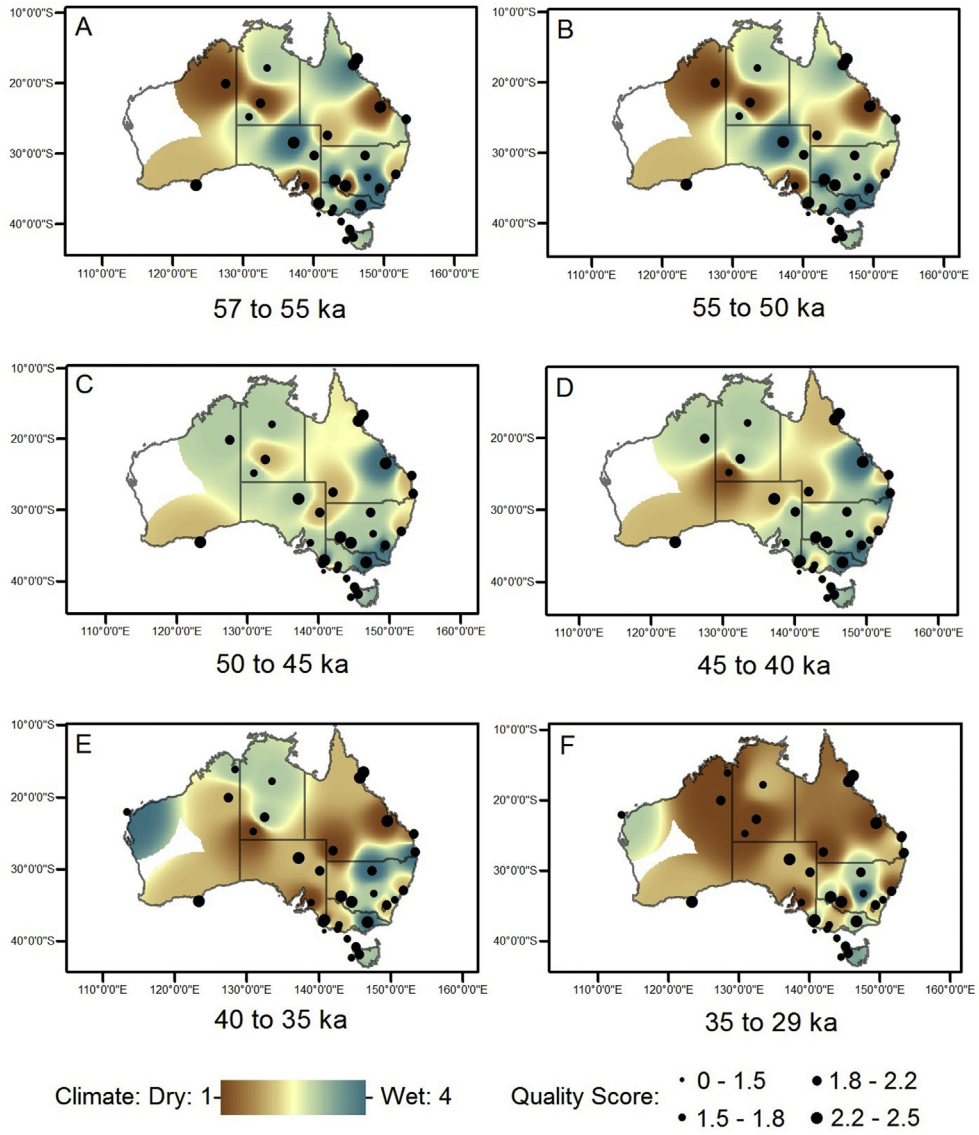

Fig. 5. Continental-scale hydroclimate through MIS 3, showing quality score for each record. Records are only included when they have hydroclimate data pertaining to the period illustrated. The interpolated surface is limited to 750 km from the active records in each period.

– as indicated by the highest-scoring records (n = 10) and the continental average (n = 40). After drying began at ~45 ka, the high-quality records indicate faster drying and remain drier on average to the end of MIS 3. In this context, it may be that small amounts of contamination by younger material in the lower quality records have resulted in these changes being inferred to occur later than in reality. Due to the lack of resolution in the source records, it was not possible to extract millennial scale variability with any accuracy. As such, assessment of the effect of Heinrich events or Antarctic isotope maxima, for example, was not possible.

4.2. Drivers of spatial and temporal hydroclimate anomalies

ENSO is a major driver of the modern hydroclimate for much of Australia, with the north-east of the continent most strongly influenced by ENSO state and variability (Risbey et al., 2009). Fossil clam shell $\delta^{18}O$ isotope records from Papua New Guinea indicate similar ENSO variability to the twentieth century at ~60 and ~40 ka (Driscoll et al., 2014), and a reduction in variability between 40 and 34 ka, in agreement with fossil corals from the same location (Tudhope et al., 2001). Recent ENSO modelling supports reduced ENSO variability in late MIS 3 from ~35 ka (Merkel et al., 2010), similar to previous models of ENSO 'strength' (Clement et al., 2001). The drying observed in Australian hydroclimate at ~40 ka (Fig. 3) may have been in part driven by the initial effect of less variable ENSO.

While clam shell $\delta^{18}O$ records indicate fewer El Niño events during MIS 3 compared to the Holocene (12 vs. 18 per century) (Driscoll et al., 2014), peat decomposition (humification) in north eastern Australia indicates a period of more frequent El Niño events centred on ~40 ka (Turney et al., 2004). The observed period of rapid drying indicated by the mean hydroclimate ~40 ka (Fig. 3) and multiple individual records (Fig. 5d and e) is likely associated with more frequent El Niño events. However, the MIS 3 hydroclimate record does not reflect a return to wetter climates associated with lower frequency of El Niño events after ~40 ka (Fig. 5e and f). There is evidence that the influence of the ITCZ and the Australian monsoon on continental hydroclimate may have been stronger during late MIS 3 than the present (Magee et al., 2004; Leduc et al., 2009), perhaps masking or modulating the effects of ENSO during this time (An et al., 2017).

Monsoonal hydroclimate in Australia is largely controlled by the seasonal southward shift of the ITCZ, which deepens the monsoonal trough (Godfred-Spenning and Reason, 2002). On longer time scales, the position of the ITCZ migrates as a result of hemispheric temperature contrast (Chiang and Friedman, 2012). A more southerly ITCZ during the southern hemisphere summer insolation peak ~47 ka (English et al., 2001; Magee et al., 2004) would lead to a stronger Australian monsoon and wetter climates in monsoon-affected regions. The fluvial archives of central and northern Australia are sensitive to Australian monsoonal hydroclimate as they drain a large proportion of northern Australia (Magee et al., 2004; Fitzsimmons et al., 2012, 2013). The wet climates evident in central and northern regions between ~50 and ~45 ka (Fig. 5c) are consistent with an intensified Australian monsoon during the insolation peak. Similarly, drying after ~48 ka (Fig. 6f) correlates with decreasing mid-latitude summer southern hemisphere insolation (Fig. 6a). This drying trend reflects the aridification of central Australia (Cohen et al., 2015) as well as the monsoon record inferred from Indonesian speleothems (Carolin et al., 2013). However, instead of a rapid decline in water availability after ~48 ka, the monsoon record indicates a more gradual, but continuous, drying of central and northern Australia.

The south westerly winds (SWW) are significantly correlated with precipitation in southern temperate Australia (Hendon et al., 2007; Fletcher and Moreno, 2011). While continental drying was occurring in late MIS 3, comparatively wetter climates persisted in records influenced by SWW variability in southern Australia and Tasmania (Fig. 5f). This pattern is consistent with observations during the LGM, at which time the SWW were found to either have strengthened or moved further north (Fletcher and Thomas, 2010; Kohfeld et al., 2013). Early movement or increasing SWW strength in late MIS 3 is additionally supported by dust records from North Stradbroke Island, the central tablelands of New South Wales and the southern Pacific Ocean, all of which show increased dust transport prior to the end of MIS 3 (Hesse et al., 2003; Petherick et al., 2008; Lamy et al., 2014).

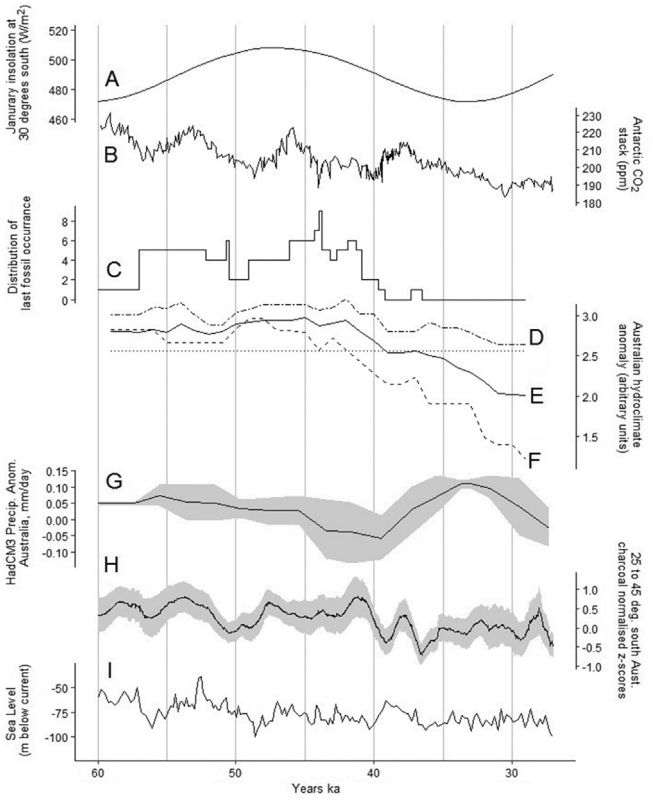

Fig. 6. A. MIS 3 January insolation at 30°S (Berger and Loutre, 1991); B. Antarctic CO_2 record stack (Köhler et al., 2017); C. the age of last megafaunal fossil occurrences (Saltré et al., 2016); D. hydroclimate record for south westerly wind influenced regions (this synthesis); E. Australian hydroclimate average (this synthesis); and F. hydroclimate record for monsoon-influenced regions (this synthesis); G. HadCM3 modelled rainfall anomaly for Australia with ±1 sigma s.d. (grey envelope) (Saltré et al., 2016); H. Australia and New Zealand sub-tropical high pressure belt (25° to 45° south) biomass burning reconstruction (Z scores of transformed charcoal influx) with ±95% bootstrap interval (grey envelope) (Mooney et al., 2011) and, I. Global sea level (Rohling et al., 2008).

4.3. The effects of changing MIS 3 climate

The human occupation of Australia, which is recorded at many sites in the southern arid interior between ~49 and ~44 ka (Bowler et al., 2003; Allen and O'Connell, 2014; Hamm et al., 2016; Clarkson et al., 2017; Tobler et al., 2017), occurred during comparatively wetter climates (Fig. 5c). Bass Strait was a barrier for human migration into Tasmania until ~43 ka, when receding sea levels created a land bridge (Lambert et al., 2008). The peak loss of megafauna occurred at 45 ± 5 ka (Fig. 6c) (Cosgrove et al., 2010; Saltré et al., 2016), during a period where the proxy data suggest generally widespread high effective moisture (Fig. 6e), albeit with

drying conditions in the monsoon-sensitive region (Fig. 6f).

Our synthesis indicates gradual continental drying from ~48 ka, which would likely have affected megafauna populations to a smaller degree than the rapid climate change indicated by the central Australian lake systems (Cohen et al., 2015). An absence of dramatic climate change corresponding to megafauna extinction has been suggested previously using modelled mean continental precipitation (Saltré et al., 2016). While our data largely support this overall conclusion, there is in fact little relationship between our mean continental hydroclimate record and modelled precipitation (Fig. 6e and g). The model predicts a gradually more arid MIS 3 from 57 ka, reaching its driest state at ~40 ka, before rainfall increases to a peak at ~34 ka. The model then infers a rapid decrease in rainfall until the end of MIS 3. Notably, the only major peak in rainfall in the model is ~10 ky later than observed in our synthesis, and much closer to the end of MIS 3.

A recent charcoal compilation for Australia and New Zealand from 25° to 45° degrees south (Mooney et al., 2011) – an area containing >70% of the records in our synthesis (Fig. 6h) – was compared to our hydroclimate synthesis. A linear regression indicated that ~33% of the variance in the charcoal record is associated with Australian hydroclimate from records south of 25° (30 records) ($r^2 = 0.33$, $p < 0.005$). The relationship suggests that decreasing charcoal influx is associated with increasing aridity over the period, potentially reflecting reduced fuel availability in response to reduced effective moisture. A possible complication is that the charcoal record synthesis contains fewer MIS 3 records than our synthesis (all 13 of the Australian MIS 3 charcoal records are included in the synthesis) and includes records from New Zealand (Mooney et al., 2011).

Increased continentality has been argued to contribute to dry Australian glacial climates, even in near-coastal records (Dodson, 1994). This affect has been observed during MIS 4 and is argued to have had a large impact on LGM water avaliability in coastal records (e.g. Donders et al., 2006; McGowan et al., 2008; Veth et al., 2017) compared to the Holocene and MIS 5. To assess the potential influence of continentality on hydroclimates of MIS 3, we performed a regression of global sea level (Rohling et al., 2008) and mean hydroclimate in the 12 records within 30 km of the coast. There was a very low r^2 of 0.05 ($p \approx 0.27$) suggesting it is unlikely that continentality during MIS 3 had a notable affect on hydroclimate.

4.4. Future research

The most fundamental problem in reconstructing Australian MIS 3 climate is the lack of data. While a number of published studies are available, they are restricted in two important ways: spatially, mirroring the location of wetland sediments that occur in a very small percentage of Australia's land mass; and temporally, in that there are few sedimentary records beyond 40 ka (Tibby et al., 2017). The limited number of MIS 3 studies have either low resolution (an average of approximately one sample every 1000 years, see supplementary material), and/or they have imprecise chronologies, with an average of only four constraining ages during MIS 3.

The problems of dating and proxy resolution could be partially addressed by resampling existing Australian palaeoclimate sites using improved dating methods with a focus on MIS 3. Re-analysis of older published records may also result in more detailed records due to new analytical and dating techniques. Additionally, increased focus on new sites, such as potential speleothem records in Nullarbor Plain cave systems (Lipar and Ferk, 2015; Heath et al., 2018), would help address spatial gaps (Fig. 4a).

Recent advances in dating of palaeoclimate archives have the potential to improve the Australian MIS 3 climate record. Refined optically stimulated luminescence (OSL) dating has significantly improved the reliability of dating beyond the radiocarbon boundary. Key recent OSL methodological improvements include the advent of single-grain techniques (e.g. Arnold et al., 2012; Arnold et al., 2014), improved statistical analyses of equivalent dose (D_e) datasets (Galbraith and Roberts, 2012), the advent of the single-aliquot regenerative protocol (Murray and Wintle, 2000) and the development of extended-range luminescence techniques (e.g. Arnold et al., 2015; Arnold et al., 2016). Age determination has also been improved by the introduction of Bayesian age modelling (e.g. Bronk Ramsey, 2009; Blaauw et al., 2018). Furthermore, techniques such as Monte Carlo Empirical Orthogonal Function analysis (Anchukaitis and Tierney, 2013; Tyler et al., 2015) allow the extraction of shared variance between sites while considering the age uncertainties.

Relatively new methods such as μXRF and hyperspectral core scanning allow for very high-resolution palaeoclimate inferences from sedimentary archives (e.g. Hahn et al., 2014; Sun et al., 2016). The introduction of new methods, which can determine past temperature from glycerol dialkyl glycerol tetraethers (GDGTs) (e.g. Tierney et al., 2008; Woltering et al., 2014; Atahan et al., 2015), chironomids (e.g. Larocque-Tobler et al., 2011; Eggermont and Heiri, 2012; Chang et al., 2015) and clumped isotopes (e.g. Affek et al., 2008; Zaarur et al., 2011; Saenger et al., 2012), and inferences of past precipitation from compound specific carbon or hydrogen isotopes from leaf waxes (e.g. Tierney et al., 2008; Feakins et al., 2014; Feakins et al., 2016), would greatly aid in the inference of Australia MIS 3 climate.

5. Conclusions

Analysis of Australian MIS 3 climate records reveals distinct hydroclimate trends. MIS 3 began relatively wet, compared to modern climates, with peak moisture availability occurring between ~49 and ~40 ka. Thereafter, continental aridity increased for the remainder of MIS 3. South westerly wind-influenced records indicate high water availability throughout MIS 3, while the monsoon-influenced records indicate a gradual drying from ~48 ka, until the end of MIS 3. Predominantly wet conditions are evident in central and northern Australia between ~50 and ~45 ka, possibly reflecting the influence of both a predominantly La Niña-like climate and a stronger Australian monsoon. These wet conditions may have aided migration of people across the continent. Lastly, the peak loss of megafauna at 45 ± 5 ka occurred at a time of generally high water availability before a transition into the comparatively dry second half of MIS 3.

Acknowledgements

This project was supported by Australian Research Council Discovery Project DP150103875 and Future Fellowship Project FT130100195. We thank Scott Mooney for providing the charcoal record, Frédérik Saltré for the modelled rainfall data as well as Antje Voelker and an anonymous reviewer for their invaluable comments on the manuscript.

Appendix A. Supplementary data

Supplementary data to this article can be found online at https://doi.org/10.1016/j.quascirev.2018.11.016.

References

Affek, H.P., Bar-Matthews, M., Ayalon, A., Matthews, A., Eiler, J.M., 2008. Glacial/

interglacial temperature variations in Soreq cave speleothems as recorded by 'clumped isotope' thermometry. Geochem. Cosmochim. Acta 72, 5351–5360.
Allen, J., O'Connell, J.F., 2014. Both half right: updating the evidence for dating first human arrivals in Sahul. Aust. Archaeol. 79, 86–108.
An, S.-I., Kim, H.-J., Park, W., Schneider, B., 2017. Impact of ENSO on East Asian winter monsoon during interglacial periods: effect of orbital forcing. Clim. Dynam. 49, 3209–3219.
Anchukaitis, K.J., Tierney, J.E., 2013. Identifying coherent spatiotemporal modes in time-uncertain proxy paleoclimate records. Clim. Dynam. 41, 1291–1306.
Arnold, L.J., Demuro, M., Navazo, M., Benito-Calvo, A., Pérez-González, A., 2012. OSL dating of the middle palaeolithic Hotel California site, Sierra de Atapuerca, north-central Spain. Boreas 42, 285–305.
Arnold, L.J., Demuro, M., Parés, J.M., Arsuaga, J.L., Aranburu, A., de Castro, B., María, J., Carbonell, E., 2014. Luminescence dating and palaeomagnetic age constraint on hominins from Sima de los Huesos, Atapuerca, Spain. J. Hum. Evol. 67, 85–107.
Arnold, L.J., Demuro, M., Parés, J.M., Pérez-González, A., Arsuaga, J.L., Bermúdez de Castro, J.M., Carbonell, E., 2015. Evaluating the suitability of extended-range luminescence dating techniques over early and Middle Pleistocene time-scales: published datasets and case studies from Atapuerca, Spain. Quat. Int. 389, 167–190.
Arnold, L.J., Duval, M., Demuro, M., Spooner, N.A., Santonja, M., Pérez-González, A., 2016. OSL dating of individual quartz 'supergrains' from the Ancient Middle Palaeolithic site of Cuesta de la Bajada, Spain. Quat. Geochronol. 36, 78–101.
Atahan, P., Heijnis, H., Dodson, J., Grice, K., Le Metayer, P., Taffs, K., Hembrow, S., Woltering, M., Zawadzki, A., 2015. Pollen, biomarker and stable isotope evidence of late Quaternary environmental change at Lake McKenzie, southeast Queensland. J. Paleoliminol. 53, 139–156.
Ayliffe, L.K., Marianelli, P.C., Moriarty, K.C., Wells, R.T., McCulloch, M.T., Mortimer, G.E., Hellstrom, J.C., 1998. 500 ka precipitation record from south-eastern Australia: evidence for interglacial relative aridity. Geology 26, 147–150.
Berger, A., Loutre, M.F., 1991. Insolation values for the climate of the last 10 million years. Quat. Sci. Rev. 10, 297–317.
Bird, M.I., Hutley, L.B., Lawes, M.J., Lloyd, J.O.N., Luly, J.G., Ridd, P.V., Roberts, R.G., Ulm, S., Wurster, C.M., 2013. Humans, megafauna and environmental change in tropical Australia. J. Quat. Sci. 28, 439–452.
Blaauw, M., Christen, J.A., Bennett, K.D., Reimer, P.J., 2018. Double the dates and go for Bayes — impacts of model choice, dating density and quality on chronologies. Quat. Sci. Rev. 188, 58–66.
Black, M.P., Mooney, S.D., Martin, H.A., 2006. A >43,000-year vegetation and fire history from Lake Baraba, New South Wales, Australia. Quat. Sci. Rev. 25, 3003–3016.
Bourman, R.P., Prescott, J.R., Banerjee, D., Alley, N.F., Buckman, S., 2010. Age and origin of alluvial sediments within and flanking the Mt Lofty Ranges, southern South Australia: a Late Quaternary archive of climate and environmental change. Aust. J. Earth Sci. 57, 175–192.
Bowler, J.M., Duller, G.A.T., Perret, N., Prescott, J.R., Wyrwoll, K.-H., 1998. Hydrologic changes in monsoonal climates of the last glacial cycle: stratigraphy and luminescence dating of Lake Woods, N.T. Australia. Paleoclimates 3, 179–207.
Bowler, J.M., Johnston, H., Olley, J.M., Prescott, J.R., Roberts, R.G., Shawcross, W., Spooner, N.A., 2003. New ages for human occupation and climatic change at Lake Mungo, Australia. Nature 421, 837.
Bronk Ramsey, C., 2009. Bayesian analysis of radiocarbon dates. Radiocarbon 51, 337–360.
Bronk Ramsey, C., 2016. Dealing with outliers and offsets in radiocarbon dating. Radiocarbon 51, 1023–1045.
Brown, J.R., Hope, P., Gergis, J., Henley, B.J., 2016. ENSO teleconnections with Australian rainfall in coupled model simulations of the last millennium. Clim. Dynam. 47, 79–93.
Burrows, M.A., Heijnis, H., Gadd, P., Haberle, S.G., 2016. A new late Quaternary palaeohydrological record from the humid tropics of northeastern Australia. Palaeogeogr. Palaeoclimatol. Palaeoecol. 451, 164–182.
Carolin, S.A., Cobb, K.M., Adkins, J.F., Clark, B., Conroy, J.L., Lejau, S., Malang, J., Tuen, A.A., 2013. Varied response of western Pacific hydrology to climate forcings over the last glacial period. Science 340, 1564.
Chang, J.C., Shulmeister, J., Woodward, C., 2015. A chironomid based transfer function for reconstructing summer temperatures in southeastern Australia. Palaeogeogr. Palaeoclimatol. Palaeoecol. 423, 109–121.
Chen, X.Y., Chappell, J., Murray, A.S., 1995. High (ground) water levels and dune development in central Australia: TL dates from gypsum and quartz dunes around Lake Lewis (Napperby), Northern Territory. Geomorphology 11, 311–322.
Chen, X.Y., Prescott, J.R., Hutton, J.T., 1990. Thermoluminescence dating on gypseous dunes of Lake Amadeus, central Australia. Aust. J. Earth Sci. 37, 93–102.
Chiang, J.C.H., Friedman, A.R., 2012. Extratropical cooling, interhemispheric thermal gradients, and tropical climate change. Annu. Rev. Earth Planet Sci. 40, 383–412.
Clarkson, C., Jacobs, Z., Marwick, B., Fullagar, R., Wallis, L., Smith, M., Roberts, R.G., Hayes, E., Lowe, K., Carah, X., Florin, S.A., Mcneil, J., Cox, D., Arnold, L.J., Hua, Q., Huntley, J., Brand, H.E.A., Manne, T., Fairbairn, A., Shulmeister, J., Lyle, L., Salinas, M., Page, M., Connell, K., Park, G., Norman, K., Murphy, T., Pardoe, C., 2017. Human occupation of northern Australia by 65,000 years ago. Nature 547, 306.
Clement, A.C., Cane, M.A., Seager, R., 2001. An orbitally driven tropical source for abrupt climate change. J. Clim. 14, 2369.
Cohen, T.J., Jansen, J.D., Gliganic, L.A., Larsen, J.R., Nanson, G.C., May, J.-H., Jones, B.G., Price, D.M., 2015. Hydrological transformation coincided with megafaunal extinction in central Australia. Geology 43, 195–199.
Cohen, T.J., Nanson, G.C., Jansen, J.D., Jones, B.G., Jacobs, Z., Treble, P., Price, D.M., May, J.-H., Smith, A.M., Ayliffe, L.K., Hellstrom, J.C., 2011. Continental aridification and the vanishing of Australia's megalakes. Geology 39, 167–170.
Colhoun, E.A., Pola, J.S., Barton, C.E., Heijnis, H., 1999. Late pleistocene vegetation and climate history of Lake Selina, western Tasmania. Quat. Int. 57–58, 5–23.
Colhoun, E.A., van de Geer, G., Mook, W.G., 1982. Stratigraphy, pollen analysis, and palaeoclimatic interpretation of Pulbeena Swamp, northwestern Tasmania. Quat. Res. 18, 108–126.
Colhoun, E.A., van der Geer, G., 1986. Holocene to middle last glaciation vegetation history at Tullabardine Dam, western Tasmania. Proc. Roy. Soc. Lond. B Biol. Sci. 229, 177–207.
Cook, E.J., 2009. A record of late Quaternary environments at lunette-lakes Bolac and Turangmoroke, Western Victoria, Australia, based on pollen and a range of non-pollen palynomorphs. Rev. Palaeobot. Palynol. 153, 185–224.
Cosgrove, R., Field, J., Garvey, J., Brenner-Coltrain, J., Goede, A., Charles, B., Wroe, S., Pike-Tay, A., Grün, R., Aubert, M., Lees, W., O'Connell, J., 2010. Overdone overkill – the archaeological perspective on Tasmanian megafaunal extinctions. J. Archaeol. Sci. 37, 2486–2503.
Croke, J., Jansen, J.D., Amos, K., Pietsch, T.J., 2011. A 100 ka record of fluvial activity in the Fitzroy River Basin, tropical northeastern Australia. Quat. Sci. Rev. 30, 1681–1695.
D'Costa, D.M., Kershaw, A.P., 1995. A late pleistocene and holocene pollen record from Lake Terang, Western Plains of Victoria, Australia. Palaeogeogr. Palaeoclimatol. Palaeoecol. 113, 57–67.
D'Costa, D.M., Grindrod, J., Ogden, R., 1993. Preliminary environmental reconstructions from late Quaternary pollen and mollusc assemblages at Egg Lagoon, King Island, Bass Strait. Aust. J. Ecol. 18, 351–366.
Dangermond, J., 2015. ArcMap. Esri, 380 New York Street, Redlands, CA 92373.
De Deckker, P., Moros, M., Perner, K., Jansen, E., 2012. Influence of the tropics and southern westerlies on glacial interhemispheric asymmetry. Nature Geosci. Lett. 5, 266–269.
Dodson, J.R., 1975. Vegetation history and water fluctuations at Lake Leake, south-eastern South Australia 50,000 B.P. to 10,000 B.P. Aust. J. Bot. 23, 815–831.
Dodson, J.R., 1977. Late Quaternary palaeoecology of Wyrie Swamp, southeastern South Australia. Quat. Res. 8, 97–114.
Dodson, J.R., 1994. Quaternary Vegetation History. Cambridge University Press, Cambridge.
Donders, T.H., Wagner, F., Visscher, H., 2006. Late Pleistocene and Holocene subtropical vegetation dynamics recorded in perched lake deposits on Fraser Island, Queensland, Australia. Palaeogeogr. Palaeoclimatol. Palaeoecol. 241, 417–439.
Driscoll, R., Elliot, M., Russon, T., Welsh, K., Yokoyama, Y., Tudhope, A., 2014. ENSO reconstructions over the past 60 ka using giant clams (*Tridacna* sp.) from Papua New Guinea. Geophys. Res. Lett. 41, 6819–6825.
Edney, P.A., Kershaw, A.P., Deckker, P.D., 1990. A late Pleistocene and Holocene vegetation and environmental record from Lake Wangoom, Western Plains of Victoria, Australia. Palaeogeogr. Palaeoclimatol. Palaeoecol. 80, 325–343.
Eggermont, H., Heiri, O., 2012. The Chironomid-temperature relationship: expression in nature and paleoenvironmental implications. Biol. Rev. 87, 430–456.
English, P., Spooner, N.A., Chappell, J., Questiaux, D.G., Hill, N.G., 2001. Lake Lewis Basin, central Australia: environmental evolution and OSL chronology. Quat. Int. 83–85, 81–101.
EPICA-Members, 2006. One-to-one coupling of glacial climate variability in Greenland and Antarctica. Nature 444, 195–198.
Feakins, S.J., Bentley, L.P., Salinas, N., Shenkin, A., Blonder, B., Goldsmith, G.R., Ponton, C., Arvin, L.J., Wu, M.S., Peters, T., West, A.J., Martin, R.E., Enquist, B.J., Asner, G.P., Malhi, Y., 2016. Plant leaf wax biomarkers capture gradients in hydrogen isotopes of precipitation from the Andes and Amazon. Geochem. Cosmochim. Acta 182, 155–172.
Feakins, S.J., Kirby, M.E., Cheetham, M.I., Ibarra, Y., Zimmerman, S.R.H., 2014. Fluctuation in leaf wax D/H ratio from a southern California lake records significant variability in isotopes in precipitation during the late Holocene. Org. Geochem. 66, 48–59.
Fitzsimmons, K.E., Cohen, T., Hesse, P.P., Jansen, J., Nanson, G.C., May, J.-H., Barrows, T.T., Haberlah, D., Hilgers, A., Kelly, T., Larsen, J., Lomax, J., Treble, P., 2013. Late Quaternary palaeoenvironmental change in the Australian drylands. Quat. Sci. Rev. 74, 78–96.
Fitzsimmons, K.E., Miller, G.H., Spooner, N.A., Magee, J.W., 2012. Aridity in the monsoon zone as indicated by desert dune formation in the Gregory Lakes Basin, northwestern Australia. Aust. J. Earth Sci. 59, 469–478.
Fletcher, M.-S., Moreno, P., 2011. Zonally symmetric changes in the strength and position of the Southern Westerlies drove atmospheric CO_2 variations over the past 14 k. y. Geology 39, 419–422.
Fletcher, M.-S., Thomas, I., 2010. A quantitative Late Quaternary temperature reconstruction from western Tasmania, Australia. Quat. Sci. Rev. 29, 2351–2361.
Freund, M., Henley, B.J., Karoly, D.J., Allen, K.J., Baker, P.J., 2017. Multi-century cool- and warm-season rainfall reconstructions for Australia's major climatic regions. Clim. Past 13, 1751–1770.
Galbraith, R.F., Roberts, R.G., 2012. Statistical aspects of equivalent dose and error calculation and display in OSL dating: an overview and some recommendations. Quat. Geochronol. 11, 1–27.

Godfred-Spenning, C.R., Reason, C.J.C., 2002. Interannual variability of lower-tropospheric moisture transport during the Australian monsoon. Int. J. Climatol. 22, 509–532.
Hahn, A., Kliem, P., Oehlerich, M., Ohlendorf, C., Zolitschka, B., 2014. Elemental composition of the Laguna Potrok Aike sediment sequence reveals paleoclimatic changes over the past 51 ka in southern Patagonia, Argentina. J. Paleolimnol. 52, 349–366.
Hamm, G., Mitchell, P., Arnold, L.J., Prideaux, G.J., Questiaux, D., Spooner, N.A., Levchenko, V.A., Foley, E.C., Worthy, T.H., Stephenson, B., Coulthard, V., Coulthard, C., Wilton, S., Johnston, D., 2016. Cultural innovation and megafauna interaction in the early settlement of arid Australia. Nature 539, 280.
Harle, K.J., 1997. Late Quaternary vegetation and climate change in southeastern Australia: palynological evidence from marine core E55-6. Palaeogeogr. Palaeoclimatol. Palaeoecol. 131, 465–483.
Harrison, S.P., Digerfeldt, G., 1993. European lakes as palaeohydrological and palaeoclimatic indicators. Quat. Sci. Rev. 12, 233–248.
Heath, P., Gouthas, G., Irvine, J., Krapf, C., Dutch, R., 2018. Microgravity surveys on the Nullarbor. ASEG Extended Abstracts 2018, 1–7.
Hendon, H.H., Thompson, D.W.J., Wheeler, M.C., 2007. Australian rainfall and surface temperature variations associated with the Southern Hemisphere annular mode. J. Clim. 20, 2452–2467.
Herzschuh, U., 2006. Palaeo-moisture evolution in monsoonal Central Asia during the last 50,000 years. Quat. Sci. Rev. 25, 163–178.
Hesse, P.P., Humphreys, G.S., Smith, B.L., Campbell, J., Peterson, E.K., 2003. Age of loess deposits in the central tablelands of New South Wales. Soil Res. 41, 1115–1131.
Hogg, A.G., Hua, Q., Blackwell, P.G., Niu, M., Buck, C.E., Heaton, T.J., Guilderson, T.P., Zimmerman, S.R.H., Palmer, J.G., Turney, C.S.M., Reimer, P.J., Reimer, R.W., 2013. Shcal13 southern hemisphere calibration, 0-50,000 years cal BP. Radiocarbon 55, 1889–1903.
Johnson, C.N., Alroy, J., Beeton, N.J., Bird, M.I., Brook, B.W., Cooper, A., Gillespie, R., Herrando-Pérez, S., Jacobs, Z., Miller, G.H., Prideaux, G.J., Roberts, R.G., Rodríguez-Rey, M., Saltré, F., Turney, C.S.M., Bradshaw, C.J.A., 2016. What caused extinction of the Pleistocene megafauna of Sahul? Proc. Roy. Soc. Lond. B Biol. Sci. 283, 1–8, 20152399.
Jouzel, J., Masson-Delmotte, V., Cattani, O., Dreyfus, G., Falourd, S., Hoffmann, G., Minster, B., Nouet, J., Barnola, J.M., Chappellaz, J., Fischer, H., Gallet, J.C., Johnsen, S., Leuenberger, M., Loulergue, L., Luethi, D., Oerter, H., Parrenin, F., Raisbeck, G., Raynaud, D., Schilt, A., Schwander, J., Selmo, E., Souchez, R., Spahni, R., Stauffer, B., Steffensen, J.P., Stenni, B., Stocker, T.F., Tison, J.L., Werner, M., Wolff, E.W., 2007. Orbital and millennial Antarctic climate variability over the past 800,000 years. Science 317, 793–796.
Kemp, J., Rhodes, E., 2010. Episodic fluvial activity of inland rivers in southeastern Australia: palaeochannel systems and terraces of the Lachlan River. Quat. Sci. Rev. 29, 732–752.
Kershaw, A.P., Bretherton, S.C., van der Kaars, S., 2007a. A complete pollen record of the last 230 ka from Lynch's Crater, north-eastern Australia. Palaeogeogr. Palaeoclimatol. Palaeoecol. 251, 23–45.
Kershaw, A.P., McKenzie, G.M., Porch, N., Roberts, R.G., Brown, J., Heijnis, H., Orr, M.L., Jacobsen, G., Newall, P.R., 2007b. A high-resolution record of vegetation and climate through the last glacial cycles from Caledonia Fen, south-eastern highlands of Australia. J. Quat. Sci. 22, 481–500.
Kohfeld, K.E., Graham, R.M., de Boer, A.M., Sime, L.C., Wolff, E.W., Le Quéré, C., Bopp, L., 2013. Southern Hemisphere westerly wind changes during the Last Glacial Maximum: paleo-data synthesis. Quat. Sci. Rev. 68, 76–95.
Köhler, P., Nehrbass-Ahles, C., Schmitt, J., Stocker, T.F., Fischer, H., 2017. Continuous record of the atmospheric greenhouse gas carbon dioxide (CO_2), raw data, in supplement to: Köhler, P et al. (2017): a 156 kyr smoothed history of the atmospheric greenhouse gases CO_2, CH_4, and N_2O and their radiative forcing. Earth Syst. Sci. Data 9 (1), 363–387. https://doi.org/10.5194/essd-9-363-2017. PANGAEA.
Lambert, F., Delmonte, B., Petit, J.R., Bigler, M., Kaufmann, P.R., Hutterli, M.A., Stocker, T.F., Ruth, U., Steffensen, J.P., Maggi, V., 2008. Dust-climate couplings over the past 800,000 years from the EPICA Dome C ice core. Nature 452, 616–619.
Lamy, F., Gersonde, R., Winckler, G., Esper, O., Jaeschke, A., Kuhn, G., Ullermann, J., Martinez-Garcia, A., Lambert, F., Kilian, R., 2014. Increased dust deposition in the Pacific Southern Ocean during glacial periods. Science 343, 403–407.
Larocque-Tobler, I., Grosjean, M., Kamenik, C., 2011. Calibration-in-time versus calibration-in-space (transfer function) to quantitatively infer July air temperature using biological indicators (chironomids) preserved in lake sediments. Palaeogeogr. Palaeoclimatol. Palaeoecol. 299, 281–288.
Leduc, G., Vidal, L., Tachikawa, K., Bard, E., 2009. ITCZ rather than ENSO signature for abrupt climate changes across the tropical Pacific. Quat. Res. 72, 123–131.
Lipar, M., Ferk, M., 2015. Karst pocket valleys and their implications on Pliocene–Quaternary hydrology and climate: examples from the Nullarbor Plain, southern Australia. Earth Sci. Rev. 150, 1–13.
Lisiecki, L.E., Raymo, M.E., 2005. A Pliocene-Pleistocene stack of 57 globally distributed benthic $\delta^{18}O$ records. Paleoceanography 20.
Longmore, M.E., Heijnis, H., 1999. Aridity in Australia: Pleistocene records of palaeohydrological and palaeoecological change from the perched lake sediments of Fraser Island, Queensland, Australia. Quat. Int. 57/58, 35–47.
Magee, J.W., Miller, G.H., Spooner, N.A., Questiaux, D., 2004. Continuous 150 k.y. monsoon record from Lake Eyre, Australia; insolation-forcing implications and unexpected Holocene failure. Geology 32, 558–888.
Maroulis, J.C., Nanson, G.C., Price, D.M., Pietsch, T., 2007. Aeolian–fluvial interaction and climate change: source-bordering dune development over the past ~100 ka on Cooper Creek, central Australia. Quat. Sci. Rev. 26, 386–404.
McGowan, H.A., Petherick, L.M., Kamber, B.S., 2008. Aeolian sedimentation and climate variability during the late Quaternary in southeast Queensland, Australia. Palaeogeogr. Palaeoclimatol. Palaeoecol. 265, 171–181.
Merkel, U., Prange, M., Schulz, M., 2010. ENSO variability and teleconnections during glacial climates. Quat. Sci. Rev. 29, 86–100.
Miller, G.H., Fogel, M.L., Magee, J.W., Gagan, M.K., 2016. Disentangling the impacts of climate and human colonization on the flora and fauna of the Australian arid zone over the past 100 ka using stable isotopes in avian eggshell. Quat. Sci. Rev. 151, 27–57.
Mooney, S.D., Harrison, S.P., Bartlein, P.J., Daniau, A.-L., Stevenson, J., Brownlie, K.C., Buckman, S., Cupper, M., Luly, J., Black, M., Colhoun, E., D'Costa, D., Dodson, J., Haberle, S., Hope, G.S., Kershaw, P., Kenyon, C., McKenzie, M., Williams, N., 2011. Late Quaternary fire regimes of Australasia. Quat. Sci. Rev. 30, 28–46.
Moss, P.T., Kershaw, A.P., 2007. A late Quaternary marine palynological record (oxygen isotope stages 1 to 7) for the humid tropics of northeastern Australia based on ODP Site 820. Palaeogeogr. Palaeoclimatol. Palaeoecol. 251, 4–22.
Moss, P.T., Tibby, J., Petherick, L., McGowan, H., Barr, C., 2013. Late Quaternary vegetation history of North Stradbroke Island, Queensland, eastern Australia. Quat. Sci. Rev. 74, 257–272.
Muller, J., Kylander, M., Wüst, R.A.J., Weiss, D., Martinez-Cortizas, A., LeGrande, A.N., Jennerjahn, T., Behling, H., Anderson, W.T., Jacobson, G., 2008. Possible evidence for wet Heinrich phases in tropical NE Australia: the Lynch's Crater deposit. Quat. Sci. Rev. 27, 468–475.
Murray, A.S., Wintle, A.G., 2000. Luminescence dating of quartz using an improved single-aliquot regenerative-dose protocol. Radiat. Meas. 32, 57–73.
Nanson, G.C., Price, D.M., Jones, B.G., Maroulis, J.C., Coleman, M., Bowman, H., Cohen, T.J., Pietsch, T.J., Larsen, J.R., 2008. Alluvial evidence for major climate and flow regime changes during the middle and late Quaternary in eastern central Australia. Geomorphology 101, 109–129.
Page, K., Nanson, G., Price, D., 1996. Chronology of Murrumbidgee River palaeochannels on the Riverine Plain, southeastern Australia. J. Quat. Sci. 11, 311–326.
Petherick, L., Bostock, H., Cohen, T.J., Fitzsimmons, K., Tibby, J., Fletcher, M.-S., Moss, P., Reeves, J., Mooney, S., Barrows, T., Kemp, J., Jansen, J., Nanson, G., Dosseto, A., 2013. Climatic records over the past 30 ka from temperate Australia – a synthesis from the Oz-INTIMATE workgroup. Quat. Sci. Rev. 74, 58–77.
Petherick, L., McGowan, H., Moss, P., 2008. Climate variability during the Last Glacial Maximum in eastern Australia: evidence of two stadials? Quat. Sci. Rev. 23, 787–802.
Petherick, L.M., Moss, P.T., Mcgowan, H.A., 2011. Climatic and environmental variability during the termination of the Last Glacial Stage in coastal eastern Australia: a review. Aust. J. Earth Sci. 58, 563–577.
Reeves, J.M., Barrows, T.T., Cohen, T.J., Kiem, A.S., Bostock, H.C., Fitzsimmons, K.E., Jansen, J.D., Kemp, J., Krause, C., Petherick, L., Phipps, S.J., Members, O.-I., 2013. Climate variability over the last 35,000 years recorded in marine and terrestrial archives in the Australian region: an OZ-INTIMATE compilation. Quat. Sci. Rev. 74, 21–34.
Reimer, P.J., Bard, E., Bayliss, A., Beck, J.W., Blackwell, P.G., Bronk Ramsey, C., Buck, C.E., Cheng, H., Edwards, R.L., Friedrich, M., Grootes, P.M., Guilderson, T.P., Haflidason, H., Hajdas, I., Hatté, C., Heaton, T.J., Hoffmann, D.L., Hogg, A.G., Hughen, K.A., Kaiser, K.F., Kromer, B., Manning, S.W., Niu, M., Reimer, R.W., Richards, D.A., Scott, E.M., Southon, J.R., Staff, R.A., Turney, C.S.M., van der Plicht, J., 2013. IntCal13 and Marine13 radiocarbon age calibration curves 0–50,000 Years cal BP. Radiocarbon 55, 1869–1887.
Risbey, J.S., Pook, M.J., McIntosh, P.C., Wheeler, M.C., Hendon, H.H., 2009. On the remote drivers of rainfall variability in Australia. Mon. Weather Rev. 137, 3233–3253.
Rodríguez-Rey, M., Herrando-Perez, S., Gillespie, R., Jacobs, Z., Saltre, F., Brook, B.W., Prideaux, G.J., Roberts, R.G., Cooper, A., Alroy, J., Miller, G.H., Bird, M.I., Johnson, C.N., Beeton, N., Turney, C.S.M., Bradshaw, C.J.A., 2015. Criteria for assessing the quality of Middle Pleistocene to Holocene vertebrate fossil ages. Quat. Geochronol. 30, 69–79.
Rohling, E.J., Grant, K., Hemleben, C., Kucera, M., Roberts, A.P., Schmeltzer, I., Schulz, H., Siccha, M., Siddall, M., Trommer, G., 2008. New constraints on the timing of sea level fluctuations during early to middle marine isotope stage 3: timing of MIS 3 sea level fluctuations. Paleoceanography 23, 1–8.
Rule, S., Brook, B.W., Haberle, S.G., Turney, C.S.M., Kershaw, A.P., Johnson, C.N., 2012. The aftermath of megafaunal extinction: ecosystem transformation in pleistocene Australia. Science 335, 1483–1486.
Saenger, C., Affek, H.P., Felis, T., Thiagarajan, N., Lough, J.M., Holcomb, M., 2012. Carbonate clumped isotope variability in shallow water corals: temperature dependence and growth-related vital effects. Geochem. Cosmochim. Acta 99, 224–242.
Saltré, F., Rodríguez-Rey, M., Brook, B.W., Johnson, C.N., Turney, C.S.M., Alroy, J., Cooper, A., Beeton, N., Bird, M.I., Fordham, D.A., Gillespie, R., Herrando-Pérez, S., Jacobs, Z., Miller, G.H., Nogués-Bravo, D., Prideaux, G.J., Roberts, R.G., Bradshaw, C.J.A., 2016. Climate change not to blame for late Quaternary megafauna extinctions in Australia. Nat. Commun. 7, 1–7.
Shepard, D., 1968. A two-dimensional interpolation function for irregularly-spaced data. Proc. 1968 ACM Nat. Conf. 517–524.
Singh, B.S., Geissler, E.A., 1985. Late Cainozoic history of vegetation, fire, lake levels and climate, at Lake George, New South Wales, Australia. Philos. Trans. Royal Soc. London. Series B, Biol. Sci. 311, 379–447.

Sun, Y., Liang, L., Bloemendal, J., Li, Y., Wu, F., Yao, Z., Liu, Y., 2016. High-resolution scanning XRF investigation of Chinese loess and its implications for millennial-scale monsoon variability. J. Quat. Sci. 31, 191–202.
Tibby, J., Barr, C., Marshall, J.C., Mgregor, G.B., Moss, P.T., Arnold, L.J., Page, T.J., Questiaux, D., Olley, J., Kemp, J., Spooner, N., Petherick, L., Penny, D., Mooney, S., Moss, E., 2017. Persistence of wetlands on North Stradbroke Island (south-east Queensland, Australia) during the last glacial cycle: implications for Quaternary science and biogeography. J. Quat. Sci. 32, 770–781.
Tierney, J.E., Russell, J.M., Huang, Y., Damsté, J.S.S., Hopmans, E.C., Cohen, A.S., 2008. Northern hemisphere controls on tropical southeast African climate during the past 60,000 years. Science 322, 252–255.
Tobler, R., Rohrlach, A., Soubrier, J., Bover, P., Llamas, B., Tuke, J., Bean, N., Abdullah-Highfold, A., Agius, S., O'Donoghue, A., O'Loughlin, I., Sutton, P., Zilio, F., Walshe, K., Williams, A.N., Turney, C.S.M., Williams, M., Richards, S.M., Mitchell, R.J., Kowal, E., Stephen, J.R., Williams, L., Haak, W., Cooper, A., 2017. Aboriginal mitogenomes reveal 50,000 years of regionalism in Australia. Nature 544, 180–184.
Tudhope, A.W., Chilcott, C.P., Mcculloch, M.T., Cook, E.R., Chappell, J., Ellam, R.M., Lea, D.W., Lough, J.M., Shimmield, G.B., 2001. Variability in the El Niño - southern oscillation through a glacial-interglacial cycle. Science 291, 1511–1517.
Turney, C.S.M., Bird, M.I., Fifield, L.K., Roberts, R.G., Smith, M., Dortch, C.E., Grün, R., Lawson, E., Ayliffe, L.K., Miller, G.H., Dortch, J., Cresswell, R.G., 2001. Early human occupation at Devil's Lair, southwestern Australia 50,000 years ago. Quat. Res. 55, 3–13.
Turney, C.S.M., Kershaw, P., Clemens, S., Branch, N., Moss, P., Fifield, L.K., 2004. Millennial and orbital variations of El Niño/Southern Oscillation and high-latitude climate in the last glacial period. Nature 428, 306–310.
Tyler, J.J., Mills, K., Barr, C., Sniderman, J.M.K., Gell, P.A., Karoly, D.J., 2015. Identifying coherent patterns of environmental change between multiple, multivariate records: an application to four 1000-year diatom records from Victoria, Australia. Quat. Sci. Rev. 119, 94–105.
van De Geer, G., Heusser, L.E., Lynch-Stieglitz, J., Charles, C.D., 1994. Paleoenvironments of Tasmania inferred from a 5–75 ka marine pollen record. Palynology 18, 33–40.
van der Kaars, S., De Deckker, P., 2002. A Late Quaternary pollen record from deep-sea core Fr10/95, GC17 offshore Cape Range Peninsula, northwestern Western Australia. Rev. Palaeobot. Palynol. 120, 17–39.
van der Kaars, S., Miller, G.H., Turney, C.S.M., Cook, E.J., Nürnberg, D., Schönfeld, J., Kershaw, A.P., Lehman, S.J., 2017. Humans rather than climate the primary cause of Pleistocene megafaunal extinction in Australia. Nat. Commun. 8, 1–7.
Veth, P., Ward, I., Ditchfield, K., 2017. Reconceptualising Last Glacial Maximum discontinuities: a case study from the maritime deserts of north-western Australia. J. Anthropol. Archaeol. 46, 82–91.
Wende, R., Nanson, G.C., Price, D.M., 1997. Aeolian and fluvial evidence for late Quaternary environmental change in the east Kimberley of Western Australia. Aust. J. Earth Sci. 44, 519–526.
Williams, N.J., Harle, K.J., Gale, S.J., Heijnis, H., 2006. The vegetation history of the last glacial-interglacial cycle in eastern New South Wales, Australia. Quat. Sci. Rev. 21, 735–750.
Woltering, M., Atahan, P., Grice, K., Heijnis, H., Taffs, K., Dodson, J., 2014. Glacial and Holocene terrestrial temperature variability in subtropical east Australia: branched GDGT distributions in a sediment core from Lake McKenzie. Quat. Res. 82, 132–145.
Zaarur, S., Olack, G., Affek, H.P., 2011. Paleo-environmental implication of clumped isotopes in land snail shells. Geochem. Cosmochim. Acta 75, 6859–6869.

Palaeogeography, Palaeoclimatology, Palaeoecology 538 (2020) 109463

Contents lists available at ScienceDirect

Palaeogeography, Palaeoclimatology, Palaeoecology

journal homepage: www.elsevier.com/locate/palaeo

Climates of the last three interglacials in subtropical eastern Australia inferred from wetland sediment geochemistry

C.W. Kemp[a,*], J. Tibby[a], L.J. Arnold[b], C. Barr[a], P.S. Gadd[c], J.C. Marshall[d,e], G.B. McGregor[d], G.E. Jacobsen[c]

[a] Geography, Environment and Population, Sprigg Geobiology Centre, University of Adelaide, Australia
[b] School of Physical Science, Environment Institute, Sprigg Geobiology Centre, Institute for Photonics and Advanced Sensing, University of Adelaide, Australia
[c] Australian Nuclear Science and Technology Organisation, Lucas Heights, Australia
[d] Queensland Department of Environment and Science, Brisbane, Australia
[e] Australian Rivers Institute, Griffith University, Brisbane, Australia

ARTICLE INFO

Keywords:
Palaeoclimate
North Stradbroke Island
Holocene
MIS 5
MIS 7
μXRF

ABSTRACT

Records of Australian climate during Marine Isotope Stages 5 and 7 (130–71 and 243–191 ka) are rare, preventing detailed assessments of long-term climate, drivers and ecological responses across the continent over glacial-interglacial timescales. This study presents a geochemistry-based palaeoclimate record from Fern Gully Lagoon on North Stradbroke Island (also known as Minjerribah) in subtropical eastern Australia, which records climates in MIS 7a–c, MIS 5 and much of the Holocene, in addition to MIS 4 (71–57 ka), and parts of MIS 6, MIS 3 and MIS 2 (191–130, 57–29 and 29–14 ka). Indicators of inorganic sedimentation from a 9.5 m sediment core – focussed on high-resolution estimates of sediment geochemistry supported by x-radiography, inorganic content and magnetic susceptibility – were combined with a chronology consisting of six radiocarbon (^{14}C) and thirteen single-grain optically stimulated luminescence (OSL) ages. Hiatuses occurred at ~178–153 ka, ~36–21 ka and ~7–2 ka and likely result from the wetland drying. Low values of locally sourced aeolian materials indicate a wet MIS 7a–c and early MIS 6 before a relatively dry MIS 5. Inorganic flux during the Holocene was up to four times greater than during MIS 5, consistent with long-term interglacial drying observed in other regions, most notably in central Australia. This study highlights the importance of employing a combination of multiple dating approaches and calibrated geochemical proxies to derive climate reconstructions and to identify depositional complexities in organic-rich wetland records.

1. Introduction

Reliable reconstructions of past interglacial climates are important for providing analogues of future climate change, as well as for better understanding ecosystem responses that are likely to accompany increases in global temperature (Turney and Jones, 2010; Harrison and Bartlein, 2012). Records of interglacial climates are similarly required to understand the long-term evolution of Australian biota including past extinction events (Kershaw et al., 2003; Miller et al., 2016; Van der Kaars et al., 2017). At present, the usefulness of Australian palaeoclimate records for either of these purposes is relatively limited, as most only extend to the Last Glacial Maximum (LGM) ~20 thousand years ago (ka) (Petherick et al., 2013; Reeves et al., 2013).

Records of Australian climate during the past three interglacials are limited, but include Lynch's Crater and the nearby ODP 820 marine record (Kershaw et al., 2007a; Moss and Kershaw, 2007) in the north-east; Lake Eyre, Lake Woods and central Australian streams and lakes (Bowler et al., 1998; Nanson et al., 2008; Cohen et al., 2015; Fu et al., 2017); and the Naracoorte Caves, Lake Selina, Lake Wangoom and Caledonia Fen in the south-east (Ayliffe et al., 1998; Colhoun et al., 1999; Harle et al., 2002; Kershaw et al., 2007b). The distribution of available records is limited in geographical scope, and does not currently include equatorial or subtropical Australian localities. Additionally, while these records infer past climate from proxies such as pollen, charcoal and palaeoshorelines, there is not as yet an Australian interglacial record utilising μXRF geochemical analysis.

Climate records derived from geochemical studies of wetland sediments have experienced a boom in the past decade, with the advent of

* Corresponding author at: Department of Geography, Environment and Population, The University of Adelaide, North Terrace, Adelaide, South Australia 5005, Australia.
E-mail address: Christopher.kemp@adelaide.edu.au (C.W. Kemp).

https://doi.org/10.1016/j.palaeo.2019.109463
Received 12 August 2019; Received in revised form 4 November 2019; Accepted 12 November 2019
Available online 19 November 2019
0031-0182/

relatively cheap, reliable, reproducible μXRF analysis (Croudace and Rothwell, 2015). Wetland geochemical records represent invaluable archives for palaeoclimatology reconstructions, providing constraints on climate change at local (e.g. Eggenberger et al., 2018; Vegas-Vilarrúbia et al., 2018; Burrows et al., 2016) and regional scales (e.g. Field et al., 2018; Pleskot et al., 2018; Profe et al., 2018), and enabling a greater understanding of internal wetland processes (e.g. Burrows et al., 2016; Kienel et al., 2017; Vegas-Vilarrúbia et al., 2018).

Here we present a multi-proxy ~209 kyr record of subtropical climatic variability from Fern Gully Lagoon focussing on past interglacials. This study is the foundation for future studies of regional climate change based on Fern Gully Lagoon sediments and assesses the validity of the site as a palaeoclimate archive. We use calibrated μXRF Itrax scanning to infer locally-derived aeolian inorganic sedimentation and assess the suitability of OSL and ^{14}C to date the complex, organic-rich sediment sequence.

2. Background

2.1. Global climate changes during recent interglacials

A recent review of global interglacial climates has demonstrated some important differences between marine isotope stage 7 (MIS 7), MIS 5 and the Holocene (Berger et al., 2015). Specifically, the MIS 7 interglacial complex was characterised by higher average global temperatures than the MIS 5 interglacial complex but had a lower temperature peak in MIS 7e than that in MIS 5e (Lisiecki and Raymo, 2005; Parrenin et al., 2013; Berger et al., 2015). The lower MIS 7e temperature is likely due to the greater difference between MIS 5e summer and winter insolation, while insolation during MIS 7e was more evenly distributed over the seasons due to lower obliquity of the Earth's orbit (Berger et al., 2015). In contrast to the warmer MIS 5e, the warmer climates of the MIS 7a–c sub-complex relative to the MIS 5a–c sub-complex are reflected in extended periods of reduced ice volume (Lisiecki and Raymo, 2005; Elderfield et al., 2012), higher sea levels (Rohling et al., 2009) and higher atmospheric CO_2 concentrations (Köhler et al., 2017). MIS 7a–c represents a rare ~20 kyr period of relatively stable, warm, mean global climate (Berger et al., 2015).

Sea surface temperature records from the West Pacific Warm Pool (WPWP) can be used to guide understanding of globally-linked, regional changes in eastern Australian climate that occurred during the previous three interglacials (Zhang et al., 2017). In particular, sea surface temperatures in the WPWP (Fig. 1) can dictate climate variability in the wider region, including the central-eastern Australian coast and the Tasman Sea (Martinez et al., 2002; Bostock et al., 2006; Pelejero et al., 2006). WPWP sea surface temperatures indicate that MIS 5e had the warmest SSTs of the last ~250 kyr (Tachikawa et al., 2014), but that the MIS 7 interglacial complex and the Holocene were/are warmer than the MIS 5 interglacial complex by an average of ~1–2 °C (Lo et al., 2017).

2.2. Australian climates during past interglacials

The available Australian MIS 7 data permits insights into broad-scale climatic trends. During late MIS 7, Lakes Eyre and Woods in central Australia, which are predominantly fed by monsoonal rains, were full, in contrast to their present mostly dry state (Bowler et al., 1998; Fu et al., 2017). Meanwhile, wet climates and open water were present in Lynch's Crater in ENSO-dominated north-eastern Australia (Kershaw et al., 2007a; Moss and Kershaw, 2007). Similarly, the speleothem record from the Naracoorte Caves in south-eastern Australia, which primarily reflects southern westerly wind-dominated rainfall, indicates wet climates, with pronounced periods of calcitic growth between ~220 and 155 ka (Ayliffe et al., 1998). These few available records indicate that Australia was wetter during late MIS 7 than the Holocene, with a more active Australian Monsoon in the north and stronger or more northerly southern westerly winds.

Central Australia was also wet during MIS 5 (Bowler et al., 1998; Cohen et al., 2015), though the average precipitation:evaporation ratio was lower than during late MIS 7. North-eastern Australian records indicate wet climates during MIS 5, but greater climate variability than during MIS 7 (Kershaw et al., 2007a; Moss and Kershaw, 2007). The pattern in the south-east of the continent is in general agreement with north-eastern records, with generally wet climates observed during MIS 5 (Edney et al., 1990; Ayliffe et al., 1998; Colhoun et al., 1999; Harle et al., 2002).

Holocene hydroclimate in Australia was drier than MIS 5 and MIS 7 in most regions. Lake Eyre and Lake Frome, which were full during MIS 5, became dry and ephemeral (Cohen et al., 2015), while speleothem growth largely ceased in the Naracoorte Caves (Ayliffe et al., 1998) suggesting weakening or more southerly south westerly winds. However, there is uncertainty about whether the Holocene was drier than MIS 5 in south-east Australia and the Wet Tropics of north-eastern Australia within each record (Edney et al., 1990; Colhoun et al., 1999; Kershaw et al., 2007a; Kershaw et al., 2007b). Uncertainty within records combined with geographical separation makes it difficult to determine climate change at a continental scale. As such, additional records from new locations are required.

2.3. Study site

North Stradbroke Island is a sand island located along the eastern coast of Australia (Fig. 1). The Island is part of the world's oldest and largest coastal dune system (Patton et al., 2019) and lies on an aeolian dust pathway from central and south-central Australia (McGowan et al., 2008; Petherick et al., 2009). The Island is a strategic location for understanding palaeoclimate, as it is situated in the subtropics (Fig. 1), with a contemporary climate that is strongly influenced by the El Niño–Southern Oscillation (ENSO) (Barr et al., 2019) and preserves the highest density of wetlands with sediment dating to the LGM in Australia (Tibby et al., 2017). As such, it has been the focus of several detailed palaeoenvironmental reconstructions (e.g. Moss et al., 2013; Barr et al., 2017; Petherick et al., 2017; Cadd et al., 2018), the longest of which extends to ~130 ka (Cadd et al., 2018). There is evidence for human occupation of the island from at least 20 ka at Wallen Wallen Creek (Fig. 1), with a Holocene increase in human occupation peaking at ~1 ka (Neal and Stock, 1986).

Fern Gully Lagoon (27.417°S, 153.460°E, 39 m ASL) is an approximately 0.8 km^2 perched, palustrine wetland (Leach, 2011) that lies within a shallow bowl of vegetated dunes at the north-western end of North Stradbroke Island. The wetland has two above-ground outflows, the largest being to the eponymous Fern Gully (Fig. 1C). The limited catchment area and highly permeable sandy soils mean the delivery of fluvially transported material to the wetland is limited. Single-grain OSL dating of a reconnaissance core from Fern Gully Lagoon determined a preliminary basal age of ~208.4 ± 32.5 ka (Tibby et al., 2017) at a depth of 9.25 m.

3. Methods

3.1. Core collection and correlation

In 2015, two ~9 m-long cores were extracted from the approximate centre of Fern Gully Lagoon (27.4174°S, 153.4600°E) using a modified Bolivia corer, itself a modification of the Livingstone-square-rod piston-sampling method (Wright, 1967). The two cores were offset by one metre horizontally and 50 cm vertically, in an attempt to provide a continuous sequence. Cores were extracted in black-painted PVC pipe and stored in black plastic sleeves, to eliminate light contamination and ensure the sediments would be suitable for luminescence dating. The first core (FG15-1) was chosen as the master core and was sampled for single-grain OSL and ^{14}C dating. The second core (FG15-2) was used to

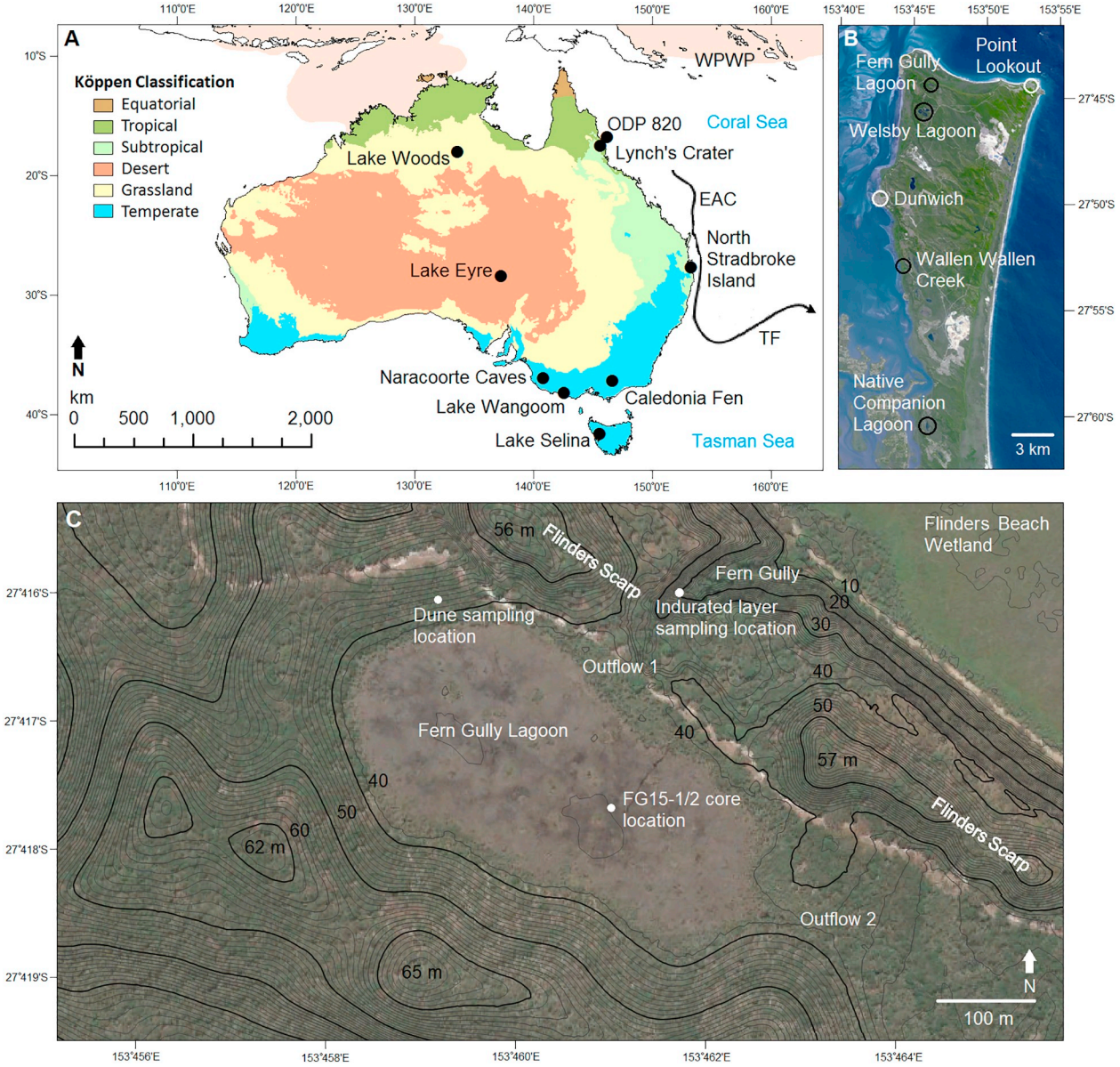

Fig. 1. A: Modified Köppen climate zones (BOM, 2005), location of Australian interglacial climate records and the approximate current positions of the west Pacific warm pool (WPWP, mean annual SST > 28 °C) boundary (pink shading; Gagan et al., 2000), the East Australian Current (EAC) and the Tasman Front (TF) (Bostock et al., 2006). B: North Stradbroke Island, with the four climate/archaeological record sites (black circles) and local towns (white circles), mentioned in the text. C: Fern Gully Lagoon combined topographic map and satellite image, indicating the coring location, locations of modern geochemistry samples, outflows and the height of surrounding dunes (m ASL). (For interpretation of the references to colour in this figure legend, the reader is referred to the web version of this article.)

fill gaps in the FG15-1 record and to provide additional sediment for ^{14}C and conventional wave dispersive x-ray fluorescence analyses.

Cores were aligned using CPLSlot sequence slotting software (Clark and Hounslow, 2009) using the eight elements with highest Itrax counts per second: silicon, titanium, zircon, potassium, calcium, iron and bromine. The correlation allowed the cores to be placed on a common depth scale.

Moisture and organic content were determined on 930 one cubic centimetre samples following Heiri et al. (2001). This record was used to target optimum OSL sample locations (i.e., locate areas with highest inorganic content, and presumably quartz content) and to calculate average water content and sediment densities for luminescence dose rate calculation (see Supplementary materials).

3.2. Itrax μXRF, magnetic susceptibility and X-radiography

To determine changes in sediment geochemistry, Itrax second-generation micro X-ray fluorescence (μXRF, Croudace et al., 2006) scanning of both cores was undertaken at the Australian Nuclear Science and Technology Organisation. Itrax scanning utilised a molybdenum x-ray tube at 30 kV and 55 mA, with a 20 second exposure time, generating a record of elemental response (counts per second) for thirty-five elements at 2 mm intervals. An X-radiograph record using the same tube at 45 kV at 30 mA and a magnetic susceptibility record were also developed.

Micro XRF data must be normalised to mitigate the closed-sum effect (Weltje and Tjallingii, 2008; Löwemark et al., 2011). However, despite an increasing number of μXRF studies (Croudace and Rothwell, 2015), there is no standardised method for normalisation. To identify all recently published methods, we undertook a review and synthesis of

μXRF in the Scopus (https://www.scopus.com/home.uri) and Web of Science (http://www.webofknowledge.com) databases. The results of this review were used to identify which normalisation methods have been utilised in recent μXRF studies, along with what (if any) validation and calibration methods were used (e.g. conventional XRF, inductively coupled plasma mass spectrometry (ICP-MS)). Further details of the database review methods and results, along with a discussion of recent μXRF methodologies are provided in the Supplementary material.

The eight most common normalisation methods identified in our review were assessed to determine the best method for normalising the Fern Gully Lagoon μXRF record. These were: total counts per second normalisation (Bouchard et al., 2011; Martin et al., 2014), centred log-ratio normalisation (Weltje and Tjallingii, 2008; Weltje et al., 2015), aluminium normalisation (Brumsack, 2006; Löwemark et al., 2011), titanium normalisation (Vegas-Vilarrúbia et al., 2018), silicon normalisation, zircon normalisation, normalisation using incoherent scattering (Compton scattering) and the ratio of incoherent to coherent scattering (Rayleigh and Compton scattering) (e.g. Guyard et al., 2007; Kylander et al., 2011; Marshall et al., 2011; Berntsson et al., 2014).

The normalised μXRF data were compared to quantitative conventional XRF analyses at twenty locations from core FG15-2, following a similar method to recent studies (e.g. Hahn et al., 2014; Falster et al., 2018; Profe et al., 2018). The conventional XRF sample locations were chosen to represent the broadest range of μXRF-derived concentrations, but where there was little within-sample variability in μXRF readings. The latter consideration was important since due to the high sediment organic content, it was necessary to sample up to 1 cm of the core to ensure sufficient material for XRF. Conventional XRF analysis was undertaken at the Commonwealth Scientific and Industrial Research Organisation in Adelaide, South Australia, using lithium-borate fusion of sample material. The glass discs created from the fusion procedure were subsequently analysed on a PANalytical Axios Advanced wavelength dispersive XRF (WD-XRF) system using an in-house silicates calibration program.

For normalisation methods without internal XRF calibration (all but centred log-ratio), μXRF counts per second were compared to absolute concentrations using simple linear regressions. The normalisation method with the highest coefficient of variation was used to identify the most suitable normalisation method for Fern Gully Lagoon sediments. For centred log-ratio, we used a Matlab script after Grant et al. (2017) to produce a multivariate centred log-ratio corrected dataset. This XRF calibration was then used to calculate the approximate mass of oxides for the composite record.

The commonly utilised μXRF incoherent/coherent scattering ratio was also evaluated as a qualitative indicator of sediment organic content (e.g. Guyard et al., 2007; Jouve et al., 2013; Field et al., 2018; Woodward et al., 2018). μXRF water content corrections were also calculated after Boyle et al. (2015), as the sediments have a high water content that is likely to affect μXRF readings.

3.3. Identification of the aeolian component in the Fern Gully Lagoon μXRF record

McGowan et al. (2008) demonstrated that the inorganic component of wetland sediments on North Stradbroke Island (NSI) is derived from two main sources; the local silicon-rich and trace element-depleted sands, and far-travelled dust, which is more clay-rich. Petherick et al. (2009) expanded on that study, analysing source material from 149 sites in central and eastern Australia to geochemically fingerprint far-travelled dust deposited in Native Companion Lagoon (Fig. 1B). High quantities of scandium, gallium, thallium and nickel characterise the clay-rich, far-travelled sediment, contrasting with the Island's rare earth element-depleted silicon-rich quartz sands (McGowan et al., 2008; Petherick et al., 2009). While scandium, gallium and nickel were identified in the μXRF scan, their concentration was too low to be accurate, and they were not considered further.

We derived a high-resolution record of calibrated μXRF silicon. Higher silicon input into wetlands is indicative of drier climate on NSI, which reduces protective vegetation cover (McGowan et al., 2008; Petherick et al., 2009). This effect is amplified by the sandy soils of NSI, which are generally loose and very dry due to their high permeability (Leach, 2011), which also restricts overland flow.

To identify the main directions of variation in the Fern Gully inorganic data, a principal component analysis (PCA) was performed using the vegan package (Oksanen et al., 2018) in RStudio (TeamRStudio, 2015; Ihaka and Gentleman, 2016). A subset of seven normalised elements comprising those with the highest counts per second (silicon, iron, calcium, bromine, zircon, potassium and titanium), along with LOI estimated organic content were used. A broken stick model was used to estimate the number of significant components in the μXRF record (Fig. S2) (Baczkowski, 2000). The PCA vectors were scaled by the species scores before being divided by the standard deviation of each element and multiplied by an equalising constant. In this way, element vectors were centred and standardised so that the relative variance of each element could be compared.

To characterise possible local sediment end members, samples were taken from the following locations:

- The surface of modern dunes ~30 m from the edge of Fern Gully Lagoon and ~30 m from the edge of nearby Welsby Lagoon.
- Sand three meters below the surface of dunes surrounding Fern Gully Lagoon.
- The surface of outflow one at Fern Gully Lagoon (Fig. 1C).
- Local rock outcrops (Point Lookout rhyolite and Dunwich sandstone).
- An indurated layer representing the B horizon of material below each of the two lagoons.

These endmember samples were scanned using Itrax μXRF and placed on the PCA using the vegan predict model (Oksanen et al., 2018).

3.4. Dating

A preliminary age obtained from Fern Gully Lagoon exceeded the radiocarbon dating limit of ~50 ka (Tibby et al., 2017). As such, we employed two dating methods to examine different depths of the core in this study: ^{14}C dating for sediments to a depth of 288 cm, and single-grain OSL dating from 171 cm to the base of the core. Four paired OSL and ^{14}C samples were collected between 171 and 288 cm, to assess age agreement.

^{14}C dating was performed on 18 macrofossil samples, including seeds, leaf material, and bark and charcoal > 3 mm diameter. Six paired ^{14}C samples were collected from different materials to identify any offset due to material properties, including absorption of humic acids and alteration by ground water residence time (Hofmann et al., 2019). Sample preparation was undertaken at the Australian Nuclear Science and Technology Organisation, where each of the samples was dissected under a stereoscope. Any identified root fragments or other foreign objects were removed. Each sample then underwent an Acid-Base-Acid (ABA) pre-treatment to remove humic acids, following Brock et al. (2010) and were freeze-dried before graphitisation and AMS measurement. After correction for isotopic fractionation using measured δ^{13}C values, the conventional ^{14}C ages were calibrated using the Southern Hemisphere Calibration Curve (SHCal13; Hogg et al., 2013).

Single-grain OSL dating was performed on 19 quartz samples collected from core sections with the highest inorganic content. The sediment samples were extracted under filtered and subdued red LED lighting, where ~12 g of bulk sediment (dry weight) was retained from the exposed core face and margins for beta and gamma dose rate determination and beta dose rate water correction (after oven drying at 100 °C). Additional bulk sediment was collected from the overlying and

underlying 10 cm depth of each OSL sample position for gamma dose rate determination and gamma dose rate water content correction. Single-grain equivalent dose (D_e) measurements and environmental dose rate assessments were made using the experimental procedures described by Demuro et al. (2013, 2015). Further details of the OSL methodologies employed in this study, including SAR suitability assessments (dose recoveries) and quality assurance criteria, are included in the Supplementary materials.

The age-depth model for Fern Gully Lagoon was constructed from the ^{14}C and OSL likelihoods using a Bayesian Poisson process depositional model in OxCal v4.2.4 (P_Sequence model: Bronk Ramsey (2009); Bronk Ramsey and Lee (2013)), which allows for randomly variable deposition rates through the age-depth profile. The P_Sequence k_0 base rigidity parameter, which controls the ability of the model to respond to variations in the prior and likelihood data, was set to a single event per 1 cm of sedimentation but was allowed to vary between 0.01 and 100 events/cm to accommodate any major fluctuations in deposition rate. This additional flexibility is at the expense of precision in the final age model and results in a liberal estimate of uncertainties inherent in the data.

As part of the assessment of modelling priors, we used a common method for identifying change in linear records: pruned exact linear time (PELT) multi-changepoint analysis (Killick and Eckley, 2014). PELT was performed on the sediment inorganic content record and the μXRF Si, Ti, K and Zr data to identify any statistically significant changes in deposition mode, including potential sedimentation hiatuses (see Supplementary material for further details and results). These independently assigned changepoint locations were used to identify separate depositional units in the OxCal modelling framework (Figs. 3, S3), each of which was represented by a separate P_Sequence with delineating start and end boundaries, nested within a master Sequence according to stratigraphic priors. Posterior dated events were automatically calculated at 1 cm intervals throughout the sequence. Further details of the Bayesian age-depth modelling method are included in the Supplementary materials.

4. Results

4.1. Core correlation

Sequence slotting revealed that the top of the two cores were vertically offset by ~97 cm, rather than the 50 cm planned (Fig. 2). The unplanned offset meant that a total of 15 cm of sediment located at the end of several core drives was not recovered, with the largest contiguous gap being 4 cm. These lost sections did not coincide with the boundaries defined using change-point analysis.

4.2. μXRF normalisation and calibration

Eight of the twelve elements from the μXRF Fern Gully Lagoon sequence had significant correlations (at $p < 0.05$) with the WD-XRF samples when normalised by total counts per second, with the four best correlated elements returning a coefficient of determination of $r^2 > 0.8$, $p < 0.05$ (Table 1, Fig. S1). Normalisation via titanium, silicon or zircon was largely unsuccessful ($r^2 < 0.5$). Of the remaining 21 recorded elements not included in WD-XRF regressions, 14 could not be considered representative of elemental concentration either due to low mean counts per second (Striberger et al., 2010; Van der Bilt et al., 2015) or having > 5% of data with zero values (Sáez et al., 2009).

A lack of correlation between the incoherent/coherent scattering ratio and measured water content ($r^2 = 0.05$, $p < 0.05$, $n = 804$) indicated that it was not possible to correct the μXRF record for water content (see Boyle et al., 2015). However, calibration of the μXRF record by conventional XRF accounts for any offset due to water content. Inorganic content estimated by the incoherent/coherent scattering ratio, as used in many recent studies (e.g. Guyard et al., 2007; Jouve et al., 2013; Burrows et al., 2016; Mackenzie et al., 2017), had a very weak relationship ($r^2 = 0.09$, $p < 0.05$) to inorganic content estimated by LOI, possibly due to the very high organic content of the core sequence.

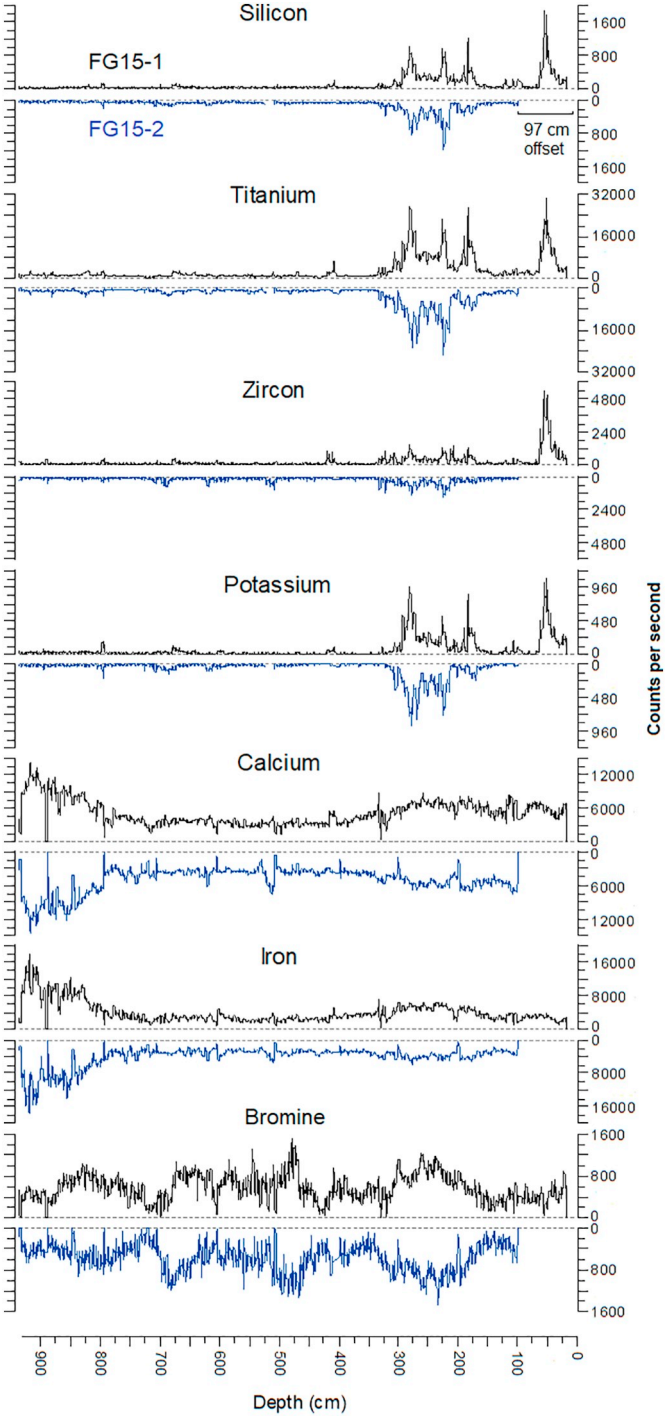

Fig. 2. Relative position of FG15-2 to FG15-1 using the seven elements exhibiting the highest counts per second.

4.3. Fern Gully Lagoon sediment composition

Fern Gully Lagoon sediments are black, finely grained and highly organic, with some macrofossils, such as roots and wood fragments. They have an average of only ~8% inorganic material by dry mass (Fig. 3). Water content is also high, at 36–93% of wet sample weight.

Table 1
Regressions of known quantities of oxides and elements via WD-XRF versus corrected µXRF data with methods ranked first in order of coefficient of determination then by number of p values < 0.05 (in bold). n = 20 for all r^2 values. Titanium, silicon and zircon normalisation had $r^2 < 0.5$, $p > 0.05$ in all cases and are not shown. cts/s: µXRF counts per second.

Element	Material quantified by XRF	Total cts/s normalised	Centred log ratio	Raw cts/s	Al normalised	Total scatter normalised	Incoherent scatter normalised
Zircon (Zr)	Pure element (ppm)	$\mathbf{r^2 = 0.93, p < 0.05}$	$\mathbf{r^2 = 0.65, p < 0.05}$	$\mathbf{r^2 = 0.92, p < 0.05}$	$\mathbf{r^2 = 0.83, p < 0.05}$	$\mathbf{r^2 = 0.92, p < 0.05}$	$\mathbf{r^2 = 0.92, p < 0.05}$
Titanium (Ti)	TiO_2	$\mathbf{r^2 = 0.88, p < 0.05}$	$\mathbf{r^2 = 0.66, p < 0.05}$	$\mathbf{r^2 = 0.90, p < 0.05}$	$\mathbf{r^2 = 0.80, p < 0.05}$	$\mathbf{r^2 = 0.90, p < 0.05}$	$\mathbf{r^2 = 0.89, p < 0.05}$
Potassium (K)	K_2O	$\mathbf{r^2 = 0.83, p < 0.05}$	$\mathbf{r^2 = 0.79, p < 0.05}$	$\mathbf{r^2 = 0.85, p < 0.05}$	$\mathbf{r^2 = 0.73, p < 0.05}$	$\mathbf{r^2 = 0.85, p < 0.05}$	$\mathbf{r^2 = 0.84, p < 0.05}$
Silicon (Si)	SiO_2	$\mathbf{r^2 = 0.80, p < 0.05}$	$\mathbf{r^2 = 0.57, p < 0.05}$	$\mathbf{r^2 = 0.78, p < 0.05}$	$\mathbf{r^2 = 0.65, p < 0.05}$	$\mathbf{r^2 = 0.77, p < 0.05}$	$\mathbf{r^2 = 0.76, p < 0.05}$
Bromine (Br)	Pure element (ppm)	$\mathbf{r^2 = 0.71, p < 0.05}$	$\mathbf{r^2 = 0.84, p < 0.05}$	$\mathbf{r^2 = 0.44, p < 0.05}$	$\mathbf{r^2 = 0.61, p < 0.05}$	$\mathbf{r^2 = 0.44, p < 0.05}$	$\mathbf{r^2 = 0.42, p < 0.05}$
Calcium (Ca)	CaO	$\mathbf{r^2 = 0.74, p < 0.05}$	$\mathbf{r^2 = 0.78, p < 0.05}$	$\mathbf{r^2 = 0.42, p < 0.05}$	$\mathbf{r^2 = 0.54, p < 0.05}$	$\mathbf{r^2 = 0.42, p < 0.05}$	$\mathbf{r^2 = 0.43, p < 0.05}$
Sulfur (S)	SO_3	$\mathbf{r^2 = 0.73, p < 0.05}$	$\mathbf{r^2 = 0.70, p < 0.05}$	$\mathbf{r^2 = 0.30, p < 0.05}$	$\mathbf{r^2 = 0.33, p < 0.05}$	$\mathbf{r^2 = 0.28, p < 0.05}$	$\mathbf{r^2 = 0.26, p < 0.05}$
Iron (Fe)	Fe_2O_3	$\mathbf{r^2 = 0.53, p < 0.05}$	$\mathbf{r^2 = 0.55, p < 0.05}$	$\mathbf{r^2 = 0.50, p < 0.05}$	$\mathbf{r^2 = 0.44, p < 0.05}$	$\mathbf{r^2 = 0.50, p < 0.05}$	$\mathbf{r^2 = 0.49, p < 0.05}$
Gallium (Ga)	Pure element (ppm)	$r^2 = 0.11$, p = 0.16	$r^2 = 0.19$, p = 0.05	$r^2 = 0.03$, p = 0.48	$\mathbf{r^2 = 0.20, p < 0.05}$	$r^2 = 0.01$, p = 0.69	$r^2 = 0.01$, p = 0.72
Aluminium (Al)	Al_2O_3	$r^2 = 0.09$, p = 0.19	$r^2 = 0.09$, p = 0.19	$\mathbf{r^2 = 0.62, p < 0.05}$	N/A	$\mathbf{r^2 = 0.67, p < 0.05}$	$\mathbf{r^2 = 0.69, p < 0.05}$
Magnesium (Mg)	MgO	$r^2 = 0.05$, p = 0.33	$\mathbf{r^2 = 0.85, p < 0.05}$	$r^2 < 0.01$, p = 0.79	$r^2 = 0.08$, p = 0.22	$r^2 = 0.02$, p = 0.60	$r^2 = 0.02$, p = 0.55
Phosphorus (P)	P_2O_5	$r^2 = 0.02$, p = 0.56	$\mathbf{r^2 = 0.46, p < 0.05}$	$r^2 = 0.11$, p = 0.14	$r^2 < 0.01$, p = 0.76	$r^2 = 0.12$, p = 0.13	$r^2 = 0.13$, p = 0.12

Fig. 3. Fern Gully Lagoon sediment stratigraphy, visible wavelength photography (brightened to show colour variation), sediment bulk density, water content, magnetic susceptibility, X-radiograph derived relative density, inorganic content and µXRF derived SiO_2 content. The four depositional boundaries used in the age model were derived from silicon µXRF counts per second (cts/s, Section 3.4 and Supplementary material). (For interpretation of the references to colour in this figure legend, the reader is referred to the web version of this article.)

Sediment density and water content remained relatively constant down core, with no overall monotonic trend (Fig. 3), demonstrating that there is little compaction of the sediments with increasing overburden pressure.

Both inorganic content and µXRF-derived silicon content exhibit several peaks and a plateau of ~10% inorganic content from ~170 to 270 cm (Fig. 2). Lower zircon levels in this part of the record likely indicate smaller average grain size (Cuven et al., 2010). There was a strong correlation ($r^2 = 0.70$, $p < 0.05$) between the LOI inorganic

Table 2
AMS radiocarbon ages. ^{14}C ages have been calibrated using the SHCal13 curve (Hogg et al., 2013) in OxCal v4.2.4. The calibrated age range shown is the 95.4% probability range (combining two or more potential calibration ranges, where they exist). All $\delta^{13}C$ values relate solely to the graphite derived from the fraction that was used for the radiocarbon measurement and have been derived using EA-IRMS. Uncalibrated ^{14}C ages have been corrected for isotopic fractionation using their measured $\delta^{13}C$ values and are quoted with their 1σ errors.

Sample ID	Lab ID (ANSTO)	Sample type	Depth (cm)	$\delta^{13}C$ (‰)	pMC (%)	Conventional ^{14}C Age (^{14}C yr BP)	Calibrated ^{14}C 95.4% probability range (cal. yr BP)
Fern Gully Core 1 (FG15-1)							
FG15 RC-1	OZU189	Terrestrial gum nut	34.5–35.5	−26.0 ± 0.2	87.83 ± 0.31	1040 ± 30	803–960
FG15 RC-2	OZU190	Terrestrial leaf fragment	34.5–35.5	−26.2 ± 0.1	90.62 ± 0.28	790 ± 30	655–730
FG15 RC-11	OZU792	Terrestrial bark fragment	78.5–79.5	−24.6 ± 0.1	24.52 ± 0.13	11,290 ± 40	13,036–13,211
FG15 RC-12*	OZU793	Reed stalk segment	78.5–79.5	−24.9[a]	46.07 ± 0.18	6225 ± 35	6952–7238
FG15 RC-3*	OZU191	Reed stalk segment	114.5–115.5	−25.7 ± 0.1	128.18 ± 0.61	Modern	Modern
FG15 RC-4	OZU192	Terrestrial seed	134.5–135.5	−24.1 ± 0.1	15.46 ± 0.11	15,000 ± 60	17,966–18,366
FG15 RC-5	OZU193	Terrestrial leaf fragment	134.5–135.5	−22.6 ± 0.1	16.49 ± 0.11	14,480 ± 60	17,392–17,849
FG15 RC-13	OZU794	Terrestrial bark fragment	158.5–159.5	−25.0 ± 0.2	13.16 ± 0.10	16,290 ± 60	19,422–19,870
FG15 RC-14*	OZU795	Reed stalk segment	158.5–159.5	−25.0[b]	78.69 ± 0.27	1925 ± 30	1736–1896
FG15 RC-6*	OZU194	Charcoal	174.5–175.5	−28.5 ± 0.1	2.94 ± 0.04	28,330 ± 120	31,637–32,682
FG15 RC-7*	OZU195	Reed stalk segment	214.5–215.5	−22.1 ± 0.3	97.97 ± 0.55	165 ± 50	Modern–281
FG15 RC-8*	OZU196	Charcoal	224.5–225.5	−26.7 ± 0.1	0.70 ± 0.03	39,880 ± 330	42,916–44,192
FG15 RC-15**	OZU796	Terrestrial bark fragment	227.5–228.5	−24.6 ± 0.1	0.71 ± 0.07	39,730 ± 810	42,343–44,960
FG15 RC-16*	OZU797	Charcoal	227.5–228.5	−26.5 ± 0.3	0.35 ± 0.06	45,400 ± 1500	46,377–[c]
FG15 RC-9*	OZU197	Charcoal	234.5–235.5	−27.2 ± 0.1	0.25 ± 0.02	48,200 ± 750	46,815–49,875
FG15 RC-10*	OZU198	Reed stalk segment	274.5–275.5	−23.4[a]	2.27 ± 0.07	30,420 ± 240	33,945–34,803
FG15 RC-17*	OZU798	Charcoal	287.5–288.5	−26.4 ± 0.1	0.41 ± 0.04	44,110 ± 850	45,785–49,430
FG15 RC-18*	OZU799	Reed stalk segment	287.5–288.5	−26.3[a]	0.96 ± 0.04	37,300 ± 360	41,178–42,297

* Age excluded from the age-depth model due to material type.
** Age eliminated from the final Bayesian model as it was identified as a major statistical outlier during initial modelling and prevented successful convergence.
[a] $\delta^{13}C$ values without associated uncertainty due to a limited number of determinations.
[b] $\delta^{13}C$ is assumed - measured value was not available.
[c] Maximum value beyond calibration range.

content and μXRF-derived silicon, indicating quartz sand is the major inorganic component of the sediment. While the magnetic susceptibility and X-radiograph records indicate variability in the lower part of the record, aligning with photographed banding (Fig. 3), the inorganic content and the μXRF silicon records indicate very little change, with largely consistent low quantities of inorganic material present.

4.4. ^{14}C dating

The AMS ^{14}C ages have a large amount of scatter (Table 2, Fig. 4). In general, the ^{14}C ages obtained from identifiable terrestrial macrofossils (gum nuts, seeds, leaves and bark fragments) are stratigraphically consistent over the uppermost 2 m of the core (n = 7) (Table 2). Three samples collected from below 1 m yield very young outliers: sample RC-3 from 115 cm has a modern ^{14}C age, and samples RC-7 and RC-14 from 159 cm and 215 cm, respectively, produced ages of < 2 cal. ka. These three samples were originally identified as reed stalk segments but were subsequently inferred to be root fragments. This re-interpretation was based on roots being identified during further sampling in the same core sections. Additional evidence for localised root penetration is apparent from some of the single-grain OSL D_e distributions (Section 4.5). Encouragingly, there is a broad agreement between the paired radiocarbon ages obtained at the same depths using terrestrial seeds and terrestrial leaf fragments (Table 2). However, there is an age offset of ~6 kyr for the replicate bark and reed stalk samples collected from a depth of 79 cm. This offset could again be attributed to misidentification of root material at this depth.

Five ^{14}C samples were single > 3 mm charcoal fragments. ^{14}C dating of charcoal can underestimate sample age in organic-rich wetlands unless prepared using a specific method to remove humic acid contamination (Nilsson et al., 2001; Turetsky et al., 2004; Brock et al., 2011). Contamination is particularly an issue for old samples where small concentrations of humic acid can produce large underestimations (e.g. 1% modern carbon contamination can cause a 15 kyr underestimation in a 50 ka sample) (Brock et al., 2011). As the charcoal samples from Fern Gully Lagoon were prepared using ABA, the resultant ages may have been inadvertently affected by humic acid contamination (Brock et al., 2010). Indeed, there is some evidence to suggest this might be the case for the three charcoal samples collected from depths of 228, 235 and 288 cm, which have statistically indistinguishable 2σ calibrated age ranges (Fig. 4, Table 2).

4.5. OSL dating

The single-grain OSL dating results are summarised in Table 3, with representative single-grain D_e distributions shown as radial plots in Fig. 5. The OSL samples from Fern Gully Lagoon exhibit a broad range of D_e distribution characteristics, indicative of spatially and temporally variable bleaching and mixing conditions at the site (e.g., Arnold et al., 2009; Arnold et al., 2007, 2008, 2012). Full discussions of the single-grain D_e distributions and statistical age models used to derive representative burial dose estimates for each sample are provided in the Supplementary materials.

The final OSL ages exhibit good stratigraphic consistency for thirteen of the nineteen samples (Table 3). The remaining six samples (FG15 OSL-1, -8, -8-2, -9, -10 and -16) yield very young, outlying and inverted ages of between 6.69 ± 2.0 ka to 21.2 ± 2.6 ka for the lowermost 7 m of the core sequence. These outlying ages in the lowermost 7 m of the core are in keeping with the complex D_e distribution characteristics observed for the six samples, which are characterised by very high overdispersion values (53–119%) and multiple discrete dose components (Fig. S7). These multimodal D_e datasets are interpreted as reflecting the presence of locally intruded young grain populations. These populations could potentially be the result of sporadic lake

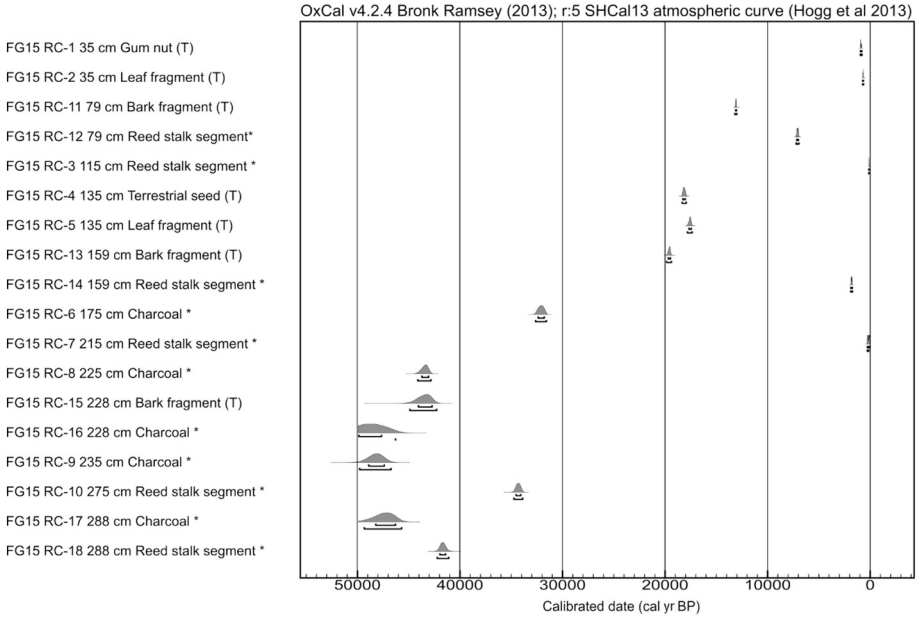

Fig. 4. Calibrated radiocarbon age probability distributions with calibrated 68.2% and 95.4% age ranges. * denotes an age excluded from the age-depth model due to material type. (T): a terrestrial source.

desiccation and the formation of deep surface cracks (a process that is visible today in analogous peat-rich wetlands on NSI) and, or, downward grain transportation via root penetration into older sediments, as has been found previously (e.g. Bateman et al., 2007; Brill et al., 2012). These interpretations are consistent with the presence of modern or near-modern organic remains at depths > 1 m in the ^{14}C study (Section 4.4).

Assuming that the multiple discrete dose components of FG15 OSL-1, -8, -8 2, -9, -10 and -16 can be explained by localised post-depositional mixing, it follows that the bulk (sample-average) dose rate of these six samples may not be entirely representative of that experienced by either dose component during burial. Owing to the impracticalities of retrospectively deriving a component-specific dose rate for the multiple identified components, these samples are not considered suitable for dating. The ages shown for these samples in Table 3 are included for indicative purposes only and have not been included as likelihood estimates in the Bayesian age model.

4.6. Bayesian age-depth model

Thirteen single-grain OSL ages and eighteen ^{14}C ages were included in the Bayesian age modelling procedure, separated by three depositional boundaries. A preliminary version of the model tested using these 31 likelihood estimates failed to converge owing to the identification of major statistical outliers. We excluded all potentially inaccurate charcoal and misidentified reed stalk ages from the second model (see Table 2). The youngest charcoal ^{14}C sample (FG15 RC-6) had an age that was consistent with the OSL sample collected at 175 cm depth (FG15 OSL-18) (see Section 4.2), suggesting that it may not be affected by humic acid contamination. However, for the sake of consistency, it was excluded from further consideration. These quality control measures resulted in only seven of the original eighteen ^{14}C likelihood estimates being included in the second Bayesian age model. A preliminary version of this model failed to converge owing to the identification of a major statistical outlier (sample FG15 RC-15). It was, therefore, necessary to eliminate this ^{14}C likelihood estimate in the final Bayesian model.

The Bayesian model for Fern Gully Lagoon has A_{model} and $A_{overall}$ values of 62.3% and 64.6%, respectively, marginally exceeding the minimum acceptance threshold of 60% and thus indicating a valid model (Bronk Ramsey, 2009). The modelling results are summarised in Table S4 and illustrated in Fig. 6. The final model indicates a basal age of 209.3 ± 28.4 ka (± 2σ) at 900 cm, in agreement with the previously measured basal age of 208.4 ± 32.5 ka on an adjacent preliminary core (Ad13069, Tibby et al. (2017)). The model reveals four distinct sedimentation phases separated by hiatuses: a late MIS 7 to early MIS 6 phase (209.3 ± 28.4 ka to 177.5 ± 25.4 ka, 930–288 cm), a late MIS 6 to late MIS 3 phase (155.2 ± 24.9 to 34.7 ± 14.5, 288–166 cm), a mid-MIS 2 to mid-Holocene phase (20.9 ± 1.4 ka to 6.5 ± 5.6 ka, 166–52 cm) and a late Holocene phase (1.7 ± 1.0 ka to 0.45 ± 0.4 ka, 52–0 cm) (± 2σ, Table S4, Fig. 6). The average sedimentation rates of these four phases are (from bottom to top) 0.20 m/kyr, 0.01 m/kyr, 0.08 m/kyr and 0.31 m/kyr.

4.7. Identifying aeolian and autochthonous wetland sediment

Broken stick analysis revealed two significant principal components in the μXRF data (Fig. S2), which combined reflect > 97% of the variance in the data. Co-varying silicon, titanium, potassium and zircon defined much of PC1. PC1 is very similar to the local aeolian signature identified by McGowan et al. (2008), and we, therefore, associate PC1 with local aeolian input. PC2 was defined by iron and calcium and is likely associated with a secondary aeolian source or internal wetland processes (Fig. 7). Unfortunately, the position of iron and calcium compounds within the sediment may have been altered post-sedimentation, such as by changing redox, rendering the identification of a source material difficult. Inorganic MIS 5 and Holocene sediments from Fern Gully Lagoon are most similar to contemporary local dune surface and subsurface samples, while the closest source material to MIS 7 inorganics is Dunwich sandstone, which contains notable quantities of iron and calcium.

4.8. Inorganic sedimentation at Fern Gully Lagoon

The influx of aeolian inorganics was highly variable over the past 209 ka (Fig. 8). Aeolian inorganic input during MIS 7a–c and early MIS 6 (209.3 ± 28.4 ka to 177.5 ± 25.4 ka) was low while other inorganic sedimentation (represented by calcium and iron dominated inputs) gradually declined. The earliest phase had a high rate of total sedimentation, but no notable inorganic peaks. During the late MIS 6 to

Table 3
Dose rate data, equivalent doses (D_e), overdispersion values, and OSL ages for lacustrine samples from Fern Gully Lagoon, NSI. The final OSL age of each sample has been calculated by dividing the D_e value by the total dose rate.

Sample (core)	Depth (cm)	Water content (% dry weight)[a]	Environmental dose rate (Gy/kyr)[b,c,d,e,f]					Equivalent dose (D_e) data			D_e (Gy)[f]	Final age (ka)[f,j]
			Beta dose rate	Gamma dose rate	Internal dose rate	Cosmic dose rate	Total dose rate	No. of grains[h]	Overdispersion (σ_b) (%)[i]	Age model[g]		
FG15 OSL-18 (1)	171–180	320/404/507	0.03 ± 0.005	0.03 ± 0.0007	0.02 ± 0.007	0.03 ± 0.003	0.11 ± 0.01	102	50.3 ± 4.2	MAM-3	3.60 ± 0.8	33.2 ± 8.0
FG15 OSL-17 (1)	181–190	342/361/497	0.03 ± 0.005	0.03 ± 0.0009	0.02 ± 0.007	0.03 ± 0.003	0.12 ± 0.01	52	50.9 ± 5.8	CAM	9.08 ± 0.7	77.7 ± 9.2
FG15 OSL-16 2 (2)	204–213	386/344/484	0.01 ± 0.003	0.02 ± 0.0006	0.02 ± 0.007	0.03 ± 0.003	0.09 ± 0.01	117	39.5 ± 2.9	MAM-3	14.3 ± 0.6	128 ± 15.3
FG15 OSL-16 (1)[k]	204–213	386/344/484	0.03 ± 0.006	0.027 ± 0.001	0.02 ± 0.007	0.03 ± 0.003	0.11 ± 0.01	50	92.2 ± 10.7	MAM-3	1.48 ± 0.1	13.3 ± 2.0
FG15 OSL-15 (1)	214–223	336/363/477	0.03 ± 0.005	0.03 ± 0.0009	0.02 ± 0.007	0.03 ± 0.003	0.12 ± 0.01	96	41.3 ± 3.6	CAM	11.4 ± 0.5	95.5 ± 9.73
FG15 OSL-14 (1)	235–244	408/378/468	0.02 ± 0.003	0.03 ± 0.0007	0.02 ± 0.007	0.03 ± 0.003	0.09 ± 0.009	33	34.5 ± 5.4	CAM	12.7 ± 0.9	135 ± 16.3
FG15 OSL-13 (1)	263–272	406/399/460	0.02 ± 0.004	0.04 ± 0.008	0.02 ± 0.007	0.03 ± 0.003	0.1 ± 0.01	37	34.0 ± 5.0	CAM	14.7 ± 0.9	132 ± 20.3
FG15 OSL-12 (1)	273–282	362/402/456	0.04 ± 0.007	0.03 ± 0.003	0.02 ± 0.007	0.03 ± 0.003	0.1 ± 0.01	131	34.4 ± 2.5	CAM	16.4 ± 0.5	137 ± 15.4
FG15 OSL-11 (1)	283–292	446/426/456	0.02 ± 0.003	0.02 ± 0.01	0.02 ± 0.007	0.03 ± 0.003	0.09 ± 0.02	82	28.9 ± 2.8	CAM	14.8 ± 0.5	171 ± 33.4
FG15 OSL-10 2 (2)	306–315	545/433/457	0.004 ± 0.001	0.007 ± 0.0003	0.02 ± 0.007	0.03 ± 0.003	0.06 ± 0.008	63	33.2 ± 3.7	CAM	13.8 ± 0.6	179 ± 22.4
FG15 OSL-10 (1)[k]	306–315	545/433/457	0.01 ± 0.003	0.01 ± 0.0005	0.02 ± 0.007	0.03 ± 0.003	0.08 ± 0.009	86	53.3 ± 6.1	MAM-3	1.65 ± 0.1	21.2 ± 2.6
FG15 OSL-9 (1)[k]	326–335	380/450/455	0.01 ± 0.002	0.02 ± 0.003	0.02 ± 0.007	0.03 ± 0.003	0.08 ± 0.009	82	118.5 ± 10.6	MAM-4	1.59 ± 0.1	20.0 ± 2.8
FG15 OSL-8 (1)[k]	405–414	572/673/477	0.009 ± 0.002	0.02 ± 0.0005	0.02 ± 0.007	0.03 ± 0.003	0.08 ± 0.008	80	76.9 ± 8.4	MAM-4	1.40 ± 0.1	19.9 ± 2.7
FG15 OSL-8 2 (2)[k]	405–414	572/673/477	0.02 ± 0.004	0.02 ± 0.0005	0.02 ± 0.007	0.03 ± 0.003	0.08 ± 0.009	51	94.8 ± 10.5	MAM-4	1.48 ± 0.1	17.5 ± 2.3
FG15 OSL-5 (1)	655–674	629/666/578	0.005 ± 0.001	0.003 ± 0.0002	0.02 ± 0.007	0.02 ± 0.002	0.05 ± 0.008	37	39.2 ± 5.7	CAM	12.6 ± 0.7	248 ± 40.6
FG15 OSL-4 (2)	777–801	438/477/577	0.007 ± 0.001	0.007 ± 0.0003	0.02 ± 0.007	0.02 ± 0.002	0.06 ± 0.008	85	32.5 ± 3.0	CAM	11.6 ± 0.5	206 ± 29.4
FG15 OSL-3 (1)	813–832	443/439/572	0.004 ± 0.001	0.008 ± 0.002	0.02 ± 0.007	0.02 ± 0.002	0.05 ± 0.008	66	26.7 ± 3.2	CAM	10.8 ± 0.4	201 ± 30.4
FG15 OSL-2 (1)	833–857	397/434/567	0.008 ± 0.001	0.007 ± 0.0005	0.02 ± 0.007	0.02 ± 0.002	0.06 ± 0.008	50	52.4 ± 5.8	MAM-4	10.4 ± 0.6	180 ± 26.4
FG15 OSL-1 (2)[k]	893–926	343/394/561	0.009 ± 0.001	0.006 ± 0.0005	0.02 ± 0.007	0.02 ± 0.002	0.06 ± 0.008	63	88.8 ± 12.8	MAM-3	0.38 ± 0.1	6.69 ± 2.0

[a] Long-term water contents used for beta/gamma/cosmic-ray dose rate attenuation, expressed as % of dry mass of mineral fraction, with an assigned relative uncertainty of ± 10%. The final beta dose rates have been adjusted for moisture attenuation using the average water content from the midpoint of each OSL sample depth. The final gamma dose rates have been adjusted using the water content determined separately for the gamma dose rate bulk sediment samples, which were collected for each OSL sample depth, as well as for the overlying and underlying 10 cm depth. The final cosmic-ray dose rates have been adjusted using the average water content measured from the contiguous 1 cm^3 bulk sediment samples collected throughout the overlying core sequence.

[b] Beta, gamma and internal dose rates have been calculated on dried and powdered sediment samples using ICP-MS and ICP-OES. The beta dose rates have been calculated on bulk sediment samples collected from each OSL sample depth. The gamma dose rates have been determined separately on bulk sediment samples collected for each OSL sample depth, as well as for the overlying and underlying 10 cm depth of each OSL sample position, following De Deckker et al. (2019).

[c] Radionuclide concentrations have been converted to alpha, beta and gamma dose rates using the published conversion factors of Guérin et al. (2011), and allowing for beta-dose attenuation (Mejdahl, 1979; Brennan, 2003) and long-term water content correction (Aitken, 1985).

[d] An internal dose rate of 0.02 ± 0.007 Gy/kyr has been included in the final dose rate calculations of all samples, based on ICP-MS U and Th measurements made on etched quartz grains from associated aeolian deposits at Welsby Lagoon (Lewis et al., in prep) and an alpha efficiency factor (*a* value) of 0.04 ± 0.01 (Rees-Jones, 1995; Rees-Jones and Tite, 1997).

[e] Cosmic-ray dose rates were calculated after Prescott and Hutton (1994), and assigned a relative uncertainty of ± 10%.

[f] Mean ± total uncertainty (68% confidence interval), calculated as the quadratic sum of the random and systematic uncertainties.

[g] SG OSL = single-grain optically stimulated luminescence; MAM-3 = three-parameter minimum age model (Arnold et al., 2009), MAM-4 = four-parameter minimum age model (Arnold et al., 2009); CAM = Central age model (Galbraith et al., 1999). MAM-3 and MAM-4 D_e estimates were calculated after adding, in quadrature, a relative error of 25% to each individual D_e measurement error to approximate the underlying dose overdispersion observed in an 'ideal' (well-bleached and unmixed) sedimentary sample from this core (FG15 OSL-3), which is consistent with global overdispersion datasets (Arnold et al., 2009).

[h] Number of D_e measurements that passed the SAR quality assurance criteria and were used for D_e determination.

[i] The relative spread in the D_e dataset beyond that associated with the measurement uncertainties for individual D_e values, calculated using the CAM.

[j] Total uncertainty includes a systematic component of ± 2% associated with laboratory beta-source calibration.

[k] Samples excluded from the Bayesian model as they contain multiple discrete dose populations when fitted with the FMM (see Section 3.5 for details).

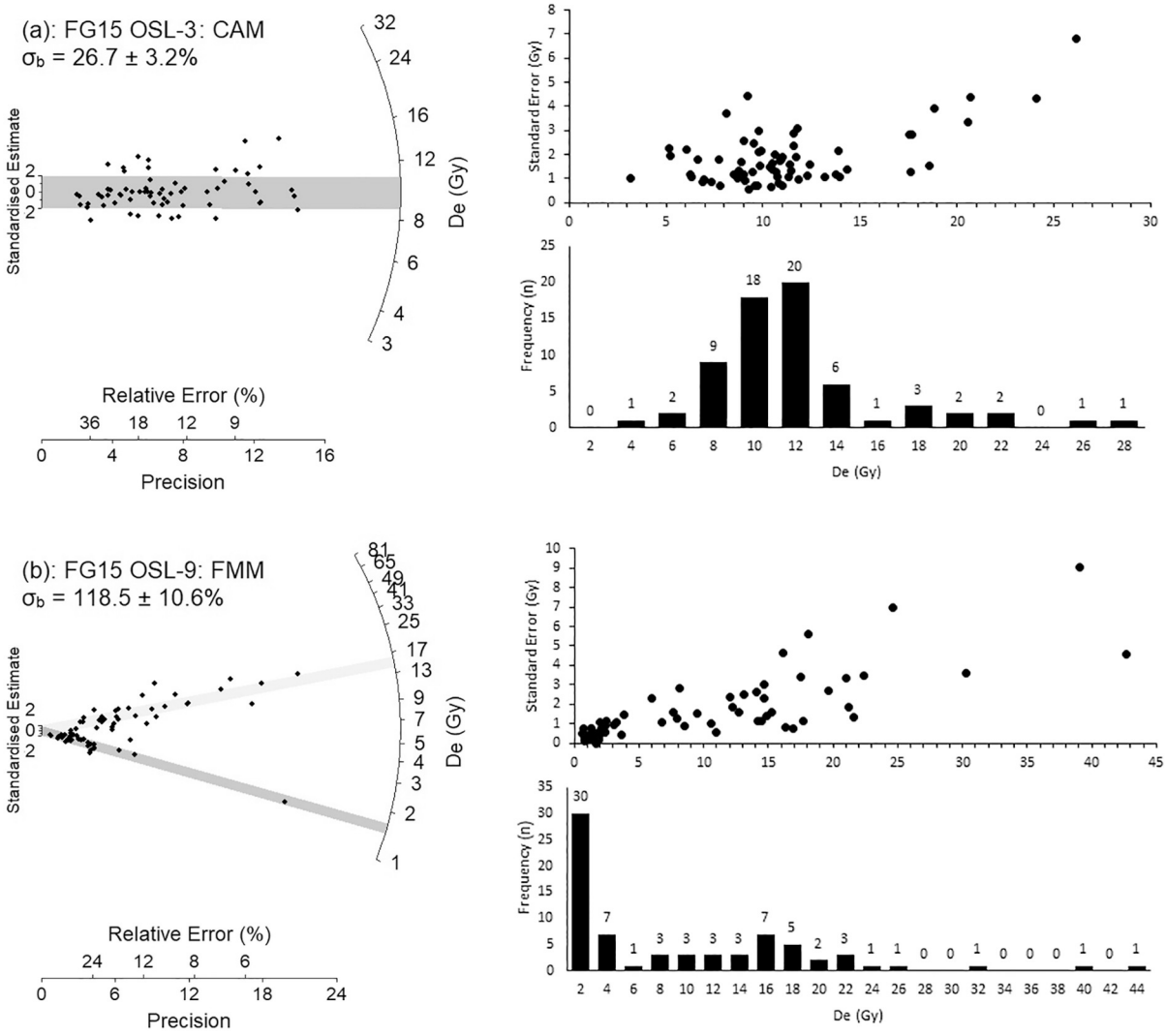

Fig. 5. Example single-grain D_e distributions shown as radial plots and frequency histograms with ranked plots of D_e versus standard error. (a) Samples FG15 OSL-3 (813–832 cm depth), which was considered suitable for dating using the central age model (CAM). The grey bar on the radial plot is centred on the CAM D_e value used to derive the final burial dose of this sample; (b) Sample FG15 OSL-9 (326–335 cm depth), which was not considered suitable for dating because it contains multiple discrete dose populations, as identified by the finite mixture model (FMM). The two dose components identified by the FMM are shown by the light and dark grey bands in the radial plot. Individual D_e estimates are presented with their 1σ error ranges, which are derived from a random uncertainty term arising from photon counting statistics for each OSL measurement, an empirically determined instrument reproducibility uncertainty of 2.5% (following the approach outlined in Jacobs et al. (2006)) and a dose-response curve fitting uncertainty determined using 1000 iterations of the Monte Carlo method implemented in Analyst (Duller, 2015).

late MIS 3 phase (155.2 ± 24.9 to 34.7 ± 14.5 ka), there were aeolian inorganic peaks at ~144 ± 10 ka (LOI, magnetic susceptibility, PC1), ~100 ± 8 ka (LOI, PC1) and ~52 ± 11 ka (PC1). During the mid-MIS 2 to mid-Holocene phase (20.9 ± 0.8 to 6.5 ± 2.8 ka), there were some small inorganic peaks from ~14 to 11 ka. Aeolian inorganic sedimentation peaks during the late Holocene, with ~95% inorganic sediments recorded at ~1.6 ± 0.5 ka (magnetic susceptibility, LOI, PC1). While wetland desiccation and cracking during dry periods, indicated by OSL D_e distributions, may have displaced quartz sand grains from their original position in the sediment, it is unlikely that this had more than a minor influence on the aeolian inorganic record, as most sediment would have remained intact.

5. Discussion

5.1. μXRF sediment analysis of highly organic wetlands

The most commonly used μXRF normalisation method (Table S5) – normalisation by total counts per second – was the most suitable for calibrating inorganic elements in the highly organic Fern Gully Lagoon sediments. However, raw counts per second had comparable or better performance than most normalisation methods, indicating that raw data may be used in some circumstances (Table 1). The best performing method for correcting μXRF data appeared to depend on the element(s) under consideration. For example, centred log-ratio correction resulted in the best correlation to WD-XRF particularly for magnesium, bromine and calcium (r^2 = 0.85, r^2 = 0.84 and r^2 = 0.78 respectively, where $p < 0.05$, n = 20 for all values), while multiple normalisation methods for aluminium had similarly good r^2 values (0.62–0.69, Table 1). For μXRF analysis of highly organic sediments, the optimal method may be to determine the most suitable normalisation method for each element before calibration, rather than using a single normalisation method. If testing of multiple normalisation methods is not possible, centred log-ratio normalisation will produce the best results in the majority of cases, as it has been mathematically proven to counter the closed sum and other distorting effects inherent in μXRF data (Weltje and Tjallingii, 2008; Croudace and Rothwell, 2015).

Several recent palaeoclimate reconstructions from wetland

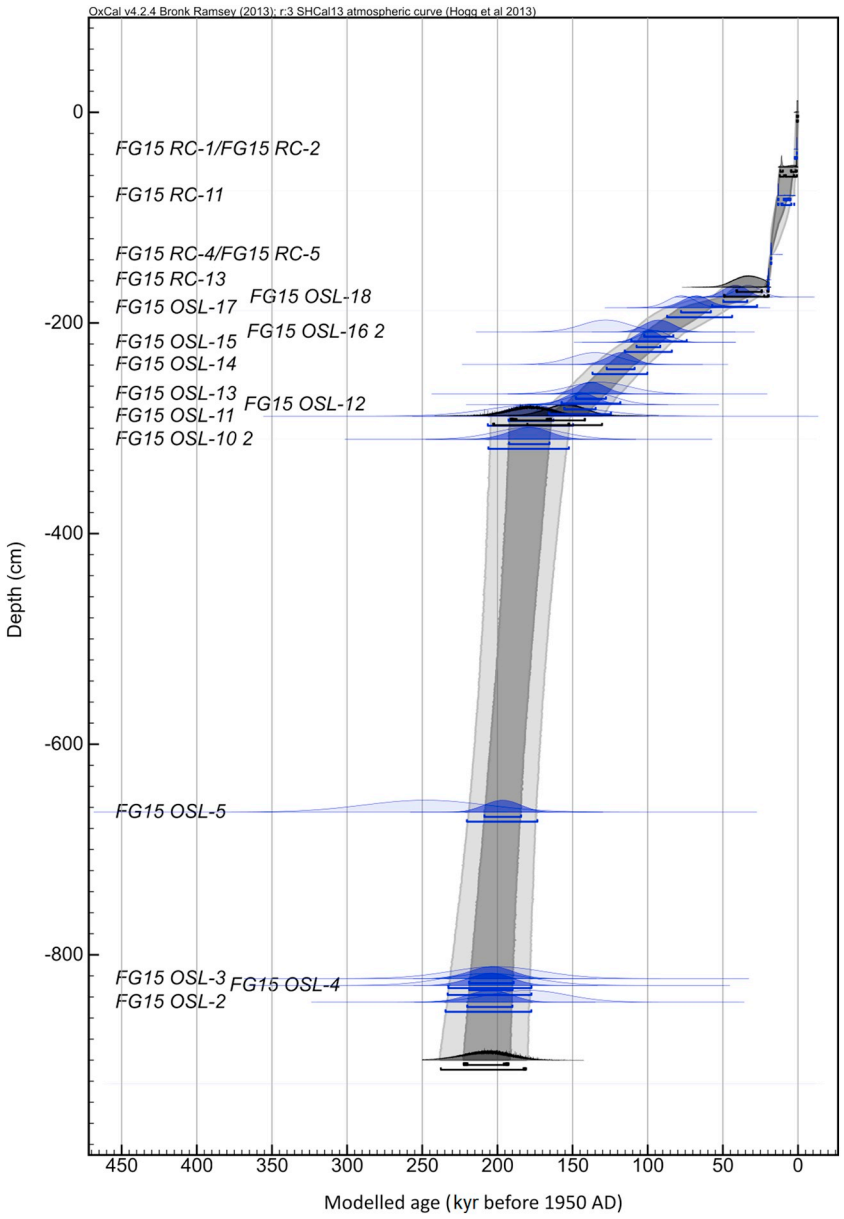

Fig. 6. Bayesian age/depth model for the Fern Gully Lagoon sequence obtained using a non-continuous deposition scenario. The prior age distributions for the dating samples (likelihoods) are shown in light blue. The modelled posterior distributions for the dating samples and unit boundaries are shown in dark blue and grey, respectively. Likelihood and posterior ages are shown on a calendar year timescale and expressed in years before 1950 CE. The 68.2% and 95.4% ranges of the posterior probabilities are indicated by the light and dark shading. (For interpretation of the references to colour in this figure legend, the reader is referred to the web version of this article.)

sediments have relied on μXRF derived iron (e.g. Rees et al., 2015; Burrows et al., 2016; Stephens et al., 2018) or magnesium (Foerster et al., 2018) records to infer, for example, waterlogged soils, redox conditions and detrital input. However, our analysis indicates that these elements may not be accurately characterised by μXRF in highly organic sediment. Bromine was used as an indicator of organic content in the Paddy's Lake record (north-western Tasmania), supported by the incoherent to coherent ratio (inc/coh) (Beck et al., 2017). However, while inc/coh and bromine correlate, neither correlated well with organic content in our study ($r^2 < 0.003$, $p = 0.132$, $n = 804$ and $r^2 = 0.05$, $p < 0.05$, $n = 804$ respectively). Indeed, the use of inc/coh requires additional stages of calibration to accurately indicate organic content (Woodward and Gadd, 2019). While some recent studies have validated the use of the μXRF inc/coh for estimating organic content (e.g. Field et al., 2018; Woodward et al., 2018), a number have not (e.g. Rees et al., 2015; Turner et al., 2015; Burrows et al., 2016; Pleskot et al., 2018). Standardising normalisation and calibration of μXRF records as a minimum requirement for μXRF derived climate studies would improve record precision and reduce uncertainty in future work.

5.2. Dating wetland sediments

Reliable dating of Australian palaeoclimate sequences that span multiple past interglacial periods has proved difficult, although luminescence dating offers a potentially useful means of filling chronological gaps across a range of palaeoenvironmental contexts (Fu et al., 2017; Roberts et al., 2018; De Deckker et al., 2019). This study highlights the complexities that can be encountered when using single-grain OSL and ^{14}C dating in organic-rich peaty wetlands. By employing both techniques, it has been possible to better diagnose complications related to material selection (e.g., root fragments and charcoal), post-depositional mixing, and heterogeneous bleaching of sand grains. While a relatively high proportion of the original dating samples were unsuitable for inclusion in the final age model (i.e. 67% of the eighteen ^{14}C samples and 32% of the nineteen OSL samples), our results highlight the general suitability of ^{14}C and OSL dating in this depositional context when targeting optimal sampling materials, laboratory protocols and scales of analysis. Careful consideration of dating quality control has proved critical for deriving a meaningful age-depth model at Fern Gully Lagoon. There is good scope for using systematic single-

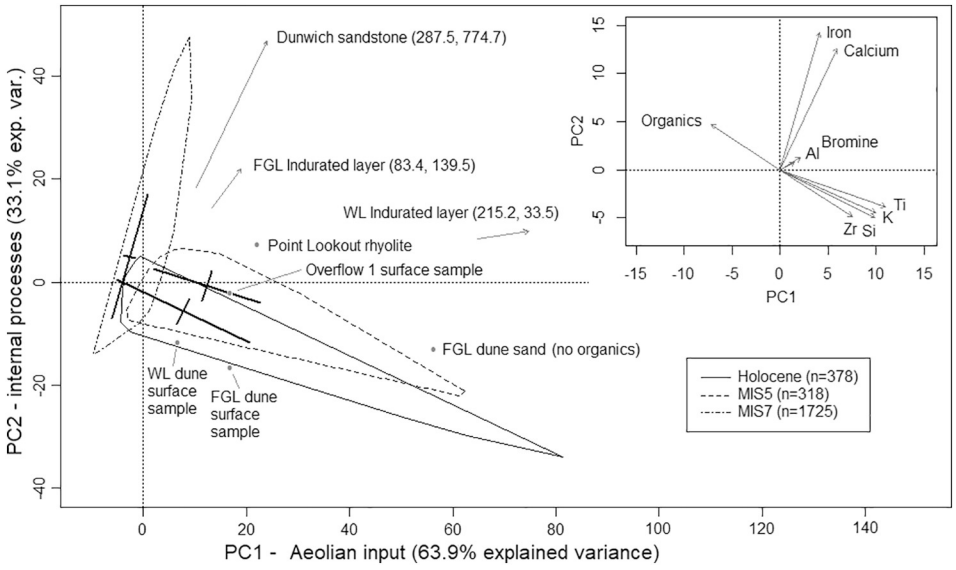

Fig. 7. PCA biplot of μXRF elements and organic content from Fern Gully Lagoon. Crosses indicate the distribution mean and one standard deviation of the two principal axes of each distribution, while the outer polygon indicates the extent of the samples. Local inorganic source materials are indicated by grey points and grey arrows where these points lie outside the plot. Al: aluminium; Ti: titanium; K: potassium; Si: silicon; Zr: zirconium.

grain OSL dating studies to refine the chronology of other Australian interglacial records.

5.3. Fern Gully Lagoon sediment hiatuses

Age-depth modelling indicates that there were three hiatuses in sedimentation at ~177 to 155 ka, ~34.7 to 20.9 ka and 6.5 to 1.7 ka. Palaeoclimate reconstructions from nearby wetland sites on North Stradbroke and Fraser Islands have revealed sedimentary hiatuses during dry periods such as the LGM (Donders et al., 2006; Woltering et al., 2014). Unfortunately, there are no nearby records of sufficient age and resolution to allow comparison of pre-MIS 5 hiatuses at FGL. The timing of two hiatuses in the Fern Gully Lagoon record during mid-MIS 6 and late MIS 3 to mid-MIS 2 are consistent with drier climates observed in a number of Australian records, both in north-east (Kershaw et al., 2007a; Moss and Kershaw, 2007) and central Australia (Fu et al., 2017). The start of the mid-MIS 3 sedimentary hiatus in Fern Gully Lagoon aligns with the commencement of widespread drying of Australia (Kemp et al., 2019), and occurs at the same time as drying in nearby Welsby Lagoon (Cadd et al., 2018). The mid-Holocene hiatus at Fern Gully Lagoon has no equivalent from Welsby Lagoon (Cadd et al., 2018), although Fern Gully Lagoon may be more hydrologically sensitive due to its smaller catchment. Lower rainfall was noted at Swallow Lagoon after ~3 ka (Barr et al., 2019), while mid-Holocene hiatuses or drier phases were recorded at Hidden Lake and Lake Allom on nearby Fraser Island (Longmore, 1997; Donders et al., 2006).

The absence of a hiatus at Welsby Lagoon during the late Holocene after ~3 ka may possibly be due to a fire which burned Fern Gully Lagoon but not Welsby Lagoon. Loss of wetland peat due to fire may exceed 50 cm in a single event (in which a peatland may burn for more than a month) – high peat density and peat moisture content lower than 16% contribute to the loss of greatest material (Ballhorn et al., 2009; Davies et al., 2013; Lukenbach et al., 2015). However, an initial study of sedimentary charcoal did not indicate higher levels during this period (Kemp, unpublished data), and there is no notable change in the calcium record (Fig. 2) which could indicate mineralisation within the sediment as the result of a major peat fire (Smith et al., 2001). Therefore, it is more likely that Fern Gully Lagoon is more hydrologically sensitive than Welsby Lagoon, and drying led to a late-Holocene hiatus, rather than loss of peat due to a major fire event.

5.4. Palaeoclimate interpretation and comparison with other records

We interpret increased aeolian inorganic sedimentation in Fern Gully Lagoon as indicative of dry climates, as reduced vegetation cover increases local wind erosion (McGowan et al., 2008). While changes in wind strength could also be a major source of changing inorganic flux, records of terrestrial dust grain size from the Tasman Sea indicate that regional wind strength was secondary to continental drying in explaining regional aeolian inorganic transport (Hesse and McTainsh, 2003). Increased biomass burning on NSI is a possible additional driver for increased inorganic sedimentation. However, macrocharcoal and the proportion of sediment inorganic matter are uncorrelated at Fern Gully Lagoon ($r^2 = 0.04$, $p > 0.05$, $n = 632$ (Kemp, unpublished data)), a situation similar to nearby Welsby Lagoon (Barr et al., 2017). Hence, it appears that increased biomass burning did not play a large role in increasing wind erosion on NSI. Sea-level transgression does not appear to drive inorganic flux to Fern Gully Lagoon as the major marine transgressions during late MIS 6 and after the LGM do not coincide with increased inorganic flux (Fig. 8). However, the lack of inorganic sediment immediately after the LGM may also be due to a change in the dominant regional wind direction which deposited sands offshore as postulated by Walker et al. (2018).

We compared our results to the ~33 kyr inorganic flux record from Native Companion Lagoon (McGowan et al., 2008; Petherick et al., 2008) (Fig. 8) and the ~37 kyr record from Tortoise Lagoon (Petherick et al., 2017). The NCL record indicates that a dry phase occurred during the LGM as well as an increase in inorganic sedimentation at ~3 ka (McGowan et al., 2008). While Tortoise Lagoon records a similar LGM peak, there is no increase late-Holocene inorganic sedimentation (Petherick et al., 2017). The LGM inorganic peak was not recorded at Fern Gully Lagoon due to a hiatus, the LGM hiatus itself indicates that Fern Gully Lagoon was similarly dry.

The Fern Gully Lagoon sequence recorded low aeolian sedimentation with low PC1 scores and the lowest inorganic content (~3%), during MIS 7a–c, indicating that it was likely the wettest interglacial of the past three in subtropical eastern Australia. This finding is similar to the record of moisture availability from central Australia, where recorded lake levels reached their highest for the past ~250 ka (Fu et al., 2017); Lynch's Crater in north-east Australia, where there were wet climates with open water present (Kershaw et al., 2007b), and Naracoorte caves in south-east Australia, where pronounced periods of calcitic growth occurred (Ayliffe et al., 1998). In comparison, there was greater aeolian input during MIS 5, indicating a drier local climate than in MIS 7a–c (Fig. 8; MIS 5 average ~0.24 kg/m^2/kyr vs average ~0.14 kg/m^2/kyr inorganics). The record also contains a notable MIS 5 dry period at 100 ± 15.6 ka. A similar comparatively drier mid-MIS 5b–d from ~110 to 90 ka has been observed in other regions, most

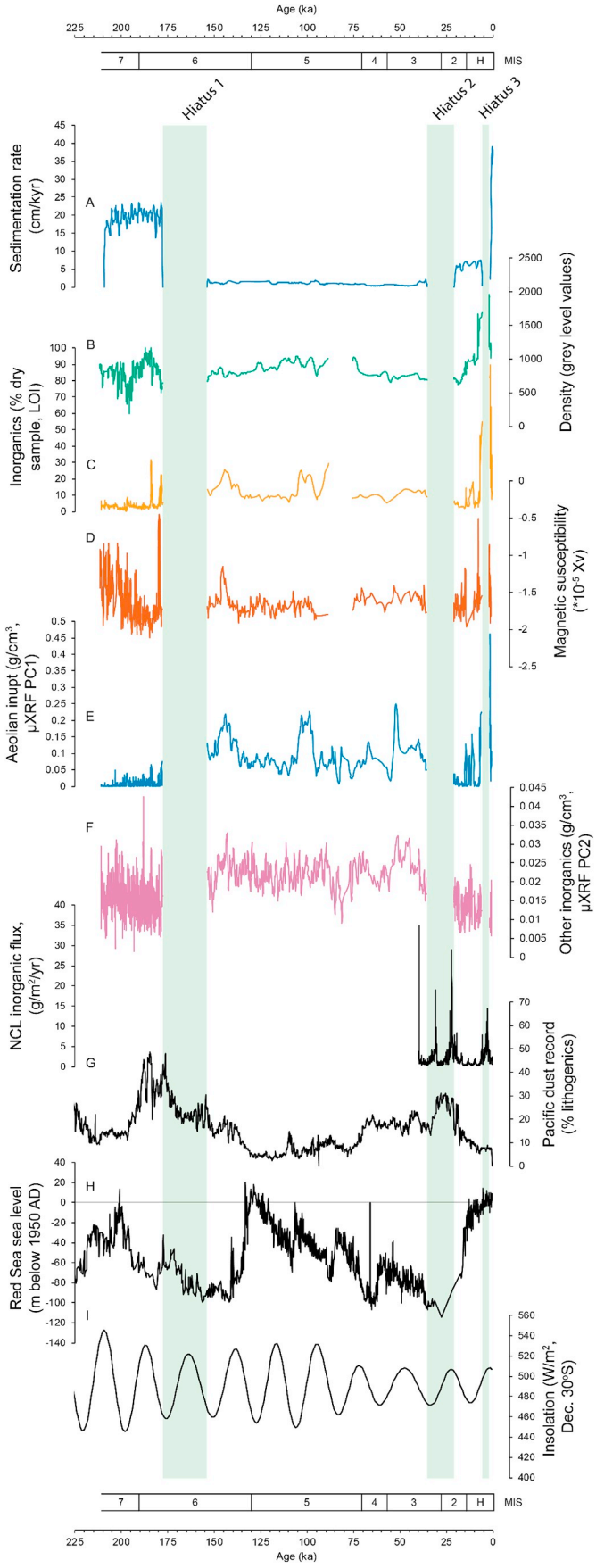

Fig. 8. Sedimentation rate (3 cm moving average), sediment density (X-radiograph), inorganic content, magnetic susceptibility, calibrated µXRF aeolian input (silicon, potassium, zircon and titanium, PC1) and other calibrated µXRF inorganic sedimentation (calcium and iron, PC2). Records for comparison are Native Companion Lagoon (NCL) (Petherick et al., 2008), an Australian dust record from the South Pacific (Lamy et al., 2014), a global sea level record from the Red Sea (Rohling et al., 2009) and December mean insolation for 30° south (Berger and Loutre, 1991).

notably in tropical north-east Australia (Kershaw et al., 2007a). Conversely, central Australian lakes maintained shallow to deep-water conditions during MIS 5 (Bowler et al., 1998; Fu et al., 2017), while calcite growth occurred after ~105 ka (Ayliffe et al., 1998).

During the Holocene, inorganic aeolian deposition at Fern Gully Lagoon averaged ~0.96 kg/m^2/kyr, four times greater than during MIS 5 and almost seven times MIS 7 levels. Greater inorganic flux, in combination with high PC1 scores, suggests the Holocene is the driest interglacial of the last three for subtropical eastern Australia. A drier Holocene relative to MIS 7a–c and MIS 5 is observed in several other Australian records, either via increased dry forest and herbaceous vegetation (Harle et al., 2002; Moss and Kershaw, 2007) or lower flows and lake filling (Maroulis et al., 2007; Nanson et al., 2008; Fu et al., 2017). Holocene drying has been attributed to increasing El Niño frequency compared to past interglacials (Moss and Kershaw, 2007), or to the extended period of high sea levels during the Holocene limiting WPWP influence on monsoonal precipitation and the warm East Australian Current (Nanson et al., 2008). Holocene inorganic sedimentation at Fern Gully Lagoon may also be influenced by human-induced biomass burning. There is a long record of human activity on the island (Neal and Stock, 1986) which may have also contributed to mobilisation of dune sands. However, the paucity of dated archaeology close to Fern Gully Lagoon currently precludes an assessment of human influence on the Fern Gully record.

The pattern of increasingly dry interglacials observed at Fern Gully Lagoon since MIS 7 is consistent with the few other Australian records covering this period, most notably in central Australia (Bowler et al., 2001; Cohen et al., 2015; Fu et al., 2017), but also in the north (Bowler et al., 1998) and south-east (Edney et al., 1990) of the continent. However, records from eastern Australia – tropical Lynch's Crater (Kershaw et al., 2007a) and alpine, temperate, Caledonia Fen (Kershaw et al., 2007b) – indicate similar climates during the Holocene and MIS 5. Similar climates between the north-eastern Lynch's Crater and Fern Gully Lagoon may be explained by the behaviour of the East Australian Current (EAC). SST records from the Tasman Sea, which record the passage of the EAC, indicate similar temperatures for MIS 5e and the Holocene (Kawagata, 2001) as a result of more southerly penetration of the EAC. The more southerly penetration of the EAC may, in turn, may have driven convective rainfall in subtropical and temperate eastern Australia somewhat independent of major continental climate drivers such as ENSO.

6. Conclusions

Analysis of a new discontinuous sedimentary record from Fern Gully Lagoon using ^{14}C dating, single-grain OSL dating and µXRF core scanning has enabled the reconstruction of a regional palaeoclimate sequence spanning the last three interglacial complexes. An evaluation of µXRF normalisation methods indicated that normalisation by total counts per second was the best method for Fern Gully Lagoon sediments.

The elemental signature of increased aeolian input to Fern Gully Lagoon, associated with drier climates, was characterised by PCA. The record indicates a relatively wet MIS 7a–c and early MIS 6 phase, a relatively drier MIS 5 interglacial complex, MIS 4 and MIS 3, and a wetter late MIS 2 which transitioned into a drier Holocene. There is

general agreement between the Fern Gully Lagoon record and central Australian lake records fed by the Australasian monsoon and records from the north- and south-east of the continent. Differences between ENSO driven north-eastern Australian records, and Fern Gully Lagoon may be due to the influence of the East Australian Current.

The increasingly dry interglacials observed from Fern Gully Lagoon may be due to more frequent El Niño events. Understanding how ENSO changes during interglacials is important in predicting future water availability due to climate change, as well as ecosystem response to increasing global temperatures. However, due to limited climate records, further study is required. The Fern Gully Lagoon record, which is sensitive to changing ENSO, may assist in answering some of these questions.

It is difficult to isolate a detailed record of hydrological change without considering changing vegetation types and biomass burning records. Ongoing analysis of multiple climate proxies such as pollen, charcoal and stable isotopes from Fern Gully Lagoon will likely result in a greater understanding of past interglacial climates and their drivers.

Supplementary data to this article can be found online at https://doi.org/10.1016/j.palaeo.2019.109463.

Declaration of competing interest

The authors declare that they have no known competing financial interests or personal relationships that could have appeared to influence the work reported in this paper.

Acknowledgements

We acknowledge Minjerribah (NSI) and the surrounding waters as Quandamooka Country, and we thank the Quandamooka Yoolooburrabee Aboriginal Corporation for their support of this research. This project was supported by the Australian Research Council Discovery Project DP150103875 and Future Fellowship Project FT130100195. Radiocarbon dating and Itrax μXRF scanning were achieved with the support of Australian Institute of Nuclear Science and Engineering grant ALNGRA16003. We would like to thank Cameron Schulz (DES) and Dr Harald Hofmann (UQ) for field assistance, and the Queensland Government for the Fern Gully Lagoon topographic map. We would also like to thank Mark Raven for WD-XRF analysis and Dr Katherine Grant for support running centred log-ratio calibration on Itrax data, as well as Chester Willard for his useful contributions to the discussion. This manuscript was improved by the contributions of two anonymous reviewers.

References

Aitken, M.J., 1985. Thermoluminescence dating. Academic press.
Arnold, L.J., Bailey, R.M., Tucker, G.E., 2007. Statistical treatment of fluvial dose distributions from southern Colorado arroyo deposits. Quat. Geochronol. 2, 162–167.
Arnold, L.J., Roberts, R.G., MacPhee, R.D.E., Willerslev, E., Tikhonov, A.N., Brock, F., 2008. Optical dating of perennially frozen deposits associated with preserved ancient plant and animal DNA in north-central Siberia. Quat. Geochronol. 3, 114–136.
Arnold, L.J., Roberts, R.G., Galbraith, R.F., DeLong, S.B., 2009. A revised burial dose estimation procedure for optical dating of young and modern-age sediments. Quat. Geochronol. 4 (4), 306–325.
Arnold, L.J., Demuro, M., Navazo, M., Benito-Calvo, A., Pérez-González, A., 2012. OSL dating of the Middle Palaeolithic Hotel California site, Sierra de Atapuerca, north-central Spain. Boreas 42, 285–305.
Ayliffe, L.K., Marianelli, P.C., Moriarty, K.C., Wells, R.T., McCulloch, M.T., Mortimer, G.E., Hellstrom, J.C., 1998. 500 ka precipitation record from southeastern Australia: evidence for interglacial relative aridity. Geology 26, 147–150.
Baczkowski, A.J., 2000. The broken-stick model for species abundances: an initial investigation. In: Internal Report STAT 00/10. University of Leeds, UK, pp. 2–25.
Ballhorn, U., Siegert, F., Mason, M., Limin, S., 2009. Derivation of burn scar depths and estimation of carbon emissions with LIDAR in Indonesian peatlands. Proc. Natl. Acad. Sci. 106, 21213.
Barr, C., Tibby, J., Moss, P.T., Halverson, G.P., Marshall, J.C., McGregor, G.B., Stirling, E., 2017. A 25,000-year record of environmental change from Welsby Lagoon, North Stradbroke Island, in the Australian subtropics. Quat. Int. 449, 106–118.
Barr, C., Tibby, J., Leng, M.J., Tyler, J.J., Henderson, A.C.G., Overpeck, J.T., Simpson, G.L., Cole, J.E., Phipps, S.J., Marshall, J.C., McGregor, G.B., Hua, Q., McRobie, F.H., 2019. Holocene El Niño–Southern Oscillation variability reflected in subtropical Australian precipitation. Sci. Rep. 9, 1627.
Bateman, M.D., Boulter, C.H., Carr, A.S., Frederick, C.D., Peter, D., Wilder, M., 2007. Preserving the palaeoenvironmental record in Drylands: bioturbation and its significance for luminescence-derived chronologies. Sediment. Geol. 195, 5–19.
Beck, K.K., Fletcher, M.-S., Gadd, P.S., Heijnis, H., Jacobsen, G.E., 2017. An early onset of ENSO influence in the extra-tropics of the southwest Pacific inferred from a 14,600 year high resolution multi-proxy record from Paddy's Lake, northwest Tasmania. Quat. Sci. Rev. 157, 164–175.
Berger, A., Crucifix, M., Hodell, D.A., Mangili, C., McManus, J.F., Otto-Bliesner, B., Pol, K., Raynaud, D., Skinner, L.C., Tzedakis, P.C., Wolff, E.W., Yin, Q.Z., Abe-Ouchi, A., Barbante, C., Brovkin, V., Cacho, I., Capron, E., Ferretti, P., Ganopolski, A., Grimalt, J.O., Hönisch, B., Kawamura, K., Landais, A., Margari, V., Martrat, B., Masson-Delmotte, V., Mokeddem, Z., Parrenin, F., Prokopenko, A.A., Rashid, H., Schulz, M., Riveiros, N.V., 2015. Interglacials of the last 800,000 years. Rev. Geophys. 54, 162–219.
Berntsson, A., Rosqvist, G.C., Velle, G., 2014. Late-Holocene temperature and precipitation changes in Vindelfjällen, mid-western Swedish Lapland, inferred from chironomid and geochemical data. Holocene 24, 78–92.
Berger, A., Loutre, M.F., 1991. Insolation values for the climate of the last 10 million years. Quat. Sci. Rev. 10 (4), 297–317.
BOM, 2005. Köppen climate classifications based on a standard 30 year climatology (1961-1990). Retrieved 29-6-2018, 2018, from. http://www.bom.gov.au/jsp/ncc/climate_averages/climate-classifications/index.jsp?maptype=kpngrp#maps.
Bostock, H.C., Opdyke, B.N., Gagan, M.K., Kiss, A.E., Fifield, L.K., 2006. Glacial/interglacial changes in the East Australian current. Clim. Dyn. 26, 645–659.
Bouchard, F., Francus, P., Pienitz, R., Laurion, I., 2011. Sedimentology and geochemistry of thermokarst ponds in discontinuous permafrost, subarctic Quebec, Canada. J. Geophys. Res. Biogeosci. 116.
Bowler, J.M., Duller, G.A.T., Perret, N., Prescott, J.R., Wyrwoll, K.-H., 1998. Hydrologic changes in monsoonal climates of the last glacial cycle: stratigraphy and luminescence dating of Lake Woods, N.T. Australia. Paleoclimates 3, 179–207.
Bowler, J.M., Wyrwoll, K.-H., Lu, Y., 2001. Variations of the northwest Australia summer monsoon over the last 300,000 years: the paleohydrological record of the Gregory (Mulan) Lakes system. Quat. Int. 82–85, 63–80.
Boyle, J.F., Chiverrell, R.C., Schillereff, D., 2015. Approaches to water content correction and calibration for μXRF core scanning: comparing X-ray scattering with simple regression of elemental concentrations. In: Croudace, I.W., Rothwell, R.G. (Eds.), Micro-XRF Studies of Sediment Cores, Developments in Paleoenvironmental Research. Springer Science and Business Media, Dordrecht.
Brennan, B.J., 2003. Beta doses to spherical grains. Radiation Measurements 37, 299–303.
Brill, D., Klasen, N., Jankaew, K., Brückner, H., Kelletat, D., Scheffers, A., Scheffers, S., 2012. Local inundation distances and regional tsunami recurrence in the Indian Ocean inferred from luminescence dating of sandy deposits in Thailand. Nat. Hazards Earth Syst. Sci. 12, 2177–2192.
Brock, F., Higham, T., Ditchfield, P., Ramsey, C.B., 2010. Current pretreatment methods for AMS radiocarbon dating at the Oxford Radiocarbon Accelerator Unit (ORAU). Radiocarbon 52, 103–112.
Brock, F., Lee, S., Housley, R.A., Ramsey, B., 2011. Variation in the radiocarbon age of different fractions of peat: a case study from Ahrenshöft, northern Germany. Quat. Geochronol. 6, 550–555.
Bronk Ramsey, C., 2009. Bayesian analysis of radiocarbon dates. Radiocarbon 51, 337–360.
Bronk Ramsey, C., Lee, S., 2013. Recent and planned developments of the program OxCal. Radiocarbon 55, 720–730.
Brumsack, H.-J., 2006. The trace metal content of recent organic carbon-rich sediments: implications for Cretaceous black shale formation. Palaeogeogr. Palaeoclimatol. Palaeoecol. 232, 344–361.
Burrows, M.A., Heijnis, H., Gadd, P., Haberle, S.G., 2016. A new late Quaternary palaeohydrological record from the humid tropics of northeastern Australia. Palaeogeogr. Palaeoclimatol. Palaeoecol. 451, 164–182.
Cadd, H., Tibby, J., Barr, C., Tyler, J., Unger, L., Leng, M., Marshall, J., McGregor, G., Lewis, R., Arnold, L., Lewis, T., Baldock, J., 2018. Development of a southern hemisphere subtropical wetland (Welsby Lagoon, south-east Queensland, Australia) through the last glacial cycle. Quat. Sci. Rev. 202, 53–65.
Clark, M., Hounslow, M., 2009. CPLSlot Version 2.4b. Monash University, Victoria, Australia.
Cohen, T.J., Jansen, J.D., Gliganic, L.A., Larsen, J.R., Nanson, G.C., May, J.-H., Jones, B.G., Price, D.M., 2015. Hydrological transformation coincided with megafaunal extinction in central Australia. Geology 43, 195–199.
Colhoun, E.A., Pola, J.S., Barton, C.E., Heijnis, H., 1999. Late Pleistocene vegetation and climate history of Lake Selina, western Tasmania. Quat. Int. 57–58, 5–23.
Croudace, I.W., Rothwell, R.G., 2015. Micro-XRF Studies of Sediment Cores: Applications of a Non-destructive Tool for the Environmental Sciences. Springer.
Croudace, I.W., Rindby, A., Rothwell, R.G., 2006. ITRAX: description and evaluation of a new multi-function X-ray core scanner. Geol. Soc. Lond., Spec. Publ. 267, 51.
Cuven, S., Francus, P., Lamoureux, S., 2010. Estimation of grain-size variability with micro X-ray fluorescence in laminated lacustrine sediments, cape bounty, Canadian High Arctic. J. Paleolimnol. 44, 803–817.
Davies, G.M., Gray, A., Rein, G., Legg, C.J., 2013. Peat consumption and carbon loss due to smouldering wildfire in a temperate peatland. For. Ecol. Manag. 308, 169–177.
De Deckker, P., Arnold, L.J., van der Kaars, S., Bayon, G., Stuut, J.-B.W., Perner, K., Lopes dos Santos, R., Uemura, R., Demuro, M., 2019. Marine Isotope Stage 4 in Australasia: a full glacial culminating 65,000 years ago – global connections and implications for

human dispersal. Quat. Sci. Rev. 204, 187–207.
Demuro, M., Arnold, L.J., Froese, D.G., Roberts, R.G., 2013. OSL dating of loess deposits bracketing Sheep Creek tephra beds, northwest Canada: dim and problematic single-grain OSL characteristics and their effect on multi-grain age estimates. Quat. Geochronol. 15, 67–87.
Demuro, M., Arnold, L.J., Parés, J.M., Sala, R., 2015. Extended-range luminescence chronologies suggest potentially complex bone accumulation histories at the Early-to-Middle Pleistocene palaeontological site of Huéscar-1 (Guadix-Baza basin, Spain). Quat. Int. 389, 191–212.
Donders, T.H., Wagner, F., Visscher, H., 2006. Late Pleistocene and Holocene subtropical vegetation dynamics recorded in perched lake deposits on Fraser Island, Queensland, Australia. Palaeogeogr. Palaeoclimatol. Palaeoecol. 241, 417–439.
Duller, Geoff, 2015. The Analyst software package for luminescence data: overview and recent improvements. Ancient TL 3, 35–42 (Epub Date: 3.24).
Edney, P.A., Kershaw, A.P., Deckker, P.D., 1990. A late Pleistocene and Holocene vegetation and environmental record from Lake Wangoom, Western Plains of Victoria, Australia. Palaeogeogr. Palaeoclimatol. Palaeoecol. 80, 325–343.
Eggenberger, S., Gobet, E., Leeuwen, J., Schwörer, C., Knaap, W., Dobben, H., Vogel, H., Tinner, W., Rambeau, C., 2018. Millennial multi-proxy reconstruction of oasis dynamics in Jordan, by the Dead Sea. J. Quat. Plant Ecol. Palaeoclim. Ancient Agric. 27, 649–664.
Elderfield, H., Ferretti, P., Greaves, M., Crowhurst, S., McCave, I.N., Hodell, D., Piotrowski, A.M., 2012. Evolution of ocean temperature and ice volume through the Mid-Pleistocene climate transition. Science 337, 704–709.
Falster, G., Tyler, J., Grant, K., Tibby, J., Turney, C., Löhr, S., Jacobsen, G., Kershaw, A.P., 2018. Millennial-scale variability in south-east Australian hydroclimate between 30,000 and 10,000 years ago. Quat. Sci. Rev. 192, 106–122.
Field, E., Tyler, J., Gadd, P.S., Moss, P., McGowan, H., Marx, S., 2018. Coherent patterns of environmental change at multiple organic spring sites in northwest Australia: evidence of Indonesian-Australian summer monsoon variability over the last 14,500 years. Quat. Sci. Rev. 196, 193–216.
Foerster, V., Deocampo, D.M., Asrat, A., Gunter, C., Junginger, A., Kramer, K.H., Stroncik, N.A., Trauth, M.H., 2018. Towards an understanding of climate proxy formation in the Chew Bahir basin, southern Ethiopian Rift. Palaeogeogr. Palaeoclimatol. Palaeoecol. 501, 111.
Fu, X., Cohen, T.J., Arnold, L.J., 2017. Extending the record of lacustrine phases beyond the last interglacial for Lake Eyre in central Australia using luminescence dating. Quat. Sci. Rev. 162, 88–110.
Gagan, M.K., Ayliffe, L.K., Beck, J.W., Cole, J.E., Druffel, E.R.M., Dunbar, R.B., Schrag, D.P., 2000. New views of tropical paleoclimates from corals. Quat. Sci. Rev. (0277-3791) 19 (1), 45–64. https://doi.org/10.1016/S0277-3791(99)00054-2.
Galbraith, R.F., Roberts, R.G., Laslett, G.M., Yoshida, H., Olley, J.M., 1999. Optical dating of single and multiple grains of quartz from Jinmium Rock Shelter, northern Australia: Part 1, experimental design and statistical models. Archaeometry 41 (2), 339–364.
Grant, K.M., Rohling, E.J., Westerhold, T., Zabel, M., Heslop, D., Konijnendijk, T., Lourens, L., 2017. A 3 million year index for North African humidity/aridity and the implication of potential pan-African Humid periods. Quat. Sci. Rev. 171, 100–118.
Guyard, H., Chapron, E., St-Onge, G., Anselmetti, F.S., Arnaud, F., Magand, O., Francus, P., Mélières, M.-A., 2007. High-altitude varve records of abrupt environmental changes and mining activity over the last 4000 years in the Western French Alps (Lake Bramant, Grandes Rousses Massif). Quat. Sci. Rev. 26, 2644–2660.
Guérin, G., Mercier, N., Adamiec, G., 2011. Dose-rate conversion factors: update. Ancient TL 29 (1), 5–8.
Hahn, A., Kliem, P., Oehlerich, M., Ohlendorf, C., Zolitschka, B., 2014. Elemental composition of the Laguna Potrok Aike sediment sequence reveals paleoclimatic changes over the past 51 ka in southern Patagonia, Argentina. J. Paleolimnol. 52, 349–366.
Harle, K.J., Heijnis, H., Chisari, R., Kershaw, A.P., Zoppi, U., Jacobsen, G., 2002. A chronology for the long pollen record from Lake Wangoom, western Victoria (Australia) as derived from uranium/thorium disequilibrium dating. J. Quat. Sci. 17, 707–720.
Harrison, S.P., Bartlein, P., 2012. Records from the past, lessons for the future: what the palaeorecord implies about mechanisms of global change. In: Henderson-Sellers, A., McGuffie, K. (Eds.), The Future of the World's Climate. Elsevier Science, pp. 403–436.
Heiri, O., Lotter, A., Lemcke, G., 2001. Loss on ignition as a method for estimating organic and carbonate content in sediments: reproducibility and comparability of results. J. Paleolimnol. 25, 101–110.
Hesse, P.P., McTainsh, G.H., 2003. Australian dust deposits: modern processes and the Quaternary record. Quat. Sci. Rev. 22, 2007–2035.
Hofmann, H., Newborn, D., Cartwright, I., Cendón, D.I., Raiber, M., 2019. Groundwater mean residence time of a sub-tropical barrier sand island. Hydrol. Earth Syst. Sci. Discuss. 1–32.
Hogg, A.G., Hua, Q., Blackwell, P.G., Niu, M., Buck, C.E., Heaton, T.J., Guilderson, T.P., Zimmerman, S.R.H., Palmer, J.G., Turney, C.S.M., Reimer, P.J., Reimer, R.W., 2013. Shcal13 Southern Hemisphere calibration, 0–50,000 years cal BP. Radiocarbon 55, 1889–1903.
Ihaka, R., Gentleman, R., 2016. R Statistical Computing Program, 331. The R Foundation for Statistical Computing.
Jacobs, Z., Duller, G.A.T., Wintle, A.G., 2006. Interpretation of single grain De distributions and calculation of De. Radiat. Meas. (1350-4487) 41 (3), 264–277. https://doi.org/10.1016/j.radmeas.2005.07.027.
Jouve, G., Francus, P., Lamoureux, S., Provencher-Nolet, L., Hahn, A., Haberzettl, T., Fortin, D., Nuttin, L., 2013. Microsedimentological characterization using image analysis and μ-XRF as indicators of sedimentary processes and climate changes during Lateglacial at Laguna Potrok Aike, Santa Cruz, Argentina. Quat. Sci. Rev. 71, 191–204.
Kawagata, S., 2001. Tasman Front shifts and associated paleoceanographic changes during the last 250,000 years: foraminiferal evidence from the Lord Howe Rise. Mar. Micropaleontol. 41, 167–191.
Kemp, C.W., Tibby, J., Arnold, L.J., Barr, C., 2019. Australian hydroclimate during Marine Isotope Stage 3: a synthesis and review. Quat. Sci. Rev. 204, 94–104.
Kershaw, P., Moss, P., Van Der Kaars, S., 2003. Causes and consequences of long-term climatic variability on the Australian continent. Freshw. Biol. 48, 1274–1283.
Kershaw, A.P., Bretherton, S.C., van der Kaars, S., 2007a. A complete pollen record of the last 230 ka from Lynch's Crater, north-eastern Australia. Palaeogeogr. Palaeoclimatol. Palaeoecol. 251, 23–45.
Kershaw, A.P., McKenzie, G.M., Porch, N., Roberts, R.G., Brown, J., Heijnis, H., Orr, M.L., Jacobsen, G., Newall, P.R., 2007b. A high-resolution record of vegetation and climate through the last glacial cycles from Caledonia Fen, southeastern highlands of Australia. J. Quat. Sci. 22, 481–500.
Kienel, U., Kirillin, G., Brademann, B., Plessen, B., Lampe, R., Brauer, A., 2017. Effects of spring warming and mixing duration on diatom deposition in deep Tiefer See, NE Germany. J. Paleolimnol. 57, 37–49.
Killick, R., Eckley, I.A., 2014. Changepoint: an R package for changepoint analysis. J. Stat. Softw. 1 (3) (2014).
Köhler, P., Nehrbass-Ahles, C., Schmitt, J., Stocker, T.F., Fischer, H., 2017. Continuous record of the atmospheric greenhouse gas carbon dioxide (CO_2), raw data. In: In Supplement to: Köhler, P et al. (2017): A 156 kyr Smoothed History of the Atmospheric Greenhouse Gases CO_2, CH_4, and N_2O and Their Radiative Forcing. Earth System Science Data, 9(1), 363–387. PANGAEA. https://doi.org/10.5194/essd-9-363-2017.
Kylander, M.E., Ampe, L., Wohlfarth, B., Veres, D., 2011. High-resolution X-ray fluorescence core scanning analysis of Les Echets (France) sedimentary sequence: new insights from chemical proxies. J. Quat. Sci. 26, 109–117.
Lamy, F., Gersonde, R., Winckler, G., Esper, O., Jaeschke, A., Kuhn, G., Ullermann, J., Martinez-Garcia, A., Lambert, F., Kilian, R., 2014. Increased dust deposition in the Pacific Southern Ocean during glacial periods. Science 343, 403–407.
Leach, L.M., 2011. Hydrology and physical setting of North Stradbroke Island. P. R. Soc. Queensland 117, 21–46.
Lisiecki, L.E., Raymo, M.E., 2005. A Pliocene-Pleistocene stack of 57 globally distributed benthic $\delta^{18}O$ records. Paleoceanography 20.
Lo, L., Chang, S.-P., Wei, K.-Y., Lee, S.-Y., Ou, T.-H., Chen, Y.-C., Chuang, C.-K., Mii, H.-S., Burr, G.S., Chen, M.-T., Tung, Y.-H., Tsai, M.-C., Hodell, D.A., Shen, C.-C., 2017. Nonlinear climatic sensitivity to greenhouse gases over past 4 glacial/interglacial cycles. Sci. Rep. 7, 4626.
Longmore, M.E., 1997. The mid-Holocene "dry" anomaly on the mid-eastern coast of Australia: calibration of palaeowater depth as a surrogate for effective precipitation using sedimentary loss on ignition in the perched lake sediments of Fraser Island, Queensland. Palaeoclimates 4, 46023.
Löwemark, L., Chen, H.F., Yang, T.N., Kylander, M., Yu, E.F., Hsu, Y.W., Lee, T.Q., Song, S.R., Jarvis, S., 2011. Normalizing XRF-scanner data: a cautionary note on the interpretation of high-resolution records from organic-rich lakes. J. Asian Earth Sci. 40, 1250–1256.
Lukenbach, M.C., Hokanson, K.J., Moore, P.A., Devito, K.J., Kettridge, N., Thompson, D.K., Wotton, B.M., Petrone, R.M., Waddington, J.M., 2015. Hydrological controls on deep burning in a northern forested peatland. Hydrol. Process. 29, 4114–4124.
Mackenzie, L., Heijnis, H., Gadd, P., Moss, P., Shulmeister, J., 2017. Geochemical investigation of the South Wellesley Island wetlands: insight into wetland development during the Holocene in tropical northern Australia. The Holocene 27, 566–578.
Maroulis, J.C., Nanson, G.C., Price, D.M., Pietsch, T., 2007. Aeolian–fluvial interaction and climate change: source-bordering dune development over the past ~100 ka on Cooper Creek, central Australia. Quat. Sci. Rev. 26, 386–404.
Marshall, M.H., Lamb, H.F., Huws, D., Davies, S.J., Bates, R., Bloemendal, J., Boyle, J., Leng, M.J., Umer, M., Bryant, C., 2011. Late Pleistocene and Holocene drought events at Lake Tana, the source of the Blue Nile. Glob. Planet. Chang. 78, 147–161.
Martin, L., Mooney, S., Goff, J., 2014. Coastal wetlands reveal a non-synchronous island response to sea-level change and a palaeostorm record from 5.5 kyr to present. The Holocene 24, 569–580.
Martinez, J.I., DeDeckker, P., Barrows, T.T., 2002. Palaeoceanography of the western Pacific warm pool during the last glacial maximum: long-term climatic monitoring of the maritime continent. In: Kershaw, P., Bruno, D., Tapper, N., Penny, D., Brown, J. (Eds.), Bridging Wallace's Line. Adv GeoEcolpp. 147–172.
McGowan, H.A., Petherick, L.M., Kamber, B.S., 2008. Aeolian sedimentation and climate variability during the late Quaternary in southeast Queensland, Australia. Palaeogeogr. Palaeoclimatol. Palaeoecol. 265, 171–181.
Mejdahl, V., 1979. Thermoluminescence Dating: Beta-Dose Attenuation in Quartz Grains. Archaeometry 21, 61–72.
Miller, G.H., Fogel, M.L., Magee, J.W., Gagan, M.K., 2016. Disentangling the impacts of climate and human colonization on the flora and fauna of the Australian arid zone over the past 100 ka using stable isotopes in avian eggshell. Quat. Sci. Rev. 151, 27–57.
Moss, P.T., Kershaw, A.P., 2007. A late Quaternary marine palynological record (oxygen isotope stages 1 to 7) for the humid tropics of northeastern Australia based on ODP Site 820. Palaeogeogr. Palaeoclimatol. Palaeoecol. 251, 4–22.
Moss, P.T., Tibby, J., Petherick, L., McGowan, H., Barr, C., 2013. Late Quaternary vegetation history of North Stradbroke Island, Queensland, eastern Australia. Quat. Sci. Rev. 74, 257–272.
Nanson, G.C., Price, D.M., Jones, B.G., Maroulis, J.C., Coleman, M., Bowman, H., Cohen, T.J., Pietsch, T.J., Larsen, J.R., 2008. Alluvial evidence for major climate and flow regime changes during the middle and late Quaternary in eastern central Australia. Geomorphology 101, 109–129.
Neal, R., Stock, E., 1986. Pleistocene occupation in the south-east Queensland coastal

region. Nature 323, 618–621.
Nilsson, M., Klarqvist, M., Bohlin, E., Possnert, G., 2001. Variation in ^{14}C age of macrofossils and different fractions of minute peat samples dated by AMS. The Holocene 11, 579–586.
Oksanen, J., Blanchet, F.G., Friendly, M., Kindt, R., Legendre, P., McGlinn, D., Minchin, P.R., O'Hara, R.B., Simpson, G.L., Solymos, P., Stevens, M.H.H., Szoecs, E., Wagner, H., 2018. Community Ecology Package, 2.5-2 ed, pp. Ordination Methods, Diversity Analysis and Other Functions for Community and Vegetation Ecologists.
Parrenin, F., Masson-Delmotte, V., Köhler, P., Raynaud, D., Paillard, D., Schwander, J., Barbante, C., Landais, A., Wegner, A., Jouzel, J., 2013. Antarctic Temperature Stack (ATS) from five different ice cores (EDC, Vostok, Dome Fuji, TALDICE, and EDML), In supplement to: Parrenin, F et al. (2013): Synchronous change of atmospheric CO_2 and Antarctic temperature during the last deglacial warming. Science 339 (6123), 1060–1063. https://doi.org/10.1126/science.1226368. (PANGAEA).
Patton, N.R., Ellerton, D., Shulmeister, J., 2019. High resolution remapping of the coastal dune fields of south east Queensland, Australia: a morphometric approach. J. Maps 15, 578–589.
Pelejero, C., Calvo, E., Barrows, T.T., Logan, G.A., De Deckker, P., 2006. South Tasman Sea alkenone palaeothermometry over the last four glacial/interglacial cycles. Mar. Geol. 230, 73–86.
Petherick, L., McGowan, H., Moss, P., 2008. Climate variability during the Last Glacial Maximum in eastern Australia: evidence of two stadials? J. Quat. Sci. Rev. 23, 787–802.
Petherick, L.M., McGowan, H.A., Kamber, B.S., 2009. Reconstructing transport pathways for late Quaternary dust from eastern Australia using the composition of trace elements of long travelled dusts. Geomorphology 105, 67–79.
Petherick, L., Bostock, H., Cohen, T.J., Fitzsimmons, K., Tibby, J., Fletcher, M.-S., Moss, P., Reeves, J., Mooney, S., Barrows, T., Kemp, J., Jansen, J., Nanson, G., Dosseto, A., 2013. Climatic records over the past 30 ka from temperate Australia – a synthesis from the Oz-INTIMATE workgroup. Quat. Sci. Rev. 74, 58–77.
Petherick, L.M., Moss, P.T., McGowan, H.A., 2017. An extended Last Glacial Maximum in subtropical Australia. Quat. Int. 432, 1–12.
Pleskot, K., Tjallingii, R., Makohonienko, M., Nowaczyk, N., Szczuciński, W., 2018. Holocene paleohydrological reconstruction of Lake Strzeszyńskie (western Poland) and its implications for the central European climatic transition zone. J. Paleolimnol. 59, 443–459.
Prescott, J.R., Hutton, J.T., 1994. Cosmic ray contributions to dose rates for luminescence and ESR dating: Large depths and long-term time variations. Radiat. Meas. (1350-4487) 23 (2), 497–500. https://doi.org/10.1016/1350-4487(94)90086-8. http://www.sciencedirect.com/science/article/pii/1350448794900868.
Profe, J., Neumann, L., Novothny, Á., Barta, G., Rolf, C., Frechen, M., Ohlendorf, C., Zolitschka, B., 2018. Paleoenvironmental conditions and sedimentation dynamics in Central Europe inferred from geochemical data of the loess-paleosol sequence at Süttő (Hungary). Quat. Sci. Rev. 196, 21–37.
Rees, A.B.H., Cwynar, L.C., Fletcher, M.-S., 2015. Southern Westerly Winds submit to the ENSO regime: a multiproxy paleohydrology record from Lake Dobson, Tasmania. Quat. Sci. Rev. 126, 254–263.
Rees-Jones, J., 1995. Optical dating of young sediments using fine-grain quartz. Ancient TL 13 (2), 914.
Rees-Jones, J., Tite, M.S., 1997. Optical dating results for British archaeological sediments. Archaeometry 36, 177–187.
Reeves, J.M., Barrows, T.T., Cohen, T.J., Kiem, A.S., Bostock, H.C., Fitzsimmons, K.E., Jansen, J.D., Kemp, J., Krause, C., Petherick, L., Phipps, S.J., Members, O.-I., 2013. Climate variability over the last 35,000 years recorded in marine and terrestrial archives in the Australian region: an OZ-INTIMATE compilation. Quat. Sci. Rev. 74, 21–34.
Roberts, H.M., Bryant, C.L., Huws, D.G., Lamb, H.F., 2018. Generating long chronologies for lacustrine sediments using luminescence dating: a 250,000 year record from Lake Tana, Ethiopia. Quat. Sci. Rev. 202, 66–77.
Rohling, E.J., Grant, K., Bolshaw, M., Roberts, A.P., Siddall, M., Hemleben, C., Kucera, M., 2009. Antarctic temperature and global sea level closely coupled over the past five glacial cycles. Nat. Geosci. 2, 500.
Sáez, A., Valero-Garcés, B.L., Giralt, S., Moreno, A., Bao, R., Pueyo, J.J., Hernández, A., Casas, D., 2009. Glacial to Holocene climate changes in the SE Pacific. The Raraku Lake sedimentary record (Easter Island, 27°S). Quat. Sci. Rev. 28, 2743–2759.
Smith, S.M., Newman, S., Garrett, P.B., Leeds, J.A., 2001. Differential effects of surface and peat fire on soil constituents in a degraded wetland of the northern Florida Everglades. J. Environ. Qual. 30, 1998–2005.
Stephens, T., Augustinus, P., Rip, B., Gadd, P., Zawadski, A., 2018. Managing land-use effects on Northland dune lakes: lessons from the past. N. Z. J. Mar. Freshw. Res. 1–21.
Striberger, J., Björck, S., Ingólfsson, Ó., Kjær, K.H., Snowball, I.A.N., Uvo, C.B., 2010. Climate variability and glacial processes in eastern Iceland during the past 700 years based on varved lake sediments. Boreas 40, 28–45.
Tachikawa, K., Timmermann, A., Vidal, L., Sonzogni, C., Timm, O.E., 2014. CO_2 radiative forcing and Intertropical Convergence Zone influences on western Pacific warm pool climate over the past 400 ka. Quat. Sci. Rev. 86, 24–34.
Team-RStudio, 2015. RStudio: Integrated Development for R. RStudio, Inc., Boston, MA.
Tibby, J., Barr, C., Marshall, J.C., Mcgregor, G.B., Moss, P.T., Arnold, L.J., Page, T.J., Questiaux, D., Olley, J., Kemp, J., Spooner, N., Petherick, L., Penny, D., Mooney, S., Moss, E., 2017. Persistence of wetlands on North Stradbroke Island (south-east Queensland, Australia) during the last glacial cycle: implications for Quaternary science and biogeography. J. Quat. Sci. 32, 770–781.
Turetsky, M.R., Manning, S.W., Wieder, R.K., 2004. Dating recent peat deposits. Wetlands 24, 324–356.
Turner, J.N., Holmes, N., Davis, S.R., Leng, M.J., Langdon, C., Scaife, R.G., 2015. A multiproxy (micro-XRF, pollen, chironomid and stable isotope) lake sediment record for the Lateglacial to Holocene transition from Thomastown Bog, Ireland. J. Quat. Sci. 30, 514–528.
Turney, C.S.M., Jones, R.T., 2010. Does the Agulhas Current amplify global temperatures during super-interglacials? J. Quat. Sci. 25, 839–843.
Van der Bilt, W.G.M., Bakke, J., Vasskog, K., D'Andrea, W.J., Bradley, R.S., Ólafsdóttir, S., 2015. Reconstruction of glacier variability from lake sediments reveals dynamic Holocene climate in Svalbard. Quat. Sci. Rev. 126, 201–218.
Van der Kaars, S., Miller, G.H., Turney, C.S.M., Cook, E.J., Nürnberg, D., Schönfeld, J., Kershaw, A.P., Lehman, S.J., 2017. Humans rather than climate the primary cause of Pleistocene megafaunal extinction in Australia. Nat. Commun. 8, 1–7.
Vegas-Vilarrúbia, T., Corella, J.P., Pérez-Zanón, N., Buchaca, T., Trapote, M.C., López, P., Sigró, J., Rull, V., 2018. Historical shifts in oxygenation regime as recorded in the laminated sediments of lake Montcortès (Central Pyrenees) support hypoxia as a continental-scale phenomenon. Sci. Total Environ. 612, 1577–1592.
Walker, J., Lees, B., Olley, J., Thompson, C., 2018. Dating the Cooloola coastal dunes of South-Eastern Queensland, Australia. Mar. Geol. 398, 73–85.
Weltje, G.J., Tjallingii, R., 2008. Calibration of XRF core scanners for quantitative geochemical logging of sediment cores: theory and application. Earth Planet. Sci. Lett. 274, 423–438.
Weltje, G.J., Bloemsma, M.R., Tjallingii, R., Heslop, D., Röhl, U., Croudace, I.W., 2015. Prediction of geochemical composition from XRF core scanner data: a new multivariate approach including automatic selection of calibration samples and quantification of uncertainties. In: Croudace, I.W., Rothwell, R.G. (Eds.), Micro-XRF Studies of Sediment Cores: Applications of a Non-destructive Tool for the Environmental Sciences. Springer, Netherlands, Dordrecht, pp. 507–534.
Woltering, M., Atahan, P., Grice, K., Heijnis, H., Taffs, K., Dodson, J., 2014. Glacial and Holocene terrestrial temperature variability in subtropical east Australia: branched GDGT distributions in a sediment core from Lake McKenzie. Quat. Res. 82, 132–145.
Woodward, C.A., Gadd, P.S., 2019. The potential power and pitfalls of using the X-ray fluorescence molybdenum incoherent:coherent scattering ratio as a proxy for sediment organic content. Quat. Int. 514, 30–43.
Woodward, C.A., Slee, A., Gadd, P., Zawadzki, A., Hamze, H., Parmar, A., Zahra, D., 2018. The role of earthquakes and climate in the formation of diamictic sediments in a New Zealand mountain lake. Quat. Int. 470, 130–147.
Wright, H.E.J., 1967. A square-rod piston sampler for lake sediments. J. Sediment. Petrol. 37, 975–976.
Zhang, S., Li, T., Chang, F., Yu, Z., Xiong, Z., Wang, H., 2017. Correspondence between the ENSO-like state and glacial-interglacial condition during the past 360 kyr. Chin. J. Oceanol. Limnol. 35, 1018–1031.